Detection of Ghrelin Species by Mass Spectrometry, a Novel Biomarker for Diagnosing Dementia?

Alanna Thomas

Supervisors:

Dr Jeffrey Davies, Dr Alwena Morgan and Dr Roberto Angelini.

Submitted to Swansea University in fulfilment of the requirements for the Degree of Doctor of Philosophy.

Swansea University
Prifysgol Abertawe

SWANSEA UNIVERSITY 2025

Table of Contents

Acknowledgements 10

List of Figures 12

List of Abbreviations 18

1. Introduction 21

1.1 Introduction to Biomarkers in Biomedical Research 22

1.1.1 Definition and Classification 22

1.1.2 Importance of Biochemical Context: Protein Structure, Function, and Post Translational Modifications 22

1.1.3 Role of Biomarkers in Precision Medicine and Neurodegenerative Disease Research 23

1.1.4 Requirements for a Viable Biomarker 24

1.2 Neurodegenerative Disease Landscape 25

1.3 Systemic Factors Influencing Neurodegeneration 27

1.3.1 The Gut–Brain Axis in Neurodegeneration 28

1.3.2 Ghrelin at the Intersection of the Gut–Brain Axis and Biomarker Research 28

1.4 Ghrelin Biology and Structural Diversity 29

1.4.1 Background of Ghrelin 29

1.4.2 Ghrelin formation 31

1.4.3 Factors Impacting Ghrelin Levels 35

1.4.3.1 Proteins Impact on Ghrelin Expression 35

1.4.3.2 Ghrelin Clearance and Half-Life 36

1.4.3.3 Animal Models of Age-Related Ghrelin Changes 37

1.4.3.4 Human Studies of Age-Related Ghrelin Changes 38

1.4.3.5 Ghrelin degradation 39

1.4.3.6 Implications for Dementia Biomarker Development 40

1.4.4 Ghrelin Receptors and Brain Localisation 41

1.4.5 Unacylated and Acyl Ghrelin and the BBB 42
1.4.6 Acyl Ghrelin Binding to GHS-R1a 47
1.4.7 The Role of Unacylated Ghrelin 48
1.4.8 Physiological Relevance of Unacylated and Acyl Ghrelin 49
1.5 Lipidation Variability and Relevance to Disease 51
1.6 Ghrelin Signalling in PD: Pathophysiological Relevance 53
1.7 Ghrelin and Biomarker Suitability 54
1.7.1 Alignment with Biomarker Criteria 54
1.7.2 Sample Collection and Preservation Challenges 56
1.7.3 Sensitivity and Specificity 56
1.7.4 Patient Stratification and Disease Stage 56
1.7.5 Biological and Pathophysiological Relevance 56
1.7.6 AG:UAG Ratio and Disease-State Reflection 57
1.7.7 Central vs. Peripheral Measurements and BBB Considerations 57
1.7.8 Clinical Interpretability and Translational Potential 57
1.7.9 Comparison with Established Blood-Based Biomarkers 57
1.7.10 Summary 58
1.8 Detection Techniques for Ghrelin Isoforms 58
1.8.1 Analytical Requirements for Quantifying AG:UAG Ratio 58
1.8.2 Immunoassays: Current Utility and Limitations 59
1.8.3 MS-Based Techniques: MALDI-TOF and LC-MS/MS 59
1.8.4 Emerging Tools: BAMS and Immune-Affinity MS 60
1.8.5 Importance of Lipid Moiety Retention and Capture Strategies 61
1.8.6 Lessons from Neurodegenerative Biomarker Assays 61
1.9 Sample Preparation and Analytical Considerations 63
1.9.1 Challenges of Complex Biological Fluids 63

1.9.2 Clearance and Simplification: Need for Lipid-Sensitive and Specific Capture 65
1.9.3 Existing Antibodies and Epitope Limitations for Acyl Ghrelin 65
1.9.4 Chromatographic Clearance or Selective Enrichment: Technical Decision Points 66
1.9.5 Bottom-Up Biomarker Development: From In Vitro Models to Human Cohorts 66
1.10 Economic and Practical Feasibility 67
1.10.1 Cost Comparison: ELISA vs. Mass Spectrometry-Based Approaches 67
1.10.2 Health Economics Implications in Large-Scale Diagnostics 68
1.10.3 Clinical Translation Potential and Cost-Benefit Balance 68
1.11 Mass Spectrometry 69
1.11.1 Overview 69
1.11.2 Ionisation Techniques 69
1.11.3 Mass Analysers 70
1.11.4 Tandem MS (MS/MS) 70
1.11.5 Summary Table of Mass Spectrometry platforms used 71
1.12 Hypotheses and Aims 71
1.13 Research Objectives 71
1.14 Context of Thesis within Wider Research Projects 72
2. Materials and Methods 73
2.1 Materials 74
2.1.1 Equipment 74
2.1.2 Reagents and Solvents 75
2.1.3 Ghrelin Standards 76
2.2 Blood and Plasma Collection 78
2.3 Ghrelin Extraction 79
2.4 Ghrelin Analysis by MALDI-TOF 79

2.4.1 Mass Spectrometer 79
2.4.2 MALDI Target Cleaning Procedure 80
2.4.3 Data and Acquisition 80
2.4.4 Statistical Analysis 81
2.5 Ghrelin Analysis by ESI-MS/MS 81
2.5.1 Positive Ion Nano Spray Settings 82
2.6 Ghrelin Analysis by LC-MS/MS 82
2.6.1 ESI Source with Orbitrap Conditions 83
2.6.2 Data and Acquisitions 83
2.7 BAMS 83
2.7.1 BAMS Optimisation for Reference Kit 83
2.7.1.1 BAMS Single Bead Immunocapture for Reference Kit 83
2.7.1.2 BAMS Single Bead Immunocapture for Ghrelin 83
2.7.1.3 Reaction Beads Arrayed 84
2.7.1.4 Eluting Analytes from Bead Arrays through MALDI Matrix Sprayer 85
3. Development of a Routine Method Protocol for the Analysis of Ghrelin using MALDI-TOF 86
3.1 Introduction 87
3.1.1 MALDI Matrix Selection 87
3.1.2 MALDI Matrix Application 88
3.1.3 Ghrelin Extraction from Biological Samples 89
3.1.3.1 Stabilisation of Ghrelin During Blood Collection 89
3.1.3.2 Internal Standard 91
3.1.3.3 Protein Precipitation 91
3.1.3.4 SPE 92
3.1.2 Aims 94
3.2 Materials and Methods 94

3.2.1 Protein Precipitation 94
3.2.2 Preparation of Matrix Surfaces 95
3.2.3 Solid Phase Extraction 95
3.2.3.1 Microelution Plate SPE 95
3.2.4 Centrifugal Filter Device 96
3.2.5 C18 Ziptips 97
3.2.6 Sample Preparation for MS Analysis 97
3.3 Results 98
3.3.1 Effect of the Seed Crystal on the Surface of the Matrix 98
3.3.2 Matrix Choice and Longevity 101
3.3.3 Quantification by MALDI-TOF 104
3.3.4 Optimization of Ghrelin Extraction from Plasma 109
3.3.4.1 Protein Precipitation 109
3.3.4.2 Protein Precipitation and the Use of C18 Ziptips 112
3.3.4.3 Inclusion of SPE in the Ghrelin Extraction Protocol 114
3.3.5 Non-Specific Binding of Ghrelin 125
3.3.5.1 Investigating the Use of Bovine Serum Albumin to Prevent Non-Specific Binding 125
3.3.5.2 Investigating the Potential Binding of Ghrelin on the MALDI Target Plate 128
3.3.6 Concentrating Ghrelin in Samples 130
3.3.6.1 Drying Samples 130
3.3.6.2 Microelution Plate 132
3.3.6.3 Testing the Use of Ammonium Hydroxide 135
3.3.7 Contamination 136
3.4 Discussion 142
3.5 Conclusion 145
4. Developing a Protocol to Analyse Ghrelin Using LC-MS/MS 146

4.1 Introduction 147
4.1.1 Aims 151
4.2 Materials and Methods 152
4.2.1 Preparation of Human and Rat Ghrelin Standards for LC-MS/MS Analysis 152
4.2.2 ESI LC-MS/MS 152
4.2.3 Liquid Chromatography-Tandem Mass Spectrometry 152
4.3 Results 155
4.3.1 Initial Method Development 155
4.3.2 Exploring Appropriate Diluent for Ghrelin Peptide 161
4.3.3 Alteration of Initial Sample Volume 163
4.3.4 Charge State Optimisation Following the Inclusion of Different Additives in the Mobile Phase During LC-MS/MS Analysis 165
4.3.4.1 Exploring the Use of Acids or Salts Within the Mobile Phase 167
4.3.4.2 Exploring the Inclusion of DMSO in Mobile Phase 172
4.3.5 Trypsin Digestion of Ghrelin Prior to MS Analysis 183
4.4 Discussion 197
4.5 Conclusion 202
5. Developing a BAMS Assay to Analyse Ghrelin 203
5.1 Introduction 204
5.1.1 Aims 206
5.2 Materials and Methods 207
An in-depth description of the material and methods for the BAMS assay are provided in Chapter 2.7. 207
5.2.1 Sample Preparation 207
5.2.2 Preparation of the BAMS Beads and their Addition to Samples 207
5.2.3 Washing Ghrelin Bound Beads 207
5.2.4 BAMS Array Assembly 208

5.2.5 Eluting Ghrelin from BAMS Reagent Beads 208
5.2.6 Data Collection of Ghrelin BAMS 209
5.2.7 Analysing BAMS MS Data 210
5.2.8 Collection of Plasma Samples 210
5.3 Results 210
5.3.1 HDX Sprayer Optimisation 210
5.3.2 Comparison and Selection of Antibody Kits 214
5.3.2.1 The Use of Rat Ghrelin as an Internal Standard to Quantify Human Ghrelin 214
5.3.3 Limit of Detection of the BAMS Assay 218
5.3.4 Performance Tests of BAMS Antibody Assays 220
5.3.4.1 Spiked Plasma Analysis 220
5.3.4.2 Neat Plasma Results 228
5.3.5 Comparison Between the Ghrelin BAMS and ELISA 235
5.3.5.1 Reproducibility of ELISA 235
5.3.5.2 Comparison of the Reproducibility of ELISA and BAMS Using Plasma from the Same Donors 238
5.3.6 Plasma Volume Reduction 241
5.4 Discussion and Conclusion 242
6. General Discussion 250
6.1 Conclusions and Discussion 251
6.2 Limitations of Body Fluid-Based Biomarkers 258
6.3 Limitations of the Work 262
6.4 Future Directions 264
6.5 Translating Ghrelin Detection to Clinical Application: Future Prospects for Biomarker Screening 266
Appendix A: Supplementary Figure and Tables. 270
References 281

Abstract

Approximately 50 million people worldwide suffer from dementia, which is characterised by memory loss and a decline in the ability to perform everyday activities. Currently, blood-based biomarkers for diagnosing neurodegenerative disorders are limited. The ‘hunger hormone’ ghrelin has previously been linked to the mediation of beneficial effects of calorie restriction on the protection of nerve cells in dementia models. Ghrelin exists in various forms, including acyl ghrelin (AG) and unacylated ghrelin (UAG). Acyl ghrelin has been shown to stimulate neurogenesis, while unacylated ghrelin inhibits the process. We have previously shown that the blood plasma AG:UAG ratio is reduced in Parkinson's disease dementia (PDD) and thus may be a potential biomarker of dementia. A major challenge is in accurately measuring these ghrelin peptides simultaneously in one assay. The main objective of this thesis is to develop a high-sensitivity mass spectrometry (MS) technique coupled with the ability to detect different species of endogenous ghrelin simultaneously from a single plasma sample. A matrix-assisted laser desorption/ionisation-time of flight (MALDI-TOF) method was developed first on exogenous human ghrelin standards, employing rat ghrelin as an internal standard (ISTD). Calibration curves for exogenous ghrelin were established with a correlation coefficient (R^2) value of 0.99 covering a range of 0.08-80 ng/mL of ghrelin, with endogenous ghrelin usually present at 0.32 ng/mL. A liquid chromatography-mass spectrometry (LC-MS) method was also developed; however, a detection limit was established at 0.4 ng/mL. Endogenous ghrelin was extracted from human plasma for quantification using MALDI-TOF. A range of traditional protein extraction techniques were used, such as protein precipitation followed by solid phase extraction (SPE), along with a novel approach termed bead-assisted mass spectrometry (BAMS). Initial results of this BAMS method showed greater capture of ghrelin compared to traditional SPE methods when extracting ghrelin. Additionally, compared to the enzyme-linked immunosorbent assay (ELISA), the reproducibility of the assay showed similar or better results than the reproducibility of the ELISA. The additional capability of BAMS to analyse multiple proteins from one plasma sample opens a new realm for not only ghrelin analysis but also additional blood-based biomarkers of disease.

Acknowledgements

I extend my heartfelt gratitude to my supervisors Dr. Jeff Davies, Dr. Alwena Morgan and Dr. Rob Angelini and everyone on the third and second floor for the support over the past few years.

Special appreciation goes to Dr. Ed Dudley, Dr. Nick Jones and Dr. James Cronin for the support over the past six years from undergraduate degree until now. You all truly helped encouraged my scientific career and gave me confidence to continue.

A profound thank you to Dr. Ann Hunter; it has been a privilege to work alongside you. Your mentorship has been invaluable, imparting knowledge and wisdom that have moulded me into the scientist I am today. I am deeply grateful for the laughter, camaraderie, and encouragement, especially when Mr LC was not giving the results I wanted.

I am immensely grateful to Kat for embarking on this extraordinary yet tumultuous journey together. Your companionship and shared experiences have provided much-needed solace. The memories of our coffee and croissant breaks with Ann will forever be cherished.

To my Mam, your unwavering belief in me since childhood has been my anchor. Thank you for nurturing my curiosity in science, from dissecting pig hearts to exploring blood under a microscope. To my sister, thank you for the stress-busting baking sessions and activities that helped me unwind. Heartfelt thank you to my brother and Shelby for the countless lifts and moments of levity amidst the challenges.

Thank you to George for sticking by me during the emotional rollercoaster of the PhD and for helping in any way possible. You have definitely made the experience more enjoyable with so many happy memories during such a stressful time.

I extend my gratitude to all my close family and friends who have stood by me with patience and understanding as I delved deeper into my PhD. Your unwavering support and belief in me have been a constant source of motivation.

Declaration

This work has not previously been accepted in substance for any degree and is not being concurrently submitted in candidature for any degree.

Signed: 

Date: 26/09/2025

STATEMENT 1

This thesis is the result of my own investigations, except where otherwise stated. Where correction services have been used, the extent and nature of the correction is marked in a footnote(s).

Other sources are acknowledged by footnotes giving explicit references. A bibliography is appended.

Signed: 

Date: 26/09/2025

STATEMENT 2

I hereby give consent for my thesis, if accepted, to be available for photocopying and for inter-library loans after the expiry of a bar on access approved by Swansea University.

Signed: 

Date: 26/09/2025

List of Figures

Figure 1.1 Formation of mature ghrelin. 32
Figure 1.2 Ghrelin-producing cells in the human stomach. 34
Figure 1.3 Ghrelin peptides crossing the blood-brain barrier..... 43
Figure 1.4 Challenges of measuring blood-based biomarkers for CNS disorders..... 64
Figure 2.1 Comparison of ghrelin standards from two suppliers – Phoenix and Tocris..... 77
Figure 2.2 Comparison of hUAG supplied by Cambridge Bioscience and Tocris..... 78
Figure 2.3 Assembling chambered slides for arraying beads..... 85
Figure 3.1 SPE steps. 93
Figure 3.2 Centrifugal filter device for 3kDa (A) and 10kDa (B). 96
Figure 3.3 Effect of seed crystal layer on matrix surface characteristics. 99
Figure 3.4 MALDI-TOF spectra were obtained of the four ghrelin species in the reflectron ion positive mode and in the m/z range 1000-5000..... 100
Figure 3.5 Comparison of the intensities of hUAG and hAG after preparation in different percentages of acetonitrile. 102
Figure 3.6 Longevity of the CHCA matrix. HAG and hUAG standards were prepared with CHCA at different time points..... 103
Figure 3.7 Calibration curves for rat ghrelin analysed by MALDI-TOF in the range of 0.08–80 ng/mL, using an internal standard (ISTD) concentration of 51 ng/mL. 104
Figure 3.8 Calibration curve of rUAG as ISTD at 51 ng/mL and rAG varying from 0.08-80 ng/mL was analysed using linear mode on the MALDI-TOF. 105
Figure 3.9. Calibration curves for the quantification of rat ghrelin species in the range of 0.08-2 ng/mL. 107
Figure 3.10: Human ghrelin standard calibration curve, hAG varying concentration between 0.08-2 ng/mL with hUAG placed as an ISTD (0.65 ng/mL). 108
Figure 3.11 The comparison of protein precipitation methods utilised for sample preparation before analysis by MALDI-TOF. 111
Figure 3.12 Comparison of the effect of using C18 ziptips on ghrelin detection following ghrelin extraction using either the Eslami et al. Rauh et al. or Sidibe et al. methods. 113

Figure 3.13 Detection of ghrelin following Protein Precipitation, SPE, and the use of C18 ziptips. 116
Figure 3.14 Comparison of 3kDa or 10kDa centrifugal filters following either the Eslami et al. or Sidibe et al. protein precipitation methods and SPE compared against without the use of centrifugal filters. 118
Figure 3.15 Comparison of C18 columns versus HLB columns following protein precipitation (Sidibe et al. method) in the extraction of rAG and rUAG 'spiked' into human plasma. 119
Figure 3.16 The impact of C18 ziptips on ghrelin retention following protein precipitation using the Sidibe method and HLB columns. 120
Figure 3.17 Comparison of ghrelin detection following HLB SPE and the use of 10Kda filters. Plasma 'spiked' with 10 ng/mL ghrelin underwent protein precipitation (Sidibe et al. method). 121
Figure 3.18 Comparing the effect of drying down the sample to concentrate. 122
Figure 3.19 Ghrelin capture from the 10kDa centrifugal filter device and flow-through. 123
Figure 3.20: Representation of ghrelin loss during the C18 ziptips protocol. 124
Figure 3.21 Calibration curve of rat ghrelin without (A) and with (B) the presence of 0.1% BSA. 126
Figure 3.22 Assessing the effect of BSA on ghrelin recovery after extraction. 127
Figure 3.23 The recovery of ghrelin following extraction in the presence or absence of BSA during both the SPE and SV steps. 128
Figure 3.24 Presence of ghrelin contamination. 129
Figure 3.25 Assessment of potential source of ghrelin contamination. 130
Figure 3.26 Effect of drying down under SV with different initial volumes and resuspending in solutions containing a different percentage of acetonitrile. 132
Figure 3.27 The analysis of ghrelin levels in continual elution followed by a wash step in either the MAX column (A) or WCX column (B). 134
Figure 3.28 Analysis of ghrelin levels of elution step 1, with and without the addition of ziptips in either MAX or WCX columns. 135
Figure 3.29 Impact of 5% ammonium hydroxide (NH4OH) on the extraction of ghrelin species. 136
Figure 3.30 Representative of MALDI-TOF spectra from potential sources of contamination, m/z range 1000-5000 Th. 139

Figure 3.31 Testing the presence of PEG contamination after deep cleaning of the MALDI target. 140
Figure 3.32 Presence of contamination within an equimolar mixture of rat ghrelin. 141
Figure 4.1 Schematic of tandem mass spectrometry (MS/MS). 148
Figure 4.2 Tryptic digestion of ghrelin peptide leads to the generation of two products, fragments 1-11 retain the acyl motif if the original substrate is AG. 151
Figure 4.3 Gradient elution for the separation of ghrelin species using HPLC. 153
Figure 4.4 HPLC Gradients for the separation of ghrelin species during a 30 minute run. 154
Figure 4.5 NanoESI with FTMS of chosen ghrelin charge state followed by MS/MS in ITMS mode to identify product ions. 156
Figure 4.6 LC Chromatograms for the 40 minute run. 157
Figure 4.7 Calibration for hAG and hUAG ranged from 0.4-40 ng/mL. 158
Figure 4.8 Calibration curve of hUAG and hAG ranging from 0.08-8 ng/mL. 159
Figure 4.9 Spectra from ghrelin in a 14 minute run versus a 40 minute run analysed by LC-MS/MS. 160
Figure 4.10 Comparison of using water and different percentages of acetonitrile during sample preparation on the peak area of ghrelin species. 162
Figure 4.12 Comparison of altering the injection volume from 1 µL to 2.5 µL on the peak area of ghrelin species following LC-MS/MS analysis. 164
Figure 4.13 Calibration curve of ghrelin species using an injection volume of 2.5 µL. 165
Figure 4.14 40 minute (A and B) versus 30 minute (C and D) LC-MS/MS run. 166
Figure 4.15 Comparison of acetic acid or formic acid on the peak area of ghrelin species $[M+5H]^{5+}$ (20 ng/mL) following LC-MS/MS analysis. 167
Figure 4.16 The distribution of different charged state ions of ghrelin ions after including either FA or AA in the mobile phase. 168
Figure 4.17 The distribution of different charged states ions of ghrelin when analysed by LC-MS using either FA or AA in the mobile phase. 170
Figure 4.18 Comparison of different combinations of acids and/or salts in the mobile phase on peak areas of the ghrelin species $[M+5H]^{5+}$ (20 ng/mL) following LC-MS/MS analysis. 171

Figure 4.19 The distribution of charged states of ghrelin ions when analysed by LC-MS, following the use of mobile phase with or without the inclusion of DMSO..... 173
Figure 4.20 Comparison of the inclusion of DMSO within the mobile phase on the peak areas of the ghrelin species $[M+5H]^{5+}$ (20 and 80 ng/mL) following LC-MS/MS analysis..... 174
Figure 4.21 Example of PEG contamination during LC-MS/MS analysis of ghrelin (20 ng/mL). 174
Figure 4.22 Presence of PEG during LC-MS/MS analysis of ghrelin (20 ng/mL). .. 175
Figure 4.23 MS and MS/MS spectra of the $[M+6H]6^{+}$and $[M+5H]^{5+}$ charged state ion..... 176
Figure 4.24 Comparison of peak areas of ghrelin after analysis using LC-MS/MS parameters monitoring the $[M+6H]^{6+}$ and $[M+5H]^{5+}$ charged states of ghrelin (analysed at 20 ng/mL) (no inclusion of DMSO)..... 179
Figure 4.25 The distribution of different charged states of ghrelin ions when analysed by LC-MS, following the use of mobile phase with or without the inclusion of DMSO..... 180
Figure 4.26 Assessing the effect of DMSO on ghrelin peak area 180
Figure 4.27 Calibration curve of hUAG, hAG, rUAG, and rAG ranging from 0.4-40 ng/mL..... 182
Figure 4.28 MS and MS/MS spectra of the trypsin digested product..... 184
Figure 4.29 Comparison of 1:20 or 1:100 (w/w) of trypsin to ghrelin on peak areas of ghrelin ($[M+2H]^{2+}$ charged stated) following LC-MS/MS analysis..... 186
Figure 4.30 MS Chromatograms and spectra of acyl ghrelin samples following digestion with trypsin suggest the presence of unacylated ghrelin at 8.6 or 8.7 minutes..... 187
Figure 4.31 Comparison of trypsin digested ghrelin peptides (1:20) analysed immediately or after 24 hours storage at 4°C..... 188
Figure 4.32 MS Chromatograms and spectra of intact ghrelin after being stored for 24 hours at 4°C. 189
Figure 4.33 Comparison of the peak areas of intact ghrelin analysed after immediate preparation (time 0) and after 24 hours of storage at 4°C. 189
Figure 4.34 LC-MS chromatograms for human and rat ghrelin after being stored for 24 hours at 4°C - with and without trypsin digestion..... 191

Figure 4.35 The presence of UAG within AG samples treated with and without trypsin was analysed at 0 and 24 hours post storage at 4˚C. 192
Figure 4.36 Comparison of alternating the trypsin digestion protocol; the original method was altered to include either a 1-hour trypsin incubation step or the use of freezing to quench the reaction. 193
Figure 4.37 Comparison of different loop volumes on the peak areas of unacylated tryptic ghrelin, 20 ng of ghrelin was injected onto the HPLC column in either 1 µL, 10 µL, 20 µL (partial), or 20 µL (full) starting injection volume. 194
Figure 4.38 Calibration curve of hUAG, hAG, rUAG, and rAG ranging from 0.4-40 ng/mL post-treatment with trypsin for 1 hour. 195
Figure 4.39 Calibration of human AG and UAG, using rat AG and UAG as internal standards, following digestion with trypsin. 196
Figure 5.1 BAMS microwell array slide that contains a gold-coated microscope slide attached to a silicone gasket. 205
Figure 5.2 Optimization of HDX sprayer conditions. 212
Figure 5.3 Visualisation of the BAMS array during MALDI-TOF analysis. 213
Figure 5.4 BAMS spectra of the protein reference. 213
Figure 5.5 Detection of human and rat ghrelin using BAMS-antibody 86. 216
Figure 5.6 MALDI-TOF analysis of an equimolar mixture of the exogenous human and rat ghrelin species. 217
Figure 5.7 Detection of human acyl and unacylated ghrelin and rat unacylated ghrelin using BAMS antibody 88. 218
Figure 5.8 Standard curve from 0.02-10 ng/mL to establish limits of detection of both human acyl and unacylated ghrelin using either antibody 86 or antibody 88. 219
Figure 5.9 Assessing the limit of detection via a standard curve with hUAG varying from 0.2-10 ng/mL and hAG as an ISTD at 2.5 pg/mL. 220
Figure 5.10 Comparison of antibody 86 versus antibody 88 from five different donors with ‘spiked’ plasma. 221
Figure 5.11 Schematic demonstrating three ghrelin antibody-coated beads after incubation in donor plasma subjected to MADLI-TOF analysis, producing an intensity ratio of AG:UAG for each bead. 222
Figure 5.12 Intra-assay variability shows the reproducibility between antibody-coated beads to quantify ghrelin levels in the same donor ‘spiked’ plasma sample. 223

Figure 5.13 Inter-assay variability. Reproducibility across independent assay runs of the same donor's spiked plasma from a single withdrawal..... 225
Figure 5.14 Comparison of mean intra-assay CV% and inter-assay CV% for each donor.. 227
Figure 5.15 Comparison of antibody 86 versus antibody 88 for the analysis of AG:UAG intensity in 'neat' plasma samples from three different donors. 228
Figure 5.16 Intra-assay variability..... 230
Figure 5.17 Inter-assay variability. 232
Figure 5.18 Comparison of mean intra-assay CV% and inter-assay CV% for each donor. 234
Figure 5.19 Intra-assay variability comparison ELISA and BAMS methods 236
Figure 5.20 Inter-assay variability comparison ELISA and BAMS methods. 238
Figure 5.21 Comparison of intra-assay %CV across different detection platforms (ELISA, BAMS using Antibody 86 spiked, and BAMS using Antibody 88 spiked) for five individual donors..... 239
Figure 5.22 Intra-Assay variability comparsion across ELISA and BAMS methods. Intra-assay variability comparison across ELISA and BAMS methods..... 240
Figure 5.23 Comparison of detection of ghrelin using different initial plasma volumes.. 242

List of Tables

Table 1.1 Ghrelin amino acid sequence with different vertebrates..... 30
Table 1.2 Summary Table: MS Platforms Used. 71
Table 2.1 Equipment and product codes..... 74
Table 2.2 Reagents and solvents alongside product codes. 75
Table 2.3 Suppliers for ghrelin standards..... 76
Table 4.1 M/Z values of ghrelin's charge state ions during protonation..... 149
Table 4.2 Peptide sequence and basic mass spectrometer parameters. 157
Table 4.3 New 8 MS/MS MRM transitions to monitor rat and human ghrelin species either focusing on $[M+5H]^{5+}$ or $[M+6H]^{6+}$charged state ion..... 177
Table 4.4 New 4 LC-MS/MS MRM transitions to monitor rat and human ghrelin species focusing on $[M+2H]^{2+}$ charged state following digestion using Trypsin. 185
Table 6.1 Comparative summary of ghrelin detection evaluated in this thesis. 254

List of Abbreviations

Aβ- amyloid beta.

AEBSF - 4-(2-aminoethyl) benzene sulfonyl fluoride hydrochloride.

AD- Alzheimer's disease.

AG – acyl ghrelin.

AHN – adult hippocampal neurogenesis.

AMPK - adenosine monophosphate-activated protein kinase.

AUC – area under the curve.

BAMS – bead-assisted mass spectrometry.

BBB – blood-brain barrier.

CHCA - α-ciano-4-hydroxycinnamic acid.

CI – chemical ionisation.

CID - collision-induced dissociation.

CNS – central nervous system.

GPCR - G-protein-coupled receptor.

CR- calorie restriction.

CSF – cerebrospinal fluid.

Da – daltons.

DC – direct current.

DG – dentate gyrus.

DI – deionised water.

DMSO – Dimethyl sulfoxide.

EDTA - ethylene diamine tetra-acetic acid-aprotinin.

ELISA – enzyme-linked immunosorbent assay.

ER – endoplasmic reticulum.

ESI – electrospray ionization.

FT – fourier transform.

GFAP – glial fibrillary acidic protein

GH – growth hormone.

GHS-R1a - growth hormone secretagogue receptor-1a.

GHRL - ghrelin and obestatin prepropeptide.

GOAT - ghrelin-o-acyltransferase.

HCL – hydrochloric acid.

HLB - hydrophilic-Lipophilic Balance.

hAG – human acyl ghrelin.

hUAG – human unacylated ghrelin.

IP-MS – immunoprecipitation mass spectrometry.

ISTD – internal standard.

ITMS – linear ion trap.

LC-MS - liquid chromatography-mass spectrometry.

MALDI – matrix-assisted laser desorption/ionization.

MCI – mild cognitive impairment.

MS – mass spectrometry.

MS/MS – tandem mass spectrometry.

M/Z – mass-to-charge ratio.

NfL - neurofilament light chain.

NMR – nuclear magnetic resonance.

PBS - phosphate Buffered Saline.

PET – positron emission tomography.

PD - Parkinson’s disease.

PDD- Parkinson’s disease dementia.

pTau – phosphorylated tau.

ROC - receiver operating characteristic.

rAG – rat acyl ghrelin.

RF – radio frequency.

rUAG – rat unacylated ghrelin.

SPE – solid phase extraction.

TFA - trifluoroacetic acid.

Th – thomson.

TOF – time-of-flight.

tTau – total tau.

UAG – unacylated ghrelin.

WT – wild type.

SGZ – subgranular zone.

88 – antibody 88.

86 – antibody 86.

Chapter

1. Introduction

1.1 Introduction to Biomarkers in Biomedical Research

1.1.1 Definition and Classification

Biomarkers are measurable indicators of biological states or processes and play a central role in both clinical and research settings. They are used to detect, characterise, and monitor diseases, as well as to guide and evaluate therapeutic interventions. Biomarkers can be molecular, histologic, radiographic, or physiologic in nature, though molecular biomarkers, particularly proteins and peptides, are among the most studied due to their accessibility and disease-specific information (Strimbu & Tavel, 2010).

Biomarkers are broadly classified based on their clinical utility. Diagnostic biomarkers identify the presence of a disease, facilitating early and accurate detection. Prognostic biomarkers provide information about the likely disease trajectory independent of treatment. Predictive biomarkers anticipate the efficacy of specific therapies, supporting personalised treatment selection. Monitoring biomarkers are used to track the course of disease or the effects of therapy over time. Pharmacodynamic biomarkers offer insight into the biological response to a therapeutic agent. Surrogate biomarkers act as substitutes for clinical endpoints, especially in research and clinical trials, where direct measures of patient benefit may be impractical or time-consuming (FDA-NIH Biomarker Working Group, 2016).

1.1.2 Importance of Biochemical Context: Protein Structure, Function, and Post Translational Modifications

Biochemical context is a critical dimension in biomarker development, particularly when proteins and peptides are the focus. A protein’s structure, including its primary amino acid sequence, folding dynamics, and interaction domains, govern its biological role and potential as a biomarker. Beyond structure and abundance, the post-translational modifications (PTMs) of proteins, such as phosphorylation, glycosylation, ubiquitination, and lipidation, introduce further complexity and biological specificity (Mann & Jensen, 2003).

These modifications are often dynamic and tissue-specific, reflecting the real-time physiological or biochemical state of cells and their microenvironments. PTMs can modulate protein stability, activity, localisation, and interactions, making them

particularly relevant in disease contexts where signalling pathways and metabolic processes are dysregulated (Walsh et al., 2005). The lipidation of peptides, for example, can affect receptor binding, bioavailability, and metabolic clearance. The acylation of ghrelin by octanoic acid was the first demonstration that lipidation could regulate peptide hormone function, making it a compelling example of how PTMs can alter bioactivity and biomarker relevance (Kojima et al., 1999).

This field remains underexplored, particularly in relation to neurodegenerative diseases, where changes in PTM patterns may represent early indicators of disease pathogenesis and progression.

1.1.3 Role of Biomarkers in Precision Medicine and Neurodegenerative Disease Research

In recent years, biomarkers have become indispensable to the advancement of precision medicine, which aims to tailor healthcare based on individual biological profiles. Neurodegenerative diseases, including Alzheimer's disease (AD), Parkinson's disease (PD), and frontotemporal dementia (FTLD), are particularly complex and heterogeneous, with varying aetiologies and progression patterns (De Strooper & Karran, 2016). As such, traditional diagnostic approaches are often insufficient, and there remains a significant unmet need for biomarkers that can stratify disease subtypes, identify early pathological changes, and guide personalised treatment strategies.

Given the high prevalence and diagnostic complexity of conditions such as AD and PD, there is a growing demand for biomarkers that can stratify subtypes, enable early detection, and be applied in large-scale screening with minimal invasiveness (Hampel et al., 2018). A blood-based prognostic biomarker of dementia, for instance, would significantly enhance clinical trial efficiency and therapeutic targeting by offering a non-invasive, cost-effective, and scalable alternative to neuroimaging or cerebrospinal fluid (CSF) analysis.

Biomarkers also provide a window into systemic factors that influence brain health, including metabolic dysregulation, hormonal signalling, and inflammatory responses. In this context, peptide hormones with neuroactive properties, such as ghrelin, have emerged as promising candidates for biomarker development, particularly given their dual roles in central nervous system function and peripheral metabolism.

1.1.4 Requirements for a Viable Biomarker

For a biomarker to be considered clinically useful, it must meet several stringent criteria. Specificity is essential, ensuring that the biomarker reliably distinguishes between health and disease, or between different disease states. Sensitivity is equally important, allowing for the detection of subtle or early pathological changes that might not yet be clinically apparent. These characteristics are particularly crucial in neurodegenerative diseases, where early intervention may alter disease trajectories (Frank & Hargreaves, 2003).

In addition to diagnostic performance, a viable biomarker must exhibit biological relevance, meaning it should be functionally or mechanistically linked to the disease process. This relevance not only enhances its validity but also increases the likelihood of consistent behaviour across patient cohorts. Finally, technical feasibility is paramount. The biomarker should be accessible in clinically obtainable samples, such as blood or CSF, and measurable through reliable, scalable, and cost-effective analytical techniques (Mayeux, 2004).

Biomarker development is further complicated by the physicochemical complexity of blood, which contains proteins, lipids, and interfering antibodies that may degrade or mask target analytes, especially when present in low abundance. For example, heterophilic antibodies in blood can produce misleading results, and proteolytic degradation of low-abundance biomarkers may impair quantification (Hampel et al., 2018). These factors necessitate the use of advanced analytical platforms, such as mass spectrometry, which can improve specificity, reduce interference, and enhance detection of post-translationally modified peptides (Domon & Aebersold, 2006).

These foundational principles provide a framework for evaluating candidate biomarkers. In the sections that follow, the discussion will focus on the neuroendocrine peptide ghrelin, its structural diversity, post-translational lipidation, and the challenges associated with developing ghrelin isoforms into clinically useful biomarkers for neurodegenerative disease.

1.2 Neurodegenerative Disease Landscape

Neurodegenerative diseases are a heterogeneous group of progressive and debilitating conditions characterised by the gradual deterioration of neuronal structure and function. Among the most prevalent are AD, PD, FTLD, and amyotrophic lateral sclerosis (ALS). These disorders are the primary causes of dementia globally, with AD alone accounting for approximately 60 to 70 percent of cases (World Health Organization [WHO], 2021).

Despite differences in their clinical presentation, major neurodegenerative diseases share several pathological hallmarks, including synaptic loss, protein misfolding and aggregation, mitochondrial dysfunction, and chronic neuroinflammation. For instance, AD is characterised by extracellular amyloid-beta (Aβ) plaques and intracellular neurofibrillary tangles composed of hyperphosphorylated tau. PD is marked by the degeneration of dopaminergic neurons in the substantia nigra and the presence of Lewy bodies, which are primarily composed of α-synuclein. These aggregated proteins disrupt cellular homeostasis, while activated glial cells perpetuate an inflammatory cascade that exacerbates neuronal damage (Heneka, Golenbock, & Latz, 2015).

In the healthy brain, neuronal maintenance is sustained through a dynamic balance between neurogenesis and neurodegeneration. This equilibrium supports synaptic plasticity and cognitive function, particularly in brain regions such as the hippocampus and cortex, which are among the earliest affected in AD and other dementias. The breakdown of this balance is associated with oxidative stress, impaired proteostasis, reduced neurotrophic support, and mitochondrial dysfunction (Mattson & Arumugam, 2018). Several molecular pathways underlie neuronal resilience, including neurotrophic signalling, mitochondrial quality control, and protein degradation systems such as the ubiquitin–proteasome and autophagy–lysosome pathways.

Recently, increasing attention has been paid to the role of lipid biology and protein acylation in maintaining neural homeostasis. The brain is a lipid-rich organ, with over 50 percent of its dry weight comprising lipids such as glycerophospholipids, sphingolipids, and cholesterol. These molecules are fundamental to the integrity of cellular membranes and are also key regulators of energy metabolism, synaptic transmission, and intracellular signalling. Disruptions in lipid metabolism, particularly within the lysosomal catabolism of sphingolipids and glycosphingolipids, have been

implicated in the pathogenesis of several neurodegenerative diseases (Wei, Wong, & Boland, 2024). For example, in FTD and PD, deficiencies in enzymes such as glucocerebrosidase lead to the accumulation of lipid intermediates like glucosylsphingosine (GlcSph) and gangliosides (Boer, van Smeden, Bouwstra, & Aerts, 2020). These lipid build-ups contribute to lysosomal dysfunction, inflammatory activation, and progressive neuronal loss.

In parallel, protein acylation has emerged as a critical post-translational modification with wide-ranging effects in the nervous system. Acylation involves the covalent attachment of fatty acid chains, including myristoyl, palmitoyl, or octanoyl groups, to proteins. This process regulates protein localisation, trafficking, membrane association, and stability. One notable example is the acylation of ghrelin, a peptide hormone that must be octanoylated to bind its receptor and exert neuroprotective functions. These include anti-inflammatory, anti-apoptotic, and metabolic effects (Young & Jialal, 2023). The bioactivity of acylated proteins such as ghrelin underscores the complex interplay between lipid metabolism and protein signalling in the brain.

Disruptions in protein acylation have been increasingly associated with neurodegenerative mechanisms. For instance, impaired palmitoylation of synaptic proteins can affect their trafficking and stability, contributing to the synaptic deficits commonly observed in AD models (Peng, Liang, & Zhang, 2024). Furthermore, acylation influences interactions with lipid rafts, which are specialised membrane domains involved in signal transduction (Yurtsever & Lorent, 2020). Lipid dysregulation can therefore indirectly impact protein function by altering membrane composition and dynamics.

Together, lipid metabolism and protein acylation are integral to the regulation of the neurogenesis–neurodegeneration balance. Lipid disturbances can lead to membrane instability and inflammation, while altered acylation patterns can disrupt cellular signalling and protein turnover. Understanding the intersection between these processes is vital for advancing our comprehension of neurodegenerative disease mechanisms.

From a clinical perspective, diagnosing neurodegenerative diseases remains challenging due to the lack of early and specific biomarkers. Symptoms are often nonspecific and overlapping, and substantial neuronal loss may occur before clinical

presentation. For example, approximately 25 percent of adults aged 75 years and older experience both AD and vascular dementia simultaneously (Ossenkoppele et al., 2015). This has led to growing interest in biomarker discovery across CSF, neuroimaging, and molecular profiling. Blood-based biomarkers, in particular, have received significant attention because of their minimally invasive nature, low cost, and feasibility for large-scale screening. Unlike CSF sampling, blood collection is more practical in both research and clinical settings and offers greater potential for longitudinal monitoring across diverse populations (Hampel et al., 2018).

In summary, neurodegenerative diseases result from multifactorial disturbances in cellular and molecular homeostasis. The convergence of lipid metabolism, protein modification, and neuroinflammatory processes reflects the complex pathology of these disorders. Investigating the roles of acylated proteins and lipid–protein interactions, particularly in the context of peptide hormones such as ghrelin, may yield novel insights and offer new avenues for early diagnosis and therapeutic intervention.

1.3 Systemic Factors Influencing Neurodegeneration

Systemic physiological factors, especially those related to metabolism, energy balance, and endocrine signalling, strongly modulate the brain's vulnerability to neurodegenerative diseases. Dietary patterns, caloric intake, and metabolic health influence neuronal plasticity, mitochondrial function, and neuroinflammation, all of which contribute to disease progression (Gomez-Pinilla, 2008). Peripheral hormones such as insulin, leptin, oestrogens, and glucocorticoids regulate neurogenesis, synaptic activity, and cognition; disruptions in their signalling (for example, in obesity or chronic stress) impair hippocampal plasticity and heighten neurodegenerative risk (Arnold et al., 2018).

A rapidly growing area highlights gut-derived hormones, particularly ghrelin, as key mediators of gut–brain communication. Ghrelin synthesised primarily by P/D1 cells in the human stomach and by their functional counterparts, X/A-like cells, in rodents, stimulates appetite via the growth hormone secretagogue receptor-1a (GHS-R1a) and also modulates neurogenesis, synaptic plasticity, and neuronal survival (Andrews et al., 2009; Bayliss et al., 2016). This activity depends on a specific octanoylation at serine-3 by ghrelin O-acyltransferase (GOAT), which is essential for receptor binding (Kojima et al., 1999; Yang et al., 2008). In Parkinson's disease dementia (PDD), a reduced acyl-to-unacylated ghrelin (AG:UAG) ratio correlates with impaired adult

hippocampal neurogenesis and cognitive decline (Hornsby et al., 2020; Song et al., 2017). Given ghrelin's bidirectional transport across the blood–brain barrier and potential for local reacylation (Banks et al., 2002; Murtuza & Isokawa, 2018), it exemplifies how systemic metabolic signals can influence central nervous system (CNS) resilience.

Together, these findings underscore the impact of systemic metabolic and hormonal factors on neurodegeneration and provide a rationale for investigating acylated peptides like ghrelin as mechanistic, blood-based biomarkers.

1.3.1 The Gut–Brain Axis in Neurodegeneration

The gut–brain axis comprises a multilayered communication network between the gastrointestinal (GI) tract and the CNS, integrating neural, endocrine, immune, and microbial signals (Carabotti et al., 2015). Afferent fibres of the vagus nerve relay information about gut luminal contents, barrier integrity, and inflammatory status directly to brainstem nuclei, while efferent vagal output modulates gut motility and immune function. Enteroendocrine cells in the epithelium secrete hormones (for example, cholecystokinin, GLP-1) that inform the CNS about nutrient availability (Gribble & Reimann, 2019).

Microbial metabolites, notably short-chain fatty acids (SCFAs), influence microglial activation and blood–brain barrier (BBB) integrity. Dysbiosis and increased intestinal permeability ('leaky gut') permit lipopolysaccharide (LPS) translocation, provoking systemic inflammation that exacerbates neuroinflammation (Sampson et al., 2016; Rieder et al., 2017). In PD, α-synuclein misfolding within enteric neurons can propagate retrogradely via vagal pathways to the dorsal motor nucleus, suggesting that gut-originating pathology may initiate or amplify central degeneration (Braak et al., 2003; Klingelhoefer & Reichmann, 2017). Thus, maintenance of gut barrier function, microbial homeostasis, and controlled immune signalling are critical systemic factors shaping neurodegenerative trajectories.

1.3.2 Ghrelin at the Intersection of the Gut–Brain Axis and Biomarker Research

Ghrelin epitomises the gut–brain axis, being released from gastric X/A-like cells in response to fasting and acting via both endocrine and neural pathways. Upon secretion, acyl ghrelin binds to GHS-R1a on vagal afferents, transmitting hunger and metabolic status to the nucleus tractus solitarius and hypothalamus (Date et al., 2002).

Circulating acyl ghrelin also traverses the BBB via a saturable transporter (Banks et al., 2002), enabling direct central effects on hippocampal and nigral neurons.

Within the CNS, acyl ghrelin engages GHS-R1a to activate intracellular cascades, phospholipase C (PLC), protein kinase C (PKC), and AMP-activated protein kinase (AMPK), that promote mitochondrial biogenesis, autophagy, and anti-inflammatory signalling (Andrews et al., 2009; Bayliss et al., 2016). These mechanisms counteract oxidative stress and support synaptic plasticity, thereby bolstering cognitive resilience. Unacylated ghrelin, unable to engage GHS-R1a, may modulate these pathways indirectly, perhaps by binding an as-yet-unidentified receptor or by competitive interference at the membrane level (Inhoff et al., 2008; Fernandez et al., 2016).

In PDD, GI dysfunction often precedes cognitive decline, and reductions in the AG:UAG correlate with impaired adult hippocampal neurogenesis and memory deficits (Hornsby et al., 2020; Song et al., 2017). Because ghrelin integrates gut-derived hormonal signals with central neuroprotective pathways, its plasma isoform levels may uniquely reflect both gut health and CNS integrity. Consequently, ghrelin's dual role in the gut–brain axis underpins its promise as a systemic biomarker for early detection and monitoring of neurodegenerative diseases.

1.4 Ghrelin Biology and Structural Diversity

1.4.1 Background of Ghrelin

Ghrelin was first discovered in 1999, as the endogenous ligand for GHS-R1a (Kojima et al., 1999). At the same time, the molecular mechanism of ghrelin action was revealed. Ghrelin activity relies on an important post-translational step, in which ghrelin is acylated (the attachment of a fatty acid) onto its third amino acid, a serine residue, generating acyl ghrelin. This acylation step is essential for growth hormone (GH) release activity that arises from acyl ghrelin binding to its cognate receptor, GHS-R1a (Kojima et al., 1999). The biological importance of this post-translational modification is underscored by the evolutionary conservation of serine at position 3 across vertebrate species (Table 1.1), suggesting strong selective pressure to preserve this specific acylation site due to its critical role in ghrelin's function (Kojima and Kangawa, 2005).

Mammalian	1 *	10	20	28
Human	GSSFLSPEHQRVQQRKESKKPPAKLQPR			
Mouse/Rat	GSSFLSPEHQKAQQRKESKKPPAKLQPR			
Dog	GSSFLSPEHQKLQQRKESKKPPAKLQPR			
Rhesus monkey	GSSFLSPEHQRAQQRKESKKPPAKLQPR			
Bovine	GSSFLSPEHQKLQ - RKEAKKPSGRLKPR			
Sheep	GSSFLSPEHQKLQ - RKEPKKPSGRLKPR			
Avian	1 *	10	20	26
Chicken	GSSFLSPTYKNIQQQKDTRKPTARLH			
Turkey	GSSFLSPAYKNIQQQKDTRKPTARLHPR			
Goose	GSSFLSPEFKKIQQQNDPAKATAKIH			
Fish	1 *	10	20	23
Rainbow trout	GSSFLSPSQKPQVROGKGK-PPRV-amide			
Goldfish	GTSFLSPAQKPQ—GRRPPRM-amide			
Zebrafish	GTSFLSPTQKPQ—GRRPPRV-amide			

Table 1.1 Ghrelin amino acid sequence with different vertebrates.

Mutation of the serine residue prevents the acylation of ghrelin by GOAT (Yang et al., 2008), unless the substitution is for threonine (Darling et al., 2015), which is consistent with the fact that threonine is present at this position in ghrelin from an alternative species, the Bullfrog (Kaiya et al., 2001). This highlights the functional flexibility of this acylation site, as both serine and threonine possess hydroxyl groups that can serve as acyl acceptors, enabling GOAT-mediated modification. However, replacing serine with non-hydroxylated residues abolishes acylation, rendering ghrelin inactive at the GHS-R1a receptor. This underscores the critical importance of the hydroxyl-bearing side chain for enabling the unique post-translational modification that defines ghrelin's endocrine function. Threonine differs from serine by having a methyl substituent in place of one of the hydrogens on the β carbon. The interchanging of threonine to serine and vice versa has long been reported, with Wan and Millner-White (1999) noting that two hydrogen bond motifs can incorporate either threonine or serine residues at the alpha-helical N-terminal. Furthermore, it has been reported that the

replacement of serine for threonine in archaeon proteasomes, Thermoplasma acidophilum (T1S mutant), does not alter the rate of proteasome hydrolysis (Seemiller et al., 1995), reinforcing the biochemical similarity between the two residues in some functional contexts. However, in ghrelin, this substitution is functionally relevant only when the acylation potential is preserved.

The acylation of ghrelin by a fatty acid, most commonly octanoic acid, was the first demonstration that peptide function can be modified by this type of post-translational modification. However, ghrelin is no longer unique in being modified in this way. For example, Wnt proteins (Willert et al., 2003; Takada et al., 2006; Coombs et al., 2010; Herr and Basler 2011; Janda et al., 2012; Nile & Hannoush 2016), Hedgehog proteins (Chamoun et al., 2001; Chen et al., 2004) and histocompatibility antigens (Schultz et al., 2018) can also be acylated by distinct fatty acids, which are reported to alter their signalling capabilities. However, ghrelin is unique in the identity and range of fatty acids that can bind to it (Hosoda et al., 2003; Gutierrez et al., 2008). Together, these studies suggest that there is an exciting and underexplored field of research into the effect of post-translational acyl modification on protein or peptide function.

1.4.2 Ghrelin formation

The ghrelin gene (GHRL) is located on human chromosome 3p25–26 and comprises five exons (Khatib, 2014). Its messenger RNA (mRNA) encodes a 117–amino-acid preproghrelin peptide, which undergoes proteolytic cleavage to yield a 94–amino-acid proghrelin intermediate. This is further processed, primarily by prohormone convertase 1/3, to generate the mature 28–amino-acid ghrelin peptide (Gahete et al., 2010; Villarreal et al., 2022) (Figure 1.1).

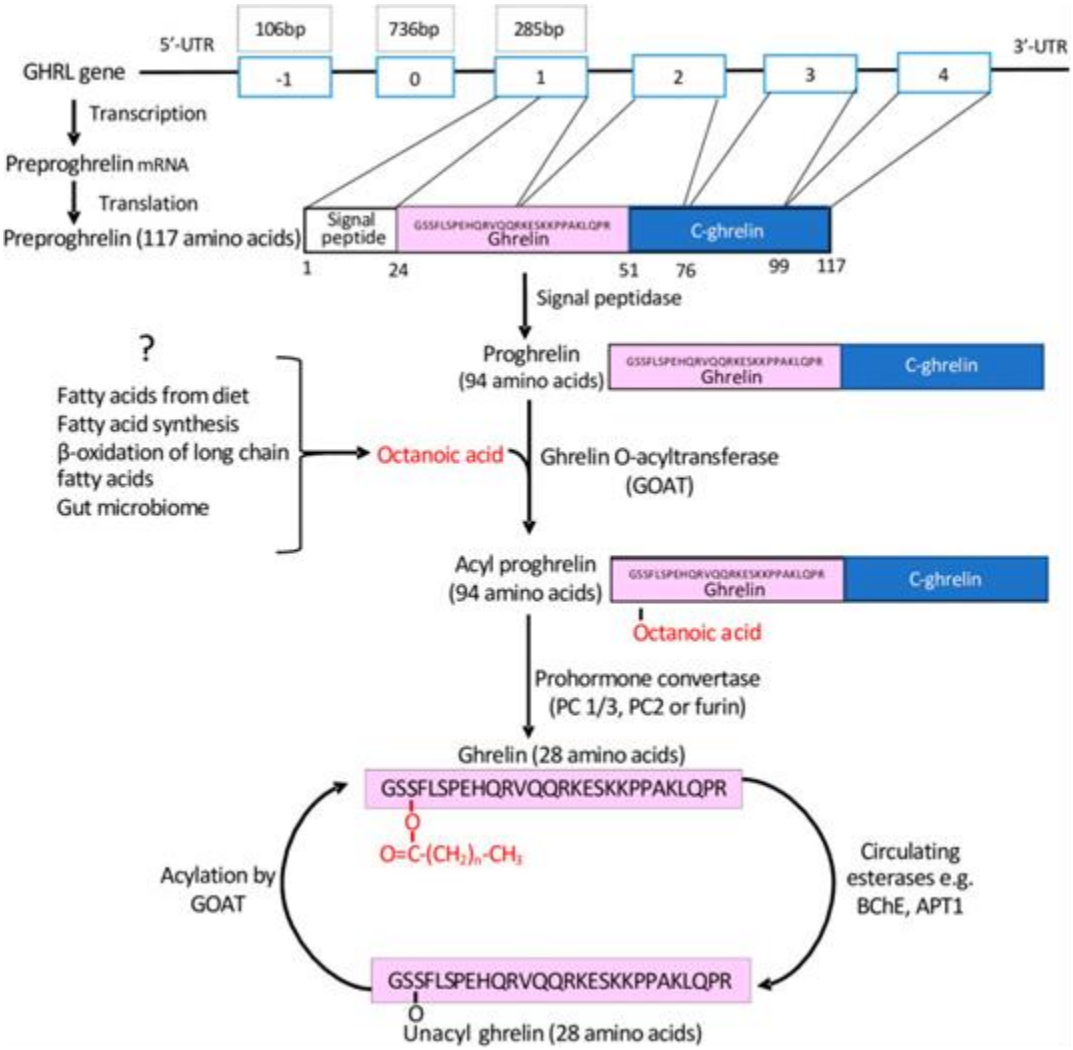

Figure 1.1 Formation of mature ghrelin.

A preproghrelin peptide (117 amino acids) is formed by a series of transcription and translation steps, followed by proteolytic cleavage, resulting in the proghrelin peptide (94 amino acids). Both proghrelin and mature ghrelin can undergo acylation by ghrelin GOAT and can be deacylated by a range of circulating esterases (Figure taken with permission from Thomas, A.S et al., 2022).

In this processing, a unique post-translational modification is introduced: an octanoyl (C8:0) fatty acid ester is attached to the serine at position 3 of ghrelin (Khatib, 2014; Thomas et al., 2022). This acylation step, catalysed by ghrelin GOAT, is essential for the peptide's ability to bind and activate GHS-R1a.

GOAT, encoded by the MBOAT4 gene and identified in 2008, is a membrane-bound enzyme with 11 transmembrane domains and two key catalytic residues (Asn307 and His338) (Gahete et al., 2010). It is highly expressed in the gastric mucosa, mirroring the distribution of ghrelin-expressing cells, but is also detectable in the hypothalamus, pituitary, and hippocampus (Villarreal et al., 2022). GOAT selectively acylates Ser3 of

ghrelin and preferentially utilises medium-chain fatty acids, particularly octanoyl-CoA (Gahete et al., 2010; Nishi et al., 2011). Dietary intake of medium-chain triglycerides (MCTs), especially those containing C8:0, significantly increases circulating octanoyl-ghrelin levels.

However, acyl ghrelin production is not strictly dependent on dietary lipids. Even in the absence of dietary fats, ghrelin-producing cells maintain acyl-ghrelin synthesis via mitochondrial β-oxidation of long-chain fatty acids (Sakata et al., 2018). Inhibition of this process with etomoxir decreases acyl ghrelin production, a deficit reversed by exogenous octanoate supplementation. In contrast, short-chain fatty acids from gut microbiota, such as acetate or butyrate, do not contribute to ghrelin acylation, and germ-free models show no change in acyl ghrelin levels (Sakata et al., 2018).

Ghrelin is synthesised predominantly by endocrine cells in the oxyntic mucosa of the stomach, specifically by P/D1 cells in humans and X/A-like cells in rodents, located mainly in the gastric fundus (Figure 1.2) (Khatib, 2014; Thomas et al., 2022). These closed-type cells release ghrelin into the bloodstream, facilitating systemic endocrine signalling. Although ghrelin is also produced in the pancreas, intestine, heart, and brain, the stomach remains the principal source of circulating ghrelin (Khatib, 2014; Villarreal et al., 2022). The majority of plasma ghrelin exists in its unacylated form, while acyl ghrelin circulates at lower concentrations.

In the brain, ghrelin acts through GHS-R1a, a G-protein–coupled receptor predominantly expressed in the hypothalamus (for example, arcuate nucleus), hippocampus, and other regions implicated in metabolism and cognition (Chen et al., 2016; Khatib, 2014). Only the acyl form binds with high affinity and activates this receptor. Unacylated ghrelin, while more abundant and capable of crossing the BBB more readily, does not bind GHS-R1a (Rhea et al., 2018). Nonetheless, unacylated ghrelin may exert GHS-R1a-independent effects on the brain.

Transport of ghrelin across the BBB occurs via carrier-mediated mechanisms and does not require GHS-R1a (Rhea et al., 2018). Acyl ghrelin is taken up into specific regions, such as the olfactory bulb, hypothalamus, and hippocampus. Areas associated with appetite, learning, and reward behaviours. This highlights the importance of ghrelin acylation in facilitating central nervous system signalling.

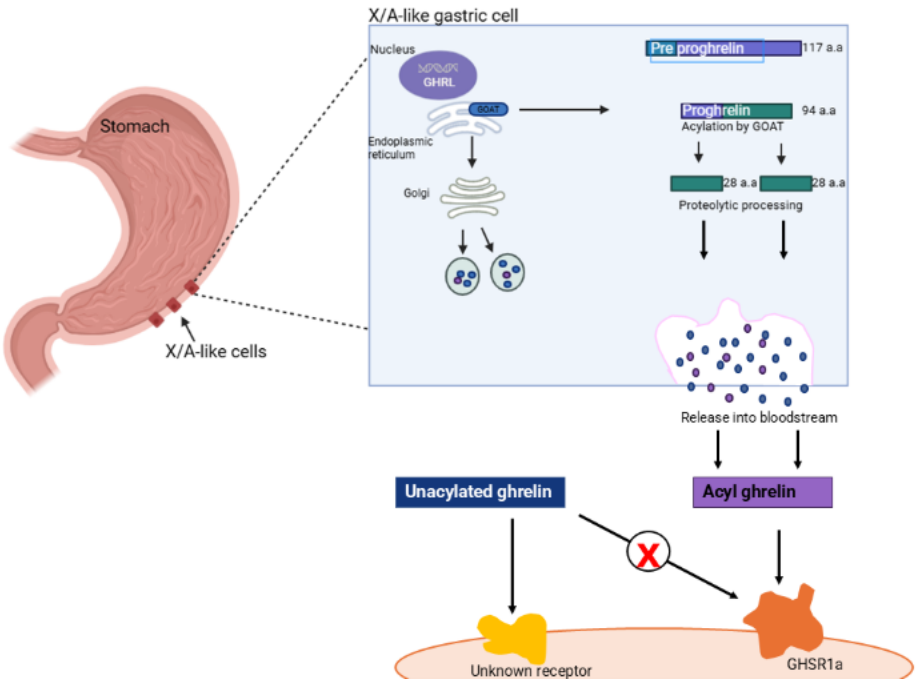

Figure 1.2 Ghrelin-producing cells in the human stomach.

Ghrelin is predominantly synthesised by endocrine P/D1 cells located in the oxyntic mucosa of the gastric fundus. These closed-type cells release ghrelin into the circulation, enabling systemic endocrine signalling. While ghrelin is also expressed in the pancreas, intestine, heart, and brain, the stomach is the primary source of circulating ghrelin. In plasma, unacylated ghrelin is the major isoform, with acyl ghrelin present at lower concentrations (Khatib, 2014; Thomas et al., 2022; Villarreal et al., 2022).

Once secreted, acyl ghrelin is rapidly deacylated in the circulation, modulating its bioactivity. Butyrylcholinesterase (BChE) hydrolyses the octanoyl group, rendering ghrelin inactive (Chen et al., 2016). Overexpression of BChE markedly lowers circulating acyl ghrelin levels. Acyl protein thioesterase 1 (APT1), secreted by immune cells during inflammation, also contributes to ghrelin deacylation and further explains the dominance of unacylated ghrelin in circulation (Satou et al., 2010).

GOAT activity and ghrelin acylation are tightly regulated by metabolic, nutritional, and hormonal cues. Fasting increases plasma ghrelin and GOAT expression, whereas feeding reverses this effect (Gahete et al., 2010). Hormones such as insulin and somatostatin downregulate GOAT, while leptin and ghrelin itself enhance its expression. In obesity, ghrelin levels are typically reduced, although GOAT expression may remain elevated, possibly as a compensatory mechanism (Gahete et al., 2010). GOAT is also sensitive to dietary fat composition, with MCT intake upregulating its expression and MCFA deprivation reducing it (Nishi et al., 2011). Inflammatory stimuli

such as lipopolysaccharide (LPS) also modulate GOAT indirectly by inducing APT1 expression (Satou et al., 2010).

Finally, the proghrelin precursor also gives rise to obestatin, a 23–amino-acid peptide derived from its C-terminal region (Cowan et al., 2016). Obestatin requires C-terminal amidation and was originally proposed to antagonise ghrelin's orexigenic effects, although its physiological relevance remains controversial. Its production represents a parallel post-translational pathway that reduces the availability of proghrelin for ghrelin synthesis, potentially modulating overall hormonal balance.

1.4.3 Factors Impacting Ghrelin Levels

1.4.3.1 Proteins Impact on Ghrelin Expression

Ghrelin secretion is primarily regulated by nutritional status, with circulating levels rising during fasting and declining postprandially as a result of gastric distension (Cummings et al., 2001). The macronutrient composition of ingested food also differentially influences ghrelin release; carbohydrates and proteins have been shown to suppress plasma ghrelin levels more effectively than dietary fats (Lomenick et al., 2009). Experimental evidence from murine models further elucidates the neuroendocrine modulation of ghrelin. For instance, intravenous administration of kisspeptin, a hypothalamic peptide known to stimulate the hypothalamic-pituitary-gonadal axis, significantly reduces plasma ghrelin concentrations and gene expression, whereas morphine, an alkaloid with inhibitory effects on reproductive function, markedly elevates both plasma ghrelin and hypothalamic mRNA levels relative to saline controls (Khazail & Mahmoud, 2022). Notably, these studies measured total ghrelin, equivalent to the acylated (active) form, without distinguishing the relative proportions of acyl versus unacylated ghrelin, thereby limiting insights into isoform-specific dynamics.

At the cellular level, nuclear receptors REV-ERBα and REV-ERBβ act as transcriptional repressors of both ghrelin and GOAT expression. Overexpression of these receptors in SG-2 cells (a stomach-derived ghrelin-secreting cell line) results in significant downregulation of ghrelin and GOAT mRNA, whereas siRNA-mediated knockdown in SG-1 cells induces their upregulation, implicating REV-ERBs in the circadian regulation of ghrelin biosynthesis (Iijima et al., 2021).

The regulation of GHRL expression involves a complex interplay of transcriptional and epigenetic mechanisms. Several transcription factors bind directly to the GHRL promoter to modulate its activity. Nkx2.2, a homeodomain transcription factor critical for pancreatic development, activates the ghrelin promoter specifically in pancreatic islet cells, directly enhancing ghrelin expression (Hill et al., 2010). Conversely, NF-κB, particularly the RelA/p65 subunit, functions as a transcriptional repressor of GHRL, as demonstrated by the suppression of ghrelin promoter activity in human TT cells (Shiimura et al., 2015). Additionally, Brain-Specific Homeobox (BSX) has been identified as an essential regulator of energy homeostasis and feeding behaviour. BSX influences the hypothalamic expression of orexigenic neuropeptides such as AgRP and NPY, which are downstream targets of ghrelin signalling (Sakkou et al., 2007).

Epigenetic regulation also plays a role in ghrelin expression. For example, Krüppel-like factor 13 (KLF13) has been implicated in modulating neural and hormonal responses associated with feeding. Wiemerslage et al. (2017) identified a DNA methylation site within the KLF13 gene correlated with altered neural reactivity to food cues and circulating ghrelin levels, suggesting KLF13's involvement in epigenetically mediated orexigenic signalling pathways.

Collectively, these findings underscore the multifaceted regulation of ghrelin secretion and gene expression, governed by nutritional cues, neuroendocrine factors, transcriptional regulators, and epigenetic mechanisms, all of which contribute to the precise modulation of this key metabolic hormone.

1.4.3.2 Ghrelin Clearance and Half-Life

Ghrelin circulates in two main forms: acyl ghrelin, the active, octanoylated peptide, and unacylated ghrelin, which is non-orexigenic. In vivo, acyl ghrelin is cleared very rapidly. Intravenous bolus studies in humans have shown an elimination half-life of approximately 9–13 minutes for acyl ghrelin, compared to 27–31 minutes for total ghrelin (predominantly unacylated ghrelin), consistent with a two-compartment model of distribution and elimination (Akamizu et al., 2004, Vestergaard et al., 2007) supported these biphasic kinetics, reporting an initial half-life of ~24 minutes and a terminal half-life of ~146 minutes for total ghrelin under sustained infusion. Methodological differences, such as bolus versus continuous infusion, likely explain some variability in half-life measurements.

In ex vivo conditions, ghrelin exhibits greater stability. Blatnik and Soderstrom (2011) found that acyl ghrelin decayed with a half-life of approximately 45 minutes in human plasma at room temperature, with about half converting to unacylated ghrelin within an hour. This slower degradation likely reflects the absence of renal clearance and tissue distribution. The authors emphasised the importance of using esterase inhibitors during sample collection to preserve endogenous acyl ghrelin and ensure accurate quantification.

Regarding ageing, direct data on ghrelin clearance in humans are limited. Hollis et al. (2013) observed lower steady-state acyl ghrelin levels in older adults but did not assess elimination kinetics directly. In rodents, however, age-related differences in degradation have been demonstrated. Ni et al. (2010) showed that foetal and neonatal rat plasma degraded acyl ghrelin more rapidly than adult plasma, even though blood esterases such as BChE and carboxylesterase increase with age. The application of serine protease inhibitors reduced acyl ghrelin degradation in adult rat plasma, suggesting that early-life clearance may involve different or more active proteolytic systems.

Overall, there is no compelling evidence that ghrelin's intrinsic clearance rate changes significantly with aging in humans. Instead, the age-related decline in circulating acyl ghrelin appears to result primarily from reduced basal secretion rather than altered elimination (Hollis et al., 2013).

1.4.3.3 Animal Models of Age-Related Ghrelin Changes

In terms of developmental expression, studies in mice have shown that gastric ghrelin mRNA rises sharply after birth, peaks around postnatal day 21, and subsequently declines to approximately 67% of its peak level by 6 months of age and to about 5% by 19 months (Liu et al., 2002). Interestingly, despite this marked reduction in transcription, circulating ghrelin concentrations remain relatively stable, between 0.1 and 0.6 ng/mL, across these ages, with a transient spike exceeding 15 ng/mL observed at postnatal day 60 in males. This suggests that post-transcriptional and post-secretory mechanisms may play a role in regulating ghrelin levels beyond gene expression alone.

Regarding tissue distribution, extra gastric sources of ghrelin also decline with age. In humans, Carraro et al. (2006) reported a strong negative correlation between adrenal ghrelin mRNA expression and chronological age (ranging from 33 to 82 years),

indicating a general down-regulation of peripheral ghrelin transcription as part of the ageing process.

When it comes to functional responsiveness, aged rodents not only produce less ghrelin but also respond differently to its biological effects. Warzecha et al. (2006) demonstrated that 7-week-old rats exhibited a significantly stronger GH and insulin-like growth factor-1 (IGF-1) response to ghrelin administration compared to neonatal or adult rats. Similarly, Nesic et al. (2013) found that intracerebral administration of acyl ghrelin led to greater food intake and weight gain in young rats compared to middle-aged animals, while older rats showed enhanced fat accumulation and elevations in circulating lipids such as triglycerides and low-density lipoprotein (LDL) following ghrelin treatment.

Taken together, these findings suggest that both ghrelin biosynthesis and its receptor-mediated physiological effects are progressively down-regulated with ageing in rodent models. This decline has important implications when attempting to extrapolate preclinical data to human aging and disease contexts.

1.4.3.4 Human Studies of Age-Related Ghrelin Changes

Fasting plasma levels of total ghrelin have been shown to decline with age. Rigamonti et al. (2002) found that individuals aged 65 years and older had circulating ghrelin levels comparable to those observed in obese subjects, and significantly lower than levels found in healthy controls with a mean age of 30. Supporting this trend, Schutte et al. (2007) reported that fasting ghrelin concentrations were lower in lean women aged 30 to 56 years compared to those aged 19 to 29 years. Additionally, data from the POWIRS cohort revealed that aging diminished the correlation between ghrelin and other metabolic markers, such as leptin and coagulation factors, suggesting a disruption in ghrelin's role within the broader metabolic regulatory network.

When specifically measuring acyl ghrelin using an ELISA, Nass et al. (2014) observed that the mean 24-hour acyl ghrelin concentration in older adults was approximately 14.7 pg/mL, nearly half the level seen in younger adults, whose mean value was around 27.8 pg/mL. Moreover, the coupling between acyl ghrelin pulses and GH secretion was significantly weakened in the older group. This disproportionate reduction in the biologically active form of ghrelin, relative to total ghrelin, highlights the importance of assessing acyl ghrelin specifically when evaluating endocrine function in ageing populations.

In terms of transcriptional regulation, Carraro et al. (2006) reported age-associated declines in adrenal ghrelin mRNA expression in humans, consistent with findings from rodent models. Notably, this decline was observed regardless of sex, providing further evidence that peripheral ghrelin gene expression diminishes as part of the ageing process.

1.4.3.5 Ghrelin degradation

Ghrelin's degradation is driven by both its peptide and lipid components. The active form, acyl ghrelin, is characterised by an n-octanoyl modification on its third serine residue, a lipidation that is essential for its receptor binding and biological activity (Kojima et al., 1999). This lipid moiety is vulnerable to hydrolysis by circulating esterases, particularly BChE and other nonspecific esterases in plasma, leading to the rapid conversion of acyl ghrelin to unacylated ghrelin (Sato et al., 2012).

While unacylated ghrelin has biological activity in its own right, it does not bind the GHS-R1a and is often considered a distinct signalling molecule. Moreover, the enzymatic breakdown of the ghrelin peptide backbone itself is mediated by proteases such as neprilysin and insulin-degrading enzyme (IDE), which are both known to increase in activity with age (Iwata et al., 2001). These age-related increases in proteolytic activity may contribute to the observed decline in active ghrelin levels in older individuals, potentially exacerbating deficits in ghrelin signalling.

Once secreted, ghrelin is inactivated through enzymatic deacylation and proteolysis. Plasma esterases remove the acyl (n-octanoyl) group from acyl ghrelin, converting it into the inactive unacylated ghrelin. De Vriese et al. (2004) demonstrated that human serum can deacylate ghrelin and identified BChE as a key enzyme. Their inhibition studies showed that BChE inhibitors reduce deacylation in human serum. Conversely, rat serum primarily relies on carboxylesterases.

Supporting this, Schopfer, Lockridge, and Brimijoin (2015) showed that purified human BChE slowly hydrolyses acyl ghrelin to unacylated ghrelin. Their findings suggest that BChE is physiologically relevant in circulating ghrelin clearance. Proteolytic degradation of the peptide backbone also contributes. De Vriese et al. (2004) identified cleavage sites within the ghrelin peptide (e.g., Ser2-Ser3, Phe4-Leu5), which generate fragments that are inactive at the receptor.

Importantly, enzymatic activity targets the lipid moiety directly. BChE and carboxylesterases hydrolyses the ester bond at Ser3, removing the octanoyl group and thereby abolishing biological activity (De Vriese et al., 2004; Schopfer et al., 2015). This process is thus a key inactivation mechanism. As deacylation removes the ghrelin receptor activity, and proteases can further degrade the resulting peptide, enzyme-mediated degradation plays a vital role in regulating ghrelin signalling.

1.4.3.6 Implications for Dementia Biomarker Development

Ghrelin's diverse roles, including its orexigenic, neuroprotective, and anti-inflammatory functions, make it a promising candidate as a blood-based biomarker for dementia. However, because normative aging significantly alters both ghrelin secretion and activity, any dementia-focused biomarker model must carefully account for these physiological changes. First, statistical analyses must adjust for age, as both total ghrelin and acyl ghrelin levels decline with advancing years, failing to do so risks conflating age-related reductions with disease-specific alterations. Furthermore, due to the disproportionately sharper decrease in acyl ghrelin, which is the biologically active form, it is critical to employ assays that accurately measure acyl ghrelin. This requires rapid sample processing protocols that include esterase inhibitors to prevent post-collection degradation, as demonstrated by Blatnik and Soderstrom (2011).

Sex differences must also be taken into account, since both animal models and some human studies suggest that ghrelin regulation may differ by sex. Incorporating sex as a stratification variable or covariate may enhance the specificity and interpretability of ghrelin-based biomarkers (Liu et al., 2002; Schutte et al., 2007). Additionally, current evidence does not support a significant change in ghrelin clearance rates with aging in humans, suggesting that observed declines in circulating levels are more likely due to alterations in secretion and gene expression rather than shifts in metabolic elimination (Hollis et al., 2013; Ni et al., 2010).

In summary, although ghrelin, particularly acyl ghrelin, declines with age, this trend may not only reflect normal neuroendocrine aging but could also identify individuals at heightened risk for reduced neuroprotection. Consequently, rigorously designed studies that control for age, sex, assay methodology, and metabolic variables will be essential for establishing ghrelin's reliability and validity as a biomarker for dementia.

1.4.4 Ghrelin Receptors and Brain Localisation

The active form of ghrelin, acyl ghrelin, binds to GHS-R1a, which is widely expressed in the CNS, including key regions such as the hippocampus, hypothalamus, substantia nigra, and ventral tegmental area (Zigman et al., 2006). These brain areas are critically involved in memory, reward processing, and homeostatic regulation, domains that are often impaired in dementia. Beyond the CNS, GHS-R1a is also expressed in peripheral tissues, including the pituitary gland and vagal afferents, underscoring the receptor's role in coordinating both central and peripheral effects of ghrelin (Kojima & Kangawa, 2005).

Within the brain, acyl ghrelin binding to GHS-R1a activates several intracellular signalling pathways, predominantly through Gq/11 proteins. This activation stimulates PLC, increases intracellular calcium levels, and triggers mitogen-activated protein kinase/extracellular signal-regulated kinase (MAPK/ERK) cascades. These signalling events modulate neuronal excitability and synaptic plasticity, thereby contributing to ghrelin's neuroprotective and cognitive-enhancing effects (Müller et al., 2015). Importantly, GHS-R1a exists alongside a splice variant, GHS-R1b, which lacks the ability to bind ghrelin but can heterodimerise with GHS-R1a, modulating receptor signalling and trafficking (Holst et al., 2003).

Animal studies have demonstrated that centrally administered ghrelin enhances hippocampal long-term potentiation (LTP), a cellular correlate of learning and memory (Diano et al., 2006). Additionally, ghrelin promotes adult hippocampal neurogenesis, protects neurons against oxidative stress, and suppresses neuroinflammatory pathways, these mechanisms are particularly relevant given that hippocampal atrophy and chronic inflammation are hallmark features of AD (Moon et al., 2009).

Receptor density and expression levels may vary with age and disease state, influencing ghrelin signalling efficacy. Some studies suggest that GHS-R1a expression in the hypothalamus and hippocampus decreases with ageing and in neurodegeneration models, potentially contributing to reduced ghrelin responsiveness in elderly populations (Malendowicz et al., 2010). However, further research is necessary to clarify these changes in humans and their relevance to dementia progression.

While GHS-R1a mediates most known effects of acyl ghrelin, some functions attributed to unacylated ghrelin or ghrelin more broadly may involve other, yet unidentified receptors or binding sites. For example, alternative ghrelin binding interactions have been proposed at receptors such as CD36 or other membrane proteins, although these mechanisms remain poorly characterised (Delhanty et al., 2012). This complexity highlights the need for continued research into ghrelin receptor biology, particularly in the context of aging and neurodegenerative diseases.

1.4.5 Unacylated and Acyl Ghrelin and the BBB

Cells within the brain have been questioned as to whether they express ghrelin. In 1999, Kojima et al. identified ghrelin mRNA in the rat stomach and brain. However, Cowley et al. (2003) reported that ghrelin-knockout mice showed no detectable mRNA in the hypothalamus compared to wild-type littermates. In contrast, other studies suggest that no brain cells express the ghrelin gene (Sakata et al., 2009; Furness et al., 2011). Despite this, the GOAT enzyme is expressed in the hippocampus (Murtuza & Isokawa, 2018; Hornsby et al., 2020), enabling local synthesis of acyl ghrelin from peripherally derived unacylated ghrelin.

The brain is protected by the BBB, a selectively permeable membrane that regulates molecular passage from the circulation into neural tissue. Both acyl ghrelin and unacylated ghrelin can cross the BBB from the periphery. In mice, acylation status and species origin influence transport directionality: murine acyl ghrelin preferentially crosses from brain to blood, whereas murine unacylated ghrelin crosses from blood to brain. Human acyl ghrelin, differing from the mouse form by only two amino acids, can cross in both directions via a saturable transport system. These amino acid differences may be critical for recognition by the influx transporter, while a separate saturable mechanism likely mediates efflux in both species (Banks et al., 2002) (Figure 1.3).

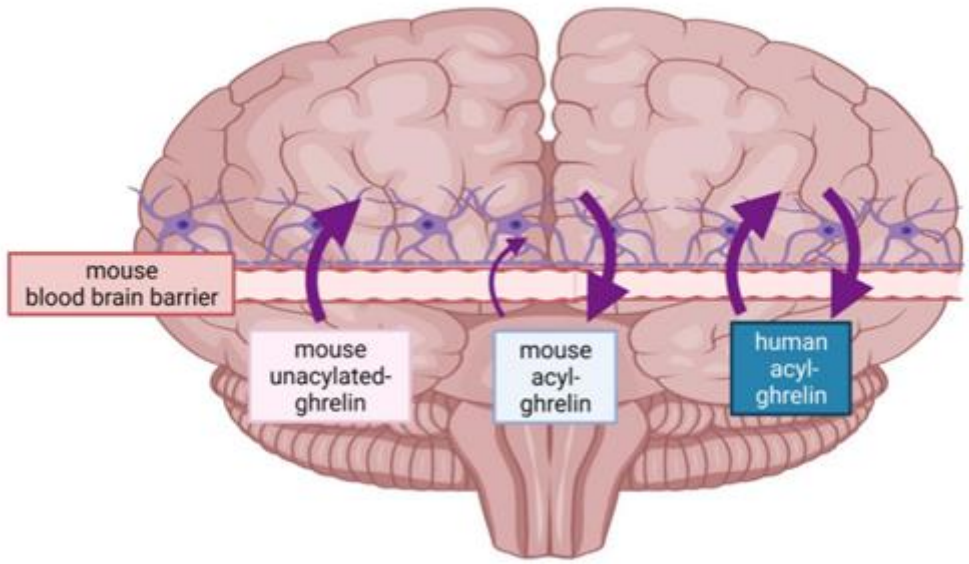

Figure 1.3 Ghrelin peptides crossing the blood-brain barrier.

Murine acyl ghrelin as shown by the arrow, prefers to cross the blood-brain barrier in the brain-to-blood direction, while murine unacylated ghrelin travels in the blood-to-brain direction. Human acyl ghrelin, which differs from mouse only in two amino acids (see Table 1.1), is capable of crossing both directions across the mouse blood-brain barrier. (Figure used with permission; Thomas A.S, et al., 2022).

The study by Banks et al., assessed both the brain:serum ratio and direct parenchymal accumulation to differentiate between ghrelin trapped in brain vasculature versus that taken up by brain tissue. This comprehensive approach confirmed that transport was not limited to capillary retention but reflected true penetration into the brain parenchyma. Additionally, Banks et al. showed that unacylated ghrelin, in contrast, crossed the BBB via a non-saturable mechanism, likely simple diffusion, indicating that it may have unregulated access to the brain. This distinction has functional implications: it suggests that unacylated ghrelin could be more consistently available in the central nervous system regardless of circulating levels, possibly allowing for local acylation by brain-expressed GOAT.

These findings demonstrate the complexity of ghrelin's central regulation and raise the possibility that species-specific sequence differences influence the neuroendocrine roles of ghrelin. Moreover, they support the hypothesis that central ghrelin actions may depend not only on peripheral levels but also on selective BBB transport mechanisms.

These initial findings on the ability of ghrelin to cross the BBB were later supported by radiolabelled ghrelin studies which also suggested that human acyl ghrelin can cross

the BBB via endocytosis (Diano et al., 2006; Pan, Tu, & Kastin 2006). A more recent study demonstrated that peripheral injections of F-ghrelin (a fluorescent analogue of acyl ghrelin) were internalised by ependymal cells of the choroid plexus and by a specific subset of tanycytes, highly specialised ependymal cells that form a barrier between CSF (a barrier between the circulating blood and the CSF space) (Uriarte et al., 2019). Accessibility of acyl ghrelin to the brain appears to occur in a dose-dependent manner. A low dose of the peripherally injected fluorescent acyl ghrelin analogue was present at low levels in the CSF and demonstrated a higher preference for the hypothalamus, while systemic administration of ghrelin through centrally injected acyl ghrelin (or high doses administered peripherally) was detected at high levels in the CSF and other regions of the brain (Cabral, Fernandez, and Perello 2013; Uriarte et al., 2019). Together, these studies suggest that both acyl ghrelin synthesised locally within the brain or derived from the periphery could impact brain function and influence neurodegenerative disorders.

Ghrelin can exert effects on the CNS by crossing the BBB. Radiolabelled tracer studies indicate that acyl ghrelin is transported across the BBB via a saturable mechanism (Banks et al., 2002), and detectable levels of circulating ghrelin enter brain regions such as the hippocampus (Diano et al., 2006). Indeed, in animal studies intraperitoneal ghrelin elevates hypothalamic neuronal activity and neurogenesis, suggesting physiologically relevant central access. Notably, PD is associated with BBB disruption (Lau et al., 2024), which could theoretically alter ghrelin's central bioavailability. Lau et al. (2024) documented widespread tight-junction changes and vascular leakage in PD, implying that peripheral hormones like ghrelin might access vulnerable brain regions more readily. Thus, circulating ghrelin can reach its CNS receptors (GHS-R1a) under normal and PD-altered conditions, allowing it to modulate feeding circuits, neuroinflammation, and neuroplasticity (Banks et al., 2002; Diano et al., 2006; Lau et al., 2024). Ghrelin production and secretion depend on gastric function, which is often impaired in PD. Gastrointestinal dysmotility is a common non-motor symptom of PD, including delayed gastric emptying (gastroparesis) and constipation. These changes can blunt normal nutrient-hormone cycles. Consistent with this, PD patients tend to exhibit lower circulating ghrelin. For example, Song et al. (2017) measured fasting plasma ghrelin in 291 early-stage PD patients and 303 controls and found that total and acyl ghrelin levels were significantly reduced in PD, regardless of disease stage.

Postprandial dynamics were also altered: PD patients showed attenuated meal-induced ghrelin suppression and blunted preprandial rises (Song et al., 2017). Unger et al. (2011) similarly reported that both PD and prodromal REM sleep behaviour disorder subjects had impaired postprandial ghrelin excursions compared to controls. These findings suggest that disease-related gastric dysfunction or weight loss in PD attenuates the normal ghrelin response. Indeed, one clinical review noted that only one study had assessed ghrelin in PD and found lower serum ghrelin in PD versus controls (Mey et al., cited in Gastroparesis review). Moreover, antiparkinsonian drugs (for example, anticholinergics, levodopa) can further delay gastric emptying and potentially feedback on ghrelin output (Mey et al., 2021). In sum, PD-related gastrointestinal abnormalities tend to suppress peripheral ghrelin production or release, which could diminish the availability of this hormone to the brain. In the CNS, ghrelin acts through its receptor GHS-R1a, which is expressed in dopaminergic and other neurons. Evidence indicates that GHS-R1a signalling is perturbed in PD. Suda et al. (2018) showed that GHS-R1a expression is markedly downregulated in induced pluripotent stem cell–derived dopaminergic neurons from patients with PARK2 mutations. In mice, pharmacological blockade of GHS-R1a in the substantia nigra produced catalepsy and motor deficits, implying that GHS-R1a loss-of-function can induce Parkinsonian symptoms (Suda et al., 2018). Thus, PD may involve functional loss of ghrelin receptor activity. GHS-R1a also heterodimerises with dopamine receptors, modifying dopaminergic signalling. Kern et al. (2014) found that unoccupied GHS-R1a (apo-GHS-R1a) forms heteromers with dopamine D2 receptors (DRD2) in hypothalamic neurons, these GHS-R1a/DRD2 complexes allosterically regulate D2 signalling. In the hippocampus, GHS-R1a and dopamine D1 receptors (DRD1) form heteromeric complexes essential for D1-dependent synaptic plasticity. Kern et al. (2015) demonstrated that DRD1 agonists elicit noncanonical Gα_q/PLC signalling only when GHS-R1a is present. Similarly, Navarro et al. (2022) identified GHS-R1a/GHS-R1b/D1R oligomers in ventral tegmental area dopamine neurons that mediate ghrelin’s effects on motivation. These interactions mean that ghrelin receptor activity can amplify residual dopamine neurotransmission. In PD, where dopamine is deficient, intact GHS-R1a might be especially important for modulating synaptic plasticity and cognition via D1 pathways (Hernandez et al., 2015). Conversely, GHS-R1a downregulation in PD dopaminergic neurons likely worsens dopaminergic deficits and might contribute to cognitive impairment (Suda et al., 2018; Kern et al., 2015). Ghrelin

also supports cellular processes that counteract PD pathology. It activates AMPK and related metabolic pathways to enhance mitochondrial function and autophagy. Bayliss and Andrews (2013) review that ghrelin promotes uncoupling protein 2 (UCP2) expression, reducing oxidative stress, and triggers AMPK-mediated mitophagy and mitochondrial biogenesis. Specifically, ghrelin inhibits mTOR signalling (via AMPK and ULK1 phosphorylation), thus stimulating autophagy and clearance of damaged organelles (Bayliss & Andrews, 2013). Experimentally, ghrelin administration increases markers of autophagy (e.g. LC3-II, Beclin-1) and decreases p62 accumulation in MPTP-lesioned mice, thereby protecting nigral neurons from α-synuclein accumulation and endoplasmic reticulum (ER) stress (Wang et al., 2020). Conversely, loss of ghrelin signalling impairs these homeostatic mechanisms. In an MPTP PD model, Xiao et al. (2024) showed that GHS-R1a knockout mice exhibited overexpression of DEPTOR (a positive regulator of early autophagy) but paradoxically developed lysosomal dysfunction. This block in autophagy flux prevented clearance of damaged mitochondria in dopaminergic neurons, exacerbating neurodegeneration. In sum, ghrelin/GHS-R1a supports mitochondrial quality control via autophagy/mitophagy, processes known to be disrupted in PD (e.g. PINK1/Parkin pathways). Any compromise of ghrelin signalling can thus aggravate the bioenergetic and proteostatic stress in PD neurons (Xiao et al., 2024; Wang et al., 2020). Clinical and experimental evidence links ghrelin alterations to PD and PDD. Population studies report lower ghrelin in PD: for example, Song et al. (2017) found reduced fasting total and acyl ghrelin in PD patients versus controls. Similarly, Unger et al. (2011) observed that PD and prodromal patients fail to suppress ghrelin normally after meals. Importantly, recent studies tie ghrelin to cognitive outcomes in PD. Plasma analysed from PD patients with and without dementia and found that the AG:UAG ratio was significantly reduced only in PDD cases (Sassi et al., 2022). Correspondingly, Hornsby et al. (2020) showed that elevating UAG (or lowering AG:UAG) in mice impaired hippocampal neurogenesis and memory, paralleling the human PDD phenotype. These studies suggest that higher unacylated ghrelin (and lower AG:UAG ratio) could serve as a circulating biomarker for PDD. Experimental models reinforce ghrelin's protective role: in mice, exogenous ghrelin administration reduces MPTP-induced microglial activation and inflammatory cytokines (IL-1β, TNF-α) in the substantia nigra, preserving dopaminergic neurons (Moon et al., 2009; Bayliss & Andrews, 2013). Conversely, GHS-R1a deletion or antagonism accelerates dopaminergic loss and PD-

like motor deficits (Suda et al., 2018; Xiao et al., 2024). Collectively, epidemiologic data on blood ghrelin, clinical correlations with weight loss and cognition, and animal studies of ghrelin modulation all implicate ghrelin in PD progression and dementia risk. These findings underscore ghrelin's multifaceted role in PD and highlight circulating ghrelin measures (especially the AG:UAG ratio) as promising biomarkers for identifying PD patients at risk for cognitive decline (Sassi et al., 2022; Song et al., 2017).

In summary, ghrelin plays a multifaceted role in the brain, influencing memory, neuroprotection, inflammation, and metabolism, all key elements in the pathophysiology of dementia. Age-related declines in ghrelin levels may contribute to cognitive decline and neurodegeneration, and emerging data support its potential as a blood-based biomarker. Further studies are warranted to validate ghrelin as a diagnostic or prognostic tool and to elucidate the mechanistic pathways linking it to dementia progression.

1.4.6 Acyl Ghrelin Binding to GHS-R1a

Acyl ghrelin binding to GHS-R1a is essential for receptor activation and downstream signalling. Unlike unacylated ghrelin, acyl ghrelin deeply penetrates the lipid membrane via its octanoyl group, increasing local concentration around the receptor by approximately 120-fold, thereby enhancing receptor engagement (Staes et al., 2010). Hydrophobic amino acids at the N-terminal, particularly around serine-3 where the octanoyl moiety is attached, play a crucial role in membrane association and receptor binding (Vortmeier et al., 2015).

Structural studies using nuclear magnetic resonance (NMR) and molecular dynamics simulations have shown that acyl ghrelin adopts a rigid helical conformation, with the octanoyl group forming a hydrophobic core that stabilises the hormone-receptor complex (Bender et al., 2019; Ferré et al., 2019). Crystal and cryoelectron microscopy structures of GHS-R1a reveal a distinctive divided binding pocket featuring a salt bridge and a hydrophobic crevasse. Phenylalanine residues within the receptor contribute critically to ligand recognition and receptor activation, and mutations in these residues impair receptor function (Shiimura et al., 2020; Wang et al., 2021).

Upon binding, acyl ghrelin activates Gq/11 protein-mediated pathways that stimulate PLC, leading to increased intracellular calcium and activation of PKC and MAPK/ERK

signalling cascades. These pathways influence multiple neuronal processes, including hormone secretion, synaptic plasticity, and gene transcription (Müller et al., 2015; Holst et al., 2004). In contrast, unacylated ghrelin shows markedly reduced affinity for GHS-R1a and does not activate these signalling cascades, underscoring the essential role of acylation in receptor engagement (Kaiya et al., 2001).

Emerging evidence also supports the concept of biased agonism at GHS-R1a, whereby different ligands induce distinct receptor conformations that selectively activate specific intracellular pathways. This phenomenon offers potential for designing therapeutics that target ghrelin signalling more precisely with fewer side effects (Smith et al., 2020). Furthermore, GHS-R1a undergoes regulated internalisation and desensitisation through clathrin-mediated endocytosis following ligand binding, mechanisms that finely tune receptor signalling duration and intensity (Roh et al., 2016).

Collectively, these molecular insights into the binding and activation of GHS-R1a by acyl ghrelin underpin the hormone's diverse physiological effects, particularly in the brain regions associated with cognition, metabolism, and neuroprotection.

1.4.7 The Role of Unacylated Ghrelin

Although unacylated ghrelin has traditionally been considered 'inactive', accumulating evidence suggests that it may exert distinct physiological effects independent of, or even antagonistic to, acyl ghrelin. For example, some studies propose that unacylated ghrelin may act as an antagonist to acyl ghrelin (Broglio et al., 2004; Gauna et al., 2005; Inhoff et al., 2008). Supporting this, Gauna and colleagues demonstrated that while acyl ghrelin stimulates glucose release from primary porcine hepatocytes, unacylated ghrelin inhibits this effect.

In addition to potential antagonism, unacylated ghrelin is increasingly recognised as having its own biological activity, possibly interfering with acyl ghrelin binding to the GHS-R or indirectly modifying its downstream effects. One hypothesis is that unacylated ghrelin binds to a currently unidentified receptor, triggering intracellular signalling pathways that modulate or counteract the effects of acyl ghrelin.

To test this, experimental approaches such as receptor deorphanization—using ligand binding assays combined with high-throughput screening of candidate G-protein coupled receptors (GPCRs) or other membrane proteins, could be employed.

Additionally, transcriptomic and proteomic profiling of cells treated with unacylated ghrelin versus acyl ghrelin can identify differential signaling cascades and molecular targets. Known signaling pathways activated by acyl ghrelin include GHS-R1a-mediated activation of PLC, increased intracellular calcium, activation of PKC, and AMPK pathways, which regulate energy homeostasis and neuroprotection. Identifying which of these pathways are selectively modulated or inhibited by unacylated ghrelin would clarify its physiological role and receptor interactions.

Acyl ghrelin is known to act through GHS-R1a, activating signalling pathways such as PLC, PKC, and AMPK, which are involved in regulating energy homeostasis, appetite, and neuroprotection. Determining whether unacylated ghrelin modulates or selectively inhibits these pathways would provide key insight into its physiological role and potential receptor mechanisms.

In support of its independent activity, Fernandez et al. (2016) showed that unacylated ghrelin binds to and acts on a specific subset of arcuate nucleus cells (neurons located in the hypothalamus that play a central role in regulating appetite, energy balance, and hormone secretion) independently of GHSR. Using a fluorescent tracker, they demonstrated that unacylated ghrelin did not affect dark phase feeding (the period during which nocturnal animals such as mice are naturally most active and consume the majority of their food). However, it did attenuate the orexigenic effects of peripherally administered acyl ghrelin (i.e., ghrelin delivered into the body outside the central nervous system, such as via subcutaneous or intraperitoneal injection, rather than directly into the brain).

These findings support the notion that unacylated ghrelin can antagonise the effects of acyl ghrelin by directly targeting hypothalamic neurons involved in appetite regulation, further challenging the notion of its inactivity.

1.4.8 Physiological Relevance of Unacylated and Acyl Ghrelin

Initially, acyl ghrelin was most widely recognised for its effects on appetite stimulation and GH release (Nakazato et al., 2001). Beyond this, acyl ghrelin has also shown a wide range of effects on cardiovascular function (Nagaya et al., 2001), skeletal muscle (Ranjit, Remmen and Ahn 2022), bone formation and osteoblast proliferation (Fukushima et al., 2005), sleep (Szentirmai et al., 2007), thymopoiesis (Dixit et al., 2007), ageing, (Rigamonti et al., 2002) and brain function (Andrews et al. 2009;

Fukushima et al., 2005; Li et al., 2013). Additionally, acyl ghrelin has been found to have neuroprotective effects within the CNS (Andrews et al., 2009; Bayliss et al., 2016). Furthermore, ghrelin plays a role in mood regulation (Lutter et al., 2008), and the promotion of neural plasticity through adult hippocampal neurogenesis (AHN) (Hornsby et al., 2016; Kent et al., 2015). More specifically in terms of its neuroprotective effects, it has been reported to promote neurogenesis and cognition (Chung et al., 2013; Chung et al., 2018; Hornsby et al., 2016). Acyl ghrelin is also considered important for the regulation of energy homeostasis (Tschöp, Smiley, and Heiman, 2000). Consistent with this, in a murine model of PD, a neurodegenerative disorder characterised by the loss of dopaminergic cells in the brain (Bertram and Tanzi 2005), the neuroprotective effect of acyl ghrelin involves the induction of mitochondrial respiration and biogenesis in the dopaminergic neurons of the substantia nigra, which depended on the metabolic regulator, AMPK (Bayliss et al., 2016). Overall, numerous studies have shown that acyl ghrelin has beneficial effects on various biological systems, Buntwal and co-workers reviewed the specific effects of acyl ghrelin on AHN in 2019.

A recent study from our group aimed to determine the role of unacylated ghrelin in the modulation of AHN and hippocampal-dependent memory (Hornsby et al., 2020). In this study, both wild-type (WT) and GOAT knock-out (GOAT-/-) mice, which lack the enzyme required to acylate ghrelin and thus have high circulating levels of unacylated ghrelin but no acyl ghrelin, were treated with exogenous unacylated ghrelin. This approach allowed for the assessment of unacylated ghrelin's direct effects on neurogenesis across genotypes and helped control for potential differences in endogenous ghrelin isoform levels. Following treatment, both WT and GOAT-/- mice showed a significant decrease in Ki67+ proliferating cells and immature Dcx+ neurons (newly generated neurons marked by the expression of doublecortin, a protein involved in neuronal migration and a widely used indicator of neurogenesis) in the subgranular zone (SGZ) of the dentate gyrus (DG), suggesting that unacylated ghrelin may exert an inhibitory effect on AHN, independent of acyl ghrelin signalling. Additionally, there was a significant reduction in the survival of new adult-born non-neuronal cells (BrdU + / Dcx) in WT mice treated with unacylated ghrelin and in vehicle-treated GOAT-/- mice. These reductions suggest that, in general, unacylated ghrelin results in reduced neurogenesis and plasticity of the hippocampus in mice.

Furthermore, GOAT-/- mice showed deficits in spatial memory, tested with the hippocampal-dependent Y-maze task, which was rescued by acyl ghrelin treatment. Together, these data suggest that altered AHN and spatial memory may be due to a combination of increased unacylated ghrelin levels and a lower level of acyl ghrelin (Hornsby et al., 2020). As previous results from the group and the literature suggested that the circulating ratio of AG:UAG could be significant in the effect of ghrelin, Hornsby et al. (2020) also investigated whether the blood plasma ratio of AG:UAG is associated with cognitive function. The AG:UAG ratio was quantified in blood plasma (using ELISA) from people with PD or PD with dementia and compared with healthy controls. Within the group of patients with PDD, a reduction in the AG:UAG ratio was reported but was unchanged in cognitively intact subjects with PD and healthy subjects. The results suggest that the circulating AG:UAG ratio may be a diagnostic biomarker of PDD and possibly could be used to monitor cognitive decline in humans. A blood-based prognostic biomarker of dementia would accelerate precision medicine-based clinical trials and therapeutic development.

1.5 Lipidation Variability and Relevance to Disease

Lipidation, the covalent attachment of lipid moieties to peptides or proteins, is a key post-translational modification that modulates molecular conformation, stability, localisation, and receptor interaction (Resh, 2013). In the case of ghrelin, lipidation refers specifically to the acylation of serine-3 by an n-octanoyl group, catalysed by GOAT, which is essential for its biological activity through the GHS-R1a receptor. This acylation distinguishes bioactive acyl ghrelin from its unacylated form, which lacks affinity for the receptor but may exert independent effects via other, less-defined mechanisms (Hosoda et al., 2000; Delhanty et al., 2012).

From a biological perspective, acyl ghrelin is inherently unstable and highly susceptible to deacylation by circulating esterases, such as BChE and acyl-protein thioesterases (Satou & Sugimoto, 2012; Mani & Zigman, 2017). This rapid conversion of AG to UAG creates a dynamic equilibrium that is sensitive to physiological and pathological influences. Consequently, the AG:UAG ratio is increasingly recognised as a potentially sensitive indicator of alterations in energy metabolism, endocrine regulation, and neurodegeneration, including in diseases such as Alzheimer's and Parkinson's (Müller et al., 2015; Stoyanova, 2014).

In PD, ghrelin has been implicated in neuroprotective pathways, including mitochondrial preservation, anti-inflammatory signalling, and dopaminergic neuron survival (Andrews et al., 2009). Disrupted ghrelin acylation in PD may reflect or contribute to metabolic impairments that precede motor symptoms. Notably, studies have shown that AG levels or AG:UAG ratios may be reduced in patients with PD, suggesting a link between altered lipidation processes and neurodegenerative pathophysiology (Stoyanova, 2014). However, precise characterisation of these alterations is contingent on the availability of robust analytical methodologies capable of distinguishing ghrelin isoforms.

Technically, the detection of lipidated ghrelin is fraught with challenges. Immunoassays such ELISA and electrochemiluminescence immunoassays (ECLIA) are widely used for clinical and research purposes but often lack the specificity required to discriminate between acyl ghrelin and unacylated ghrelin with high fidelity. Antibody cross-reactivity, matrix effects, and susceptibility to sample degradation complicate interpretation, particularly in plasma or serum (Blatnik & Soderstrom, 2011; Delhanty et al., 2012).

In contrast, MS-based techniques offer superior molecular resolution and specificity. LC-MS, including LC-MS/MS platforms, allows direct quantification of acyl and unacylated ghrelin by monitoring specific mass-to-charge ratios and retention times. Studies have demonstrated the successful application of LC-MS to ghrelin detection, particularly when coupled with acyl-stabilisation protocols using esterase inhibitors and rapid processing (Thomas et al., 2022). Immunoprecipitation-MS (IP-MS) provides an additional level of selectivity by enabling targeted enrichment of ghrelin isoforms before MS analysis, thereby improving sensitivity and minimising matrix interference. Similarly, MALDI-TOF MS has been explored for high-throughput peptide profiling, although its utility in ghrelin lipidation studies remains limited due to ionisation variability and sensitivity constraints (Yin et al., 2015).

The complexity of detecting ghrelin acylation is not unique. Comparable challenges are observed in the study of lipidation in autophagy, particularly regarding microtubule-associated protein 1 light chain 3 (LC3). In this context, lipidated LC3 (LC3-II) is covalently bound to phosphatidylethanolamine and associates with autophagosome membranes, while its non-lipidated form (LC3-I) remains cytosolic (Mizushima et al., 2010). Importantly, assays must distinguish these lipidation states to accurately

measure autophagic flux. In practice, the LC3-II:LC3-I ratio is typically assessed using Western blotting, which exploits differences in electrophoretic mobility between the lipidated and non-lipidated forms. Although mass spectrometry can detect PE-conjugated LC3 peptides and confirm the presence of lipidation sites, it is not yet routinely used to quantify LC3-II:LC3-I ratios due to challenges in recovering hydrophobic peptides, ionisation inefficiency, and the lack of appropriate internal standards (Wilkinson et al., 2015). Thus, Western blotting remains the gold standard for LC3 ratio quantification, while MS offers high-resolution structural insights without yet replacing traditional methods. This limitation parallels the difficulties in ghrelin detection, where differentiating AG from UAG by MS or immunoassay faces analogous biochemical and analytical hurdles. Both systems underscore the critical importance of precise assay design when quantifying lipidated versus non-lipidated forms in biomarker research.

Ultimately, accurate quantification of ghrelin variants, particularly the AG:UAG ratio, has significant potential as a biomarker for metabolic and neurodegenerative diseases. However, this potential will only be realised through the refinement of detection strategies and a deeper understanding of how ghrelin lipidation varies across disease states. Standardising pre-analytical protocols, improving antibody specificity, and leveraging mass spectrometry innovations are essential steps towards this goal.

1.6 Ghrelin Signalling in PD: Pathophysiological Relevance

Beyond its peripheral metabolic functions, acyl ghrelin exerts central neuroprotective effects that are particularly relevant to PD. GHS-R1a, the ghrelin receptor, is expressed in dopaminergic neurons within the substantia nigra pars compacta, one of the primary regions affected by PD-related neurodegeneration (Andrews et al., 2009). Activation of GHS-R1a promotes mitochondrial biogenesis and function via AMPK and PGC-1α signalling, enhances autophagic clearance, and reduces oxidative stress, all of which are critical pathways implicated in PD pathology (Bayliss & Andrews, 2013; Stoyanova, 2014).

Notably, GHS-R1a is capable of forming heterodimers with dopamine D1 and D2 receptors, modulating dopaminergic neurotransmission, a mechanism particularly relevant in the striatum and midbrain, where dopaminergic signalling is disrupted in PD (Schellekens et al., 2013). This receptor crosstalk suggests that altered ghrelin levels or receptor function could directly affect PD-associated motor and non-motor

symptoms. Furthermore, preclinical studies have shown that ghrelin administration protects dopaminergic neurons against neurotoxic insults (for example, MPTP) and may even improve motor function in PD animal models (Andrews et al., 2009).

There is also emerging evidence of systemic alterations in ghrelin dynamics in PD patients. Several studies report lower circulating acyl ghrelin levels and AG:UAG ratios in individuals with PD, potentially reflecting impaired ghrelin acylation or increased deacylation under disease conditions (Stoyanova, 2014). Given that ghrelin is primarily produced in the stomach, these changes may not directly result from central neurodegeneration. However, central effects could still arise due to altered GHS-R1a signalling, receptor distribution, or blood-brain barrier permeability. Additionally, neurodegenerative processes may indirectly impact ghrelin signalling through inflammation, autonomic dysfunction, or altered gut-brain axis activity, which are all common features in PD.

Taken together, the interaction between ghrelin biology and PD pathology, via mitochondrial regulation, receptor dimerization, dopaminergic modulation, and autophagy, supports the hypothesis that ghrelin lipidation and signalling may play an active role in disease progression. This reinforces the potential utility of AG:UAG ratio as a mechanistically informed biomarker not only for PD diagnosis but also for tracking disease-related metabolic or neurochemical shifts. Incorporating such mechanistic insights into biomarker development strategies may improve specificity, provide early diagnostic value, and ultimately support more personalised treatment approaches for PD and related neurodegenerative disorders.

1.7 Ghrelin and Biomarker Suitability

1.7.1 Alignment with Biomarker Criteria

As discussed in Section 1.1, a viable biomarker must meet several critical criteria to be considered suitable for clinical or research applications. These include high specificity and sensitivity, biological and clinical relevance, stability, reproducibility, accessibility, and an ability to reflect central pathology when used in peripheral samples (Pepe et al., 2001; Strimbu & Tavel, 2010; Blennow & Zetterberg, 2018; Mullane & Williams, 2019).

Specificity refers to the biomarker's capacity to accurately distinguish individuals with the disease from those without, thereby minimising false-positive results and ensuring

diagnostic precision. Complementing this, sensitivity is the ability to correctly identify those affected by the disease, including early or subtle pathological changes, reducing false negatives (Pepe et al., 2001). The combination of specificity and sensitivity underpins the clinical utility of a biomarker.

Reproducibility and accuracy are also essential, as biomarkers must provide consistent and reliable measurements within and across laboratories, populations, and over time (Mullane & Williams, 2019). Equally important is biological and clinical relevance; a biomarker should reflect underlying disease mechanisms or correlate strongly with disease progression or severity, thus providing meaningful insights into pathology (Blennow & Zetterberg, 2018).

Ghrelin, particularly its acylated and unacylated isoforms, exemplifies many of these attributes. Its measurable presence in peripheral blood, involvement in central neurobiological and metabolic pathways, and emerging evidence of association with diverse pathological states underscore its potential as a biomarker for neurodegenerative and other diseases. For example, Grönberg et al. (2017) identified ghrelin as a prognostic marker in breast cancer, highlighting its broader clinical relevance. Similarly, Alnasser et al. (2020) demonstrated ghrelin's diagnostic promise in inflammatory conditions, reinforcing its role as an indicator of systemic pathological states.

Accessibility is another crucial consideration; biomarkers should be measurable through minimally invasive or non-invasive methods such as blood or saliva sampling to facilitate longitudinal monitoring (Strimbu & Tavel, 2010). Furthermore, stability during sample collection, processing, and storage is vital to preserve biomarker integrity and ensure accurate quantification (Delhanty et al., 2012).

Lastly, in the context of CNS disorders like neurodegenerative diseases, it is imperative that peripheral biomarker levels meaningfully correspond to central pathology. This relationship is often modulated by the integrity of the BBB, which regulates substance exchange between the brain and systemic circulation. Biomarkers that readily cross the BBB or whose peripheral levels mirror brain changes have enhanced utility for disease monitoring (Blennow & Zetterberg, 2018; Mullane & Williams, 2019).

Together, these criteria, specificity, sensitivity, reproducibility, biological relevance, accessibility, stability, and the central-peripheral relationship, constitute a robust framework for evaluating the suitability of ghrelin and other candidates as biomarkers.

1.7.2 Sample Collection and Preservation Challenges

A significant challenge in using ghrelin as a biomarker arises from its biochemical instability. Acyl ghrelin is rapidly deacylated by circulating esterases such as BChE (Hosoda et al., 2004; Blatnik & Soderstrom, 2011). Accurate quantification requires strict pre-analytical protocols, including use of esterase inhibitors, immediate chilling, acidification of blood samples, and rapid processing (Delhanty et al., 2012). Variability in sample handling contributes to inter-laboratory inconsistencies, impeding standardisation and clinical translation.

1.7.3 Sensitivity and Specificity

Preliminary clinical studies indicate that plasma acyl ghrelin levels and the AG:UAG ratio may differentiate PDD from PD without dementia and cognitively healthy controls (Song et al., 2017; Sassi et al., 2022). However, these findings are inconsistently replicated, likely due to confounding factors such as metabolic comorbidities (obesity, diabetes), which influence circulating ghrelin (Bayliss & Andrews, 2013). Large-scale, stratified studies accounting for these factors are required to robustly establish ghrelin's sensitivity and specificity across neurodegenerative subtypes.

1.7.4 Patient Stratification and Disease Stage

Neurodegenerative diseases exhibit heterogeneity in clinical presentation and pathology, with biomarker levels potentially varying by disease stage or subtype (Postuma et al., 2015; Jack et al., 2018). Stratifying patients by clinical phenotype and disease progression may enhance biomarker accuracy and clinical relevance. For PD, understanding how ghrelin levels change relative to motor and cognitive symptom onset is critical. Longitudinal, pre-symptomatic sampling remains challenging but is necessary to evaluate ghrelin's potential for early diagnosis (Frisoni et al., 2017; Postuma et al., 2017).

1.7.5 Biological and Pathophysiological Relevance

Ghrelin's neuroprotective effects, including synaptic plasticity enhancement, mitochondrial support, and anti-inflammatory properties, support its pathophysiological relevance in neurodegeneration (Moon et al., 2009; Xiao et al.,

2024). Acyl ghrelin activates GHS-R1a, which interacts with dopaminergic neurons, central to Parkinsonian pathology. Reduced ghrelin levels and receptor availability have been observed in AD patients and correlate with cognitive decline (Akimoto et al., 2013; Spitznagel et al., 2010; Kordonowy et al., 2012).

1.7.6 AG:UAG Ratio and Disease-State Reflection

The ratio of acyl to unacylated ghrelin potentially offers a more sensitive indicator of disease-specific metabolic disruptions than absolute concentrations alone. This ratio reflects the balance of enzymatic activities (GOAT, deacylation enzymes) and physiological state. Altered AG:UAG ratios in PDD and AD may indicate neuroendocrine or energy metabolism dysfunction, possibly linked to brain–gut axis alterations or hypothalamic involvement. However, longitudinal studies directly assessing this ratio in dementia cohorts are scarce and constitute a vital area for future investigation.

1.7.7 Central vs. Peripheral Measurements and BBB Considerations

Though ghrelin is primarily synthesised peripherally, its central effects depend on transport across the BBB via saturable mechanisms (Diano et al., 2006). BBB integrity is often compromised in advanced PD and AD (Lau et al., 2024), potentially disrupting the correlation between peripheral ghrelin levels and central nervous system activity. This complicates interpretation and suggests a need to assess BBB status and correlate plasma ghrelin with CNS-specific markers or imaging findings.

1.7.8 Clinical Interpretability and Translational Potential

Despite these complexities, ghrelin holds translational promise. It is measurable via minimally invasive blood sampling, has well-characterised CNS actions, and its levels can be modulated by pharmacological or dietary interventions. Clinical interpretability may improve when ghrelin measurement is integrated into multi-biomarker panels, combining neurofilament light chain (NfL, a cytoskeletal protein released upon axonal injury), tau, and inflammatory markers, enhancing diagnostic accuracy in complex or mixed dementia presentations (Janelidze et al., 2020; Thijssen et al., 2020).

1.7.9 Comparison with Established Blood-Based Biomarkers

In contrast to classical biomarkers such as Aβ, tau, and NfL, which closely track structural neurodegeneration, ghrelin reflects systemic neuroendocrine-metabolic alterations. While this may reduce disease specificity, it offers an opportunity to detect

early systemic changes preceding overt neurodegeneration. Moreover, unlike phosphorylated tau (pTau) or Aβ assays that require ultra-sensitive platforms such as single molecule enzyme-linked immunosorbent assay (SIMOA) (Single Molecular Array) or mass spectrometry, ghrelin isoforms can potentially be measured using more accessible immunoassays, though isoform specificity and stability remain obstacles.

1.7.10 Summary

Ghrelin meets several core biomarker criteria, especially biological relevance and accessibility, but faces challenges related to stability, reproducibility, interpretability, and standardisation. The AG:UAG ratio may serve as a more physiologically meaningful parameter than absolute ghrelin concentrations. Although unlikely to replace established AD or PD biomarkers, ghrelin could augment early-stage detection and differential diagnosis within multi-marker strategies. Future progress hinges on rigorous validation, harmonisation of measurement protocols, and incorporation into longitudinal clinical studies.

1.8 Detection Techniques for Ghrelin Isoforms

1.8.1 Analytical Requirements for Quantifying AG:UAG Ratio

Accurate quantification of the AG:UAG ratio is essential for evaluating the biomarker potential of ghrelin species in neurodegenerative disease. Traditional methods of measuring acyl and unacylated ghrelin, such as ELISA, radioimmunoassay (RIA), and Western blotting, are limited in both sensitivity and selectivity. These techniques typically fail to distinguish between acyl and unacylated ghrelin within the same sample and cannot differentiate between acylated species with varying fatty acid chain lengths. This limitation is partly due to the immunogenic targeting of peptide termini (typically N- or C-termini) while the acyl modification on Ser3 is poorly immunogenic and difficult to detect using standard antibody-based methods.

Given that different ghrelin isoforms may exert distinct biological effects, a more advanced and sensitive analytical platform is needed to reliably quantify the AG:UAG ratio and to characterise the fatty acid moiety bound to acyl ghrelin. Such specificity and resolution can only be achieved using MS-based approaches, which have been instrumental in the initial identification and characterisation of ghrelin isoforms (Nishi et al., 2005; Gutierrez et al., 2008).

1.8.2 Immunoassays: Current Utility and Limitations

Immunoassay-based platforms, including ELISA and RIA, remain widely used for ghrelin quantification due to their relatively low cost, high throughput, and straightforward implementation. However, as outlined in Section 7.1, their reliance on antibodies recognising terminal regions of the peptide provides minimal information about the acyl chain attached to acyl ghrelin. Commercial ELISAs are typically single-plex, requiring separate reactions for acyl and unacylated forms, and they do not capture the full diversity of circulating isoforms.

While lateral flow immunoassays offer potential for rapid, point-of-care applications, they share similar specificity limitations and often have reduced sensitivity compared to laboratory-based assays. Consequently, although immunoassays are valuable for large-scale screening and clinical workflows, they are inherently limited in their ability to resolve the detailed structural and compositional features necessary for precise AG:UAG quantification in biomarker discovery.

1.8.3 MS-Based Techniques: MALDI-TOF and LC-MS/MS

MS offers greater analytical power for the detection of neuropeptides such as ghrelin. Both MALDI-TOF and LC-MS/MS are capable of providing high specificity, sensitivity, and the ability to resolve small structural differences. MALDI-TOF is attractive for its rapid throughput and ease of sample preparation; however, it suffers from matrix effects, reduced resolution, and poor signal reproducibility, especially in complex biological matrices like plasma. Although MALDI can simultaneously detect acyl and unacylated ghrelin, its capacity to resolve minor mass shifts associated with different fatty acid chains remains limited.

LC-MS/MS enables precise quantification through multiple reaction monitoring (MRM), a targeted acquisition mode in which specific precursor ions (representing the peptide of interest) are selected and fragmented, and only predefined fragment ions are monitored. This double level of selectivity, first for the intact molecule, then for a characteristic fragment, greatly enhances both specificity and sensitivity. MRM is especially useful for detecting low-abundance biomarkers in complex matrices like plasma, as it reduces background noise and improves reproducibility. Several studies have used LC-MS to quantify acyl and unacylated ghrelin in human plasma (Rauh et al., 2007; Sidibe et al., 2014), but a protocol allowing simultaneous monitoring of all

ghrelin isoforms using MRM has not yet been established. One significant complication in MS-based workflows is the requirement for deproteination of plasma, as high-abundance proteins interfere with signal quality. This necessitates complex and time-consuming sample preparation, which can result in analyte loss and variability.

1.8.4 Emerging Tools: BAMS and Immune-Affinity MS

Bead-assisted mass spectrometry (BAMS) is an emerging tool designed to overcome some of the limitations of traditional MS workflows. BAMS allows for direct analysis of plasma without the need for extensive protein removal. In this approach, magnetic or polymeric beads are functionalised with affinity ligands to selectively capture target peptides from complex matrices. After washing and elution, captured peptides can be analysed directly by MALDI or LC-MS. BAMS enhances throughput and reproducibility while reducing sample loss, making it a promising platform for the sensitive detection of ghrelin isoforms.

Another promising approach is immune-affinity MS (IA-MS), which combines antibody-based enrichment with MS detection. This method has demonstrated considerable success in quantifying low-abundance proteins in plasma, such as Aβ and tau isoforms. In AD research, IP-MS has achieved diagnostic accuracies upwards of 90% for Aβ42/Aβ40 ratios (Ovod et al., 2017; Janelidze et al., 2021). The key advantage of IA-MS is its ability to combine the selectivity of immunoaffinity enrichment with the structural resolution of MS, enabling both qualitative and quantitative assessment. In contrast, immunomagnetic reduction (IMR), which detects antigen-antibody binding through changes in magnetic signals without prior peptide enrichment, has shown limited ability to detect differences in plasma Aβ42 levels between Alzheimer's patients and controls (Teunissen et al., 2018). This discrepancy likely arises from IMR’s lower specificity and sensitivity compared to IA-MS, as matrix interference and peptide aggregation can obscure subtle biomarker changes. Such findings show a broader uncertainty in protein biomarker research, even biologically relevant targets may go undetected if the analytical method lacks sufficient precision, sensitivity, or robustness in complex biological matrices like plasma. Applying IA-MS to ghrelin detection could allow targeted enrichment of acyl ghrelin while preserving its labile lipid moiety, something traditional immunoassays cannot achieve. To date, this approach remains

underexplored for ghrelin but offers substantial promise, particularly when combined with multiplexed MRM workflows.

1.8.5 Importance of Lipid Moiety Retention and Capture Strategies

A critical consideration in acyl ghrelin quantification is the preservation of the labelled acyl modification, most commonly an octanoyl group bound to the Ser3 residue of the peptide. This lipid moiety is highly susceptible to enzymatic hydrolysis by esterases present in plasma, leading to rapid conversion of acyl to unacylated ghrelin ex vivo. Therefore, pre-analytical strategies must include immediate sample acidification, cooling, and the addition of esterase inhibitors (e.g., AEBSF or PMSF) to prevent degradation. Failure to stabilise acyl ghrelin during sampling and storage can result in significant underestimation of its physiological levels.

Capture strategies that protect and preserve the lipid moiety during extraction are equally vital. For example, affinity enrichment using lipid-specific antibodies or hydrophobic interaction materials can preferentially retain the acylated form. Additionally, selective SPE techniques using C18 columns under acidic conditions may offer a balance between recovery and acyl group preservation. These strategies may be essential for measuring accurate and biologically meaningful AG:UAG ratios, particularly when these metrics are intended for clinical or diagnostic use.

1.8.6 Lessons from Neurodegenerative Biomarker Assays

The development of blood-based biomarkers for neurodegenerative diseases, particularly AD, provides a valuable framework for evaluating the analytical and translational requirements needed to advance ghrelin isoform detection. Techniques such as IP-MS have been pivotal in detecting the plasma Aβ42/Aβ40 ratio with high diagnostic accuracy. For instance, the assay developed by Ovod et al. (2017), which utilised proteolytic digestion of plasma-derived Aβ peptides prior to MS analysis, achieved an area under the curve (AUC) of 0.89, demonstrating strong concordance with CSF-based measurements. However, these assays are limited by peripheral Aβ expression and the influence of comorbid conditions such as cardiovascular disease, which can confound the plasma Aβ42/Aβ40 ratio (Lewczuk et al., 2010; Pannee et al., 2014; Roeben et al., 2016).

Similarly, the measurement of pTau isoforms using MS and SIMOA platforms has yielded promising results. Among the pTau isoforms, pTau217 has shown the greatest

performance, with an R^2 value of 0.89 between plasma and CSF, compared to 0.76 for pTau181 and 0.30 for pTau231 (Janelidze et al., 2022). These findings have been replicated using immunoassay platforms, with Spearman's correlation coefficients ranging from moderate (<0.65) to strong (>0.86), depending on the isoform and cohort (Bayoumy et al., 2021).

Importantly, recent developments have seen the translation of these research assays into clinically validated diagnostics. In May 2025, the U.S. Food and Drug Administration (FDA) granted marketing authorisation for the Lumipulse® G β-Amyloid Ratio (1-42/1-40) test and Lumipulse® G pTau217 assay for use in adults aged 55 years and older presenting with cognitive impairment (FDA, 2025). This marked the first FDA-cleared blood-based biomarker test for AD pathology, showing a 91.7% concordance rate with PET or CSF-based biomarker status, and a 97.3% negative predictive value when used in symptomatic individuals (Quanterix, 2025). These advances affirm that blood-based biomarkers can achieve clinically relevant diagnostic accuracy through integration of immunoaffinity enrichment and high-resolution detection, whether via MS or advanced immunoassay systems.

Moreover, the measurement of NfL, has demonstrated utility as a general marker of neurodegeneration. SIMOA-based assays have shown a high correlation between CSF and plasma concentrations of NfL ($R^2 = 0.89$), and increased levels in individuals with mild cognitive impairment (MCI) and AD dementia (Gisslen et al., 2016; Preische et al., 2019). However, defining universally accepted diagnostic cut-off values remains challenging due to inter-cohort variability. For example, Palmqvist et al. (2020) reported markedly different plasma NfL cut-offs across two cohorts: in the Swedish BioFINDER-1 study (mean age ~72 years; 57% female), the optimal cut-off was 41.9 pg/mL (sensitivity 82%, specificity 32%), whereas in the independent BioFINDER-2 cohort (mean age ~70 years; 53% female), the optimal cut-off was 26.5 pg/mL (sensitivity 67%, specificity 38%). BRAAK staging data were not uniformly available, but the cohort included individuals spanning the preclinical to dementia stages of AD, including cognitively unimpaired amyloid-positive participants.

These differences highlight the difficulty of determining universally valid cut-off points for NfL, where a higher threshold may lead to under-diagnosis of early-stage cases, and a lower threshold may increase false positives. Moreover, while NfL is a sensitive marker of axonal damage, it is not disease-specific and may be more valuable when

interpreted in combination with other pathophysiologically relevant biomarkers, such as Aβ or tau, to improve diagnostic accuracy and stage-specific discrimination in neurodegenerative disease contexts.

Taken together, these developments provide key lessons for the analytical validation of ghrelin isoforms. First, high diagnostic value can be achieved through targeted enrichment strategies combined with sensitive and specific detection platforms. Second, isoform-level resolution, as demonstrated with pTau217 and Aβ peptides, is essential to capture biologically meaningful variation. Finally, regulatory acceptance of blood-based biomarkers requires robust validation across diverse populations and careful control of pre-analytical and clinical confounders. These insights will inform the approach taken in this thesis to develop mass spectrometry-based techniques for quantifying AG:UAG ratios and characterising acyl ghrelin variants in plasma.

By drawing on these methodological frameworks, future ghrelin isoform assays may benefit from similar multi-modal strategies, particularly those that combine immuno-enrichment with lipid-stabilising workflows and high-resolution MS detection. The development of such robust analytical platforms will be critical in validating ghrelin's potential as a blood-based biomarker for neurodegenerative disease.

1.9 Sample Preparation and Analytical Considerations

1.9.1 Challenges of Complex Biological Fluids

Identifying reliable blood-based biomarkers for neurodegenerative diseases poses several significant challenges (see Figure 1.4). For a biomarker to be detectable in blood, it must cross the BBB, often resulting in markedly lower concentrations compared to CSF (Hampel et al., 2018). Moreover, biomarkers may exhibit diurnal fluctuations, with protein levels in both blood and CSF varying throughout the day (Hampel et al., 2018). The timing of sample collection thus critically impacts assay sensitivity, as biomarker levels may peak at various times in CSF and blood compartments. Importantly, some biomarkers may not cross the BBB at all, limiting their utility in blood-based diagnostics (Hampel et al., 2018; Snyder et al., 2014; Zetterberg & Burnham, 2019).

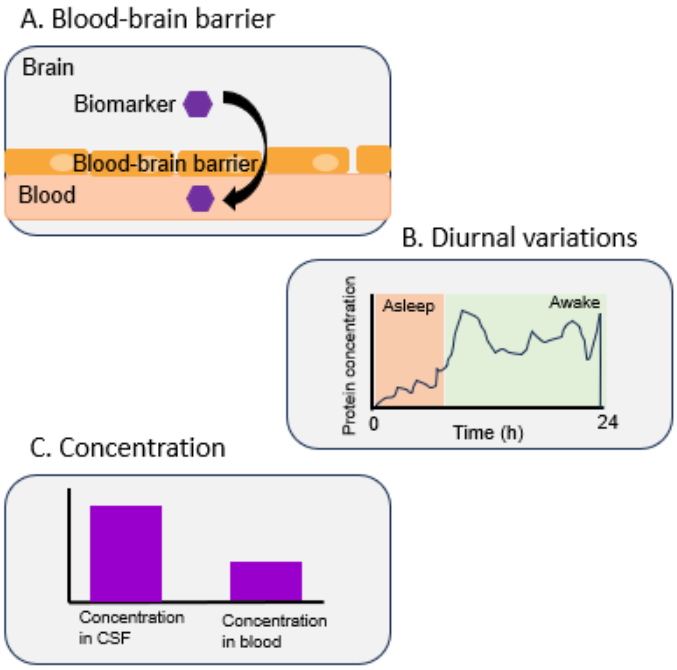

Figure 1.4 Challenges of measuring blood-based biomarkers for CNS disorders.

A: The biomarker must be able to cross the blood-brain barrier to be detected. B. Diurnal variations in protein levels. Both the blood and the CSF exhibit fluctuations in protein levels during the day. As biomarker levels can peak at varying times for CSF and blood, the biomarker assay must sample at a peak concentration or sufficient sensitivity to detect the biomarker. C. Variation of concentration. Biomarker levels can differ between blood and CSF, and plasma levels are often lower (Adapted from Hampel et al., 2018).

Blood is a complex biological matrix composed of diverse compounds such as proteins, lipids, and nucleic acids, which contribute to variability in analytical results and pose additional challenges for biomarker quantification (Hampel et al., 2018; Lista, Faltraco, Prvulovic, & Hampel, 2013). The presence of heterophilic antibodies, endogenous antibodies that can interact non-specifically with assay antibodies, can cause assay interference, leading to false-positive or false-negative results. This phenomenon is more pronounced in blood, compared to CSF where antibody levels are significantly lower (Zetterberg & Burnham, 2019). Additionally, proteolytic degradation of biomarkers can occur in plasma or during hepatic metabolism, further complicating accurate detection (Hampel et al., 2018).

Another layer of complexity arises from comorbid conditions common in patients with neurodegenerative diseases. Disorders such as respiratory, rheumatic, and cardiovascular diseases frequently coexist, potentially altering circulating protein levels and confounding biomarker interpretation (Henriksen et al., 2014).

1.9.2 Clearance and Simplification: Need for Lipid-Sensitive and Specific Capture

A critical analytical consideration for acyl ghrelin detection is the molecule's biochemical instability. Acyl ghrelin, characterised by an essential n-octanoyl lipid modification on serine-3, is highly susceptible to enzymatic deacylation by circulating esterases such as butyrylcholinesterase (Chen et al., 2015; Kojima et al., 1999). This rapid degradation necessitates the use of specialised sample collection methods, including acidification and esterase inhibition, to preserve the active form for analysis (De Vriese et al., 2004). Effective capture of acyl ghrelin thus requires lipid-sensitive analytical techniques or antibodies capable of discriminating the acylated isoform.

In the context of blood sample complexity, simplifying the matrix via chromatographic clearance or selective enrichment prior to analysis becomes essential. Techniques such as immunoaffinity enrichment or LC are often employed to reduce background noise and improve sensitivity (Blatnik & Soderstrom, 2011). The decision to employ chromatographic clearance versus direct immunoassays depends on assay goals, throughput, and available instrumentation, representing a key technical decision point in assay development.

1.9.3 Existing Antibodies and Epitope Limitations for Acyl Ghrelin

A limiting factor in acyl ghrelin biomarker development is the availability and specificity of antibodies. Most commercial antibodies target peptide epitopes that do not discriminate between acyl and unacylated forms, which can confound measurements of the biologically active isoform (Pemberton & Richards, 2008). Antibodies recognising the lipid modification are less common and technically challenging to produce due to the small and labile nature of the acyl group.

Consequently, assays must be carefully validated to ensure specificity for acyl ghrelin, often relying on complementary methods such as mass spectrometry to confirm isoform identity (Cao et al., 2018; Hornsby et al., 2022). This epitope limitation illustrates the need for multi-modal analytical approaches that combine immunochemical and chromatographic techniques.

1.9.4 Chromatographic Clearance or Selective Enrichment: Technical Decision Points

The analytical workflow for ghrelin isoform detection must balance sensitivity, specificity, and practicality. Bottom-up approaches employing sample fractionation via LC prior to MS can enrich target peptides, reduce matrix effects, and improve quantitative accuracy (Blatnik & Soderstrom, 2011). However, these methods increase assay complexity and processing time. Alternatively, immunoassays offer high throughput but may suffer from cross-reactivity and lack of isoform specificity without prior chromatographic separation (Blatnik & Soderstrom, 2011; Pemberton & Richards, 2008). Emerging hybrid approaches such as IA-MS seek to combine the advantages of antibody-based capture with the molecular resolution of MS (Hornsby et al., 2022).

The choice of method depends on intended application: discovery-phase studies may prioritise sensitivity and isoform discrimination, while clinical screening may emphasise throughput and reproducibility.

1.9.5 Bottom-Up Biomarker Development: From In Vitro Models to Human Cohorts

A robust biomarker pipeline often begins with mechanistic in vitro models to characterise biomarker biology, isoform biochemistry, and degradation pathways under controlled conditions (Chen et al., 2015). This foundational understanding informs assay design and sample handling protocols. Subsequently, assays are optimised in complex biological matrices, including plasma and CSF, with careful attention to pre-analytical variables such as anticoagulant choice, processing time, and storage conditions (De Vriese et al., 2004; Blatnik & Soderstrom, 2011). Finally, validated assays are applied to well-characterised human cohorts, including longitudinal studies, to evaluate biomarker performance in clinical settings (Song et al., 2017; Sassi et al., 2022). This phased approach, from molecular characterisation to clinical validation, aligns with established biomarker development frameworks and increases the likelihood of successful translation (Pepe et al., 2001).

In summary, the complexities of biological matrices and the biochemical instability of ghrelin isoforms necessitate carefully optimised analytical workflows balancing sensitivity and specificity. These technical challenges must be considered alongside

economic and practical factors, which will be explored in the following section, addressing the cost comparison between ELISA and MS approaches, health economic implications, and the feasibility of clinical translation in large-scale diagnostics.

1.10 Economic and Practical Feasibility

1.10.1 Cost Comparison: ELISA vs. Mass Spectrometry-Based Approaches

The clinical adoption of ghrelin-based biomarkers is contingent not only upon their analytical robustness but also on economic and practical considerations. This section evaluates the comparative costs of prevalent assay platforms, the broader health economics implications of deploying these biomarkers at scale, and the critical balance between clinical utility and cost-effectiveness in translation to routine practice. In the UK, ELISA assays are commonly used in both clinical and research settings due to their accessibility and ease of use. For ghrelin quantification, specialised ELISA kits are required for both acyl ghrelin and unacylated ghrelin measurements. These kits are typically supplied by Fischer Scientific and produced by Bertin Bioreagent. Each 96-well kit costs approximately £574 (Fischer Scientific UK, 2024), and since both the acyl-ghrelin and unacylated ghrelin assays are necessary to fully characterise ghrelin species, the reagent cost effectively doubles to around £1,148 per 96 samples. This reagent cost translates to roughly £12 per sample just for consumables, excluding labour, equipment depreciation, and overheads. While ELISA platforms require relatively modest laboratory infrastructure, commonly available across NHS and academic labs, the cumulative expense of reagents for large cohort studies or routine clinical screening can be considerable.

By contrast, MS-based approaches necessitate significant initial investment, with high-resolution instruments costing between £250,000 and £450,000 (Medical Research Council, 2020). However, MS assays offer multiplexing capabilities, allowing simultaneous quantification of multiple biomarkers, which can reduce the per-sample cost when scaled appropriately. Current estimates place MS analysis costs at £80 to £250 per sample depending on assay complexity, sample preparation, and throughput (Baker & Thompson, 2021). Despite higher upfront costs and technical complexity, MS methods provide superior specificity and sensitivity, potentially justifying the investment in settings where comprehensive biomarker panels are required.

1.10.2 Health Economics Implications in Large-Scale Diagnostics

Implementing biomarker assays at scale requires careful consideration of health economic impacts, extending beyond assay costs to include effects on patient outcomes and healthcare resource allocation. Early, accurate detection of neurodegenerative diseases via ghrelin-based biomarkers may enable timely therapeutic interventions and delay disease progression thus potentially reducing overall long-term care expenditures and improving quality-adjusted life years (Pepe et al., 2001; Hampel et al., 2018). Health economic models should integrate assay sensitivity and specificity, disease prevalence, and downstream cost savings from early diagnosis. While MS-based techniques currently incur higher upfront and operational expenses, their enhanced diagnostic accuracy may justify deployment in specialised or high-risk populations. In contrast, ELISA-based approaches may be more suitable for broad population screening due to lower cost and operational simplicity, albeit with potential compromises in analytical specificity and biomarker isoform resolution (Blatnik & Soderstrom, 2011; Pemberton & Richards, 2008).

1.10.3 Clinical Translation Potential and Cost-Benefit Balance

Successful clinical translation depends on selecting the right platform for the right stage of the diagnostic pathway. While MS offers molecular-level specificity and can unambiguously differentiate ghrelin isoforms and post-translational modifications, alternative multiplex immunoassay platforms, such as SIMOA and Luminex, are increasingly used in UK research and diagnostic laboratories. SIMOA enables ultra-sensitive detection of low-abundance proteins, while Luminex facilitates simultaneous analysis of multiple analytes via bead-based immunoassays. Both generally require lower capital investment than MS and can deliver high-throughput results within shorter assay times (National Institute for Health and Care Excellence [NICE], 2023).

However, these immunoassay-based platforms share the same dependency on antibody recognition as ELISA, meaning that analytical specificity for lipid-modified peptides such as acyl ghrelin can be limited. Given these trade-offs, a tiered diagnostic approach could be economically and clinically optimal: rapid, large-scale screening using ELISA/multiplex immunoassays, followed by confirmatory MS analysis for cases requiring detailed isoform resolution. To achieve adoption, assays must undergo rigorous validation, secure reimbursement pathways, and demonstrate clinical utility within robust health economic frameworks.

1.11 Mass Spectrometry

1.11.1 Overview

MS is a highly sensitive analytical technique that determines the mass-to-charge ratio (m/z) of ionised molecules. In a typical MS workflow, an analyte is (1) converted from solution or solid phase into gas-phase ions by an ionisation source, (2) separated according to m/z by a mass analyser, and (3) detected to produce a mass spectrum. The spectrum displays signal intensity versus m/z and serves as a fingerprint that can be used for identification (via exact mass and fragmentation patterns) and quantification (via signal intensity or extracted ion chromatograms).

MS is widely used in proteomics and lipidomics, offering high selectivity, low sample consumption, and the ability to quantify multiple analytes simultaneously, including ghrelin isoforms. In this thesis, MS was applied using three platforms: **MALDI-TOF**, **LTQ-Orbitrap**, and **electrospray Ionisation (ESI) via Nanomate**.

Key performance parameters are:

- **Mass accuracy**: closeness of measured m/z to true m/z (important for elemental composition and confident assignment).
- **Resolving power**: ability to distinguish near-isobaric ions (critical for complex peptide mixtures and PTM discrimination).
- **Sensitivity**: lowest amount detectable with acceptable signal-to-noise.
- **Dynamic range and linearity**: range over which signal is proportional to analyte concentration (affects quantitation).

1.11.2 Ionisation Techniques

Ionisation is critical as MS detects only charged molecules. Two common ion sources used in this thesis are:

- **ESI**: Produces multiply charged ions via a high-voltage spray, ideal for coupling with LC and suitable for peptides <10 kDa. It operates in positive mode for ghrelin detection.
- **MALDI**: Produces mostly singly charged ions by laser ablation of a matrix–analyte crystal. MALDI is useful for analysing intact peptides, including ghrelin.

1.11.3 Mass Analysers

MS instruments separate ions by their m/z ratios using various analysers. This thesis employed:

- **Time-of-Flight (TOF)**: Separates ions based on their flight time. Used with MALDI, TOF provides high sensitivity and is suitable for intact peptide detection.
- **Quadrupole and Linear Ion Trap (LTQ)**: Used for ion filtering and fragmentation.
- **Orbitrap**: Offers high-resolution and accurate mass measurements via ion oscillation in an electric field, ideal for complex peptide mixtures.

1.11.4 Tandem MS (MS/MS)

Tandem MS provides structural information by fragmenting a precursor ion and recording its fragment ion spectrum. Fragmentation techniques commonly used for peptides include collision-induced dissociation (CID) in ion traps/quadrupoles, higher-energy collisional dissociation (HCD) in Orbitrap systems, and electron-transfer dissociation (ETD) for labile PTMs or preserving labile modifications. MS/MS is essential for peptide identification, localisation of PTMs and distinguishing acylation variants of ghrelin

1.11.5 Summary Table of Mass Spectrometry platforms used

Instrument	Ionisation Method	Mass Analyser(s)	Key Features	Application in Thesis
MALDI-TOF	MALDI (soft ionisation)	TOF	Singly charged ions, fast analysis, high sensitivity, matrix-assisted	Detection of intact AG and UAG peptides
LTQ-Orbitrap	ESI (through atmospheric pressure ionization, API)	Linear Ion Trap + Orbitrap	High resolution, accurate mass, MS/MS via CID and tandem-in-time	Structural analysis and quantification via LC-MS
Nanomate (ESI)	Chip-based ESI (NanoESI)	Coupled with Orbitrap	Low sample volume, gentle ionisation, ideal for low-abundance analytes	Direct infusion of ghrelin isoforms for MS analysis

Table 1.2 Summary Table: MS Platforms Used.

1.12 Hypotheses and Aims

Primary Hypothesis: MS-based techniques, particularly when combined with enrichment strategies such as BAMS and LC-MS provide a robust analytical platform for detecting ghrelin variants in clinical matrices.

1.13 Research Objectives

1. Develop a MALDI-TOF method that can identify unacylated and acyl ghrelin within the same sample.
2. Develop an LC-MS method that can detect both ghrelin species simultaneously.
3. Optimise the extraction of ghrelin from plasma.
4. Develop a bead-assisted mass spectrometry method that can detect ghrelin.
5. Compare the bead-assisted mass spectrometry method with the use of traditional ELISA.

1.14 Context of Thesis within Wider Research Projects

Parts of the work presented in this chapter contributed to wider research efforts within our group and associated collaborations, combining both academic research and translational studies. This chapter focuses on the optimisation of mass spectrometry workflows to enable the detection and quantification of ghrelin species, with the aim of advancing the discovery of ghrelin as a potential biomarker.

Relevant outputs from this PhD include:

- *Review article* on ghrelin biology and its roles in brain and metabolic health, published in *Cells* (PMC9280358): https://pmc.ncbi.nlm.nih.gov/articles/PMC9280358/
- Contribution to a *study* investigating the impact of the 5:2 diet on neurogenesis and systemic biomarkers (*Neurobiology of Aging*, PMID: 37987211): https://pubmed.ncbi.nlm.nih.gov/37987211/
- Involvement in a *clinical trial* exploring the neuroprotective roles of circulating hormones, including ghrelin, and their interactions with brain-infiltrating T cells (in progress).

These outputs reflect the broad scope of the project, which has combined fundamental analytical method development with applied research questions relating to brain health, metabolism, and potential clinical biomarkers.

Chapter

2. Materials and Methods

2.1 Materials

2.1.1 Equipment

Product	Supplier	Product Number
QuickPick starter kit with tools and tips	Catlag + medsystems	QRE-24001SP
QuickPick Tips Bulk 500	Catlag + medsystems	QRE-24500
Bruker AutoFlex MALDI Mass Spec.	Bruker	
Eppendorf ThermoMixer C	Eppendorf	
BAMS Starter Kit	Adeptrix	C0008
Unacylated Ghrelin (human) easy sampling EIA kit	Bertin	501190
Acylated ghrelin (human) easy sampling EIA kit	Bertin	501160
Oasis PST uElution Method Development Plate	Oasis	186004713
MALDI-TOF stainless steel target	Bruker	8280784
Ziptips	Millipore	ZTC185096
Lowbind tips 1-200 ul	Sorenson	10470T
0.1-10ul gradient multi-fit pipette tips	Sorenson	23580T
Waters QuanRecovery MaxPeak 12x32 mm Polypropylene 300 ul screw cap vials	Waters	186009186
Protein LoBind tube 0.5 mL	Eppendorf	022431064
Protein LoBind Tube 1.5 mL	Eppendorf	022431081
3 um Fortis C18 150x2.1 mm		F18-020385190
VACUETTE® TUBE 6 mL K3E K3EDTA	Greiner Bio-one	456038
Oasis HLB 6 cc Vac Column, 200 mg Sorbent per Column, 30 µm,	Waters	WAT106202
Amicon® Ultra 0.5 mL Centrifugal Filters – 3kDa	Millipore	UFC5003
Amicon® Ultra 0.5 mL Centrifugal Filters – 10kDa	Millipore	UFC5010

Table 2.1 Equipment and product codes.

2.1.2 Reagents and Solvents

Item	Product code	Company
5-sulfosalicylic acid dihydrate >99%	5965-83-3	Sigma Aldrich
Trichloroacetic acid, ACS, 99% min	76-03-9	Alfa Aesar
Ethanol absolute ≥99.8%	64-17-5	VWR Chemicals
Water, HPLC for Gradient Analysis	7732-18-5	Fisher Chemical W/0106/17 Fisher Scientific
Methanol, for HPLC	67-56-1	Fisher Scientific
Acetonitrile, HPLC grade >99.8	75-05-8	Fisher Scientific
Acetone, analytical reagent grade	67-64-1	Fisher Scientific
α-Cyano-4-hydroxycinnamic acid	28166-41-8	Sigma Aldrich
n-dodecyl-b-D-maltoside, UTROL grade	324355-1GM	Merk Millipore
10x Dulbecco's PBS	1960454	MP biomedical
Hydrochloric acid 1.18 analytical grade	H/1200/PB15	Fisher Scientific
Ammonium citrate dibasic	09633-100G	Sigma Aldrich
Ammonium bicarbonate	A6141-5OOG	Sigma Aldrich
Trypsin resuspension buffer	V542A	Progema
Sequencing grade modified trypsin	V5118	Progema
AEBSF (4-(2-Aminoethyl)-benzenesulfonyl fluoride.	A8456	Sigma Aldrich
Potassium chloride	P9541	Sigma Aldrich
DMSO, anhydrous, 99.8% (original DMSO tested)	67-68-5	Thermo Scientific
Pierce DMSO, LC-MS grade (used for the majority of the study)	85190	Thermo Scientific

Table 2.2 Reagents and solvents alongside product codes.

2.1.3 Ghrelin Standards

When indicated, ghrelin standards were used for quantification. A table of the ghrelin standards, including their structures, is shown below (Table 2.3).

Common name	Structure	Counter ion	Peptide purity	Supplier	Product number
Ghrelin (human)	^{n}Octanoyl Gly-Ser-Ser-Phe-Leu-Ser-Pro-Glu-His-Gln-Arg-Val-Gln-Gln-Arg-Lys-Glu-Ser-Lys-Lys-Pro-Pro-Ala-Lys-Leu-Gln-Pro-Arg	TFA	≥95%	Tocris	1463
			≥ 96%	Phoenix	031-30
Des-ghrelin (human)	Gly-Ser-Ser-Phe-Leu-Ser-Pro-Glu-His-Gln-Arg-Val-Gln-Gln-Arg-Lys-Glu-Ser-Lys-Lys-Pro-Pro-Ala-Lys-Leu-Gln-Pro-Arg	TFA	≥95%	Tocris	2260
			≥ 95%	Phoenix	031-32
			>95%	Bachem AG (supplied by Cambridge bioscience)	4042605.1000
Ghrelin (rat)	^{n}Octanoyl Gly-Ser-Ser-Phe-Leu-Ser-Pro-Glu-His-Gln-Lys-Ala-Gln-Gln-Arg-Lys-Glu-Ser-Lys-Lys-Pro-Pro-Ala-Lys-Leu-Gln-Pro-Arg	TFA	>95%	Tocris	1465
			≥ 97%	Phoenix	031-31
Des-ghrelin (rat)	Gly-Ser-Ser-Phe-Leu-Ser-Pro-Glu-His-Gln-Lys-Ala-Gln-Gln-Arg-Lys-Glu-Ser-Lys-Lys-Pro-Pro-Ala-Lys-Leu-Gln-Pro-Arg	TFA	>95%	Tocris	2951
			≥ 95%	Tocris	031-33

Table 2.3 Suppliers for ghrelin standards.

Ghrelin peptides were originally sourced via Phoenix Pharmaceuticals (USA), which is known for high-quality peptides. During the course of the PhD, increasing international shipping costs led to a transition to Tocris Bioscience (UK-based) as an alternative supplier. To ensure consistency and comparability between these sources, MALDI-TOF analysis was performed on both Phoenix and Tocris peptides (Figure 2.1).

Notably, commercially available acylated ghrelin is predominantly octanoylated (C8), which corresponds to a monoisotopic m/z of 3370 for human acyl ghrelin. This chain length is added enzymatically at Ser3 and is crucial for ghrelin's biological activity. While alternative acyl chain lengths (e.g., C6 or C10) are biologically possible and

have been detected in biological samples, such variants are not typically included in commercially available standards.

Given that acyl chain length directly affects the molecular weight of ghrelin, MALDI-TOF is particularly well-suited to detect such differences. A shift of ±14 Da per CH_2 group allows for resolution of alternative acyl species. In our analyses, both Phoenix and Tocris acyl ghrelin preparations consistently showed a peak at m/z 3370, confirming the presence of the expected octanoyl modification and supporting the equivalence of the standards across suppliers.

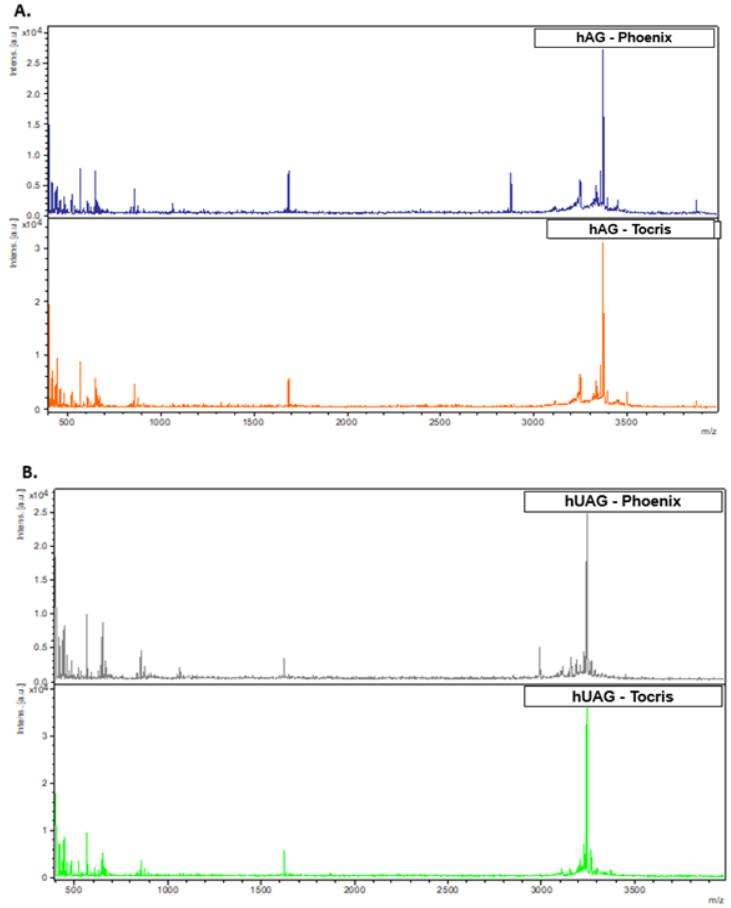

Figure 2.1 Comparison of ghrelin standards from two suppliers – Phoenix and Tocris. Ghrelin standard (15 ng/mL) was prepared in 0.1% TFA and added onto a stainless-steel target in a ratio of 1 part peptide to 3 parts CHCA matrix (5 mg/mL, dissolved in 40% acetonitrile and 0.1% TFA) in a volume of 1.5 µL.

A. hAG. B. hUAG. Both companies supplied standards of high purity.

Upon investigation, both human unacylated and acyl ghrelin provided by Phoenix and Tocris did not show any significant changes, both appearing to be of a high standard.

However, in November 2022, Tocris discontinued only the human unacylated ghrelin peptide and, therefore, an alternative source was needed. Human unacylated ghrelin was purchased from a company called Bachem AG, which was also tested on MALDI-TOF to compare its purity with the Tocris standard (Figure 2.2).

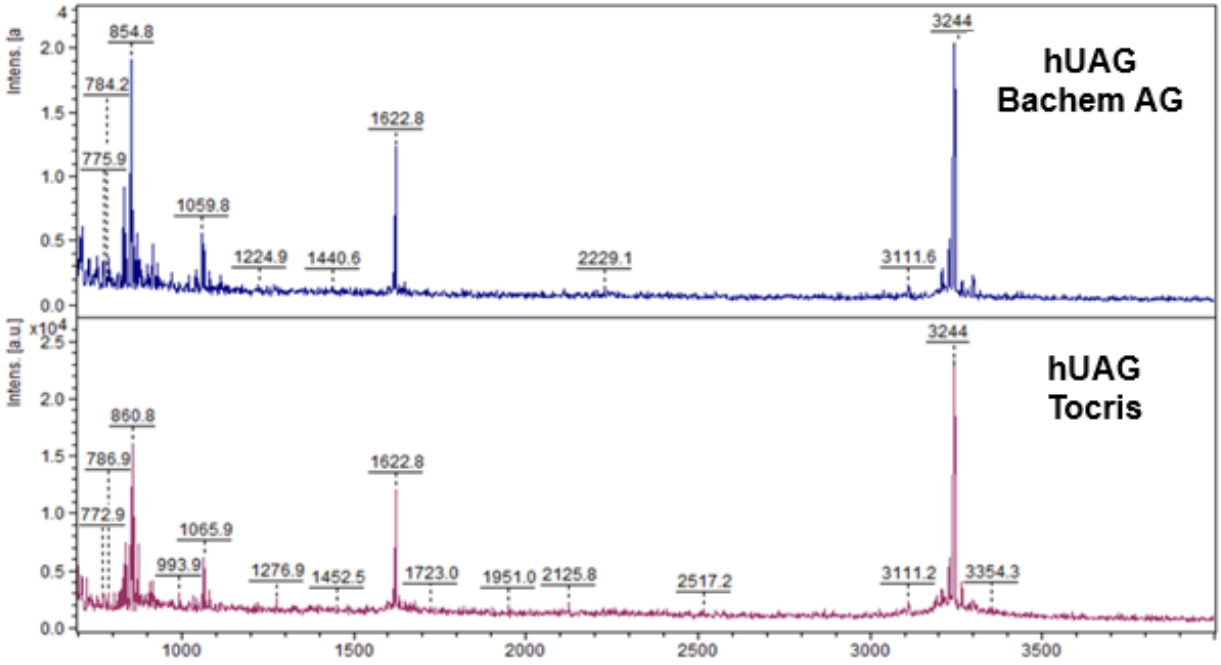

Figure 2.2 Comparison of hUAG supplied by Bachem AG and Tocris.

Ghrelin standard (15 ng/mL) was prepared in 0.1% TFA and added onto a stainless-steel target in a ratio of 1 part peptide to 3 parts CHCA matrix (5 ng/mL, dissolved in 40% acetonitrile and 0.1% TFA) in a volume of 1.5 µL No differences of concern were noted.

Similarly, with the switch from Phoenix to Tocris, no significant differences were seen within the standard from Bachem AG, both standards from Tocris and Bachem AG showed a similar purity.

2.2 Blood and Plasma Collection

Human donor blood was collected (Swansea University Medical School (SUSM) Research Ethics Committee (RESC), project reference 2022-0029) into vacutainer ethylene diamine tetraacetic acid-aprotinin (EDTA)-plasma tubes and gently inverted to ensure that the anticoagulant and blood were thoroughly mixed. EDTA functions by chelating calcium ions, thereby preventing coagulation and preserving plasma components, which is essential for downstream peptide analysis (Lippi, Salvagno, Montagnana, & Guidi, 2006). 4-(2-aminoethyl) benzenesulfonyl fluoride hydrochloride (AEBSF) (2 mg/mL) was added and gently mixed to ensure inhibition of proteinase activity. AEBSF is a protease inhibitor that inhibits serine proteases, which is

necessary to avoid the deacylation of acyl ghrelin (Blatnik and Soderstorm 2011). Within 3 hours of blood collection, the blood was centrifuged at 2,000xg for 15 minutes at 4 ± 2°C. After centrifugation, three layers are formed, the top layer being plasma (yellow), the second layer being a thin white layer containing leukocytes and platelets, which is white, and the bottom red layer containing red blood cells. Plasma was transferred to separate sterile Eppendorf tubes (1.5 mL), and each sample was labelled and stored at -80°C until required.

2.3 Ghrelin Extraction

Ghrelin was extracted via protein precipitation followed by SPE. Optimisation for protein precipitation and SPE is described in 3.2.3 and 3.2.4 but briefly, plasma samples at 1 mL first underwent protein precipitation following the addition of 500 µL sulfosalicylic acid. Samples were then placed on ice for 30 minutes followed by a 40-minute centrifugation at 17,500xg. After protein precipitation, SPE was carried out using a Hydrophilic-lipophilic balance (HLB) column with the following protocol: The columns were washed and conditioned by adding 1 mL of 60% acetonitrile in 0.1% TFA repeated three times, followed by 1 mL of saline three times, and then loading of the samples. After the samples were loaded and washed with 1 mL 5% acetonitrile in 0.1% TFA followed by 1 mL 10% acetonitrile in 0.1% TFA, and finally the samples were eluted with 500 µL of 60% acetonitrile in 0.1% TFA.

2.4 Ghrelin Analysis by MALDI-TOF

2.4.1 Mass Spectrometer

The MALDI-TOF Bruker ultrafleXtreme was used for the analysis in positive ion reflector mode (studies in linear mode were attempted and stated where applicable). The laser used was a smartbeam2, version 2.

Refer to Chapter 3.2 for the optimisation of MALDI-TOF for ghrelin analysis. Standard ghrelin solutions and dilutions were made in 0.1% TFA and spotted on a stainless-steel target in a ratio of 1-part peptide to 3-part matrix α-cyano-4-hydroxycinnamic acid (CHCA, 5 ng/mL) dissolved in 40% acetonitrile and 0.1% TFA in a volume of 1.5 µL. Each sample was spotted in triplicate on the target, with two MS acquisitions carried out per spot. This resulted in six spectra being obtained for one sample. Flex analysis 3.3. was used to analyse the data, which was first processed using smooth and

subtractive functions from the baseline before the identification of the peaks. Relative peaks were exported to Excel, followed by a GraphPad prism for analysis.

2.4.2 MALDI Target Cleaning Procedure

After each experiment, the MALDI-TOF target was cleaned. The cleaning procedure was optimised during the work and is stated throughout the chapter.

Cleaning Procedure 1:

1. The sample/matrix spots were cleaned from the surface of the MALDI target plate with a wet tissue immersed in 70% ethanol.
2. Wet a tissue with water and wipe the surface of the MALDI target.
3. Let the target completely dry for at least 15 minutes at room temperature.

Cleaning procedure 2:

1. The sample/matrix spots were cleaned from the surface of the MALDI target plate with a wet tissue immersed in 70% ethanol.
2. Cover the target with a layer of 80% TFA diluted in HPLC-grade water aqueous TFA (100 µL).
3. Rinse the target with deionised water and wipe dry.
4. Let the target completely dry for at least 15 minutes at room temperature.

Cleaning procedure 3:

1. The sample/matrix spots were cleaned from the surface of the MALDI target plate with a wet tissue immersed in 70% ethanol.
2. Transfer the MALDI target to a crystalising dish (8x4 cm) and overlay the surface of the target with 70% ethanol. Place in the ultrasonic bath and sonicate for 5 minutes.
3. Cover the target with a layer of 80% TFA diluted in HPLC-grade water (100 µL).
4. Rinse the target with deionised water and wipe dry.
5. Let the target completely dry for at least 15 minutes at room temperature.

2.4.3 Data and Acquisition

Flex analysis 3.3 was used for data analysis. Processing of the mass spectrum contained smoothing and subtracting the baseline from the mass spectrum and using

the find toggle to identify the masses. The output was recorded in an Excel document / GraphPad prism, where data analysis was carried out.

2.4.4 Statistical Analysis

All statistical analyses were conducted using GraphPad Prism (version 8.0.1). Throughout the study, two-way analysis of variance (ANOVA) was used to assess the effects of experimental conditions on ghrelin signal intensity. This approach was applied to compare the influence of two independent factors—such as acetonitrile concentration, matrix composition, or ionisation parameters—and ghrelin form (acylated vs. unacylated)—on MALDI-MS signal intensity. Two-way ANOVA enabled assessment of both main effects and interactions between variables. Where significant effects were observed, Tukey's multiple comparisons test was used for post hoc analysis to identify specific group differences while controlling the family-wise error rate. Assumptions of normality and homogeneity of variance were assessed using Prism's built-in diagnostics, and statistical significance was defined as $p < 0.05$.

For each MALDI-MS experiment, two laser shots were acquired per spot across three spots per sample, yielding six spectra per run. Each run was independently repeated on three separate days to account for both intra- and inter-run variability. Unless otherwise specified, the six spectra from each run were averaged to generate a single mean intensity value per sample per day. These daily averages were then compared across experimental conditions. All graphical data are presented as mean ± standard error of the mean (SEM), reflecting the precision of the group mean estimates. For transparency, when n = 3, this refers to three independent experimental runs, reflecting inter-run variability. In cases where only intra-run variability is shown, n is reported as 1.

2.5 Ghrelin Analysis by ESI-MS/MS

To help optimise the conditions for LC-MS, we first evaluated the ghrelin standards using the Triversa Nanomate (Advion) coupled with a Thermo Scientific LTQ Orbitrap XL. All standards were diluted in 20% mobile phase B for LC-MS and added to a 96-well plate compatible with Nanomate which is held at 10°C. The acquisition was first required in FTMS where the CID was altered (ranging from 20-23) until a stable signal of the ghrelin peptide was achieved, allowing the identification of the ions of the MS2 products in ITMS.

2.5.1 Positive Ion Nano Spray Settings

Sample volume injected: 8 µL.

The volume of air to aspirate after the sample: 1.5 µL.

Gas pressure: 0.4 psi.

Voltage to apply: 1.53 kv.

2.6 Ghrelin Analysis by LC-MS/MS

Intact ghrelin species: Ghrelin samples were made to a concentration in the range of 0.08-80 ng/mL (depending on the experiment) and were diluted in 0.1% plasma using 20% acetonitrile and water.

Trypsin digestion of ghrelin: for protease digestion, trypsin (Progema, V5117) was added to a final protein: protease ratio of either 1:100 or 1:20 (w/w). For the 1:20, a mixture of, 4 ng/mL of trypsin (Progema, V5117), 80 ng/mL of ghrelin, and 50 mM ammonium bicarbonate was added and placed on a shaker overnight at 37°C at 500 rpm. For the 1:100, a mixture of 0.80 ng/mL of trypsin, 80 ng/mL of ghrelin, and 50 mM ammonium bicarbonate was added and placed on a shaker overnight at 37°C at 500 rpm. After overnight incubation of 16 hours, 2% of acetic acid was added to the mixtures and centrifuged for 20 minutes at 9000xg, 37°C.

For method development, please refer to Chapter 4.2.3. Ghrelin samples either intact or tryptic peptides were placed in a cooling tray set to 4 ° C in an HPLC autosampler (Ultimate 3000). The sample was injected by sampling the needle at either 1 µL or 20 µL and loaded into the sample loop, to be injected into the mobile phase within the HPLC system. Unless stated otherwise, the mobile phase A consisted of water, 2% acetonitrile 0.2% acetic acid, and 1% dimethyl sulfoxide (DMSO) while mobile phase B consisted of acetonitrile with 0.2% acetic acid and 1% DMSO. Separation of the ghrelin peptide was carried out on a Fertis C18 column (3 µM, 150x2.1 mm, F18-020703) at a flow rate of 200 µL/min. The duration of the run was 25 minutes with a 5-minute equilibration step before the next run could begin. Thermo Xcalibur software was used to identify correct peaks with MS2 spectra of the targeted species and was used to confirm the identification. Peak lists and their intensities were exported to Excel, and statistical analysis was performed using GraphPad prism.

2.6.1 ESI Source with Orbitrap Conditions

Sheath Gas flow rate: 0 µL/min.

Spray voltage: 0 kv.

Capillary temperature: 200°C.

Capillary voltage: 39 kv.

2.6.2 Data and Acquisitions

Confirmation of the ghrelin species was made by manual analysis of the MS2 spectra of the target species using Thermo Xcalibur software. Data was outputted to Excel for organisation and the generation of calibration curves. Statistical analysis was carried out using GraphPad prism, focusing on a two-way ANOVA with Tukey post hoc analysis, and $P<0.05$ was considered statistically significant.

2.7 BAMS

2.7.1 BAMS Optimisation for Reference Kit

2.7.1.1 BAMS Single Bead Immunocapture for Reference Kit

BAMS reference beads (#21070002, Adeptrix) were provided from the BAMS reference peptide immunocapture kit (SKU C0124, Adeptrix), the entire 15 beads of the reference beads were added to a 1.5 mL Eppendorf and incubated overnight at 4°C on the ThermoMixer at 1,200 rpm with the lyophilised reference protein (#21070002, Adeptrix) which was resuspended in 100 µL of HPLC grade water. After overnight incubation, the beads were washed with buffer A (100 mM KCl, 100 mM Tris-HCl, pH 8.0) for 10 minutes, followed by a wash with buffer B (ammonium bicarbonate buffer 10 mM, pH 8.0) twice for two minutes and finally a wash of two minutes with buffer C (deionised water). Each incubation took place on the thermomixer at 1,200 rpm at 4°C with each wash volume consisting of 700 µL.

2.7.1.2 BAMS Single Bead Immunocapture for Ghrelin

ADX086 and ADX088 BAMS antibody kits were provided, each consisting of a 96-well plate with three antibody-functionalised beads per well. For each sample, one well (containing three beads) was used. Prior to incubation, the beads were gently washed in 1× phosphate-buffered saline (PBS) for one minute to remove any residual storage solution. The washed beads were then transferred to an Eppendorf tube and incubated

overnight with the target sample at 4 °C and 1,100 rpm using an Eppendorf ThermoMixer.

Following incubation, the beads were subjected to a series of wash steps to reduce nonspecific binding and remove unbound components. All washes were performed at 500xg and room temperature in a total wash volume of 750 µL. The first wash was carried out using Wash Buffer A, composed of 1 M potassium chloride, 0.2% n-dodecyl-D-maltoside, and 10% acetonitrile in 1× PBS at pH 7.4, and incubated for 10 minutes. This was followed by a second wash using Wash Buffer B, which contained 100 mM potassium chloride, 0.2% n-dodecyl-D-maltoside in 1× PBS at pH 7.4, also for 10 minutes. The third wash step employed Wash Buffer C, composed of 50 mM ammonium bicarbonate (ABC) at pH 8.0, again for 10 minutes. A fourth wash followed using Wash Buffer D, consisting of 10 mM ABC at pH 8.0, for 5 minutes. Finally, the beads were washed twice in deionised water, each for 2 minutes. After each wash step, the beads were carefully transferred into a fresh Eppendorf tube to avoid carryover and cross-contamination.

2.7.1.3 Reaction Beads Arrayed

Microwell slides were assembled using a gold-coated microscope slide and a silicone gasket to create a defined array of 88 × 26 wells. To ensure proper seating, 100 µL of deionised water was added to each chamber, and the assembled slide was balanced with a counterweight and centrifuged at 355 × g for 5 minutes. Following centrifugation, three reference beads were added to at least four separate chambers. Bead positioning was achieved by placing a magnet beneath the slide, inverting the array, and gently tapping it against an absorbent surface to allow the beads to settle into individual wells. Magnetic attraction retained the beads within the wells. The magnet, stainless-steel clips, and silicone gasket were then removed to complete the arraying process. The workflow is illustrated in Figure 2.3.

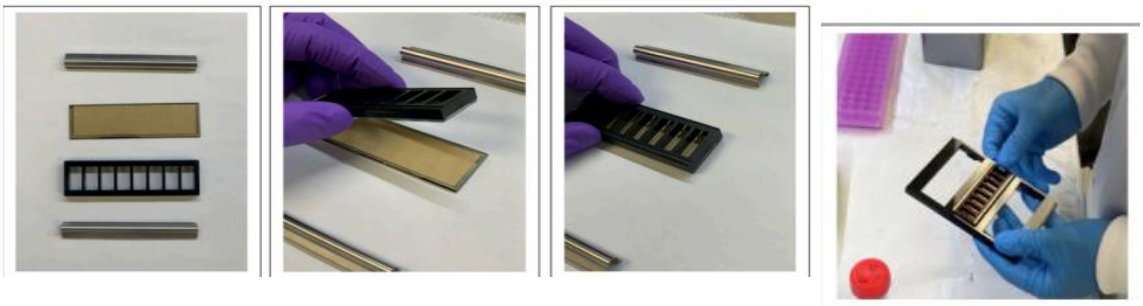

Figure 2.3 Assembling chambered slides for arraying beads. A suitable multi-chamber frame is chosen and placed on top of the microwell array. Its position is secured by inserting stainless steel clips into the groove of the chamber frame. The chambered slide is inserted into the slide tray ready for centrifugation [Adapted with permission from BAMS kit protocol].

2.7.1.4 Eluting Analytes from Bead Arrays through MALDI Matrix Sprayer

Matrix was applied to the microwell array using an automated sprayer that generated a fine mist of α-cyano-4-hydroxycinnamic acid (CHCA) solution. The acidic matrix gradually displaced deionised water in the wells, facilitating analyte elution from affinity beads. As the solvent evaporated, analytes co-crystallised with the matrix and formed discrete spots localised at the bottom of each well. The matrix solution contained 5 mg/mL CHCA, 50% (v/v) acetonitrile, 0.4% (v/v) trifluoroacetic acid (TFA), and 10 mM diammonium citrate. Spraying was conducted at 30 °C, and the matrix was applied immediately after placing the array in the chamber. Following deposition, the array was dried at room temperature for ~30 minutes, during which beads shrank, and matrix crystallised. Beads were then removed using a nitrogen gas stream, followed by removal of the silicone gasket. The array was photographed using a smartphone with flash to identify analyte-containing spots, which appeared as crescent-shaped with a central matrix void. In contrast, matrix-only spots displayed uniform coverage.

2.7.1.5 Measuring Microarrays of Bead Eluted Analytes

This protocol is optimised for use with the Bruker Ultraflex mass spectrometer and Bruker FlexControl data acquisition software. The microwell slide is inserted into a Moveable Top Plate II slide adaptor, positioned on a clean, flat surface (e.g., white laboratory-grade paper) to avoid contamination. Once secured in the adaptor, the assembly is loaded into the instrument's sample chamber. The system is then allowed to reach vacuum equilibrium prior to initiating data acquisition.

Chapter

3. Development of a Routine Method Protocol for the Analysis of Ghrelin using MALDI-TOF

3.1 Introduction

This chapter will develop and optimise a protocol for analysing ghrelin by MALDI-TOF. As outlined in Chapter 1, MALDI-TOF has several advantages in comparison to ELISA, such as its sensitivity, speed, and low sample volume. The ability of MALDI-TOF to detect analytes using small sample volumes makes this method ideal for detecting ghrelin from plasma samples (or even CSF), which can often only be obtained in small volumes from patients. Furthermore, MALDI-TOF has been regularly used within the NHS since 2010, primarily focussing on the control of microbial infections (Elbehiry et al., 2022), including the evaluation of gram-positive and gram-negative bacteria. As such, the integration of MALDI-TOF into clinical practices is firmly established, making it an ideal tool for detecting ghrelin as a blood-based biomarker. In this chapter, MALDI-TOF analysis is conducted using the Bruker ultrafleXtreme MALDI-TOF/TOF instrument. In contrast, Guiterrez et al. utilised the Applied Biosystems Proteomics analyser for ghrelin detection via MALDI-TOF, while Satou et al. (2010) employed the bench-top MALDI-TOF Voyager DE Biospectrometry. Notably, the benchtop MALDI-TOF instrument offers a reduced resolution of 10,000 compared to the Applied Biosystems device, which provides a resolution of 5000, and the ultrafleXtreme instrument, which offers a resolution power exceeding 40,000.

Several careful considerations are required whilst optimising a MALDI-TOF method including matrix selection, the application of matrices such as sample preparation, matrix-to-analyte ratio, laser intensity, and spot size. This chapter will investigate these varied factors to develop a routine method protocol for the analysis of ghrelin using MALDI-TOF.

3.1.1 MALDI Matrix Selection

The selection of an appropriate MALDI matrix is important for the analytical process. The matrix is composed of crystallised molecules that act as a buffer between the sample and the laser. The matrix can also aid in the ionisation of the sample, facilitating its movement along the flight tube so that it may be subsequently detected. There are a small number of universally accepted desirable characteristics of a matrix, one such characteristic is for a matrix to have a molecular weight that is as low as possible while still being large enough to be stable under vacuum and to evaporate

easily. Secondly, to ensure rapid and efficient absorbance of the laser during irradiation, a matrix needs to have a strong optical absorption, usually in the ultraviolet or infrared range. Moreover, for a matrix to be used in aqueous solutions, it must also contain a polar group. Finally, in most cases, the matrix contains a visual aid using a chromophore. Matrices vary greatly and as such have a range of different uses, with some matrices proving better for lipids, while others are more beneficial for proteins or peptides. A matrix that has commonly been reported in the use of peptides is CHCA; this matrix works well in peptides smaller than 5000Da (Beavis 1992; Cohen and Chait 1996) and is therefore suitable for a peptide such as ghrelin. Previous publications of ghrelin detection employed CHCA as a matrix (Guiterrez 2005; Satou et al., 2010). Thus, for my work, I will use CHCA as a matrix for MALDI-MS analysis.

3.1.2 MALDI Matrix Application

In the literature, various techniques have been explored for preparing samples for MALDI analysis, with the dried droplet method being the most used (Gutierrez 2005; Vorm 1994). This method involves mixing a saturated matrix solution with a smaller volume of an analyte solution. A droplet of this mixture, typically 0.3 to 2 µL in volume, is then spotted/deposited on the MALDI plate, which is typically a metal plate equipped with sample application sites. After the droplet has dried at room temperature, resulting in complete evaporation of the liquid and formation of crystals, the MALDI plate containing the sample is loaded into the mass analyser for further analysis. Two distinct follow-up techniques can be utilised for matrix application: the thin-layer and sandwich methods. In the thin-layer method, the droplet of the matrix solution is dried under a gentle stream of air, and subsequently, the sample of interest is deposited on top of the matrix crystal, followed by another round of drying under a gentle stream of air. On the contrary, the sandwich method involves an additional step in which a droplet of matrix solution is deposited on top of the dried thin layer preparation, resulting in the formation of a matrix-sample sandwich. A disadvantage common to both MALDI techniques is a low shot-to-shot reproducibility and a strong dependence on the sample preparation method. Furthermore, spectral variations can be obtained because of the impact position on the surface of the deposited sample. Additionally, the variation in shot-to-shot is observed as the laser irradiates a spot on the sample and therefore ablates layers of the deposit. As a result, the homogeneity

of the deposit is of the highest importance, and improvements in homogeneity give rise to greater reproducibility of the signal detected.

Another difficulty in quantitative work for MALDI is competitive ionisation/ion suppression. In any mixture, there are analytes present that have a higher affinity for charge than others and therefore are more successful when competing for available protons (Duncan, Order and Hunsucker, 2008). As a result, when analysing numerous samples, it is important to keep the sample composition/sample matrix constant. The importance of sample preparation is to prepare the sample into the most appropriate form for analysis which can reduce the complexity of the sample and thus minimising the background and potential interfering peaks. These methods must be highly reproducible with the minimisation of potential contaminants that can cause higher variability between samples and ion suppression. Techniques such as LC-MS can also include an ‘online separation' before MS analysis; however, this is rarely/not used during MALDI-MS as it requires additional instrumentation adding to the complexity, and as a result, during MALDI-MS multiple analytes are present on the target simultaneously and therefore compete for the available charge during each desorption/ionisation event (such as laser shot). As part of the investigations within this chapter, I will investigate different methods for preparing the sample droplet for MALDI-MS analysis.

3.1.3 Ghrelin Extraction from Biological Samples

3.1.3.1 Stabilisation of Ghrelin During Blood Collection

In 2004, Hosoda and Kangawa established the standard for the measurement of ghrelin and noted the importance of appropriate sample preparation due to the instability of acyl ghrelin. Within this study, they assessed the reliability of ghrelin measurements in plasma, the effect of pH on ghrelin stability in plasma, the stability of ghrelin during freeze-thawing, and the half-life of ghrelin in rats. Their study suggested that the presence of ester bonds within acyl ghrelin causes instability within the peptide, with potential degradation taking place both chemically and enzymatically. Enzymatic degradation is likely due to esterase activity in samples that convert acyl ghrelin back to unacylated ghrelin (Gutierrez et al., 2008). Thus, sample preparation is vital to ensure accurate estimation of the AG:UAG ratio (Blatnik et al., 2012). In the study by Hosoda and Kangawa, optimal blood collection included the collection of

blood samples in EDTA tubes and the centrifugation of the samples for 30 minutes at 4°C. In untreated plasma, acyl ghrelin decreased by 40% at 6 hours after storage at 37°C. During this time, ghrelin levels were maintained in samples stored at 4°C or after acidification of plasma to pH 3-4. For samples that underwent four freeze-thaw cycles, no changes in acyl ghrelin levels were observed in acidified plasma while untreated plasma showed a decrease in acyl ghrelin levels from the second freeze-thaw cycle onwards. Finally, the half-life of synthetic human acyl ghrelin was reported to be 8 minutes after intravenous administration in an anaesthetised rat (Hosoda and Kawanga et al., 2004).

Since then, Blatnik and Soderstrom (2010) published a guide to stabilise acyl ghrelin in plasma. The study reported that the half-life of acyl ghrelin in plasma was around 45 minutes, with 50% of acyl ghrelin degraded to unacylated ghrelin at the 60-minute mark. Since Hosoda and Kangawa's work, there have been investigations into the use of a protease inhibitor AEBSF. Blatnik and Soderstorm discovered that the addition of AEBSF to blood did not result in detectable loss of acyl ghrelin and the addition of hydrochloric acid to AEBSF did not show any improvement in the stability of acyl ghrelin. They also concluded that the use of fasted samples treated with AEBSF resulted in the highest levels of ghrelin. In 2016, further investigations were performed to establish the most effective esterase inhibitor to prevent deacylation (McGovner-Gooch et al., 2016). Here, they compared acyl ghrelin levels in blood treated with AEBSF and methoxy arachidonyl fluorophosphonate (MAFP). Overall, MAFP was able to produce a twofold increase in acyl ghrelin compared to AEBSF. This difference arises because AEBSF selectively inhibits serine proteases that cleave peptide bonds, but it does not target esterases responsible for removing lipid modifications such as ghrelin’s octanoyl group. In contrast, MAFP is a broad-spectrum inhibitor of serine hydrolases, including esterases and lipid-modifying enzymes like phospholipases and fatty acid amide hydrolase (FAAH), allowing it to effectively prevent deacylation of acyl ghrelin during sample preparation. However, despite their discovery, when tested by our laboratory group, the addition of MAFP (stock arrived in methyl acetate and diluted into dimethyl sulfoxide before use, 5 μM final concentration added to blood) to blood samples resulted in haemolysis that would affect our work using ELISA kits, and thus we routinely use AEBSF to stabilise our blood samples, including all plasma samples described in this chapter.

3.1.3.2 Internal Standard

A valuable tool to improve the precision of quantitative analysis is the addition of an ISTD before protein precipitation. An ISTD is a standard of a known amount that is added to every sample that is analysed. The selected ISTDs should have chemical and physical properties similar to those of the analyte of interest and, in terms of mass spectrometry, have a comparable ionisation response. As a result, the most appropriate standard would be a stable isotope-labelled form of the analyte of interest (Yang et al., 2019). Examples include deuterated ghrelin ([13C6] Leu5)-G) added to plasma in a 0.1 ppm solution (Thomas et al., 2021). Despite the success shown in the use of stable isotope-labelled ghrelin, this often comes at a high cost compared to other standards and is often not readily available. An alternative approach is to use ghrelin compounds from different species that are similar but not identical, as an ISTD. For example, rat ghrelin differs from human ghrelin by only two amino acids, and therefore, it exhibits similar characteristics and offers a cost-effective alternative to a deuterated standard. In support of this, several mass spectrometry-based studies have successfully used rat ghrelin as an ISTD to quantify human ghrelin (Rauh et al., 2007; Sidibe et al., 2014). Therefore, for the experiments described here, the intention is to use rat ghrelin as an ITSD to enable the quantification of human ghrelin.

3.1.3.3 Protein Precipitation

Protein precipitation is a common technique used to prepare biological samples for mass spectrometry analysis. The process involves the removal of larger proteins and other contaminants from the samples, resulting in a more purified matrix for the protein of interest. In this thesis, three methods of protein precipitation were explored based on previous research using mass spectrometry to quantify ghrelin. The first method published by Rauh et al. (2007) which showed a good capture of ghrelin, involved the addition of 50 µL of acetonitrile and 50 µL of sulfosalicylic acid (100 g/L) per 200 µL of plasma in a low-bind protein Eppendorf. The sample was mixed and centrifuged at 4°C at 36,000xg for 10 minutes (Rauh et al., 2007). The second method performed partial protein precipitation after the addition of 250 µL of sulfosalicylic acid solution (100 mg/mL) to 500 µL plasma. The mixture was homogenised on a MixMate mixer for 1 minute at 1500 rpm, followed by centrifugation for 30 minutes at 16,000xg (Sidibe et al., 2014). Lastly, a third method by Eslami et al. (2016) carried out protein precipitation followed by ghrelin MS analysis after the addition of a solution of

sulfosalicylic acid, acetonitrile, and plasma in a 1:1:4 ratio (v/v/v), followed by mixing and centrifugation at 24104xg for 10 minutes at 4°C (Eslami et al., 2016). All three methods described above were able to successfully capture and detect ghrelin. A general trend in all three methods showed the inclusion of sulfosalicylic acid during protein precipitation. In 2021, another paper on ghrelin analysis was published, whereby 5 µL of a 5% ammonium hydroxide solution was added to the samples to prevent nonspecific binding of ghrelin to albumin or other larger proteins within the plasma. This was followed by protein precipitation, whereby 75 µL of sulfosalicylic acid solution (100 mg/mL) was added to 250 µL of plasma, followed by centrifugation at 17,000xg for 10 minutes (Thomas et al., 2021). In this chapter, I will investigate the use of these three methods in the development of an effective protocol for ghrelin extraction from plasma.

3.1.3.4 Solid Phase Extraction (SPE)

SPE is a technique that enables the isolation of proteins based on their chemical and physical properties. The technique is widely used in mass spectrometry sample preparation, often to clean the sample, reduce sample complexity, and concentrate the analyte of interest (Bladergroen and van der Burgt, 2015). The chemical and physical properties of a compound will determine whether a compound will reside in the stationary solid phase or the mobile liquid phase during the clean-up process. The stationary phase is often packaged in a solid column in the shape of a column or a small column within a well of an SPE plate. The stationary phase itself is usually made up of silica or polymer-based sorbents and adopts one of three methods of adsorption: reversed-phase/nonpolar, normal phase/polar, or ion exchange chromatography. To begin with, the analyte of interest may be retained in the stationary phase if it has a greater affinity to it rather than the sample matrix, and any compounds with a low affinity to the stationary phase remain in the mobile liquid phase and are eluted from the column. In the case of proteins and peptides, the most widely used SPE method is the reverse phase. The general process of SPE can be seen in Figure 3.1.

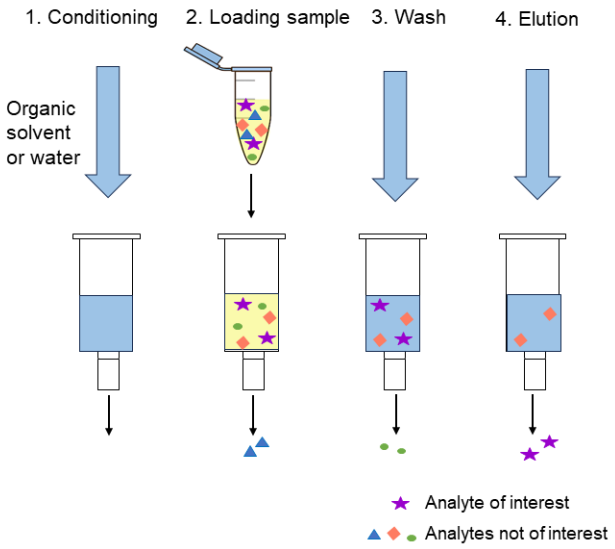

Figure 3.1 SPE steps.

1. Conditioning the column. 2. Loading the sample with the analyte of interest. 3. Wash step – remove impurities. 4. Elution of analyte of interest.

SPE consists of four stages, the first stage involves conditioning or equilibrating the solvent to wet the sorbent. The second stage is the loading of the sample onto the column, for example, the plasma, with the analyte of interest. During this step, if the analyte of interest has a high affinity for the solid phase, then it will bind to it, as will several alternative compounds that are not of interest. The third step involves washing to remove some of these impurities, followed by collection of the analyte of interest during the final elution step.

Research using SPE techniques in the extraction of ghrelin dates to the 2000s, when the Sep-Pak C18 column was used in several studies (Hosoda 2003; Kojima et al., 2000; Nishi et al., 2005). The use of C18 columns has remained common within ghrelin research, with papers still reporting their use until 2012 (Akamizu et al., 2012). All the methods have thus far used similar columns with varying types of mobile phase and the elution phase differing slightly but containing the consensus of using saline and 0.1% TFA for the mobile phase, which retains ghrelin in the stationary phase. This is generally followed by using acetonitrile with 0.1% TFA as the solvent for the elution step. In 2021, the use of reverse-phase polymeric HLB columns for the separation of ghrelin was employed with a mixture of acetonitrile and water as eluate (Thomas et al., 2021). Within this chapter, I will investigate the use of these different methods to extract ghrelin from plasma samples before MALDI-MS analysis.

To conclude, MALDI is an excellent tool for proteomics, but careful consideration is required for quantitative analysis, including optimisation of the experimental parameters. As highlighted, sample preparation is of key importance with optimisation needed to increase the reproducibility of the application.

3.1.2 Aims

The general aims of this chapter are to develop and optimise:

1. A sample preparation protocol for the extraction of ghrelin from plasma
2. A MALDI-TOF protocol to detect and quantify both acyl and unacylated ghrelin that is present in plasma.

3.2 Materials and Methods

3.2.1 Protein Precipitation

Before optimisation of protein precipitation using four different methods, 10,000 pg/mL of rat acyl or unacylated ghrelin was added to 1000 µL of human plasma. The first method identified by Eslami et al., 2016 involved protein precipitation after the addition of 250 µL of sulfosalicylic acid and 250 µL acetonitrile to plasma. Similarly, a method by Rauh et al., 2007, used the addition of 250 µL of sulfosalicylic acid and 250 µL of a 50:50 mixture of water and acetonitrile to the plasma. The third method based on a study by Sidibe et al. (2014) involved the addition of 500 µL sulfosalicylic acid to plasma. Finally, the fourth method used the addition of 10% trichloroacetic acid (TCA) to plasma, which had been previously used in an alternative lipidomic/MS-based project. After the addition of the solvents, as stated above, all samples from each method were placed on ice for 30 minutes and then centrifuged for 40 minutes at 17,500xg. The supernatant was removed and prepared for deposition on the MALDI stainless steel target as described in Section 3.2.2. Alternatively, the supernatant underwent further clean-up using SPE, centrifugal filters, speedvac, or C18 ziptips. C18 ziptips are pipette-tip based solid-phase extraction tools containing a small bed of C18 reverse-phase resin, which selectively binds hydrophobic peptides and proteins. They are commonly used for sample desalting and concentration prior to mass spectrometry or other analytical techniques, allowing efficient removal of salts and other contaminants while retaining peptides such as ghrelin.

3.2.2 Preparation of Matrix Surfaces

The stainless steel MALDI-TOF target plates were washed in the following order: 1. 100% methanol scrub (gently), 2. Deionised water rinses 3. 100% ethanol scrub. The plates were left to dry at room temperature. The matrix surface was prepared using the seed crystal method with CHCA (5 mg/mL) dissolved in acetone (apart from during matrix surface comparison studies, in which the seed crystal versus the dried droplet methods were compared). Approximately 1 µL of matrix solution is spotted on the MALDI-TOF stainless-steel target, the acetone causes the matrix to evaporate quickly and therefore the transfer must be completed quickly. The saturated matrix was allowed to dry at room temperature before the plate was inserted into the MALDI-TOF for analysis.

3.2.3 Solid Phase Extraction

The C18 columns have traditionally been used as a method of sample purification and clean-up. For this protocol, the C18 or HLB columns were used with the following protocol: Each column was first washed three times with 60% acetonitrile with 0.1% TFA, followed by equilibration by adding 3 mL of saline three times. The supernatant from step 3.2.1 (500 µL) was then loaded onto the column and washed with 1 mL 5% acetonitrile in 0.1% TFA followed by 1 mL 10% acetonitrile in 0.1% TFA, and finally, the samples were eluted with 500 µL of 60% acetonitrile in 0.1% TFA.

3.2.3.1 Microelution Plate SPE

An alternative method of SPE tested in place of traditional C18 or HLB columns was the use of an oasis microelution method development plate (186004713, Oasis). The 96-well microelution plate has advantages such as elongated/thinner well shapes, allowing for increased sorbed bed height with a large surface area. As a result, this technique is ideal for small plasma volumes and avoids the drying step, as it can elute the sample to 25 µL with a starting volume of 750 µL. The microelution plate protocol consisted of plasma mixed 1:1 with 4% phosphoric acid (H_3PO_4) in a final volume of 750 µL before loading onto the columns, the columns were washed with a volume of 750 µL with 5% ammonium hydroxide (NH_4OH) followed by a 20% acetonitrile wash and finally eluted 25 µL in 1% TFA in 75:25 Acetonitrile/H_2O. The sample was then analysed by MALDI MS.

3.2.4 Centrifugal Filter Device

Following SPE, the use of centrifugal filters was investigated, which is a device used to concentrate and desalt samples through the application of centrifugal force. The filter devices included either a 10kDa or 3kDa filter (which allowed the passage of molecules that were less than 10kDa or 3kDa, respectively). The working principle of a centrifugal filter involves the following steps:

Sample Loading: 500 µL of supernatant is loaded after protein precipitation and SPE (section 3.2.1 and 3.2.3) into the centrifugal filter device. The sample is typically placed in a filter unit which consists of a filter membrane suspended between two chambers.

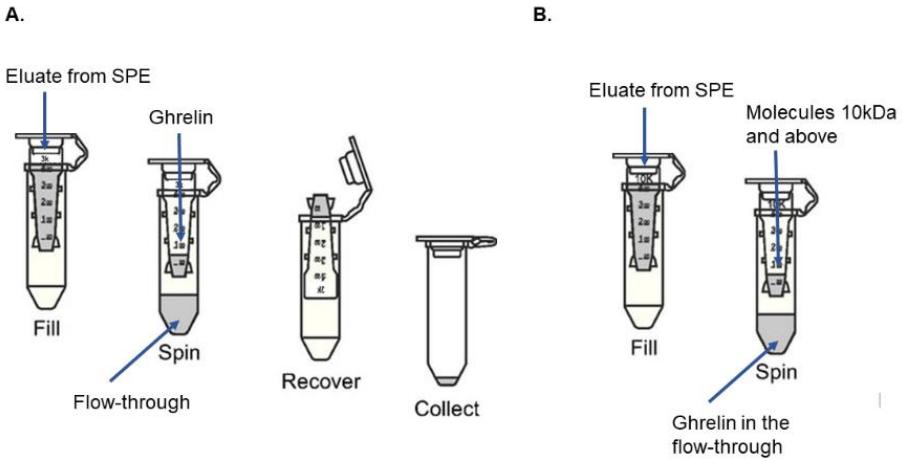

Figure 3.2 Centrifugal filter device for 3kDa (A) and 10kDa (B).

Centrifugation: The loaded filter unit is then placed in a centrifuge for 30 minutes at 14,000xg. When the centrifuge spins at high speeds, a centrifugal force is generated, causing the liquid component of the sample to move outward through the filter membrane while retaining the desired particles or molecules of a particular mass within the filter unit.

Elution: Once the centrifugation process is complete, the concentrated sample, now enriched with the retained molecules of interest, can be eluted. This is achieved by placing the filter device upside down in a clean tube and centrifuged for 2 minutes at 1000xg.

The samples were then applied to the MALDI target and analysed.

3.2.5 C18 Ziptips

Samples after protein precipitation (section 3.2.1) or SPE (section 3.2.3) are transferred to a fresh Eppendorf ready for the C18 ziptip protocol. Initially, the ziptips were pre-wetted by aspirating and dispensing the wetting solution, composed of 50% acetonitrile with 0.1% TFA, three times to fully activate the C18 reverse-phase resin. Following pre-wetting, the tips were equilibrated by aspirating and dispensing 0.1% TFA solution three times to prepare the resin for peptide binding. The peptide-containing samples were then processed by aspirating and dispensing the sample through the ziptip ten times, ensuring sufficient binding of the peptides to the resin. After binding, the ziptips were washed three times with 0.1% TFA to remove unbound contaminants and salts. Finally, peptides were eluted from the resin by dispensing 5 µL of a solution CHCA matrix dissolved in 40% acetonitrile. The eluted samples were then subjected to analysis by MALDI-MS.

3.2.6 Sample Preparation for MS Analysis

In addition to ghrelin samples derived from the protein precipitation step (3.2.1), ghrelin standards and dilutions of the samples were prepared in 0.1% plasma, diluted by 0.1% TFA on the MALDI-TOF stainless steel target. Before ‘spotting,’ the ghrelin samples or standards were mixed in a 1-part peptide mixture with 3 parts of the matrix, CHCA (5 mg/mL) in 40% acetonitrile and 0.05% TFA. A volume of 1.5 µL of this mixture was spotted directly onto the MALDI target plate in triplicate. For each spot, two spectra were acquired, resulting in a total of six spectra collected per sample using the MALDI-TOF mass spectrometer. To determine the variability of different matrix surfaces and the range of the assay, a seed crystal comparison study and a calibration curve were first performed. The seed crystal comparison study consisted of coating part of the target with seed crystal and another section of the target using a dried droplet method. For the seed crystal, CHCA (5 mg/mL) dissolved in acetone was first added to coat the plate and upon drying, the 1:3 peptide matrix mixture was spotted directly on top. The dried droplet method consists of spotting the 1:3 peptide matrix mixture directly onto the target (without prior addition of acetone).

For the calibration curve, ghrelin was added at concentrations ranging from 0.08 to 80 ng/mL, with the internal standard (ITSD) concentration varying depending on the

specific experiment described in the corresponding section. This broad calibration range was selected to reflect the wide variability in circulating ghrelin levels reported in the literature. In healthy individuals, fasting plasma levels of acylated ghrelin typically range from approximately 30 to 80 pg/mL (equivalent to 0.03 to 0.08 ng/mL), with total ghrelin concentrations averaging around 1 ng/mL (Cummings et al., 2001;). Des-acyl ghrelin represents the predominant circulating form, comprising roughly 90% of total ghrelin in plasma (Gahete et al., 2013). However, these levels can vary depending on nutritional status and disease state. For example, patients with anorexia nervosa exhibit markedly elevated total ghrelin levels, with reports as high as 13 ng/mL (Shiiya et al., 2002), while obesity is associated with significantly reduced ghrelin concentrations (Pulkkinen et al., 2010). Thus, a wide calibration range was necessary to account for both physiological and pathological variations in ghrelin levels.

3.3 Results

3.3.1 Effect of the Seed Crystal on the Surface of the Matrix

The even coating of the seed crystal matrix onto the target before depositing the peptide matrix mixture is a common method used in the MALDI-TOF sample preparation to achieve optimal results. This approach helps ensure that the matrix and analyte are evenly distributed at the target spot, facilitating efficient desorption and ionisation during MALDI-TOF analysis. However, some studies report the use of a dried droplet method (Gutierrez 2005; Vorm 1994). This method involves depositing a droplet containing the peptide and matrix onto the target and allowing it to dry. Therefore, the seed crystal and dried droplet methods were compared to confirm which was most appropriate in the context of ghrelin analysis. Figure 3.3A shows the visual results of the dried droplet method. In this case, uneven clusters of crystals and sparse spots were observed, suggesting that the distribution of the matrix and analyte was not uniform. Asymmetrical drying or uneven distribution of the matrix and analyte resulted in the formation of localised concentrations of the matrix and analyte, leading to irregular crystallisation, which can lead to spot-to-spot variation in the resulting spectra. Figure 3.3B shows a visual representation of the even coating achieved using the seed crystal method. The image shows a well-defined spot with a uniform distribution of the matrix on its surface. The flat surface and consistent shape of the crystals indicated that the matrix and analyte had crystallised uniformly, which is described to obtain high-quality spectra.

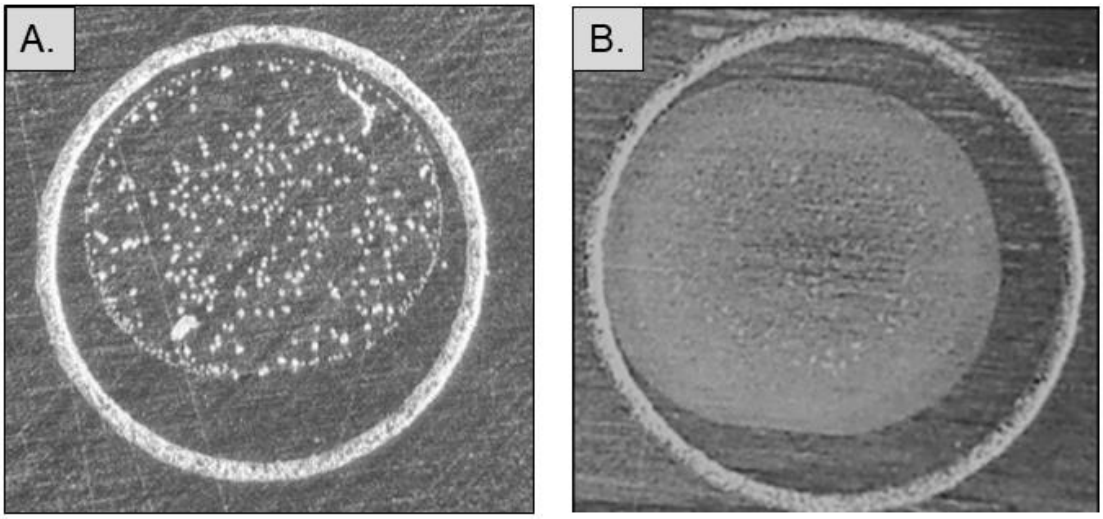

Figure 3.3 Effect of seed crystal layer on matrix surface characteristics.

A. Dried droplet method, crystals formed creating a non-homogenous environment. B. Seed crystal method, smooth, even layer created within the spot.

The visual analysis of Figure 3.3 suggests that the seed crystal method results in a more homogeneous layer. To provide further insight into the stability of the analytes prepared using both methods, an equimolar mixture of rat and human, acyl and unacylated ghrelin species was prepared at a concentration of 15 ng/mL. The mixture was spotted onto the MALDI target using either the seed crystal or dried droplet method. The analysis showed that the dried droplet method resulted in 'noisier' and lower intensity signals compared to the seed crystal method (Figure 3.4A). This is likely due to the crystal formation as can be seen in Figure 3.3A. The seed crystal method, as shown in Figure 3.4B (bottom panel), demonstrates clearer spectra at a higher intensity of ~4000-6000 arbitrary unit (a.u.), indicating greater signal quality compared to the dried droplet method which produced a signal of ~1000-1200 a.u. (Figure 3.4A). ANOVA analysis confirmed that all ghrelin species exhibited significantly higher mean intensities with the seed crystal method compared to the dried droplet method (Figure 3.4C). Specifically, rat unacylated ghrelin and rat acyl ghrelin demonstrated significant increases ($P < 0.01$), while human unacylated ghrelin and human acyl ghrelin also showed significant improvements ($P < 0.05$).

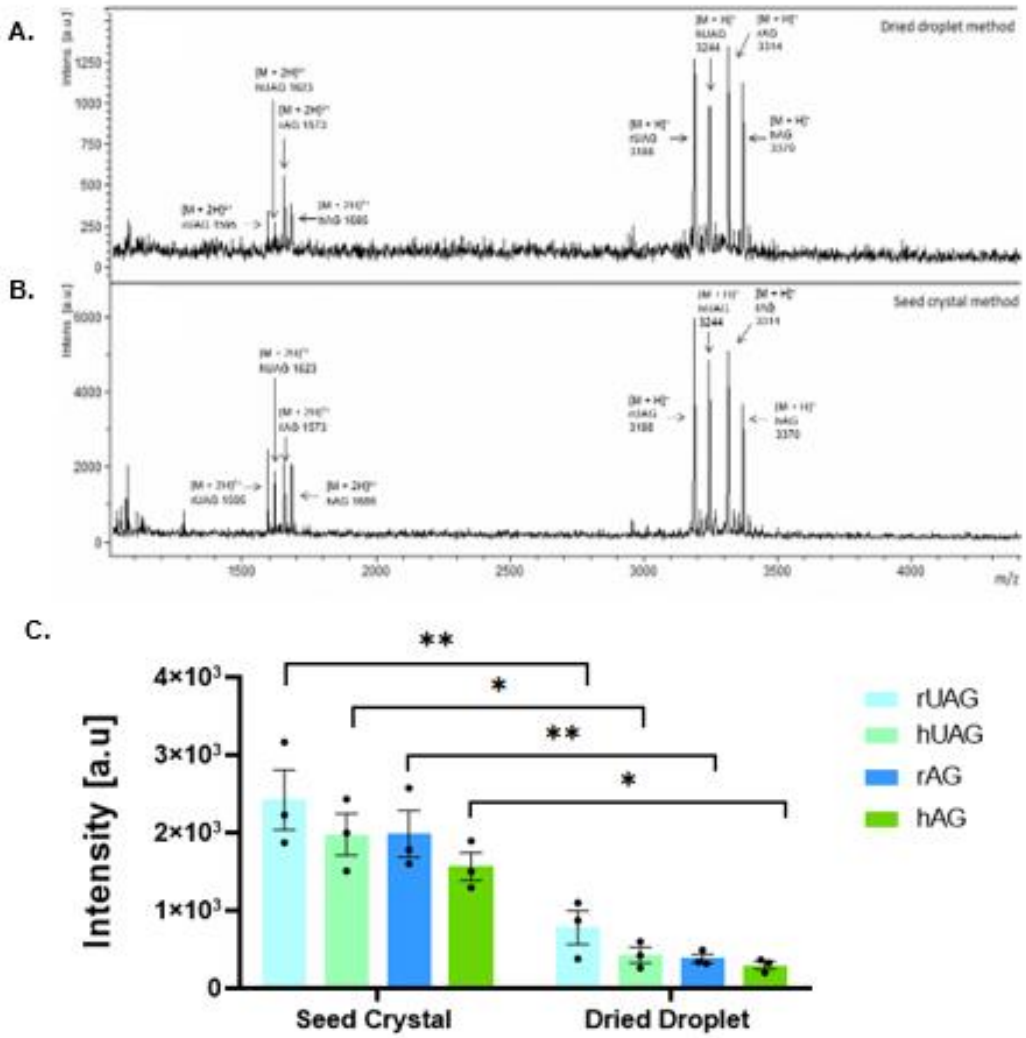

Figure 3.4 MALDI-TOF spectra were obtained of the four ghrelin species in the reflectron ion positive mode and in the m/z range 1000-5000.

The x-axis represents the mass-to-charge ratio (m/z), while the y-axis shows signal intensity in arbitrary units (a.u.), corresponding to the peak height of each ion detected. Peaks labelled as $[M+H]^+$ represent the singly protonated molecular ions (monoisotopic species) of each peptide, while the $[M+2H]^{2+}$ peaks indicate the same peptides carrying two protons, resulting in a doubly charged species. The labelled peaks correspond to the following ghrelin species: Rat unacylated ghrelin: $[M+H]^+$ at m/z 3188 and $[M+2H]^{2+}$ at m/z 1595. Human unacylated ghrelin: $[M+H]^+$ at m/z 3244 and $[M+2H]^{2+}$ at m/z 1623. Rat acyl ghrelin: $[M+H]^+$ at m/z 3314 and $[M+2H]^{2+}$ at m/z 1657. Human acyl ghrelin: $[M+H]^+$ at m/z 3370 and $[M+2H]^{2+}$ at m/z 1686 A. Spectra acquired using dried droplet method. B. Spectra obtained using the seed crystal method. A and B. Example spectra of the six spectra obtained. C. Two-way ANOVA with Tukey's multiple comparisons correction was performed to evaluate statistical significance. For each condition, spectra were acquired from three independent runs (N = 3). Each run consisted of three spots per sample, with two spectra acquired per spot (six spectra per run). The six spectra from each run were averaged to produce a single mean value, and the data presented represent the mean ± SEM calculated across the three independent runs. $P < 0.05$ was considered significant; **$P < 0.001$.

3.3.2 Matrix Choice and Longevity

To optimise the MALDI-TOF analysis of the ghrelin peptide, the selection of an appropriate matrix is crucial as it can significantly induce the ionisation process. Based on previous studies by Zhao et al. (2021) and Gutierrez et al. (2005), CHCA has been reported as a matrix that works effectively with peptides and proteins, including ghrelin. Therefore, CHCA was selected as the sample matrix. The solvent chosen to dissolve CHCA is also important. One solvent commonly used for CHCA in MALDI-TOF analysis is acetonitrile due to its compatibility with peptides and proteins, moderate volatility, and ability to induce crystal formation (Bradnt et al., 2010, Tsai et al., 2017). To determine the optimal percentage of acetonitrile in the matrix for our study, an equilibrium concentration of human acyl and unacylated ghrelin was prepared at a concentration of 15 ng/mL, dissolved in acetonitrile varying from 40-70% acetonitrile. The spectra obtained from the analysed samples show that the presence of acetonitrile in the matrix can significantly influence the ionisation and detection of acyl and unacylated ghrelin during MALDI-TOF analysis (Figure 3.5). In both the spectra highlighted in Figure 3.5 and the statistical analysis, it was observed that human acyl and unacylated ghrelin produced spectra that were significantly ($P<0.001$) more intense while dissolved in 40% acetonitrile, compared to the other percentages of acetonitrile (Figure 3.5).

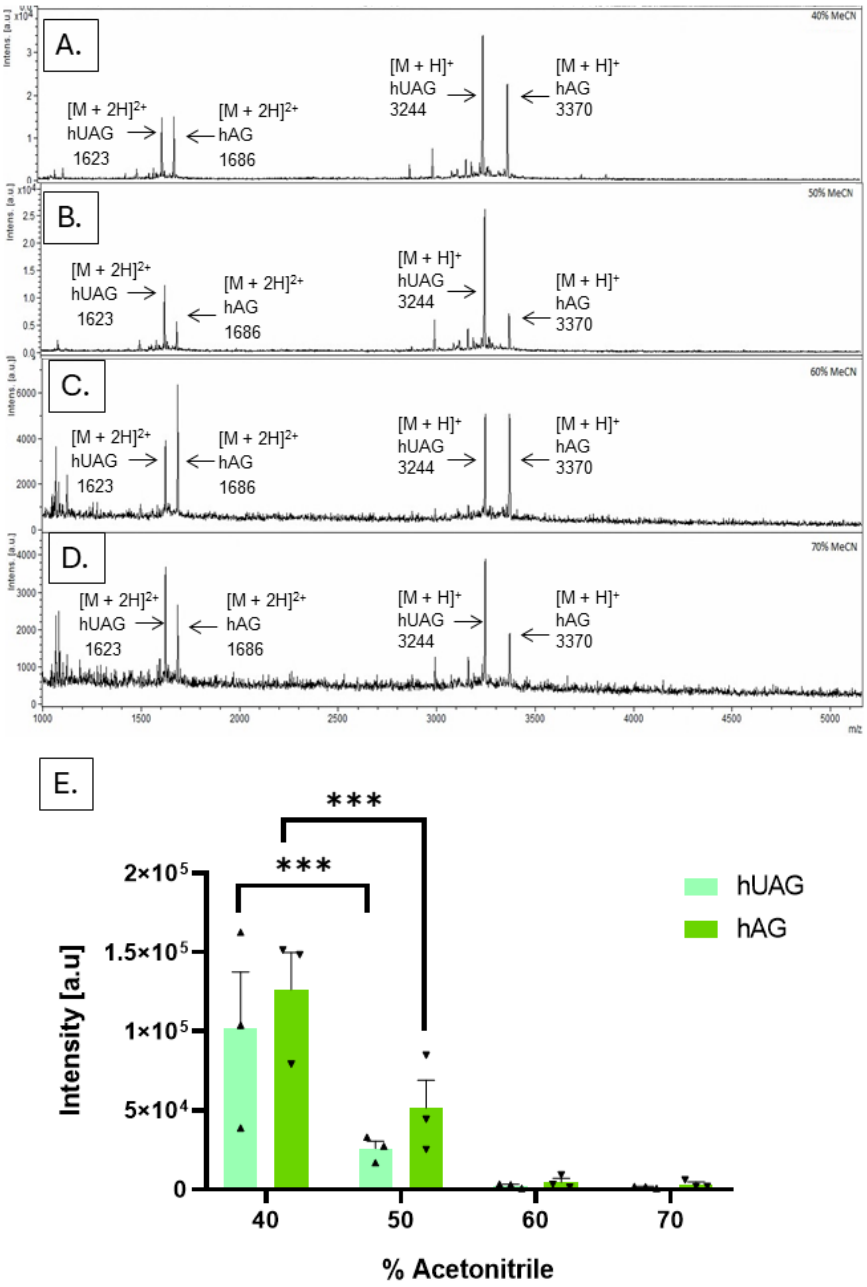

Figure 3.5 Comparison of the intensities of hUAG and hAG after preparation in different percentages of acetonitrile.

Equimolar concentrations of hAG and UAG were prepared in different percentages of acetonitrile followed by MALDI-TOF analysis. A–D. MALDI-TOF spectra obtained in reflectron-ion positive mode across the m/z range 1000–5000 Th. A. 40% acetonitrile. B. 50% acetonitrile. C. 60% acetonitrile. D. 70% acetonitrile. E. Two-way ANOVA with Tukey's multiple comparisons correction was performed to evaluate statistical significance. For each condition, spectra were acquired from three independent runs (N = 3). Each run consisted of three spots per sample, with two spectra acquired per spot (six spectra per run). The six spectra from each run were averaged to produce a single mean value, and the data presented represent the mean ± SEM calculated across the three independent runs. $P < 0.05$ was considered significant; **$P < 0.01$.

These findings indicate that the percentage of acetonitrile in the matrix significantly influences the ionisation and detection of human ghrelin species during the MALDI-TOF analysis.

The longevity of the matrix once prepared was also investigated. More specifically, the stability and performance of the matrix over time were assessed. Fresh human acyl and unacylated ghrelin standards were prepared at various times after forming one solution of CHCA, time 0 (immediately after matrix preparation), 24 hours, 48 hours, and 72 hours after preparation. The results revealed that there were no significant changes in either of the ghrelin species between the different time points (Figure 3.6). This suggests that the matrix remained stable and maintained its performance over the expected period. However, despite the results suggesting that the longevity of the matrix is consistent up to 72 hours, as good practice, a fresh matrix was prepared every 48 hours.

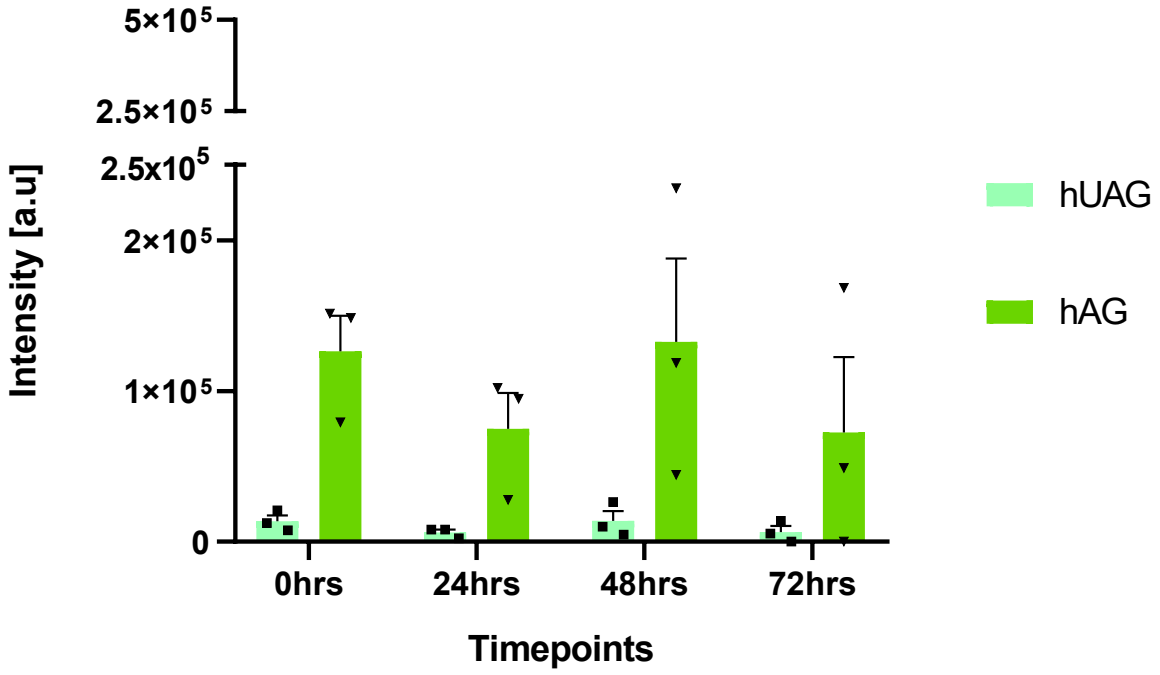

Figure 3.6 Longevity of the CHCA matrix. HAG and hUAG standards were prepared with CHCA at different time points.

Time 0 (immediately after matrix preparation), 24 hours, 48 hours, and 72 hours after matrix preparation. Two-way ANOVA was performed with Tukey corrections. $P<0.05$ is considered statistically significant. The data shown represent mean +/- SEM across three independent runs (N=3).

3.3.3 Quantification by MALDI-TOF

To enable the quantification of ghrelin in human plasma, calibration curves were generated for exogenous ghrelin standards. The first step in optimisation involved generating calibration curves with rat ghrelin, which will be used as an ISTD. By incorporating higher levels of ghrelin concentration within the calibration curve, the dynamic range of the instrument was assessed. The calibration curve was constructed using a ten-point calibration approach, covering a concentration range from 0.08-80 ng/mL (Figure 3.7). The ISTD was included at 51 ng/mL. Two sets of calibration curves were performed: one used rat acyl ghrelin as the internal standard with varying amounts of rat unacylated ghrelin, while the other used rat unacylated ghrelin as the internal standard with varying amounts of rat acyl ghrelin. This was done to ensure an accurate representation of the signal suppression and overall intensity readings, as acyl and unacylated ghrelin may have slightly different affinities during MALDI analysis. The R^2 obtained for both standard curves were greater than 0.9, indicating a stronger linear relationship between the concentration of ghrelin species and the corresponding signal intensities (Figure 3.7).

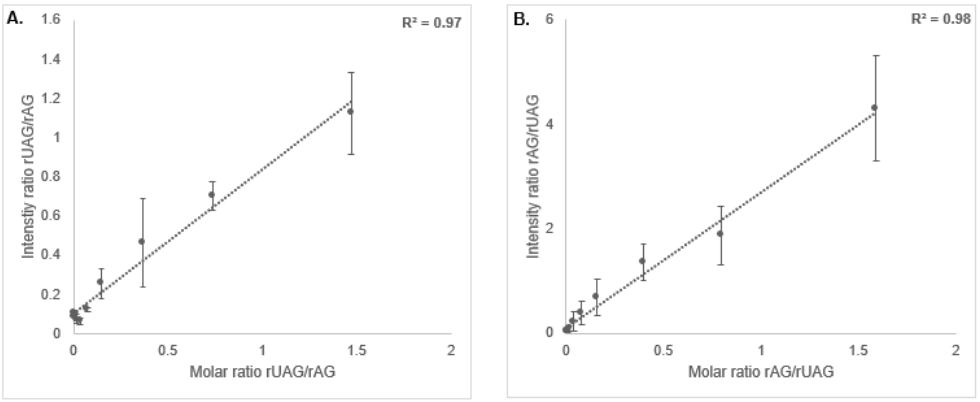

Figure 3.7 Calibration curves for rat ghrelin analysed by MALDI-TOF in the range of 0.08–80 ng/mL, using an ISTD concentration of 51 ng/mL.

A. Calibration with rAG as the ISTD and variable rUAG (expressed as a molar ratio). B. Calibration with rUAG as the ISTD and variable rAG (expressed as a molar ratio). Each calibration point represents the average signal intensity calculated from three independent runs (n = 3). For each run, six spectra were acquired per calibration point (two spectra from each of three spots), and these six spectra were averaged to produce a single mean value for that run. The final plotted point is the mean of these three-run means, and error bars represent the standard deviation across runs, reflecting inter-run variability. Trendlines represent linear regression fits, and R^2 values are reported to indicate goodness of fit. Error bars show the standard deviation, reflecting variability in measured signal intensities.

The reflector mode of the MALDI-TOF technique offers significant advantages over the linear mode, including improved mass accuracy and resolution. This was the initial rationale for selecting the reflector mode for the analysis. However, when the stability of analytes during their passage through the reflector becomes a concern, particularly for unstable or easily fragmented molecules, the linear mode may be more appropriate due to its gentler ion handling. Although ghrelin is a relatively small peptide, which would generally be suitable for reflector mode, its potential instability and susceptibility to fragmentation during analysis warranted further investigation to determine the most appropriate mode for its detection. After excluding the saturated data points at the two highest concentrations, the linear mode showed good linearity, with a correlation coefficient of $R^2 = 0.99$ (Figure 3.8), comparable to that of reflectron mode ($R^2 = 0.99$; Figures 3.7). However, due to the evident saturation in the linear mode at higher concentrations and the advantages of reflectron mode, such as superior mass accuracy and resolution, the reflectron mode was selected for all subsequent analyses.

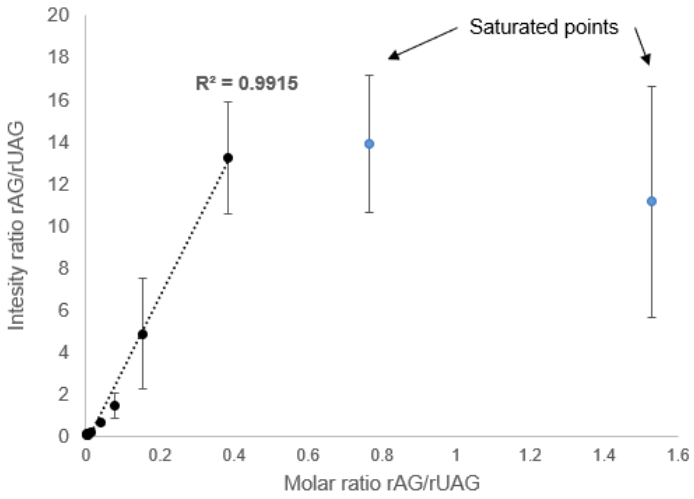

Figure 3.8 Calibration curve of rUAG as ISTD at 51 ng/mL and rAG varying from 0.08-80 ng/mL was analysed using linear mode on the MALDI-TOF.

Each calibration point represents the average signal intensity calculated from three independent runs (N = 3). For each run, six spectra were acquired per calibration point (two spectra from each of three spots), and these six spectra were averaged to produce a single mean value for that run. The final plotted point is the mean of these three-run means, and error bars represent the standard deviation across runs, reflecting inter-run variability. Trendlines represent linear regression fits, and R^2 values are reported to indicate goodness of fit. Error bars show the standard deviation, reflecting variability in measured signal intensities. Saturated points are included in the graph for transparency but were excluded from the regression analysis.

The next objective was to assess whether adjusting the ISTD concentration could improve calibration curve performance. The ISTD is typically placed near the midpoint of the calibration range to ensure consistent quantification and minimise risks of signal suppression or competition. However, in some cases, it may be deliberately positioned elsewhere—for example, to reduce ionisation competition in mass spectrometry-based assays, where high analyte or matrix concentrations can interfere with ionisation efficiency. Adjusting the ISTD concentration in such cases can help stabilise the signal and improve accuracy in specific parts of the curve. To address this, the calibration curve was re-evaluated using a reduced concentration range of 0.08–2 ng/mL, with two different ISTD concentrations tested: 0.65 ng/mL and 1.3 ng/mL (Figure 3.9). Rat acyl ghrelin showed good linearity as an ISTD at both 1.3 ng/mL and 0.65 ng/mL, with R^2 values of 0.96 and 0.97, respectively (Figures 3.9A and 3.9B). Similarly, when rat unacylated ghrelin was used as the ISTD, strong linearity was observed with R^2 values of 0.95 at 1.3 ng/mL and 0.93 at 0.65 ng/mL (Figures 3.9C and 3.9D). Although slight differences in R^2 values were noted, all calibration curves demonstrated strong linear correlations between ghrelin concentration and signal intensity. Overall, varying the ISTD concentration had minimal effect on the linearity of the calibration curves. Consequently, 0.65 ng/mL, which lies closer to the midpoint of the calibration range, was selected for subsequent analyses.

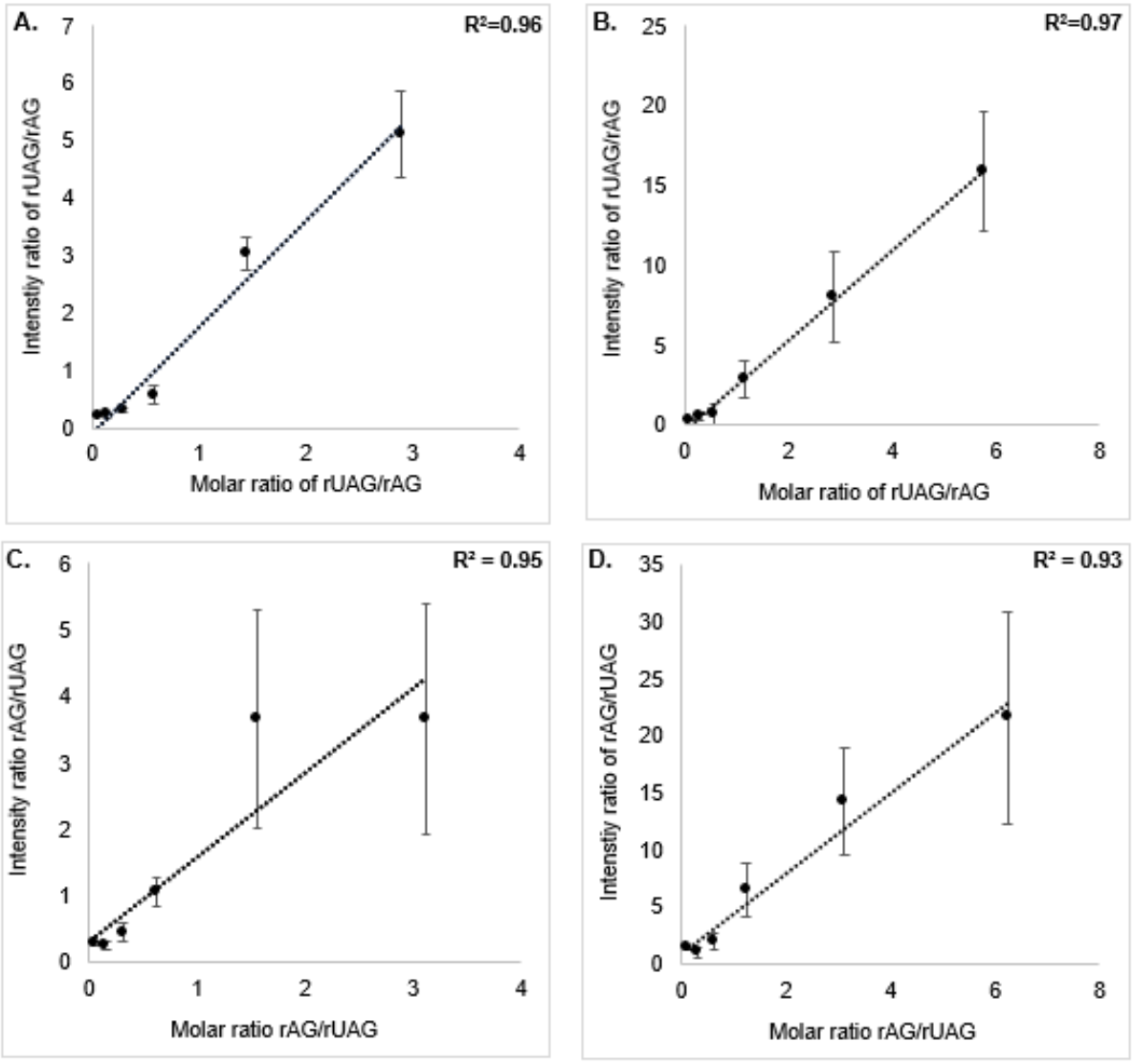

Figure 3.9. Calibration curves for the quantification of rat ghrelin species in the range of 0.08-2 ng/mL with ISTD either at 1.3 ng/mL (A and C) or 0.65 ng/mL (B and D). A B. rAG is used as the ISTD, with rUAG at varying concentrations. C, D, rUAG is used as the ISTD, with rAG at varying concentrations. Each calibration point represents the average signal intensity calculated from three independent runs (N = 3). For each run, six spectra were acquired per calibration point (two spectra from each of three spots), and these six spectra were averaged to produce a single mean value for that run. The final plotted point is the mean of these three-run means, and error bars represent the standard deviation across runs, reflecting inter-run variability. Trendlines represent linear regression fits, and R^2 values are reported to indicate goodness of fit. Error bars show the standard deviation, reflecting variability in measured signal intensities.

After the successful optimisation of the calibration curve with the rat ghrelin standards, a calibration curve of the human standards was carried out. For this calibration curve, human acyl ghrelin was placed as the variable, ranging from 0.08-2 ng/mL, and the human unacylated ghrelin was used as the ISTD at 0.65 ng/mL. The graph was plotted as the molar ratio of human acyl ghrelin/human unacylated ghrelin against the intensity ratio of human acyl ghrelin/human unacylated ghrelin (Figure 3.10). The calibration curve generated for the human ghrelin standards had a strong linear correlation, shown by the R^2 value at 0.95.

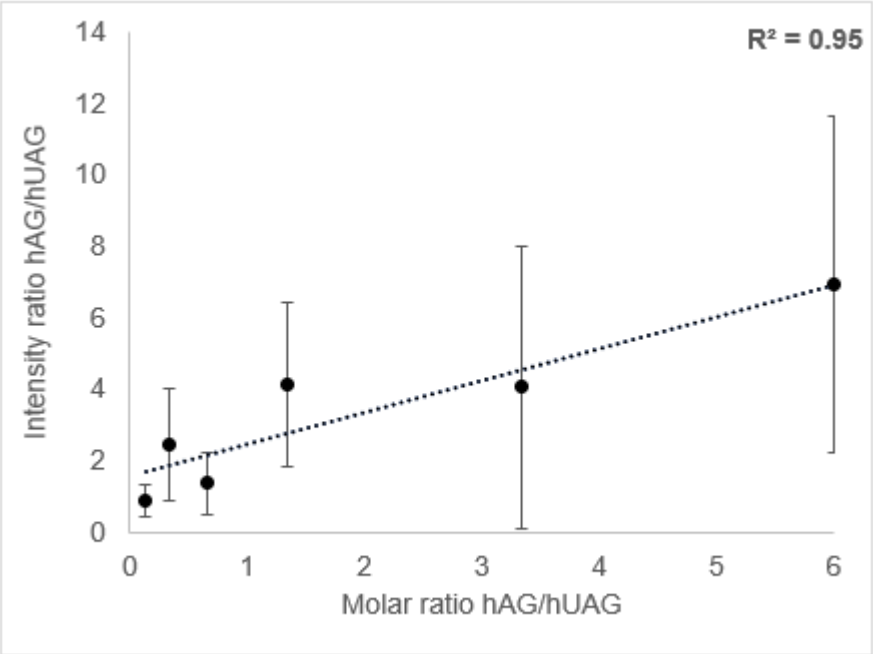

Figure 3.10: Human ghrelin standard calibration curve, hAG varying concentration between 0.08-2 ng/mL with hUAG placed as an ISTD (0.65 ng/mL).

Each calibration point represents the average signal intensity calculated from three independent runs (N = 3). For each run, six spectra were acquired per calibration point (two spectra from each of three spots), and these six spectra were averaged to produce a single mean value for that run. The final plotted point is the mean of these three-run means, and error bars represent the standard deviation across runs, reflecting inter-run variability. Trendlines represent linear regression fits, and R^2 values are reported to indicate goodness of fit. Error bars show the standard deviation, reflecting variability in measured signal intensities.

To conclude, calibration curves were successfully optimised for both rat and human ghrelin, allowing continuation into ghrelin extraction from plasma.

3.3.4 Optimization of Ghrelin Extraction from Plasma

3.3.4.1 Protein Precipitation

The extraction of ghrelin, a small peptide with a molecular weight of approximately 3000Da, requires protein precipitation as an initial step in its extraction from plasma to eliminate large proteins and purify the sample. A comprehensive investigation of the literature on ghrelin and MS analysis led to the selection of three methods of protein precipitation for further investigation: Rauh et al. 2007, Sidibe et al. 2014 and Eslami et al. 2016. Furthermore, a method using trichloroacetic acid (TCA) which had been used within the Davies laboratory was also tested (these methods are described in detail in Section 3.2.2, Protein Precipitation). All of these methods were selected for further investigation to see which was the most effective in our laboratory setting using plasma 'spiked' with rat ghrelin. After the initial protein precipitation, the deproteinised supernatant was then analysed via MALDI-TOF.

None of the methods successfully captured human ghrelin and, as such, the graphs throughout this chapter only demonstrate rat ghrelin. The Eslami et al. methodology when assessed, exhibited significantly higher levels of both rat acyl and unacylated ghrelin compared to the Rauh et al. methodology tested (Figure 3.11A) ($P<0.05$). The TCA method did not produce detectable data, indicating its inefficacy in isolating ghrelin and leading to its exclusion as a viable protein precipitation method. Notably, whilst the methodology by Rauh et al was not as efficient for ghrelin capture compared to the Eslami et al. and Sidibe et al. method, it seemed potentially promising for extracting both acyl and unacylated ghrelin at a similar ratio.

Overall, the protein precipitation methodology described by the Eslami et al., Sidibe et al., and Rauh et al. protocol, reported lower levels of ghrelin than expected with the highest signal intensity of 10^3 after protein precipitation compared to the 'spiked' concentration which exhibits signal intensities of 10^5. Upon extrapolating the predicted concentration from the generated calibration curves, the Sidibe et al. protein precipitation method demonstrated an overall 53% ghrelin loss for rat unacylated ghrelin and a 72% loss for rat acyl ghrelin, whilst Eslami et al. exhibited 40% loss for rat unacylated ghrelin and 65% loss for rat acyl ghrelin. Rauh et al. method ghrelin levels fell below the calibration curve. As such, further investigations were conducted

on all three methods to gain a more comprehensive understanding and determine the most suitable method for extracting ghrelin from plasma.

To explore whether modifying the precipitation protocol could improve recovery, an additional adaptation was applied to each method. After solvent addition as per the original protocols, samples were placed on ice for 30 minutes, followed by extended centrifugation at 17,500×g for 40 minutes (Figure 3.11B). These modified protocols were directly compared to their original versions.

The adapted Eslami method showed a significant improvement in rat unacylated ghrelin detection ($P < 0.0001$), while no significant change was observed for acyl ghrelin. In contrast, the adapted Rauh method showed significantly increased detection of both rat acyl and unacylated ghrelin ($P < 0.0001$ for both). The Sidibe method did not show any improvement with the modified protocol. These results suggest that introducing a cooling step and longer centrifugation may enhance peptide recovery, particularly for unacylated ghrelin in acetonitrile-containing protocols.

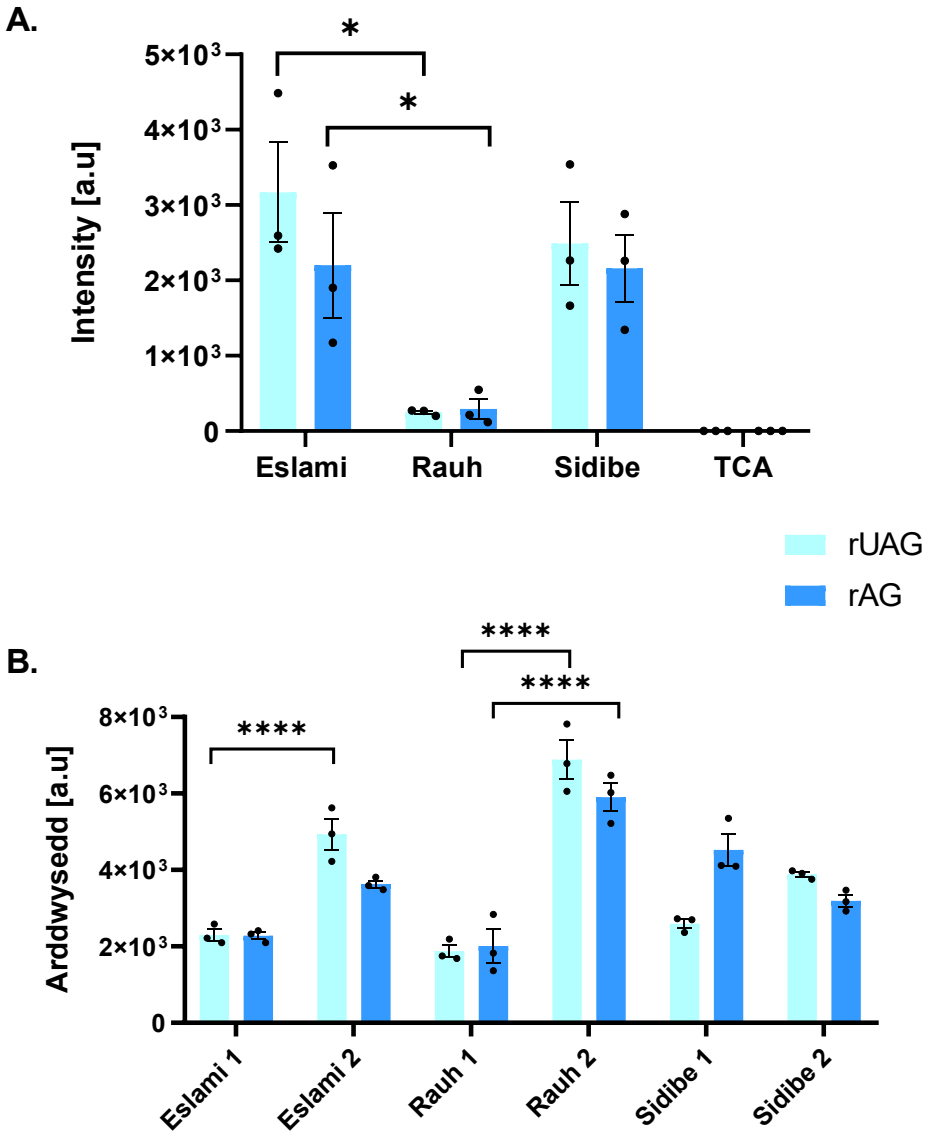

Figure 3.11 The comparison of protein precipitation methods utilised for sample preparation before analysis by MALDI-TOF.

A. Comparison of four protein precipitation methods (Eslami, Sidibe, Rauh, and TCA) for the extraction of rat acyl and unacylated ghrelin from plasma prior to MALDI-TOF analysis. B. Evaluation of adapted versions of the Eslami, Rauh, and Sidibe protocols. Each method was modified to include a 30-minute incubation on ice followed by centrifugation at 17,500×g for 40 minutes. Bar labels "1" and "2" denote the original and adapted versions of each method, respectively. Significant improvements were observed for rat unacylated ghrelin using the Eslami 2 protocol ($P < 0.0001$) and for both acylated and unacylated ghrelin using Rauh 2 ($P < 0.0001$). No significant differences were observed for the Sidibe method following adaptation. Data represent mean ± SEM from three independent replicates ($N = 3$). Two-way ANOVA was performed with Tukey's multiple comparison test; $P < 0.05$ was considered statistically significant.

3.3.4.2 Protein Precipitation and the Use of C18 Ziptips

The use of C18 ziptips was investigated as a method of further sample clean-up following the initial protein precipitation methods described by Rauh et al. Sidibe et al. or Eslami et al. C18 ziptips can offer advantages in terms of desalting samples and concentrating an analyte of interest which can facilitate its detection by MS.

The results did not show significant differences ($P>0.05$) among the protein precipitation methods themselves with versus without the use of C18 ziptips (Figure 3.12). However, a statistically significant difference was observed in rat unacylated ghrelin when comparing the Eslami et al. method with C18 ziptips, versus the Rauh method with the use of C18 ziptips ($P<0.001$). There was also a significant increase in rat unacylated ghrelin when comparing the Sidibe et al. method with C18 ziptips in comparison to the Rauh et al. method with the C18 ziptips ($P<0.001$). The results suggest, in the case of rat unacylated ghrelin, that both the Eslami et al. and Sidibe et al. methods outperformed the Rauh et al. method after incorporating C18 ziptips into the protocol. Additionally, for the Sidibe et al. method, rat unacylated ghrelin was detected at a higher intensity than the rat acyl ghrelin ($P<0.01$), suggesting that the method worked better for rat unacylated ghrelin. The use of C18 ziptips was then continued to be explored following the use of all three protein precipitation methods in conjunction with SPE.

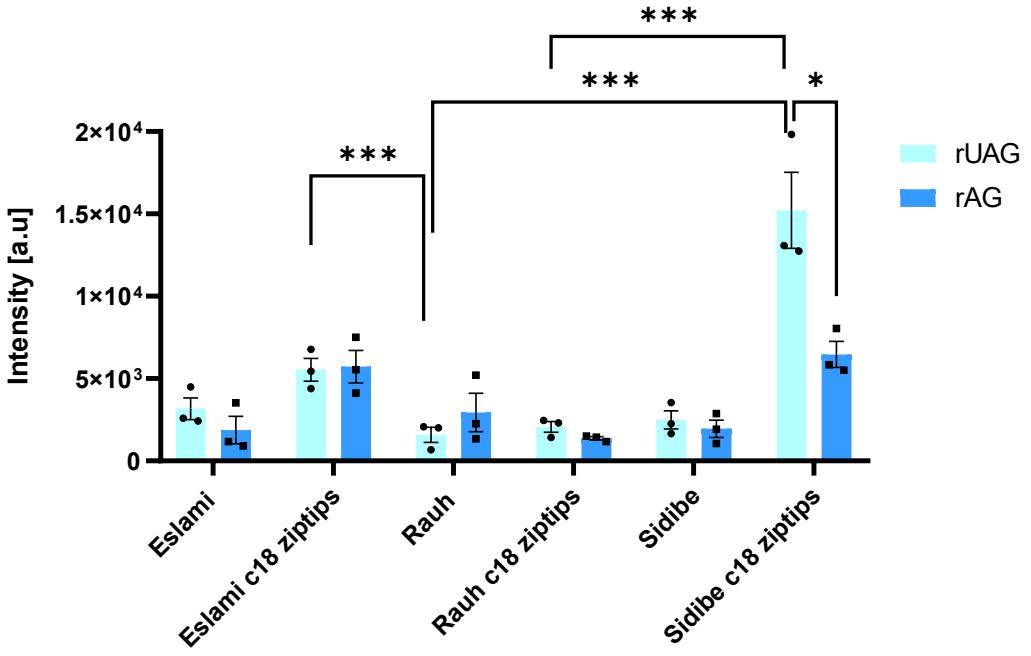

Figure 3.12 Comparison of the effect of using C18 ziptips on ghrelin detection following ghrelin extraction using either the Eslami et al. Rauh et al. or Sidibe et al. methods.

Exogenous rat AG or UAG was added to plasma and extracted using protein precipitation methods as described by Eslami et al, Rauh et al., or Sidibe et al., followed by samples being cleaned via the use of C18 ziptips followed by MALDI-TOF. The data presented in the figure represents the mean values along with the standard error of the mean (SEM). Two-way ANOVA was performed with Tukey corrections. $P<0.05$ is considered statistically significant. *** $P<0.001$, *$P<0.01$. The data shown represent mean +/- SEM. N=3.

The results obtained using the Eslami et al. and Sidibe et al. method demonstrated a reduction in 'spiked' ghrelin loss with the utilisation of C18 ziptips. Specifically, when using regular tips, Eslami et al. methodology indicated a ghrelin loss of 41% for rat unacylated ghrelin and 65% for rat acyl ghrelin, whereas with C18 ziptips, the losses were only 4% and 7%, respectively. Likewise, the results obtained using Sidibe et al., methodology reported ghrelin loss of 53% for rat unacylated ghrelin and 63% for acyl ghrelin when using the regular tips, whilst the C18 ziptips showed losses of 28 and 7%, respectively. Conversely, results using the Rauh et al. methodology showed a reduction of 70% and 45% in rat acyl and unacylated ghrelin loss with regular tips, while C18 ziptips resulted in losses of 61% and 75% for rat unacylated and acyl ghrelin, respectively. These results suggest a potential benefit of using C18 ziptips in minimising ghrelin loss.

3.3.4.3 Inclusion of SPE in the Ghrelin Extraction Protocol

An ANOVA comparison was performed to evaluate the effectiveness of protein precipitation and SPE protocols for peptide recovery across the three published workflows (Sidibe, Eslami, Rauh) as shown in Figure 3.13A. The main focus was on comparing the same ghrelin species (rat acyl ghrelin vs. rat acyl ghrelin, rat unacylated ghrelin vs. rat unacylated ghrelin) within and across methods to assess whether SPE improved peptide recovery relative to protein precipitation.

There were no significant differences observed between protein precipitation and solid-phase extraction within the same ghrelin group across any method. Within the Eslami protocol, rat unacylated ghrelin levels were significantly higher than rat acyl ghrelin using both protein precipitation and SPE methods ($P < 0.01$). A similar trend was observed within the Sidibe method, where rat unacylated ghrelin was significantly elevated compared to rat acyl ghrelin when using protein precipitation, although the level of significance was lower ($P < 0.05$).

When comparing performance across extraction methods, the Eslami SPE approach for rat unacylated ghrelin yielded significantly higher values than Rauh's protein precipitation method (**$P< 0.0001$). Eslami's protein precipitation method for rat unacylated ghrelin also significantly outperformed Rauh's SPE protocol (**$P < 0.0001$). Furthermore, Eslami SPE for rat unacylated ghrelin performed significantly better than Sidibe's SPE method (*$P < 0.001$), and the Eslami protein precipitation method for rat unacylated ghrelin also yielded superior results relative to Sidibe's SPE approach. Additionally, Sidibe's protein precipitation method for rat unacylated ghrelin showed a significant increase ($P < 0.01$) when compared to Rauh's SPE method.

Overall, these data indicate that Sidibe's protein precipitation protocol generally provides superior peptide recovery compared to SPE within the same method, while the Eslami SPE method shows improved performance relative to Sidibe SPE but not to Sidibe protein precipitation. The Rauh protocol appears less sensitive to the choice of extraction method but is outperformed by Sidibe protein precipitation.

Figure 3.13B presents a comparative analysis of peptide recovery across the Eslami, Rauh, and Sidibe extraction protocols, with and without C18 ziptip purification, for both rat unacylated ghrelin and rat acylated ghrelin. Within the Eslami method, no significant differences were seen between with and without C18 ziptips.

The Sidibe method with C18 ziptips showed significantly higher recovery for both rat unacylated ghrelin ($P < 0.0001$) and rat acyl ghrelin ($P<0.001$) compared to Eslami samples without C18. However, Eslami with C18 ziptips had significantly higher recovery than Rauh for rat unacylated ghrelin both without C18 ($P<0.01$) and with C18 ($P<0.01$). Rat acyl ghrelin within Eslami C18 was also shown to have significantly better recovery than Rauh without C18 ($P<0.05$).

Within Sidibe C18 ziptip samples, rat unacylated ghrelin was recovered significantly better than rat acyl ghrelin ($P<0.0001$).

Sidibe samples treated with C18 ziptips also outperformed Rauh in all comparisons for both peptides ($P<0.0001$). Across the Rauh method, no significant differences between rat acyl and unacylated ghrelin were shown, and no clear benefit from C18 purification.

To summarise, Sidibe C18 ziptips samples consistently showed the highest recovery among all groups.

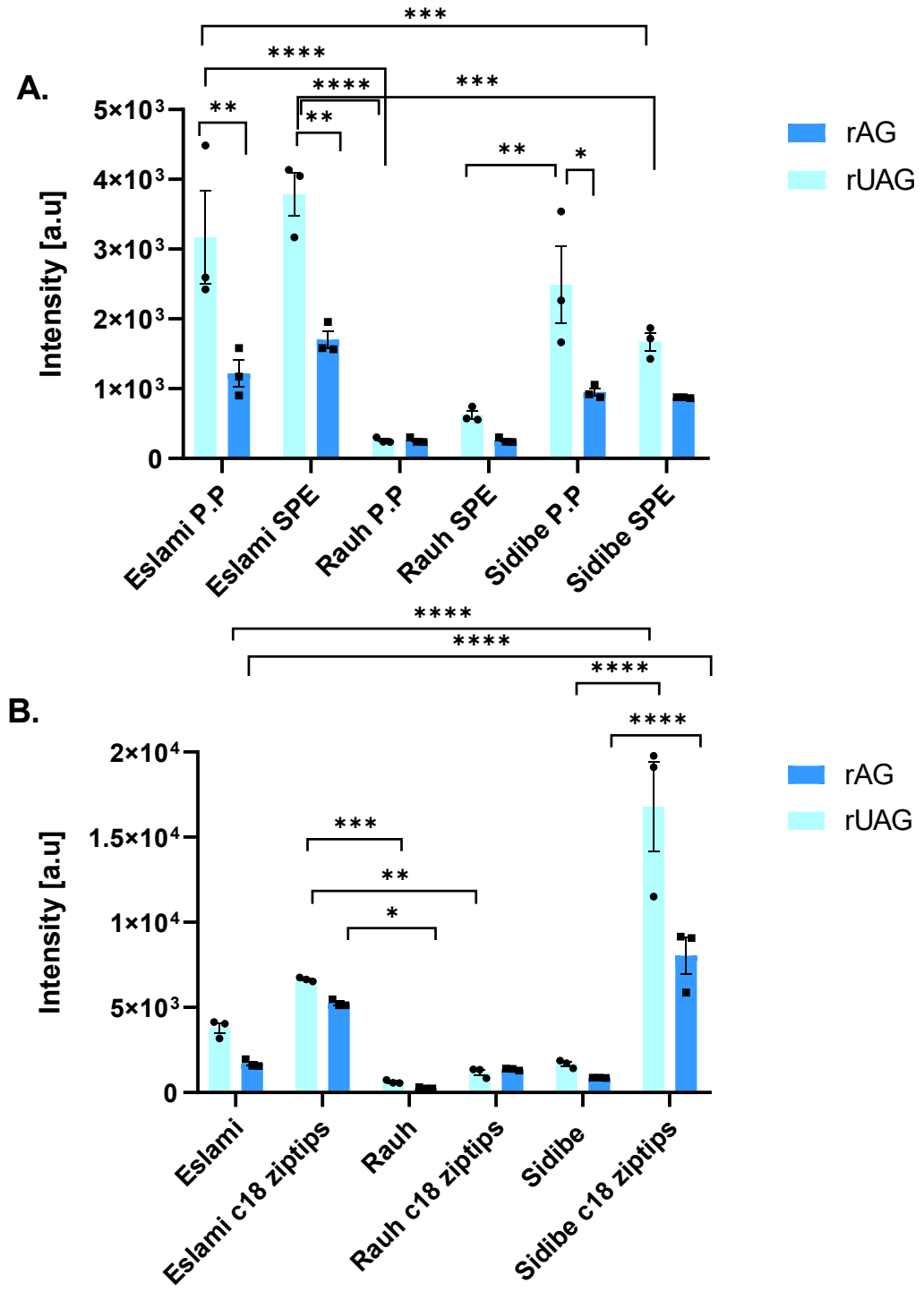

Figure 3.13 Detection of ghrelin following Protein Precipitation, SPE, and the use of C18 ziptips. A. Ghrelin extracted after protein precipitation (P.P. on the graph) versus protein precipitation followed by SPE. B. Ghrelin extracted using protein precipitation and SPE but using, regular tips versus C18 ziptips before MALDI-TOF analysis. Two-way ANOVA was performed with Tukey corrections. P<0.05 is considered statistically significant.****<0.001, *** P<0.001, **P<0.01, *P<0.05. The data shown represents mean +/- SEM. N=3.

Due to the low intensities of ghrelin observed after SPE, alternative options were explored to concentrate ghrelin in samples post-SPE. One such option investigated was the use of centrifugal filter devices known for their ability to purify and concentrate samples effectively (Yang and Sumbria 2021). In this study, the use of 10kDa or 3kDa molecular weight cutoff filters (MWCO) after performing SPE was investigated for their potential to concentrate ghrelin in samples (Figure 3.14).

Within the Eslami dataset, SPE of rat unacylated ghrelin was significantly higher than the 3 kDa centrifugal filter ($P < 0.05$), while the 10 kDa centrifugal filter of rat unacylated ghrelin was significantly greater than the 3 kDa centrifugal filter ($P < 0.0001$). In contrast, for rat acyl ghrelin, the 3 kDa centrifugal filter was significantly higher than the 10 kDa centrifugal filter ($P < 0.001$). When comparing across datasets, the Sidibe 3 kDa centrifugal filter of rat unacylated ghrelin was significantly greater than the Eslami 3 kDa centrifugal filter ($P < 0.001$), and the Sidibe 3 kDa centrifugal filter of rat acyl ghrelin was also significantly higher than the Eslami 3 kDa centrifugal filter ($P < 0.0001$). Furthermore, the Sidibe 10 kDa centrifugal filter of rat acyl ghrelin was significantly higher than the Eslami 10 kDa centrifugal filter ($P < 0.0001$) and also significantly greater than the Sidibe SPE of rat acyl ghrelin ($P < 0.0001$). Collectively, these findings indicate that the choice of centrifugal filter influences the relative recovery of rat unacylated and acyl ghrelin, with the 10 kDa filter favouring recovery of rat unacylated ghrelin, whereas the 3 kDa filter preferentially retains rat acyl ghrelin. In addition, the consistent differences between the Eslami and Sidibe datasets highlight the impact of methodological variation or sample preparation on ghrelin recovery, underscoring the importance of extraction strategy in determining biomarker yield and reproducibility.

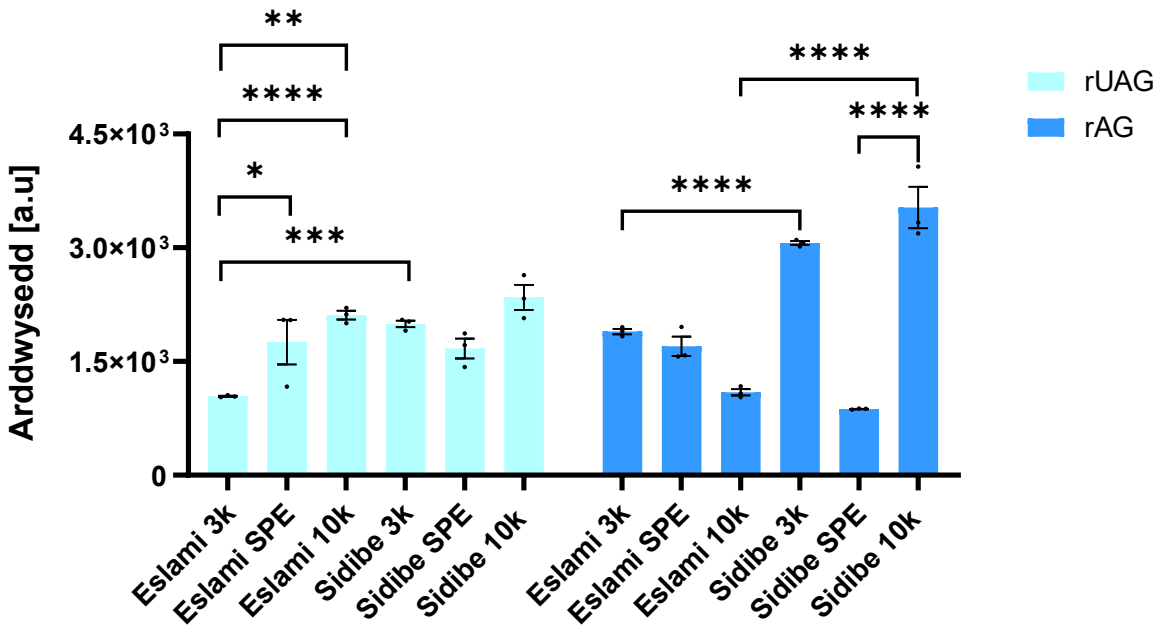

Figure 3.14 Comparison of 3kDa or 10kDa centrifugal filters following either the Eslami et al. or Sidibe et al. protein precipitation methods and SPE compared against without the use of centrifugal filters.

Two-way ANOVA was performed with Tukey corrections. P<0.05 is considered statistically significant. **** P<0.0001, ***P<0.001, * P<0.05. The data shown represents mean +/- SEM. N=3. Statistical significance is shown only for selected comparisons (Eslami SPE vs 3k vs 10k, and Sidibe SPE vs 3k vs 10k) for clarity. Additional statistically significant comparisons, including between Eslami and Sidibe protocols, are described in the results text and summarised in Supplementary Figure S1.

To address the persistently low intensity of ghrelin after extraction, alternative SPE columns were explored. C18 HLB columns were identified as a potential alternative and subjected to testing. HLB columns differ from C18 columns in their composition; whilst C18 contains a fully porous silica-based packing, HLB columns utilise a fully porous polymeric packing. Ghrelin exhibits both polar and nonpolar characteristics because of the presence of lysine and arginine residues, as well as the addition of the octanoyl group. Previous studies have reported on the dual nature of ghrelin (Eslami et al., 2016). Typically, more traditional silica-based sorbents, such as C18 columns, are known to be more effective with nonpolar analytes (Waters Corp). However, oasis HLB columns possess the advantage of being able to extract both polar and nonpolar analytes. This characteristic is particularly relevant in the case of ghrelin, where acylated and unacylated forms may exhibit slightly different properties. Thus, it was anticipated that the HLB columns might be appropriate for the wide range of acyl and unacylated species of ghrelin.

The HLB columns demonstrated a significantly improved intensity of ghrelin for both rat acyl ($P<0.01$) and unacylated ghrelin ($P<0.05$) compared to the traditional C18 columns (Figure 3.15). Based on these results, they were selected as the preferred choice to conduct SPE from this point onwards.

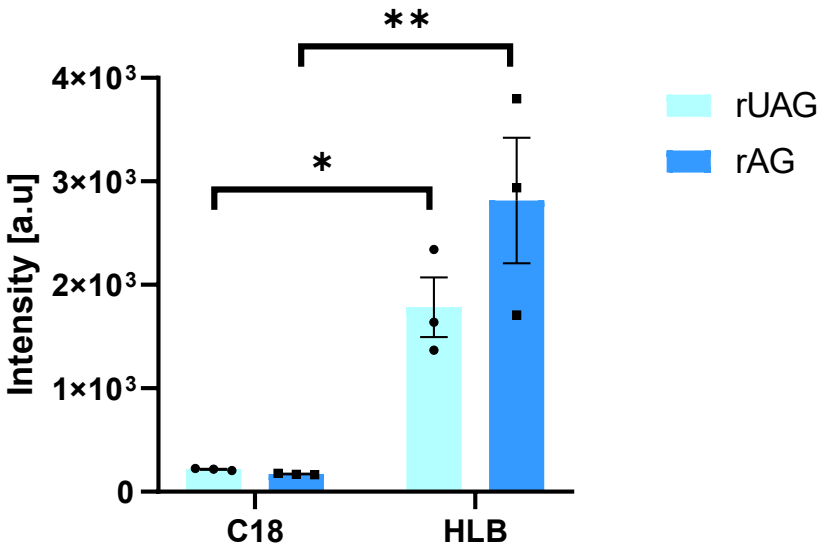

Figure 3.15 Comparison of C18 columns versus HLB columns following protein precipitation (Sidibe et al. method) in the extraction of rAG and rUAG 'spiked' into human plasma.
Two-way ANOVA with Two-way ANOVA performed with Tukey corrections. $P<0.05$ is considered statistically significant. ** $P<0.01$, * $P<0.05$. The data shown represents mean +/- SEM. N=3.

Given the better performance of HLB columns in the retention of ghrelin, we further explored the possibility of enhancing ghrelin retention by combining them with C18 ziptips after the use of HLB columns. The results suggest that the addition of C18 ziptips did not significantly improve ghrelin retention compared to using HLB columns alone (Figure 3.16). This is similar to the results in Figure 3.12 where ziptips also failed to improve ghrelin retention after the use of C18 columns. These results indicate that the inclusion of C18 ziptips in the workflow after the use of HLB SPE separation did not contribute to enhanced ghrelin retention and therefore the use of C18 ziptips was excluded from the protocol.

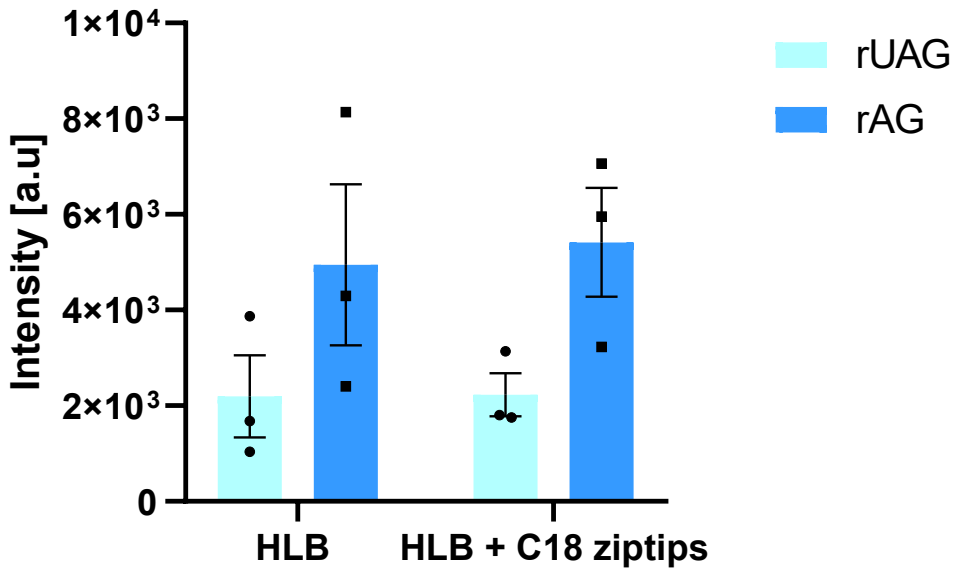

Figure 3.16 The impact of C18 ziptips on ghrelin retention following protein precipitation using the Sidibe method and HLB columns.

Analysed by MALDI-TOF. Two-way ANOVA was performed with Tukey corrections. P<0.05 is considered statistically significant. The data shown represents mean +/- SEM. N=3.

Another option for consideration was the use of centrifugal filters after the HLB columns. The application of centrifugal filters after the Sidibe et al. method of protein precipitation followed by SPE previously demonstrated that 10kDa filters in the case of rat acyl ghrelin obtained the best ghrelin levels (Figure 3.14). As a result, the application of 10kDa filters was further explored after protein precipitation and SPE now that the HLB columns were being employed. Overall, no significant improvement in levels for either 'spiked' rat acyl or unacylated ghrelin was observed (Figure 3.17). The use of both HLB columns and centrifugal filters did not yield significant improvements in ghrelin detection, thus alternative approaches were pursued to improve sample retention and extraction. An approach investigated was drying the sample utilising vacuum desiccation (speedvac) to concentrate the analyte and potentially achieve higher intensities during MALDI-TOF analysis.

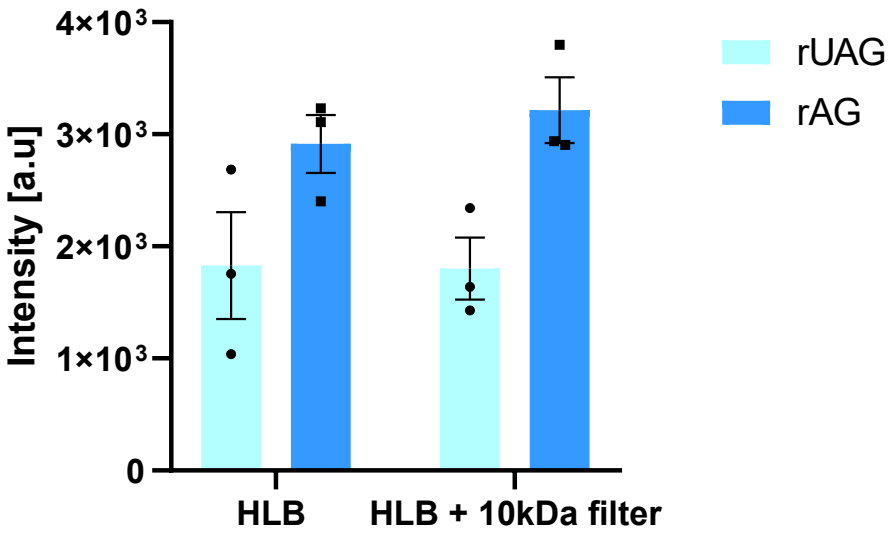

Figure 3.17 Comparison of ghrelin detection following HLB SPE and the use of 10Kda filters. Plasma 'spiked' with 10 ng/mL ghrelin underwent protein precipitation (Sidibe et al. method). SPE uses HLB columns and the use of 10kDa filters. Samples were analysed by MALDI-MS, and Two-way ANOVA was performed with Tukey corrections. P<0.05 is considered statistically significant. The data shown represents mean +/- SEM. N=3.

The impact of drying on ghrelin recovery was assessed using plasma samples subjected to protein precipitation (Sidibe et al. method) followed by SPE with HLB columns. Samples were subsequently dried under vacuum either immediately after SPE or following centrifugation using 10kDa filters. In both cases—whether drying was performed after SPE or after the 10kDa filtration—lower levels of ghrelin were detected (Figure 3.18).

For rat acyl ghrelin, significantly greater retention was observed when samples were processed with SPE alone or with SPE followed by 10kDa filtration, without drying ($P < 0.05$). Furthermore, acyl ghrelin recovery with SPE followed by 10kDa filtration was significantly higher than in comparison to 10kDa filtration step with speedvac ($P < 0.001$).

Regarding rat unacylated ghrelin, samples that underwent both 10kDa filtration and vacuum drying exhibited significantly lower ghrelin levels compared to SPE alone ($P < 0.05$). Additionally, SPE combined with 10kDa filtration (without drying) resulted in significantly higher recovery than either SPE with vacuum drying ($P < 0.01$) or the combination of 10kDa filtration and vacuum drying ($P < 0.01$).

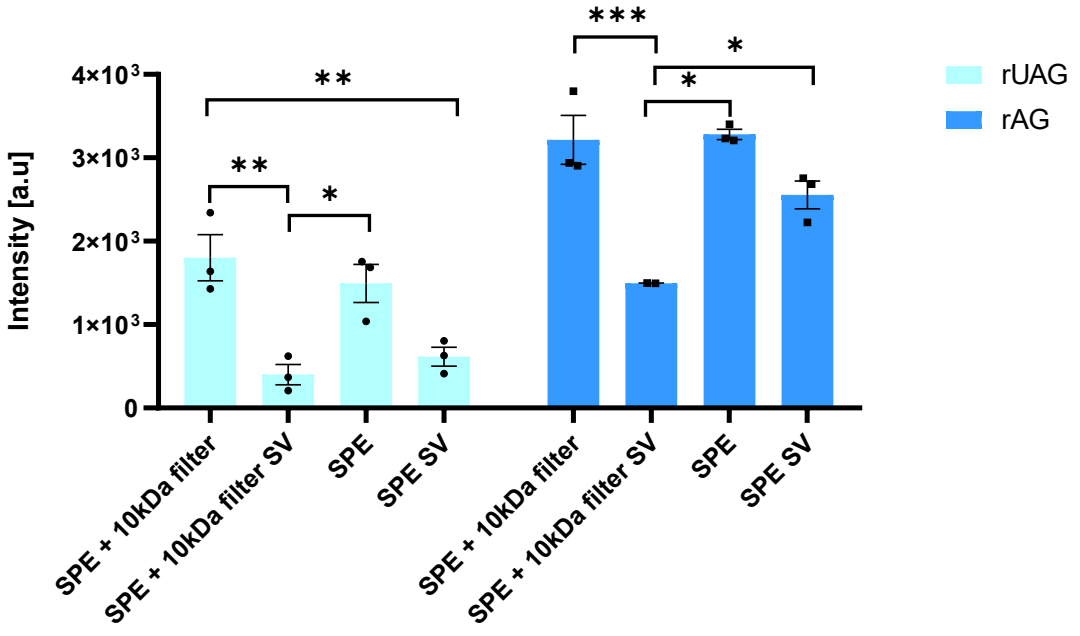

Figure 3.18 Comparing the effect of drying down the sample to concentrate.
Plasma 'spiked' with 10 ng/mL ghrelin underwent protein precipitation (Sidibe et al. method) followed by SPE (HLB column) and was then either dried down under vacuum using a speed vac (SV) immediately or after undergoing centrifugation using 10kDa filters. Samples were then analysed by MALDI-MS. Two-way ANOVA was performed with Tukey corrections. P<0.05 is considered statistically significant. * P<0.05, ** P<0.01, **P<0.001. The data shown represents mean +/- SEM. N=3.

Considering the low levels of ghrelin, the possibility of loss of ghrelin was investigated. Therefore, the next objective was to pinpoint the stages or factors of the sample preparation process that could be responsible for the low ghrelin levels observed. To assess the potential loss of ghrelin following the use of 10kDa filters, the flow-through (filtrate) and the 10kDa filter (retentate) were assessed. Given ghrelin's molecular weight (~3 kDa), it was expected to pass through the 10 kDa filter and be recovered in the flow-through fraction. However, the results demonstrated a more complex picture (Figure 3.19). For rat unacylated ghrelin, although a notable portion of the analyte was detected in the overspill fraction, a substantial amount remained in the 10kDa filter retentate. Across replicates, rat unacylated ghrelin levels in the filter were consistently higher than in the overspill fraction. Similarly, rat acyl ghrelin showed a substantial presence in both the filter retentate and the overspill, with in some cases even higher amounts detected in the filter than in the overspill. This finding suggests that both forms of ghrelin were partially retained by the filter, contrary to the expected complete passage of these peptides through a 10kDa MWCO membrane.

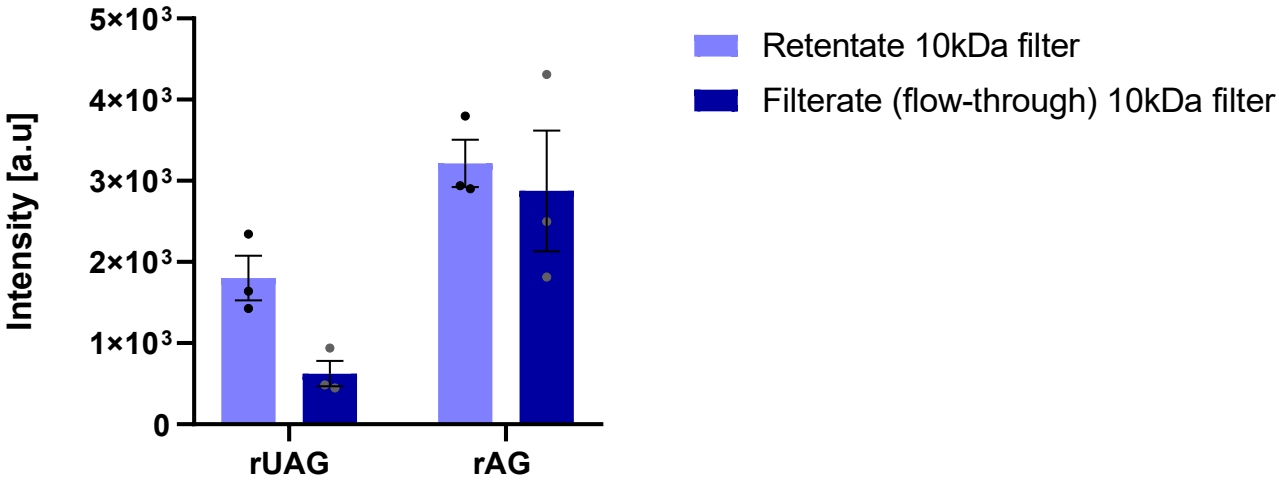

Figure 3.19 Ghrelin capture from the 10kDa centrifugal filter device and flow-through.
Plasma 'spiked' with 10 ng/mL rat ghrelin underwent protein precipitation (Sidibe et al. method) and SPE (HLB) followed by 10kDa filters, both the retained (retentate) and flow-through (filtrate) fractions were analysed by MALDI-TOF. The data shown represents mean +/- SEM. N=3.

Due to the substantial loss of ghrelin observed during the centrifugal filtration step, further investigations were conducted to identify other potential points of peptide loss within the sample preparation workflow. One such point was the use of C18 ZipTips, which operate similarly to SPE columns. In this protocol, the ZipTip is first primed before the sample containing ghrelin is aspirated and dispensed multiple times, with the expectation that the peptide binds to the C18 resin while unbound components remain in the Eppendorf tube. The retained peptides are then eluted directly onto the MALDI-TOF target for analysis.

To assess the efficiency of this step, an equimolar solution of rat ghrelin standard (10 ng/mL) in water containing 0.01% trifluoroacetic acid (TFA) was processed using the C18 ZipTip protocol. Both the eluate and the leftover solution from the final step, where no ghrelin should theoretically remain, were analysed by MALDI-TOF.

As shown in Figure 3.20, a considerable proportion of rat unacylated ghrelin remained in the leftover solution following the ZipTip procedure, with consistently higher levels detected in the leftover fraction compared to the ZipTip eluate across all replicates. This indicates poor retention or inefficient elution of rat unacylated ghrelin, suggesting

that the peptide may not effectively bind to the C18 matrix or is inadequately recovered during elution.

Similarly, although rat acyl ghrelin was generally recovered in greater amounts in the ZipTip eluate, substantial quantities were still present in the leftover fraction. In some cases, the peptide levels in the leftover solution were comparable to or even exceeded those in the eluate, further highlighting inconsistencies in peptide recovery.

These findings reveal notable limitations of the current C18 ZipTip protocol, particularly for rat unacylated ghrelin, and suggest that factors such as suboptimal peptide binding, insufficient elution strength, or procedural losses may contribute to these inefficiencies.

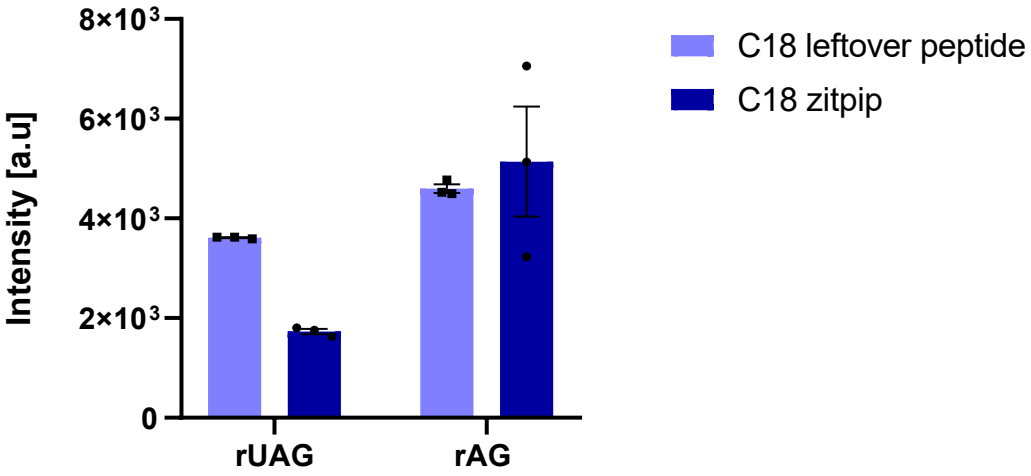

Figure 3.20: Representation of ghrelin loss during the C18 ziptips protocol.
Plasma 'spiked' with 10 ng/mL ghrelin underwent protein precipitation (Sidibe et al. method) and SPE (HLB column) followed by C18 ziptips and analysed by MALDI-MS. The data shown represents mean +/- SEM. N=3.

Another aspect that was investigated in relation to ghrelin loss was the nonspecific binding of ghrelin molecules to various surfaces encountered during the sample preparation process. It was hypothesised that ghrelin could potentially remain bound to the original Eppendorf tubes or other components, resulting in lower levels of ghrelin being measured in the final samples. This phenomenon could contribute to the low intensity of ghrelin signals observed.

3.3.5 Non-Specific Binding of Ghrelin

3.3.5.1 Investigating the Use of Bovine Serum Albumin to Prevent Non-Specific Binding

To mitigate the issue of nonspecific binding during protein extraction, the utilisation of bovine serum albumin (BSA) was explored. BSA is known for its ability to reduce nonspecific binding and enhance protein stability. The underlying concept is that BSA molecules would bind to potential sites where nonspecific binding might occur, thereby preventing the protein of interest from adhering to these surfaces. To evaluate the effectiveness of BSA in minimising nonspecific binding, the calibration curve described in Chapter 3.3.3, Figure 3.9, was repeated without the addition of BSA (Figure 3.21A) and with the addition of 0.1% BSA in the solution used to dilute the standard (Figure 3.21B). Rat acyl ghrelin was used as an ISTD at 0.65 ng/mL with rat unacylated ghrelin varying from 0.08-2 ng/mL. Additionally, the tips and Eppendorf tubes used in the experiment were coated with 0.1% BSA to minimise the chances of ghrelin binding to these surfaces. Although the addition of BSA showed some improvement in the calibration curve (R^2 of 1 compared to without BSA with R^2 of 0.99), the calibration curve without BSA was already well quantified and showed little room for improvement.

After successfully conducting the calibration curve in the presence of 0.1% BSA, further experiments were performed to assess the effect of including BSA during sample preparation. These experiments included coating 10kDa centrifuge filters, HLB columns, Eppendorf (used during the drying stage), and regular tips versus C18 ziptips with 0.1% BSA before use (Figure 3.22). Overall, the use of BSA during sample preparation did not significantly improve ghrelin retention and overall observed ghrelin levels.

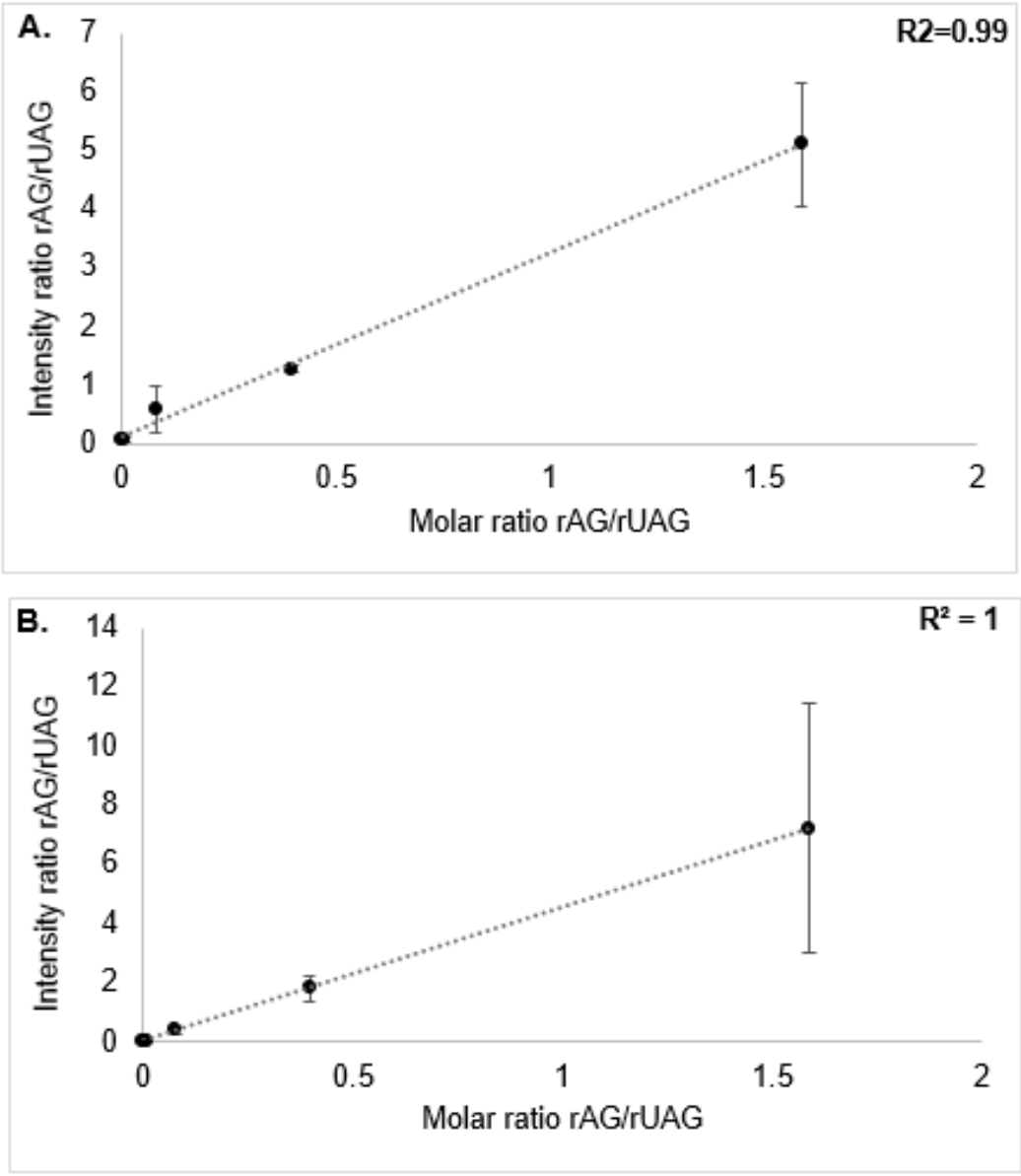

Figure 3.21 Calibration curve of rat ghrelin without (A) and with (B) the presence of 0.1% BSA. rAG as ISTD at 51 ng/mL and rUAG varying from 0.08-2 ng/mL. Analysed by MALDI-TOF N=3. The final plotted point is the mean of these three-run means, and error bars represent the standard deviation across runs, reflecting inter-run variability. Trendlines represent linear regression fits, and R^2 values are reported to indicate goodness of fit.

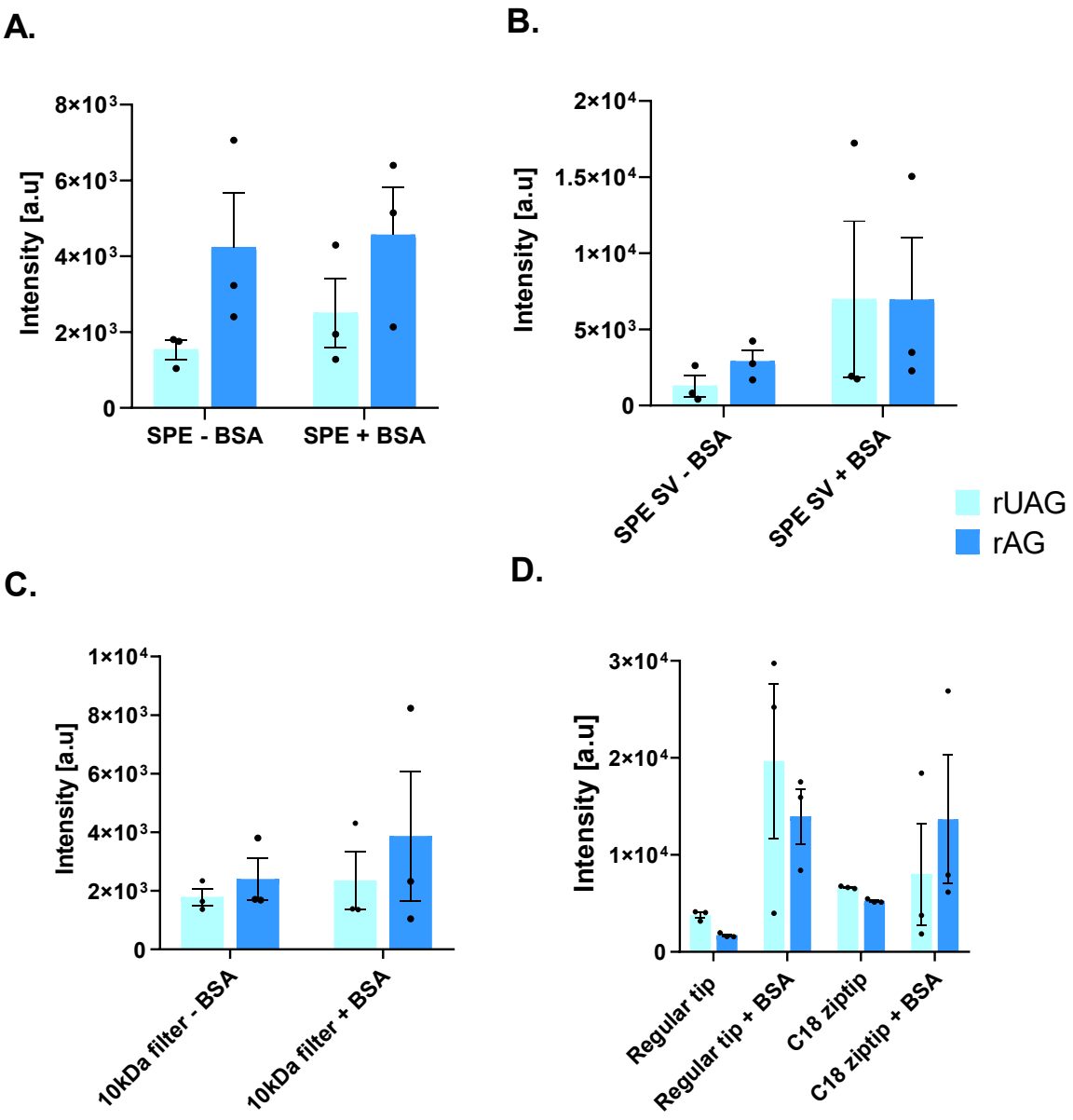

Figure 3.22 Assessing the effect of BSA on ghrelin recovery after extraction.
Plasma 'spiked' with 10 ng/mL ghrelin underwent protein precipitation (Sidibe et al. method) and SPE (HLB column) with and without conditioning with 0.1% BSA (A), and then either clean-up using 10kDa filters with and without conditioning with 0.1% BSA (B) or concentration by drying under vacuum (SV) using tubes with and without conditioning with 0.1% BSA (C) clean-up using C18 ziptips with and without conditioning with 0.1% BSA (D). Two-way ANOVA was performed with Tukey corrections. $P<0.05$ is considered statistically significant. The data shown represents mean +/- SEM. N=3.

A side-by-side comparison of the effect of using BSA during both SPE and the drying down steps was investigated to determine whether BSA could aid in increased ghrelin extraction compared to conditioning using BSA during SPE alone. Again, no significant differences were observed, suggesting that drying the sample or conditioning with BSA

did not significantly increase the recovery of ghrelin (Figure 3.23). Further research may be necessary to explore alternative approaches or modifications to the sample preparation method to mitigate ghrelin losses more effectively.

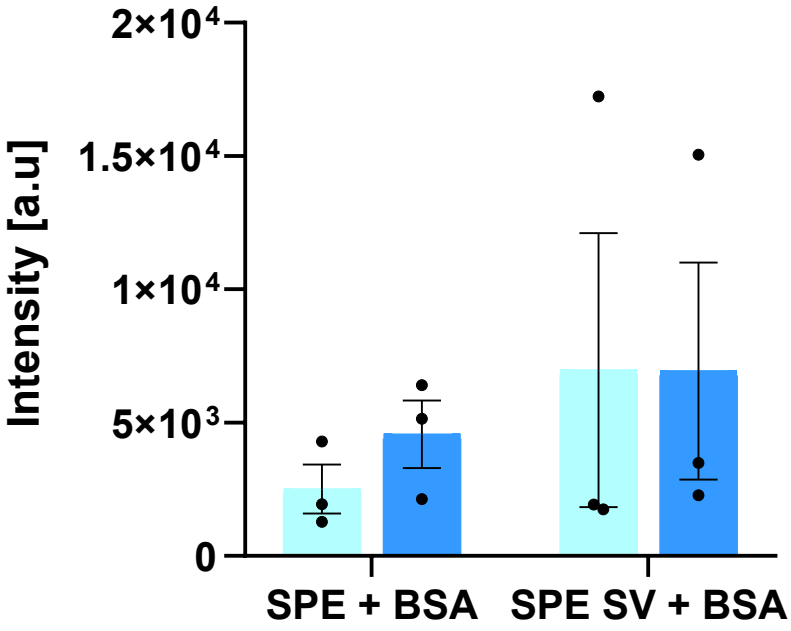

Figure 3.23 The recovery of ghrelin following extraction in the presence or absence of BSA during both the SPE and SV steps.

Plasma 'spiked' with 10 ng/mL ghrelin underwent protein precipitation (Sidibe et al method) and SPE (HLB column) drying down under vacuum (SV) following conditioning with 0.1% BSA Samples analysed by MALDI-TOF. Two-way ANOVA was performed with Tukey corrections. $P<0.05$ is considered statistically significant. The data shown represents mean +/- SEM. N=3.

3.3.5.2 Investigating the Potential Binding of Ghrelin on the MALDI Target Plate

During a detailed investigation of the potential sources of ghrelin loss during the sample preparation phase, ghrelin was observed to be present during the MALDI-TOF analysis of 'blank samples' (Figure 3.24A). To identify the source of contamination, the matrix alone was examined to determine whether it contained traces of ghrelin. No ghrelin signals were detected in the matrix alone (Figure 3.24B), suggesting that the matrix was not the source of ghrelin contamination.

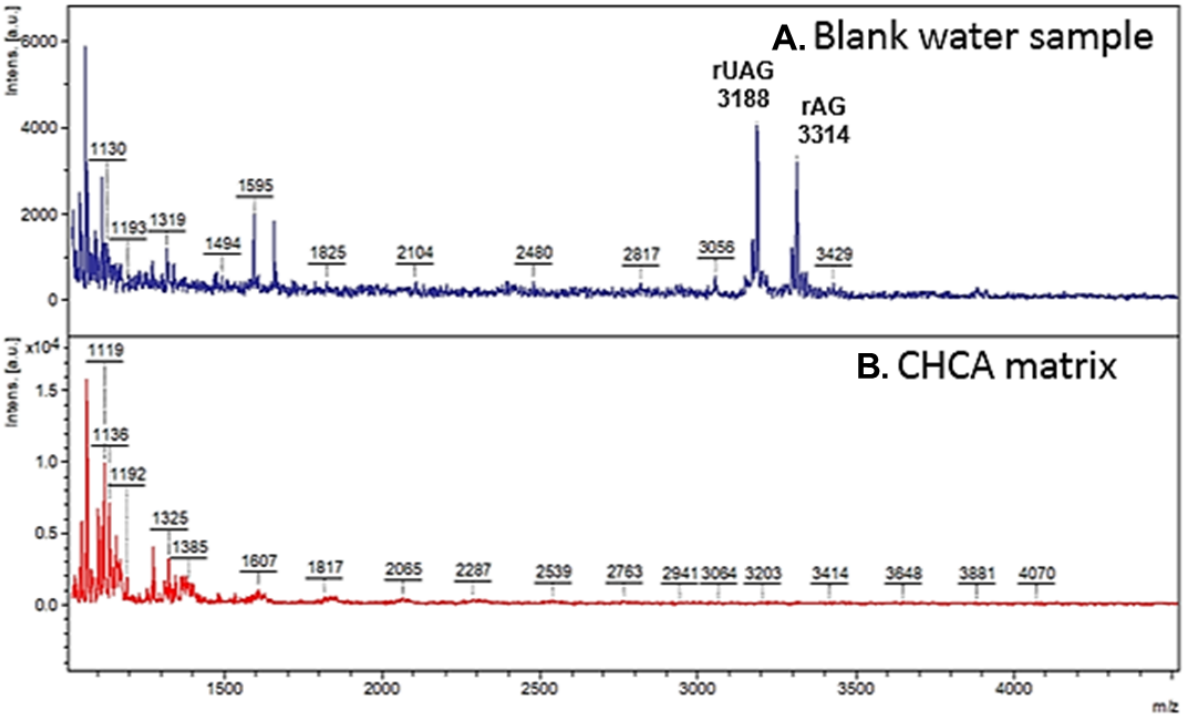

Figure 3.24 Presence of ghrelin contamination.

Presence of rat ghrelin in a blank water sample during MALDI-TOF analysis (A), but absence in matrix alone (B). Example of one MALDI-TOF spectra out of 12.

Additional tests were carried out using a different MALDI target, water source, and pipette (Figure 3.25) to identify factors that could contribute to the presence of ghrelin in the MALDI spectra. First, the regular MALDI target used was examined under different conditions. Regardless of the water source and pipette used, ghrelin species were consistently observed in the spectra obtained after using the regular MALDI target (Figure 3.25 A-C). This indicated that ghrelin could accumulate on the target surface over time despite cleaning between experiments (see Section 2.4, Cleaning Procedure 1), leading to contamination. Thus, a new MALDI target plate that had not previously been exposed to ghrelin was tested (Figure 3.25 D-F). Under the same experimental conditions, no ghrelin species were detected in the spectra obtained from the new target. This confirmed that the contamination was specific to the regularly used MALDI target.

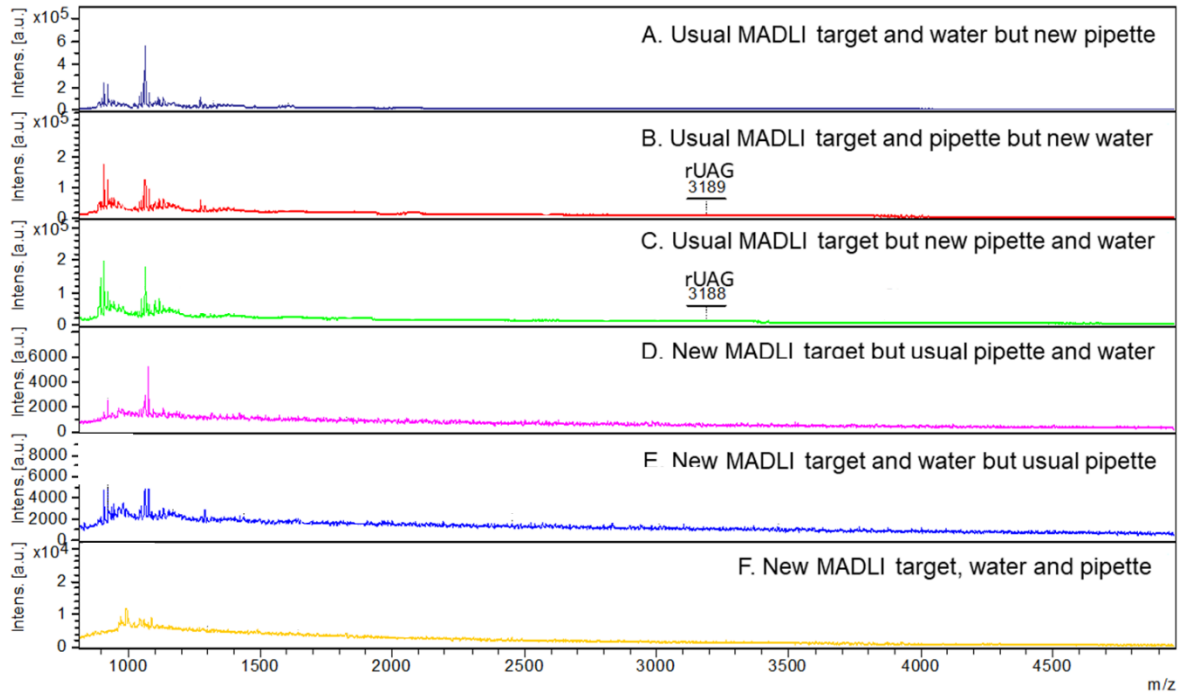

Figure 3.25 Assessment of potential source of ghrelin contamination.

MALDI analysis was carried out on A. Usual MALDI target and water but new pipette. B. Usual MALDI target and pipette but new water. C. Usual MALDI target but new pipette and water. D. New MALDI target but usual pipette and water. E. New MALDI target and water but usual pipette. F. New MALDI target, water, and pipette. Example of one MALDI-TOF spectra out of 12.

Based on these observations, it was concluded that ghrelin can build up on the MALDI target over time, leading to contamination of subsequent samples. To mitigate this issue, a more rigorous cleaning protocol was implemented for the MALDI target to effectively remove residual ghrelin and prevent cross-contamination between samples. More specifically, to prevent cross-contamination, the target was cleaned using 80% TFA solution (outlined in Section 2.4, Cleaning Procedure 2) before each subsequent analysis. Following the implementation of the new extensive cleaning protocol, subsequent analysis of the MALDI target revealed that there was no presence of ghrelin.

3.3.6 Concentrating Ghrelin in Samples

3.3.6.1 Drying Samples

To address the issue of low ghrelin signal after SPE, further investigations were performed to evaluate the impact of sample concentration by vacuum drying on ghrelin recovery. Unlike earlier experiments, which combined drying with protein precipitation, SPE, or 10 kDa filtration, these tests focused solely on drying down ghrelin standards

under vacuum, without prior sample clean-up. Equimolar mixtures of all ghrelin species, including human and rat forms, were prepared at a final concentration of 40 ng, as this concentration had previously produced robust MALDI-MS signals.

Initially, the effect of drying volume was assessed by comparing samples that were dried from either 5 µL or 25 µL starting volumes and subsequently resuspended in a fixed volume of 5 µL of 50% acetonitrile, which was the standard resuspension solvent used in previous experiments (Figure 3.26A). This experiment aimed to determine whether a smaller starting volume, which reduces drying time, could improve recovery, as extended drying times with larger volumes could potentially lead to ghrelin loss. Interestingly, despite the higher theoretical concentration expected from drying down 25 µL, both rat and human acyl-ghrelin showed significantly higher intensity when dried from the smaller 5 µL volume (rat acyl ghrelin, $P<0.001$; human acyl ghrelin, $P < 0.0001$). This suggested that ghrelin loss during prolonged drying could be more impactful than the concentration effect of the larger volume.

At the same time, a second set of experiments was performed to examine whether the percentage of acetonitrile in the resuspension solvent influenced peptide recovery after drying. Samples were dried from a 25 µL volume and then resuspended in 5 µL of either 5% or 50% acetonitrile (Figure 3.26B). This was motivated by the possibility that using high acetonitrile concentrations, both during resuspension and in the matrix solution itself, might reduce peptide solubility or cause sample loss during spotting. Across all ghrelin species tested, resuspension in 5% acetonitrile significantly improved signal intensity compared to 50% acetonitrile (rat unacylated ghrelin, $P<0.01$; human unacylated ghrelin, $P< 0.01$; rat acyl-ghrelin, $P < 0.0001$; human acyl ghrelin, $P< 0.01$).

Although not tested in this set of experiments, another approach worth exploring in future work would be to resuspend the dried peptide directly into the MALDI matrix solution, which may further streamline sample preparation and potentially improve recovery.

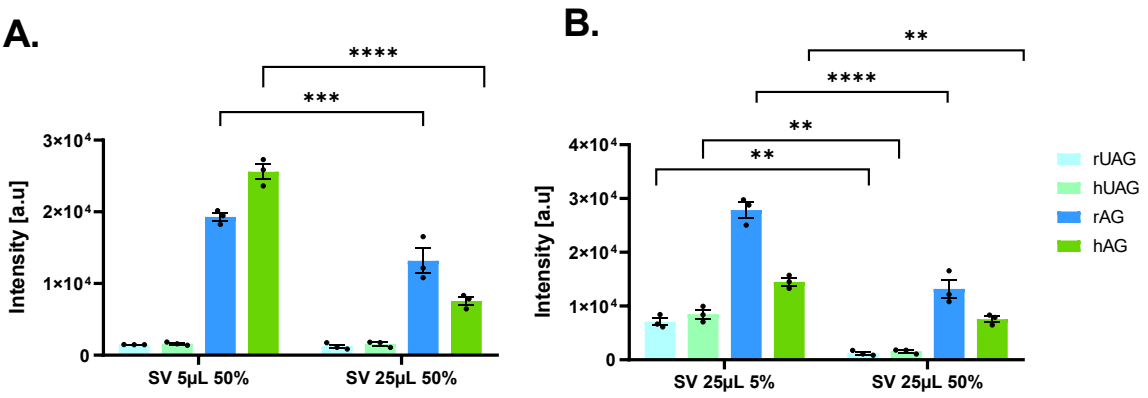

Figure 3.26 Effect of drying down under SV with different initial volumes and resuspending in solutions containing a different percentage of acetonitrile.

In panel A, 40 ng of hUAG, rUAG, hAG, and rAG was added into either a 5 µL or 25 µL volume, dried under vacuum, and then resuspended in 5 µL of 50% acetonitrile. In panel B, samples dried from a 25 µL volume were resuspended in 5 µL of either 5% or 50% acetonitrile to assess the impact of acetonitrile concentration on signal intensity. Two-way ANOVA with Tukey correction was performed; $P < 0.05$ was considered statistically significant.****$P<0.0001$, ***$P < 0.001$, **$P < 0.01$. Data are presented as mean ± SEM, with $N = 3$.

3.3.6.2 Microelution Plate

To address the concentration issues encountered previously, a different method of SPE was used using a µElution plate. The µElution plate was divided into two sections, with one half containing Oasis MAX packaging, which is designed for acidic compounds, and the other half containing WCX, which is designed for strong bases. This approach was designed to optimise the retention and recovery of ghrelin species during the extraction process. According to the recommendation of the Waters protocol for peptides, rat ISTD was added to plasma and mixed 1:1 with 4% phosphoric acid (H_3PO_4) at a volume of 750 µL. Protein precipitation methods were not used before using the µElution plate as the addition of H_3PO_4 breaks the binding of the peptide to protein and dilutes the sample, decreasing viscosity and increasing the contact time with the sorbent. The final elution could be completed in 25 µL of 1% TFA in 75/25 Acetonitrile/H_2O. As such, with a 750 µL load and a 25 µL elution, the sample can be concentrated up to a factor of x30.

To test whether one elution of 25 µL was enough to elute ghrelin from the plate, the elution step was repeated ten times from the same well and each eluate was kept separate and analysed individually for the presence of ghrelin. Following the final/tenth

elution, a wash step was performed, and the presence of ghrelin was tested (Figure 3.27). During this analysis, both the MAX and WCX columns were tested which is highlighted in Figure 3.26A and B, respectively. Endogenous human ghrelin was not detected using this protocol and thus only the ISTD, rat ghrelin, is observed within the figure. Similarities between the MAX and WCX columns are seen in the analysis. With both columns, it can be observed that the intensity of ISTD rat acyl ghrelin in both elutions 1-3 ($P<0.001$) for the MAX and 1-2 (Elution 1, $P<0.001$ and elution 2 $P<0.001$) for WCX is significantly higher than the rat unacylated group. Additionally, in both MAX and WCX, rat ghrelin ISTD was observed in all ten elution steps and during the wash stage. The intensity of rat ghrelin decreases throughout elution. In the case of the MAX column (Figure 3.27A), most of the ghrelin is captured by elution 4, suggesting that at least a 100 µL elution is needed. For the WCX column (Figure 3.26B), ghrelin is captured mainly by elution 3, indicating that at least a 75 µL volume would be needed to capture all ghrelin. The increase of the elution volume from 25 µL as the protocol suggests, removes the benefits of using the microelution plate as the concentration factor decreases. For the MAX column, rat unacylated ghrelin obtained a 92% loss of ghrelin, while rat acyl ghrelin only obtained a 20% loss. In comparison, for the WCX, the rat unacylated ghrelin resulted in a 99% loss, while the rat acyl ghrelin only obtained a 1% loss.

Upon sharing our results with the manufacturers of the microelution plate, our experts advised us to continue with a 25 µL elution and to use C18 ziptips. As such, the first elution of the microelution plate was used to evaluate the effect of C18 ziptips. A significant decrease in rat acyl ghrelin levels ($p<0.001$ for MAX and $p<0.0001$ for WCX) after the use of C18 ziptips was observed, while rat unacylated ghrelin levels remained unchanged (Figure 3.28). These findings suggest that the use of C18 ziptips may not effectively concentrate the ghrelin sample as expected based on previous findings (Figure 3.16). Furthermore, rat acyl ghrelin appeared at a significantly higher intensity than rat unacylated ghrelin for both the MAX and WCX columns ($P<0.0001$). In terms of rat acyl ghrelin, the WCX column performed significantly better ($P<0.0001$) for ghrelin intensity compared to MAX, with rat unacylated ghrelin showing no significance between both. Suggesting that the plate might be more suitable for the extraction of acyl ghrelin compared to that of unacylated ghrelin.

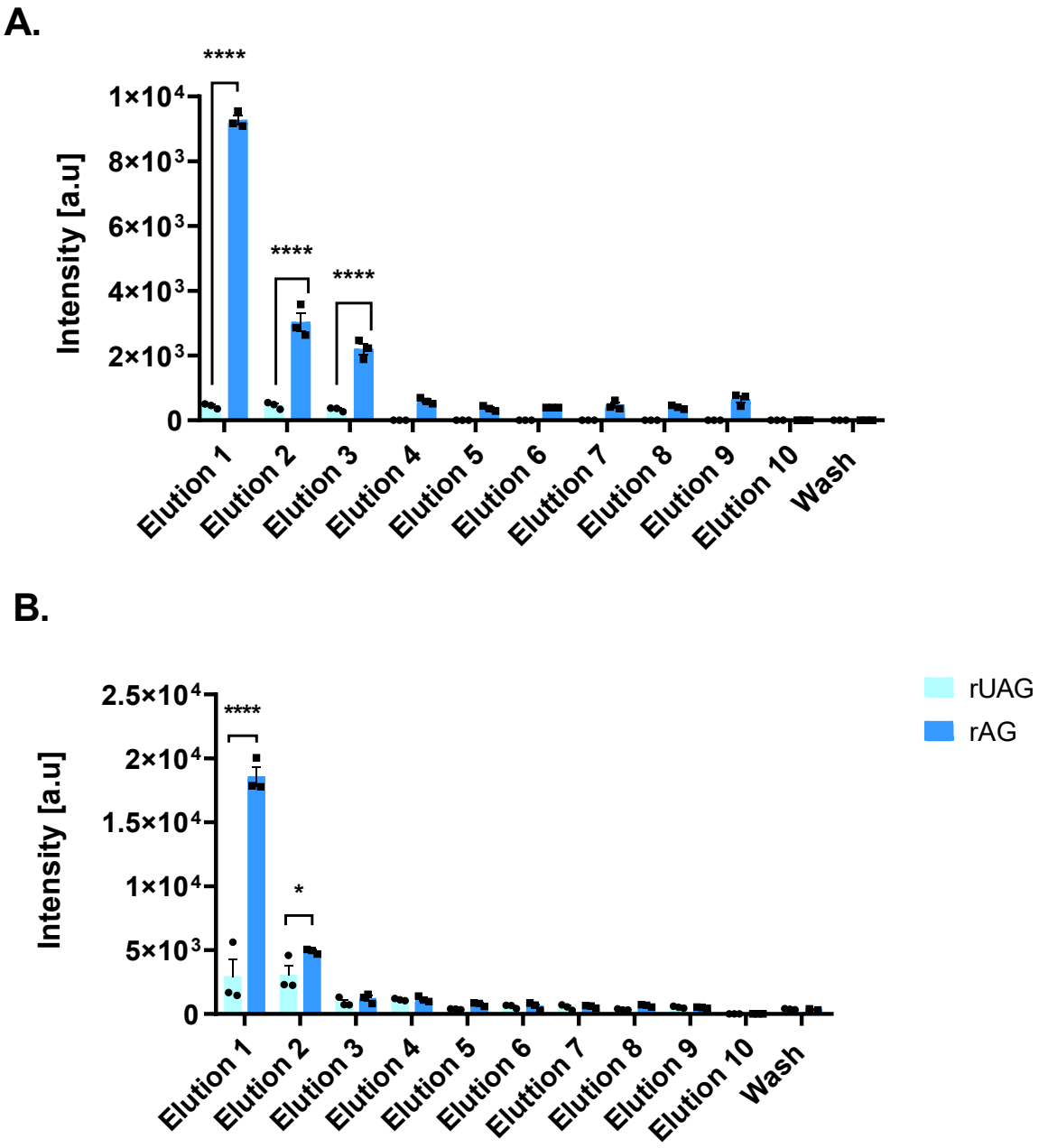

Figure 3.27 The analysis of ghrelin levels in continual elution followed by a wash step in either the MAX column (A) or WCX column (B).

Plasma was 'spiked' with 10 ng/mL rat ghrelin and treated with H_3PO_4 followed by SPE using a microelution place (MAX or WCX columns). Multiple sample eluates were carried out. Samples were analysed by MALDI-TOF. Two-way ANOVA was performed with Tukey corrections. $P<0.05$ is considered statistically significant. ***$P<0.01$, ****$P<0.001$. The data shown represent mean +/- SEM. N=3.

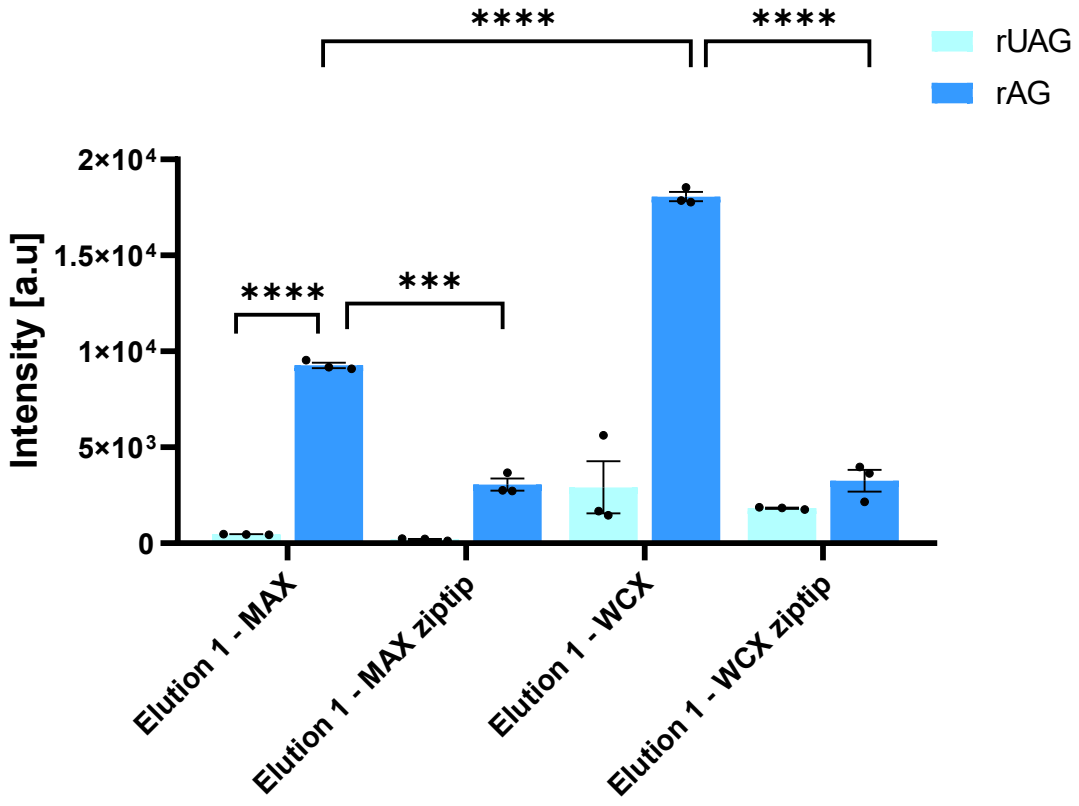

Figure 3.28 Analysis of ghrelin levels of elution step 1, with and without the addition of ziptips in either MAX or WCX columns.

Two-way ANOVA was performed with Tukey corrections. P<0.05 is considered statistically significant. ***P<0.001, ****P<0.0001. The data shown represent mean +/- SEM. N=3.

3.3.6.3 Testing the Use of Ammonium Hydroxide

As ghrelin is a small peptide, it has an increasing likelihood of binding to albumin and other larger proteins. To prevent nonspecific binding of ghrelin to these proteins and thus increase ghrelin extraction, ammonium hydroxide, which has previously been used for ghrelin analysis (Thomas et al., 2021), was added to plasma alongside ISTD. In this experiment, 5% ammonium hydroxide (NH_4OH) was introduced into plasma samples 'spiked' with rat ISTD (10 ng/mL) and vortexed for two minutes. Following the application of ammonium hydroxide, protein precipitation (Sidibe method) is performed with subsequent processing by SPE (HLB columns). Two analytical steps were carried out to evaluate the effects of the addition of ammonium hydroxide: (1) analysis after protein precipitation and (2) analysis after protein precipitation and SPE. In this run (N = 1), the addition of 5% NH_4OH to plasma samples following protein precipitation appeared to increase rat acyl ghrelin levels, potentially by disrupting ghrelin's binding

to larger proteins; however, due to contamination in subsequent experiments, only intra-run variation was available, and further replicates are needed to confirm these preliminary observations (Figure 3.29A–B).

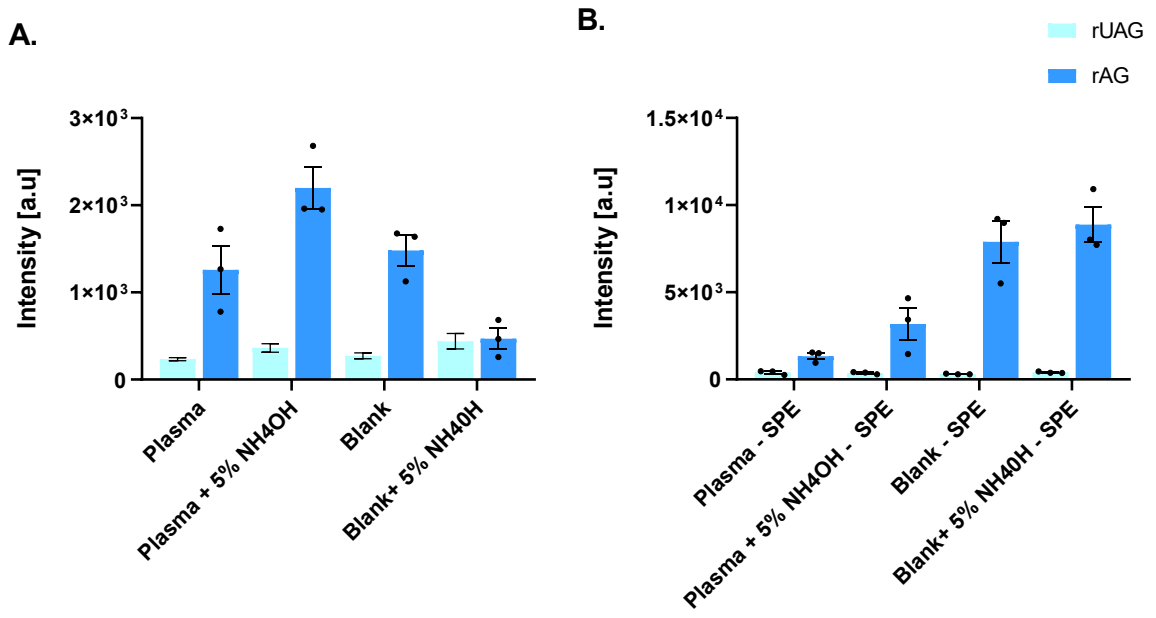

Figure 3.29 Impact of 5% ammonium hydroxide (NH4OH) on the extraction of ghrelin species. Plasma or water treated with or without 5% NH_4OH was 'spiked' with 10 ng/mL rat ghrelin, and samples then underwent protein precipitation (Sidibe et al. method) before being analysed directly by MALDI MS (A) or undergoing SPE separation (HLB Column) before MALDI-TOF analysis. Bars represent the mean ± SEM of three technical replicates per condition within a single experimental run (N=1). Error bars reflect technical variation only and do not indicate biological variability.

3.3.7 Contamination

Following the NH_4OH testing, as described above, a contamination issue became apparent when using the MALDI-TOF, which prevented any further MALDI-TOF analysis. One significant limitation associated with mass spectrometry analysis is the potential for contamination, particularly from polymer polyethylene glycols (PEG). PEG is a very common contaminant and is present in detergents, chemical wipes, and plastics, thus making the identification of the source of PEGs difficult. Because of the abundance of PEGs in everyday laboratory exposure, PEGs are likely to present within samples constantly but at a lower level compared to the samples of interest and thus are suppressed during the ionisation/analysis. However, PEGs can become problematic when the initial analyte of interest is present at low levels, as is the case

for ghrelin. In this situation, as PEG itself is easily ionised, it may suppress the analyte of interest and, in some cases, contamination could render ghrelin levels undetectable.

During routine MALDI-TOF analysis of samples, such as for Figure 3.28, some of the spectra showed signs of PEG contamination which has not previously been seen for any of the earlier results described above. Thus, to identify the source of contamination observed in the spectra readings, a thorough investigation was carried out. Figure 3.30 (A) shows MS spectra from the experiment where contamination was originally seen. The samples analysed included plasma treated with 5% NH_4OH, a rat ghrelin equimolar mix in water, and water treated with 5% NH_4OH. Typical spectra for PEG contamination are observed in the plasma sample treated with 5% NH_4OH, in the water sample, and in the rat ghrelin equimolar mix sample. To further investigate contamination, MS spectra were collected from the samples and HPLC grade solvents most used during the experimental protocol Figure 30. Interestingly, both 5% NH_4OH and acetonitrile showed evidence of contamination. It is noteworthy that MALDI-TOF analysis often has 'background noise' at some level that is related to certain solvents and matrix. This is reduced when analysing samples, as the analyte of interest, will suppress this background noise. This normal background noise can be seen in the acetone of Figure 3.29B and is noted throughout the figure where indicated. This can be identified when looking at the spectra closer and the repeated units of ‘noise’ that are seen. PEG often repeats itself within a pattern of 44kDa, which allows it to be distinguished from background noise. As contamination was observed in both acetonitrile and NH_4OH, this suggests that contamination may not be specific to a particular solvent but rather a more general issue. The contamination might arise from a source other than the solvents themselves, such as the equipment or reagents used in the sample preparation process. In the subsequent investigation, the common solvents acetone and acetonitrile were re-analysed and compared with fresh solvents that had not been previously used (Figure 3.30 C). The spectra obtained from both sets of solvents revealed signs of contamination. However, the use of a different batch of acetone appeared to remove the contamination, suggesting that the contamination may be related to the specific acetone. The contamination observed in acetonitrile was consistent, even when using a brand-new solvent. This implies that the source of contamination in acetonitrile may be inherent and not limited to a particular batch or source.

To remove the source of contamination, a new deep cleaning of the MALDI target was performed at the mass spectrometry facility where PEGs from detergents are less likely to be present (see section 3.2, cleaning protocol 3). The cleaning of the MALDI-TOF differed with the additional use of 70% ethanol in the ultrasonic bath followed by the 80% TFA which was used in the previous cleaning. Following the deep cleaning of the MALDI target, a more extensive test was conducted to ensure the absence of contamination. This test involved assessing the matrix used, including both the matrix that was regularly used in addition to the matrix from a new batch, and analysing different spots on the target. In Figure 3.31A, the results of the matrix test showed that there were no PEGs in the regularly used matrix or the new batch. This indicated that the matrix itself was not the source of contamination and supports the effectiveness of the cleaning procedure. Furthermore, analysis of different spots on the target also revealed that there was no presence of PEGs. This suggests that the previously observed contamination was successfully removed by deep cleaning the target. An equimolar of rat ghrelin was tested using regular equipment such as solvents, tips, and Eppendorf's versus a different batch. No contamination, in the form of PEGs, was detected in the solvents, tips, or Eppendorf's. Overall, these comprehensive tests support the conclusion that the deep cleaning procedure effectively removed the contamination source.

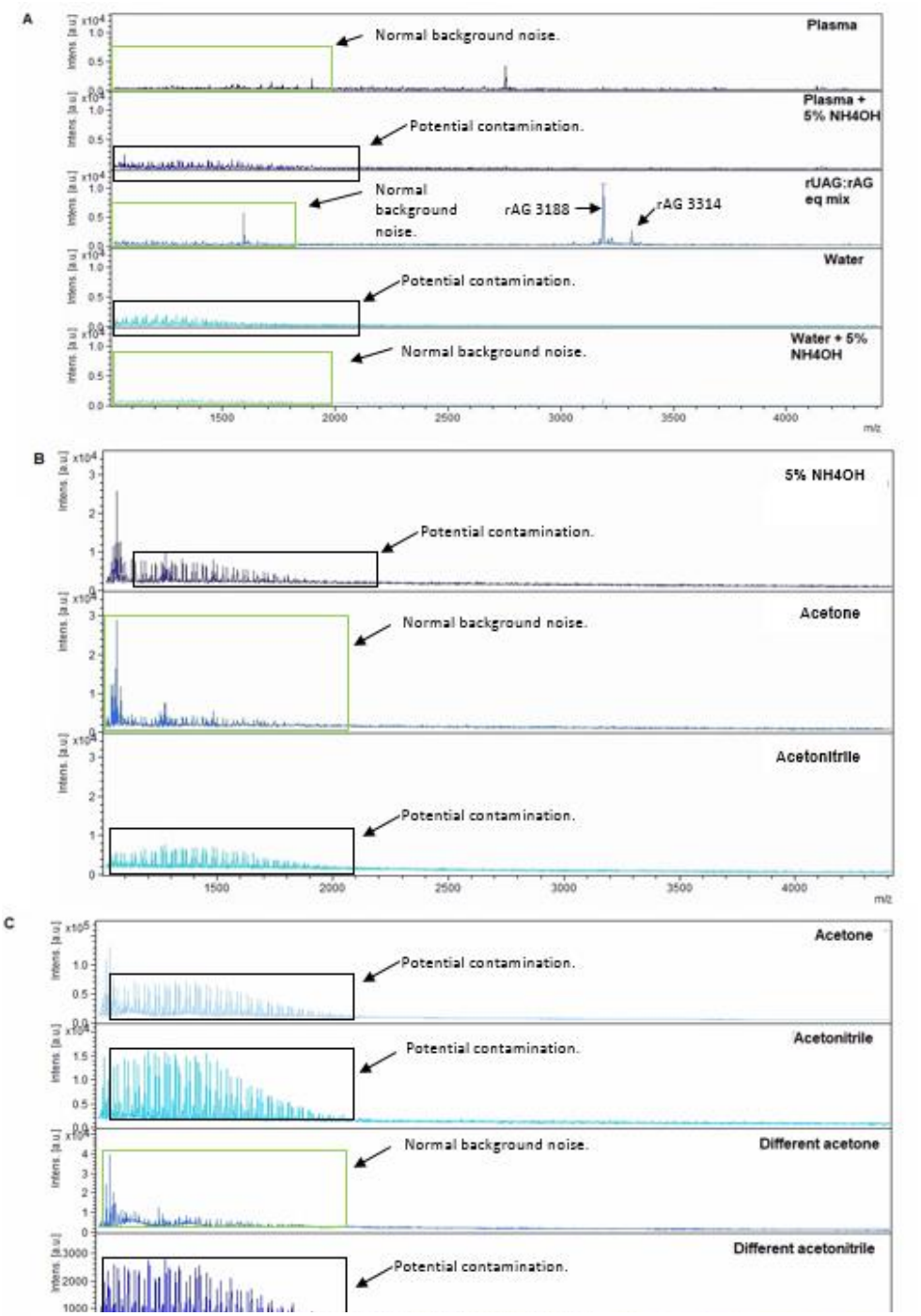

Figure 3.30 Representative of MALDI-TOF spectra from potential sources of contamination, m/z range 1000-5000 Th. A. samples of plasma, plasma sample containing 5% ammonium hydroxide, a rat ghrelin equimolar mix, water, and water with 5% ammonium hydroxide. B. Analysis of different solvents that were used regularly to identify the potential source of the contamination sources was conducted (5% sodium hydroxide, 100% acetone and 100% acetonitrile) C. The effect of changing solvents on the presence of PEGs was assessed (original acetone, original acetonitrile, fresh acetone, fresh acetonitrile). Example of one MALDI-TOF spectra out of 12.

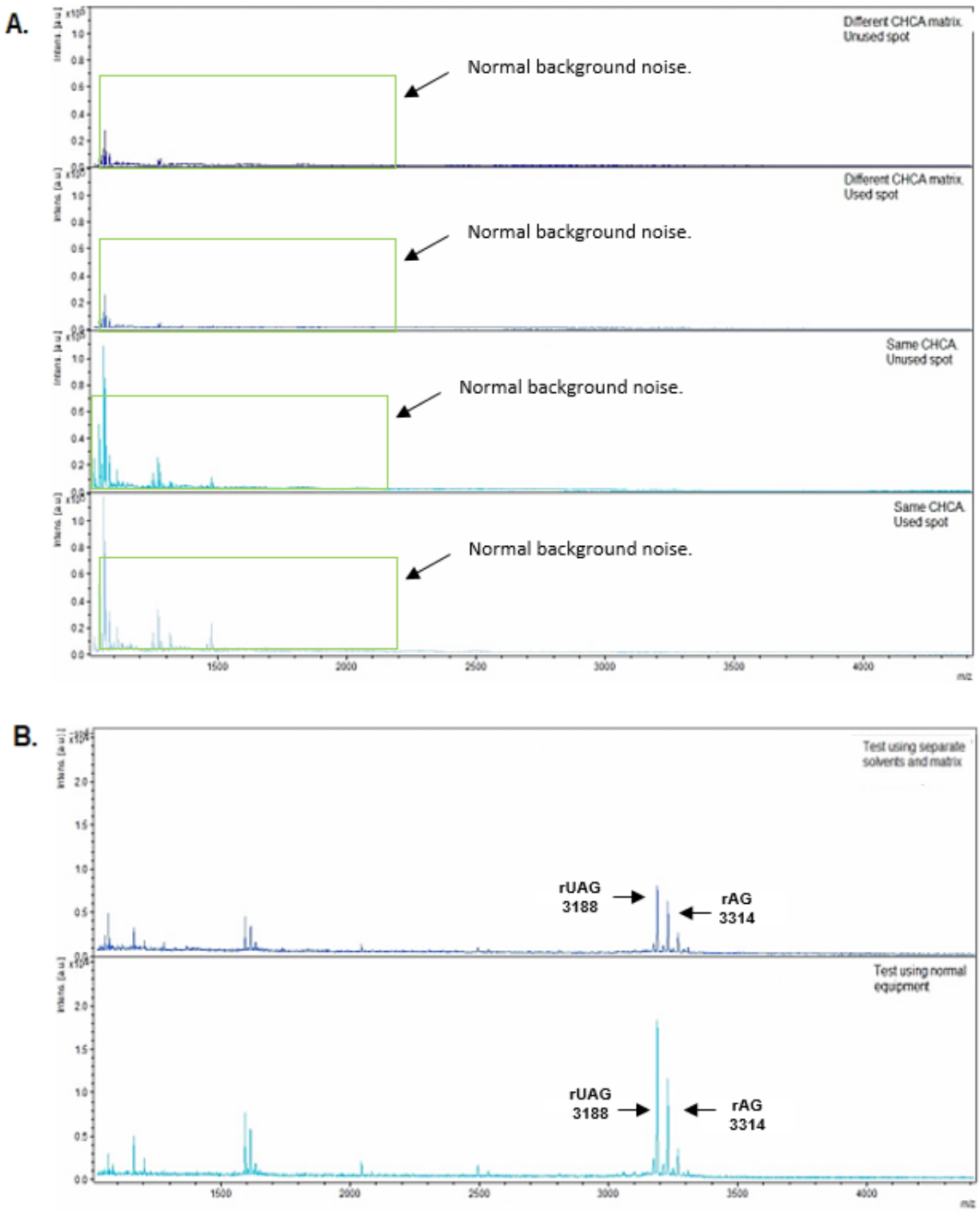

Figure 3.31 Testing the presence of PEG contamination after deep cleaning of the MALDI target. A. The matrix used is evaluated, including both the regular matrix and a new batch. Additionally, different spots on the target are analysed. B. Equimolar mix of rat ghrelin using regular equipment versus new equipment. Example of one MALDI-TOF spectra out of 12.

Despite extensive cleaning and investigation efforts, the reappearance of PEG during sample analysis indicated that the source of contamination was not resolved. In Figure 3.32, an equimolar mixture of rat ghrelin was tested before the continuation of work, however contamination by PEG was observed again.

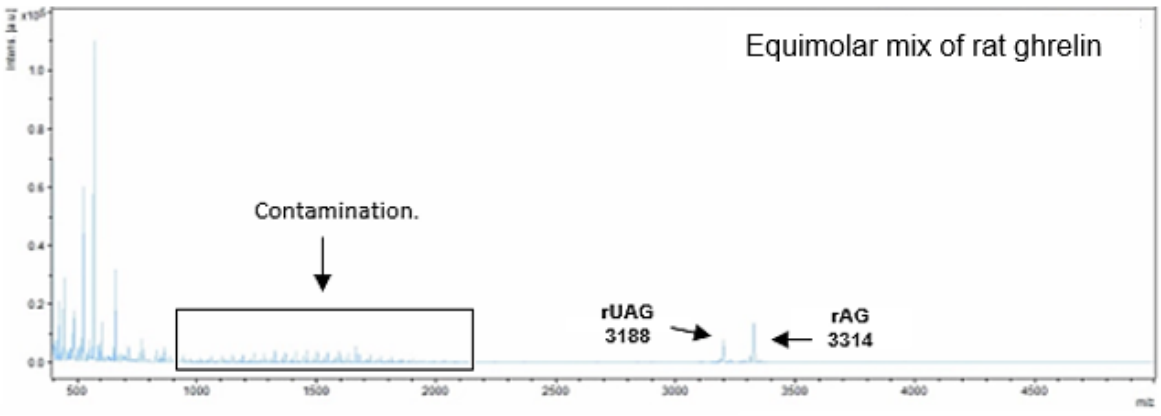

Figure 3.32 Presence of contamination within an equimolar mixture of rat ghrelin.
Example of one MALDI-TOF spectra out of 12.

The origin of PEG contamination appears to be external to the solvents, tips, Eppendorf, and the MALDI target. A deep cleaning of the MALDI-TOF source was also implemented several times, which did not resolve the issue long-term.

3.4 Discussion

MALDI-TOF analysis is a powerful technique for the identification and quantification of peptides and proteins, but it is not without limitations. This scientific discussion aims to address several methodological considerations encountered during the analysis of ghrelin using MALDI-TOF.

In concordance with the literature, the seed crystal method for depositing samples onto the MALDI-TOF target proved to be the most efficient for analysing ghrelin (Vorm 1994; Yun et al., 2022). CHCA was selected as the matrix based on its effectiveness with peptides and proteins. Numerous studies have reported dissolving CHCA in a range of 40-70% acetonitrile (Sun et al., 2008; Singor et al., 2013, Friedemann, Tougu, and Paulmaa 2020; Leszyk 2010) with 50% acetonitrile most reported for ghrelin analysis (Gutierrez et al., 2008; Schopfer et al., 2015). Here, it was discovered that 40% acetonitrile was the most optimal for the ghrelin analysis.

Throughout the sample preparation, differences were observed between acyl and unacylated ghrelin in terms of their extraction. This can be explained by the dual characteristics of ghrelin. The presence of several lysine and arginine residues gives ghrelin polar properties, whilst the addition of an octanoyl group, which is nonpolar, provides acyl ghrelin with polar and nonpolar properties (Kojima et al., 2001; Bednarek et al., 2000). Previously, the use of C18 SPE columns for ghrelin extraction was reported (Kojima et al., 2000; Hosoda, 2003; Nishi et al., 2005) which is used for multi-compound mixes. However, the results in this chapter demonstrated low ghrelin levels following SPE. The WCX column for rat acyl ghrelin performed the best. For future work, exploring a two-step protocol for SPE could help ghrelin with retention, such as using WCX for acyl ghrelin and collecting the loading phase (where unacylated ghrelin should wash through) and exploring the use of a WAX column for unacylated ghrelin, which should retain polar compounds better, but also lead to a more extensive protocol. Another route to explore is the stir-based solvent extraction (SBSE) method, which is an analytical technique used to extract and concentrate samples. This was previously used successfully for ghrelin detection by Eslami et al., 2016, allowing ghrelin detection down to 0.02 ng/mL, however, it is a time-consuming procedure that requires conditioning of the bars for 24 hours before SBSE and 45 minutes for the SBSE protocol, followed by desorption via ultrasonic treatment for a further 30

minutes. The stir bars also require reconditioning between extractions, which takes 30 minutes.

Within this chapter, it was discovered that concentrating the ghrelin samples via speedvac, resulted in lower ghrelin results compared to not drying down. An explanation for this is reported in the literature which states that peptide loss during drying is a result of peptide precipitation and adsorption in containers such as Eppendorf (Pezeshki et al., 2009; Berka and Luklova et al., 2017). It has been reported that surface adsorption could be compensated with additives such as PEGs, but these are unfavourable for MALDI-TOF analysis and introduce a new problem (Midwoud et al., 2007).

To help decrease peptide binding to tubes, the use of 0.1% BSA was explored (Kovalchuk, Anikanov, Ivanova, Ziganshin and Govorun 2015). However, no improvement was observed while using 0.1% BSA, although the use of BSA could be explored further by testing a range of BSA concentrations.

Ghrelin loss was also reported following the use of centrifugal filters and C18 ziptips, further complicating the sample preparation steps. Likewise, to our results, Cunningham et al. also reported the use of centrifugal filters, and significant sample loss was observed with low-abundance peptide analysis (Cunningham et al., 2013). Here, they suggest the use of a more aqueous solution to elute the sample, although in the case of acyl ghrelin, which has nonpolar properties, increasing the polarity of the elution solution could decrease the elution of acyl ghrelin. The loss of sample during the ziptip procedure and SPE, in general, could be the result of several issues highlighted in a paper by Bugyi et al. 2023. In the case of ghrelin, during the ziptip procedure, ghrelin was observed in the wash steps, which may indicate an incorrect pH for the wash solvent, which was described as a frequent problem by Bugyi et al. 2023. It was also highlighted within this paper that achieving a correct pH that works for different peptides can be challenging. As such, with acyl and unacylated ghrelin obtaining different polarities, this proves a challenge and may be the result of the ghrelin loss observed.

The loss of ghrelin can also be explained by its potential binding to a larger protein, such as human albumin, which is removed during protein precipitation. Original studies investigating ghrelin by mass spectrometry did not account for the binding of ghrelin

to albumin (Rauh et al., 2007, Gutierrez et al., 2008, Eslami et al., 2016). However, studies have shown that ghrelin binds to human albumin through the albumin fatty acid binding sites and the ghrelin octanoyl moiety (Heppner et al., 2012; Lufrano et al., 2016). It has also been shown that the fatty acid side chain for ghrelin acylation, although predominately reported to be C8, a range of fatty acids can also bind. Heppner et al., 2012, suggested that C16 acyl ghrelin was more effective than C8 acyl ghrelin with greater stability of the acyl group and provides ghrelin a more effective anchor for binding to the cell membrane, compared to C8 acyl ghrelin. As albumin is known to bind longer-chain fatty acids, it is possible that C16 acyl ghrelin is bound to albumin and stays in circulation longer. Thus, as a result, having acyl ghrelin with varying fatty acid side chains creates a mixture of ghrelin peptides freely within plasma and some bound to larger proteins. Thomas et al., 2021, reported using 5% NH_4OH to separate the binding of ghrelin and other plasma proteins such as albumin. The use of 5% NH_4OH was investigated within this chapter to explore if this could increase ghrelin capture, although due to evident contamination, only one experiment was carried out, and as such repeated experiments are needed to explore if NH_4OH can increase ghrelin capture.

During MALDI-TOF analysis, fluctuations in the relative intensities of rat unacylated ghrelin and rat acyl ghrelin were observed across certain experiments, with occasional reversals in signal dominance between these two species. These variations were likely influenced by several factors including differences in extraction recovery, matrix crystallisation effects, and potential ion suppression phenomena inherent to MALDI analysis. Additionally, differing ionisation efficiencies between the acylated and unacylated forms of ghrelin may contribute to such variability.

While these shifts in intensity did not consistently impact the calculated ratios beyond the observed coefficients of variation, they highlight the importance of cautious interpretation of intensity-based ratios in MALDI-TOF experiments. Future work may benefit from employing isotopically-labelled internal standards to more accurate for such variations and improve ratio reliability

At the end of this chapter, contamination within the MALDI-TOF was noted with efforts to remove the contamination, which proved to be difficult. Contamination by polymers such as PEG remains difficult, as their presence results in ion signal suppression on

the MALDI-TOF (Zhao and O'Connor, 2007). It has been suggested that the use of titanium dioxide within protein samples may remove PEGS (Zhao and O'Connor 2007), although it adds to the already extensive proteomics sample preparation.

Due to the chemical differences between acyl and unacylated ghrelin, mainly the lipid group present on acyl ghrelin, it is possible that separate sample preparation steps may be needed to handle each form properly. In this study, both forms were processed under the same conditions. However, acyl ghrelin often showed lower recovery and weaker signal intensity. This suggests that acyl ghrelin may need a slightly different approach to improve its detection, especially if this method were to be used in a clinical setting where accurate measurement is important. One of the key issues identified was the need for a two-step elution, which adds time and complexity to the process and could make the method harder to apply in high-throughput or routine clinical workflows. Future work should look into ways of simplifying this, such as using a single-step elution or finding extraction methods that work well for both forms of ghrelin at the same time. While this chapter focused mainly on method development, these findings are in line with other studies using MALDI-TOF to measure ghrelin (Gutierrez et al., 2008; Eslami et al., 2016) and could be helpful for developing more efficient protocols that are better suited for clinical or biomarker-based studies.

3.5 Conclusion

The results shown above serve to highlight the challenges associated with MALDI-TOF analysis of ghrelin. Before MALDI-TOF analysis, it is important not only to extract ghrelin but also to desalt and concentrate the sample for optimal results. Here, ghrelin loss is extensive, with peptides being lost during the washing steps and drying down. Furthermore, the hydrophobic property of ghrelin means that it can precipitate or stick to the surface of containers. As a result, we explored an alternative novel technique of bead-assisted mass spectrometry to avoid such extraction issues (Chapter 5).

Chapter

4. Developing a Protocol to Analyse Ghrelin Using LC-MS/MS

4.1 Introduction

Both ESI and MALDI are commonly used ionisation methods for ghrelin analysis and MS-based proteomic analysis in general. As highlighted in the previous chapter, MALDI is a soft ionisation technique that uses a matrix to absorb the laser energy and produce ions with minimal fragmentation. ESI also uses soft ionisation and both ionisation steps for MALDI and ESI occur through the addition (or removal) of protons to produce $[peptide+nH]^{n+}$ molecular ions, which exist within the positive mode of ionisation. ESI offers an advantage over MALDI-TOF as it can produce both single and multiply charged protonated ions which can be used to confirm the identity of a peptide.

A single stage ESI-MS is the most similar to MALDI-MS, with both being useful for the determination of a protein's molecular weight by the detection of the m/z of related ions. Tandem mass spectrometry (MS/MS) consists of two mass analysers connected via a collision cell. Tandem MS can isolate a specific m/z (precursor/parent ion) that can be subjected to CID. Following the first round of MS detection, the precursor ion(s) (the ion(s) of interest) are allowed into the quadruple filter based on their m/z (either a range of m/z or one specific m/z) and are fragmented by dissociation. During CID, the ions are collided with a stream of inert gas which causes them to fragment and separate based on their m/z ratios which are then detected in a second mass analyser (Figure 4.1). CID results in the production of fragment or product ions, a specific 'fingerprint' for a peptide, thus offering more information about the molecular structure of the analyte and a further tool for identification. When the MS is set up to monitor several specified precursor/parents to product/daughter ions (also called 'transitions') simultaneously, this is called multiple reaction monitoring (MRM) which is commonly used during LC-MS/MS.

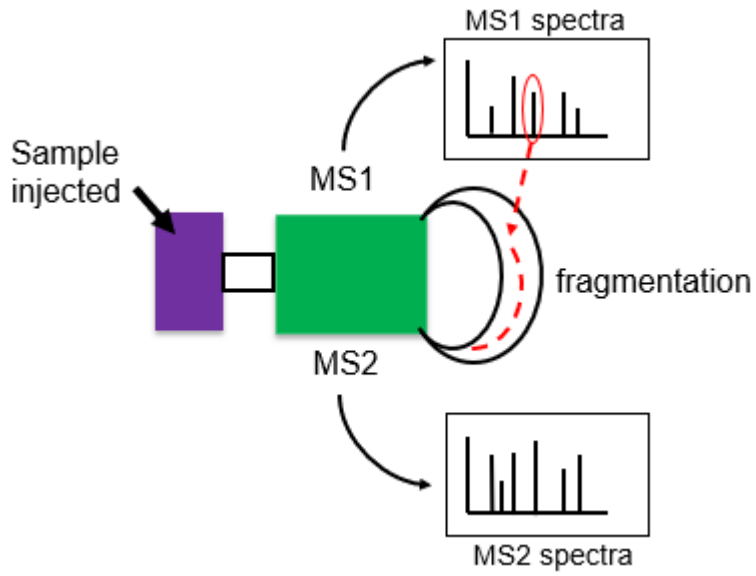

Figure 4.1 Schematic of tandem mass spectrometry (MS/MS).

Upon sample injection, the analyte enters the mass spectrometer whereby it is ionised, accelerated, and analysed by mass spectrometry which results in MS1 spectra. Ions from MS1 are fragmented and analysed again by mass spectrometry in MS2. Note, that some instruments utilise a single mass analyser for both rounds of MS whilst others may have multiple mass analysers.

For a more in-depth analysis, ESI and tandem MS can be coupled with HPLC separation, termed LC-MS/MS. Combining the time of elution following HPLC separation and the MS/MS spectra of a molecule provides extra strength of identification for the molecule under analysis, you may get some molecules with a similar (or the same) mass or MS/MS profile (for example, different oxysterols), combining with time gives extra reassurance that you are looking at the same/correct molecule each time. A disadvantage of ESI-MS is that a peptide can generate several ions with a different charged state. The potential disadvantage of this is that a greater number of charged state ions are generated, which results in a decrease in the overall intensity of those detected ions, as such for detection and quantification purposes it is more beneficial to generate fewer more intense ions.

Intact ghrelin is a peptide that contains more than one basic site that can be protonated, and thus, it can form more than one positively charged state. As a result, ghrelin can exist as $[M+H]^{+}$, $[M+2H]^{2+}$, $[M+3H]^{3+}$, $[M+4H]^{4+}$, $[M+5H]^{5+}$, $[M+6H]^{6+}$, $[M+7H]^{7+}$, $[M+8H]^{8+}$ during ESI MS analysis (m/z highlighted in table 4.1).

Charged state	Rat AG	Rat UAG	Human AG	Human UAG
$[M+H]^{+}$	3313.8491	3187.7449	3369.8864	3243.7822
$[M+2H]^{2+}$	1657.4291	1544.3778	1685.4469	1622.3947
$[M+3H]^{3+}$	1105.2890	1063.2562	1123.9671	1081.9322
$[M+4H]^{4+}$	829.2183	797.6922	843.2271	811.7010
$[M+5H]^{5+}$	663.5762	638.3553	674.7831	649.5622
$[M+6H]^{6+}$	553.1481	532.1307	562.4872	541.4698
$[M+7H]^{7+}$	474.2704	456.2555	482.2758	464.2609
$[M+8H]^{8+}$	415.1125	399.3495	422.1172	406.3542

Table 4.1 M/Z values of ghrelin's charge state ions during protonation.

Rauh et al. (2007), utilised ESI coupled to a quadrupole mass spectrometer for the detection and quantification of acyl and unacylated ghrelin species within the plasma. Here, the triple-charged $[M+3H]^{3+}$ and quadrupole-charged $[M+4H]^{4+}$ ions of ghrelin were the most intense during MS analysis. Their analysis used a mobile phase that had a pH of ~ 5. To note, the most intense signal for the peaks can vary depending on the overall pH of the mobile phase, as such, several different charge states of any peptide can appear under different pHs. For example, Sidibe et al. 2014, observed the 7-fold charged $[M+7H]^{7+}$ ion of ghrelin as the most intense whilst using an overall pH of 2 within the mobile phase.

The purpose of this chapter is to optimise an LC-MS/MS method to analyse ghrelin, focusing on increased sensitivity and reproducibility. Sensitivity in LC-MS/MS correlates to the ionisation efficiency of analyte molecules in solution. The ionisation in ESI can be influenced by the mobile-phase buffers and therefore, choosing the appropriate buffer is important for the sensitivity of an LC-MS/MS method. An additive that is commonly included in the mobile phase of LC-MS/MS includes acetic acid, formic acid, and/or their ammonium salts (Lupo et al., 2017). An acid modifier for ESI is often included as it can donate/remove protons and as such, aid in in the ionisation of the analyte. Alternatively, buffer salts (such as ammonium formate or ammonium acetate) can aid by increasing the ionisation efficiency of polar neutral compounds such as ghrelin (Lupo et al., 2017). The success of using acetic acid, formic acid (FA), and their ammonium salts for ghrelin analysis is seen in Rauh et al. 2007, whereby mobile phase A for the LC-MS/MS consisted of ammonium acetate and methanol

containing 0.1% acetic acid whilst mobile phase B consisted of ammonium acetate and methanol containing 0.1% formic acid. Here, quantification of human ghrelin was successfully noted following extraction from 1 mL of human plasma, within the range of 0.07-72 ng/mL. In 2014, Sidibe et al. explored the use of cubic-selected reaction monitoring which included LC separation on a SIL-HTC HPLC system using mobile phase A consisting of 0.2% formic acid, 0.01% TFA in water and mobile phase B consisting of 0.2% formic acid, 0.01% TFA in acetonitrile. Successful quantification of human acyl and unacylated ghrelin was reported within a linear range between 0.02-80 ng/mL. Zemenova et al. 2016 also reported using 0.1% formic acid in water for their LC-MS/MS mobile phase A and 0.1% formic acid in acetonitrile for mobile phase B. Here, the six-fold charged ions $[M+6H]^{6+}$ were utilised as ghrelin precursors for MRM and ranges of 1-250 µg/mL of acyl and unacylated ghrelin were detected with 80-100% accuracy. Other techniques discussed in this chapter include direct infusion, which involves pumping the sample directly into the mass spectrometer via a syringe and syringe pump which delivers a regular flow of liquid. Direct infusion can be used to optimise conditions of the ESI source, such as spray voltage and sheath gas flow. This should be carried out before embarking on the longer LC-MS/MS runs which typically take between 30-40 minutes. The above methods are top-down proteomic approaches where intact ghrelin peptide is measured, and thus, due to the presence of multiple basic amino acids in ghrelin, multiple charge states are produced. As such, there will be a need to focus on increasing sensitivity by increasing the intensity of one of the charged states and/or decreasing the spread/number of the charged states. Another way to increase the sensitivity is using a bottom-up approach whereby the protein undergoes digestion either enzymatically or chemically before analysis. In terms of ghrelin analysis, this has been explored recently by Thomas et al in 2021. Here, ghrelin species underwent tryptic digestion, generating an 11 amino acid fragment (t1-11), with one arginine residue at the C-terminus and the inclusion of the acyl modification at serine position 3 (Figure 4.2).

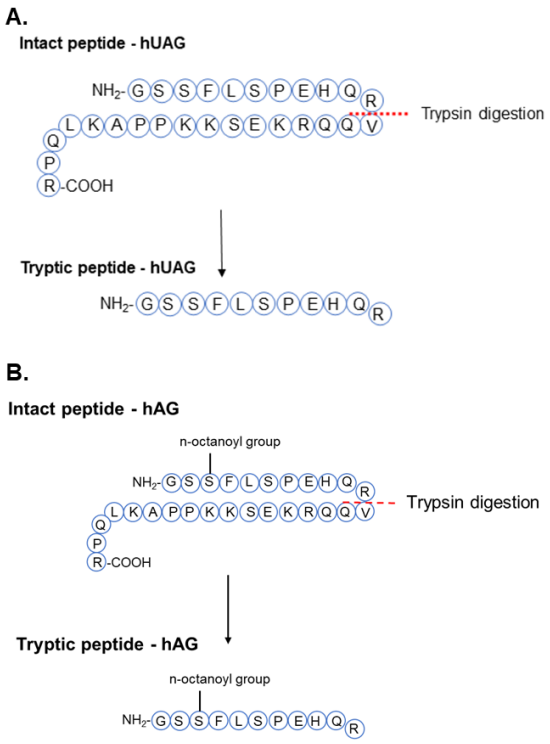

Figure 4.2 Tryptic digestion of ghrelin peptide leads to the generation of two products, fragments 1-11 retain the acyl motif if the original substrate is AG. A. hUAG. B. hAG.

The main charged state ions following the digest were reported as being the $[M+2H]^{2+}$ ions at m/z 622 and 685 for unacylated and acyl ghrelin, respectively. Whilst analysis of intact ghrelin concentrated on the $[M+5H]^{5+}$ ions at m/z 650 and 675 for unacylated and acyl ghrelin, respectively. Overall, the paper showed that the fragmented peptides analysed following tryptic digestion separated better during HPLC at a higher intensity than was seen for intact ghrelin, resulting in better LC-MS/MS analysis.

4.1.1 Aims

This chapter aims to optimise an LC-MS/MS method that can not only identify acyl and unacylated ghrelin simultaneously but also to try and distinguish (and quantify) different forms of acyl ghrelin (for example, ghrelin bound by different fatty acids).

The objectives of the chapter are as follows:

1. Optimise an LC-MS/MS method that can detect and quantify endogenous human acyl and unacylated ghrelin using rat ghrelin as an internal standard.
2. Assess ghrelin levels within human plasma samples.
3. Develop a method to analyse the different species of acyl ghrelin.

4.2 Materials and Methods

4.2.1 Preparation of Human and Rat Ghrelin Standards for LC-MS/MS Analysis

For ESI LC-MS/MS ghrelin standards were diluted to 2 ng/mL in 20% of mobile phase B (acetonitrile with either 0.1% acetic or formic acid and with or without DMSO, depending on the method used). For LC-MS/MS ghrelin standards were diluted to a range of 0.08-80 ng/mL in either HPLC-grade water or 20% acetonitrile.

4.2.2 ESI LC-MS/MS

Before LC-MS/MS analysis, ghrelin standards were analysed on the Triversa Nanomate (Advion) coupled with a Thermo Scientific LTQ Orbitrap XL (Thermo Scientific). The Nanomate was first tuned and calibrated in the positive mode before samples were analysed. All standards were diluted in 20% B mobile phase (which is where ghrelin is eluted onto the LC-MS/MS). 40 µL of the sample (2 ng/mL ghrelin) was added by direct infusion into the MS, where the acquisition was first carried out in FTMS until a stable signal was achieved followed by identification of MS2 product ions in ITMS. A range of CID energies (20-23) was tested on each peptide to determine the most suitable CID for LC-MS/MS analysis.

4.2.3 Liquid Chromatography-Tandem Mass Spectrometry

Samples were separated and analysed using an Agilent 1100 HPLC (section 4.3.1) or Ultimate 3000 HPLC (section 4.3.2 and onwards) system coupled with Thermo Orbitrap LTQ XL. After sample preparation (described in 4.2.1), the samples were placed in the autosampler of the HPLC system. Either 1 µL, 2.5 µL or 20 µL of the sample was injected via the sampling needle and loaded into a sample loop ready for injection into the mobile phase within the HPLC system which runs through the column at 25°C. During method development, the mobile phase and run lengths were optimised as follows:

Method 1: Mobile phase A consisted of HPLC grade water, 2% acetonitrile and 0.1% acetic acid whilst mobile phase B contained acetonitrile with 0.1% acetic acid. Separation of the ghrelin peptides was performed using a Fertis C18 column at a flow rate of 200 µL per minute. Two HPLC run lengths were tested, one being 30 minutes with a 10-minute equilibration (Figure 4.3 A), and the other was a run of 9 minutes with a 5-minute equilibration (Figure 4.3 B). The voltage of the needle during positive electrospray ionisation was set to 3.5 kv and the temperature of transfer capillary and

gas was 325°C and the sheath gas flow rate was 10. A full-MS scan in a range from 400-1700 m/z with a 30000 resolution was used as well as targeted MS2 in ITMS using the following specified MRM MS/MS transitions 1. Parent mass with an m/z of 638 with product ion of interest at m/z 762 and therefore scanned between 761-763 for rat unacylated ghrelin $[M+5H]^{5+}$. 2. Parent mass with a m/z of 663 with product ion of interest at m/z 793 and therefore scanned between 792-794 for rat acyl ghrelin $[M+5H]^{5+}$. 3. Parent mass with an m/z of 650 with product ion of interest at m/z 776 and as such scanned between 775-777 for human unacylated ghrelin $[M+5H]^{5+}$. And finally, 4. Parent mass with an m/z of 674 with product ion of interest at m/z 807 and as such scanned between 806-809 for human acyl ghrelin $[M+5H]^{5+}$. Please note, as ghrelin has multiple charge states and often the single charge sate M+ at m/z 3000 was not frequently observed, the MS was restricted to monitoring within a m/z 400 to 1700 range to maintain instrument sensitivity.

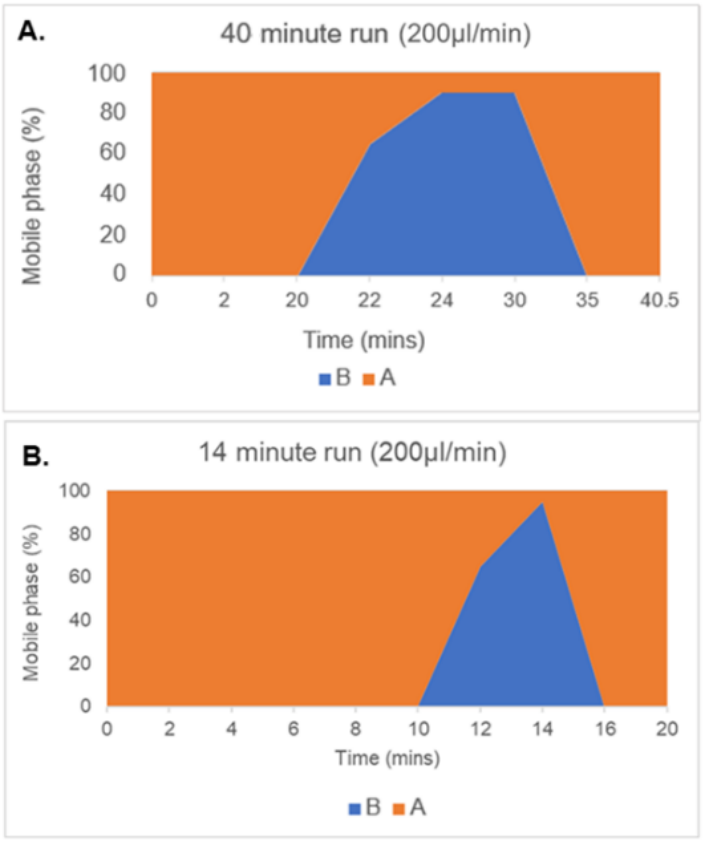

Figure 4.3 Gradient elution for the separation of ghrelin species using HPLC.

The gradient used for the initial method development, a 40-minute run (A), alongside the attempted shortened run at 14 minutes (B). Unless stated otherwise, mobile phase A contains HPLC-grade water with 2% acetonitrile and 0.1% acetic acid. Mobile phase B contains acetonitrile with 0.1% acetic acid. The flow rate was 200 µL/min.

Method 2: After preparation of the ghrelin standards, the samples were placed in the cooling tray of the HPLC autosampler, set at 4°C.The sample was injected via the sampling needle with the specific volume used stated in the results section. The sample was loaded into the sample loop to be injected into the mobile phase within the HPLC system at 25°C. For some experiments, (stated where necessary in the results), the mobile phase A consisted of water, 2% acetonitrile, 0.1% acetic acid, and 1% DMSO whilst mobile phase B consisted of acetonitrile with 0.1% acetic acid and 1% DMSO. As stated above, separation of the ghrelin peptide was carried out using a Fertis C18 column at a flow rate of 200 µL per minute. For some experiments (stated where necessary in the results), the duration of the run was 25 minutes with a 5-minute equilibration step (Figure 4.4). The voltage of the needle during positive electrospray ionization was set to 3.5 kv, the temperature of transfer capillary and gas was 325°C and the sheath gas flow rate was 15. An FTMS scan in the m/z range of 400-1700 was carried out with a resolution of 30000, alongside targeted MS/MS carried out in ITMS mode (Table 4.3)

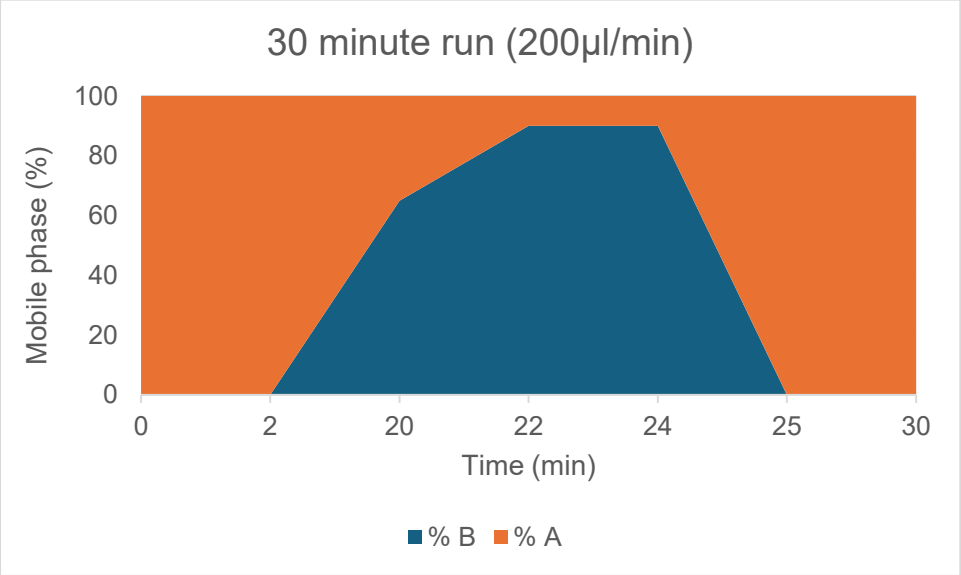

Figure 4.4 HPLC Gradients for the separation of ghrelin species during a 30-minute run.
Mobile phase A consisted of HPLC grade water, 2% acetonitrile, 0.02% acetic acid, and 1% DMSO whilst mobile phase B contains acetonitrile with 0.02% acetic acid and 1% DMSO.

4.3 Results

4.3.1 Initial Method Development

Initially, ghrelin standards were analysed through ESI LC-MS/MS using the Nanomate to optimise the conditions for the ESI such as spray voltage, drying gas flow, temperature, and tube lens for LC-MS/MS analysis. This step was also first performed prior to LC-MS/MS to confirm ghrelin's accurate mass and determine the most appropriate MS/MS transitions to be included during MRM and the most effective collision energies required for MS/MS analysis. During FTMS mode, the $[M+5H]^{5+}$ precursor ion was the most intense and thus was selected in ITMS mode. After testing various collision energies, a CID of 20 gave the most appropriate balance of sufficient fragmentation of the precursor ion without over fragmenting it. The product (or daughter) ion seen in MS2 selected for the MS/MS MRM was based on its ability to distinguish between the acyl and unacylated ghrelin rather than the most intense ion, to ensure specificity (Figure 4.5). During this process, the MS is set up to carry out a continual rotation (within milliseconds) of one scan event in FTMS, scanning a mass range of 400-1700, followed by four scans in ITMS, one for each of the MRM transitions being monitored for each ghrelin species, as summarised in the table below (Table 4.2). These MRM parameters were used in conjunction with a 40-minute HPLC run (as described in the method section 4.2.3). An example of the LC-MS/MS traces obtained during MRM monitoring of all four human and rat acyl and unacylated ghrelin is shown in Figure 4.6.

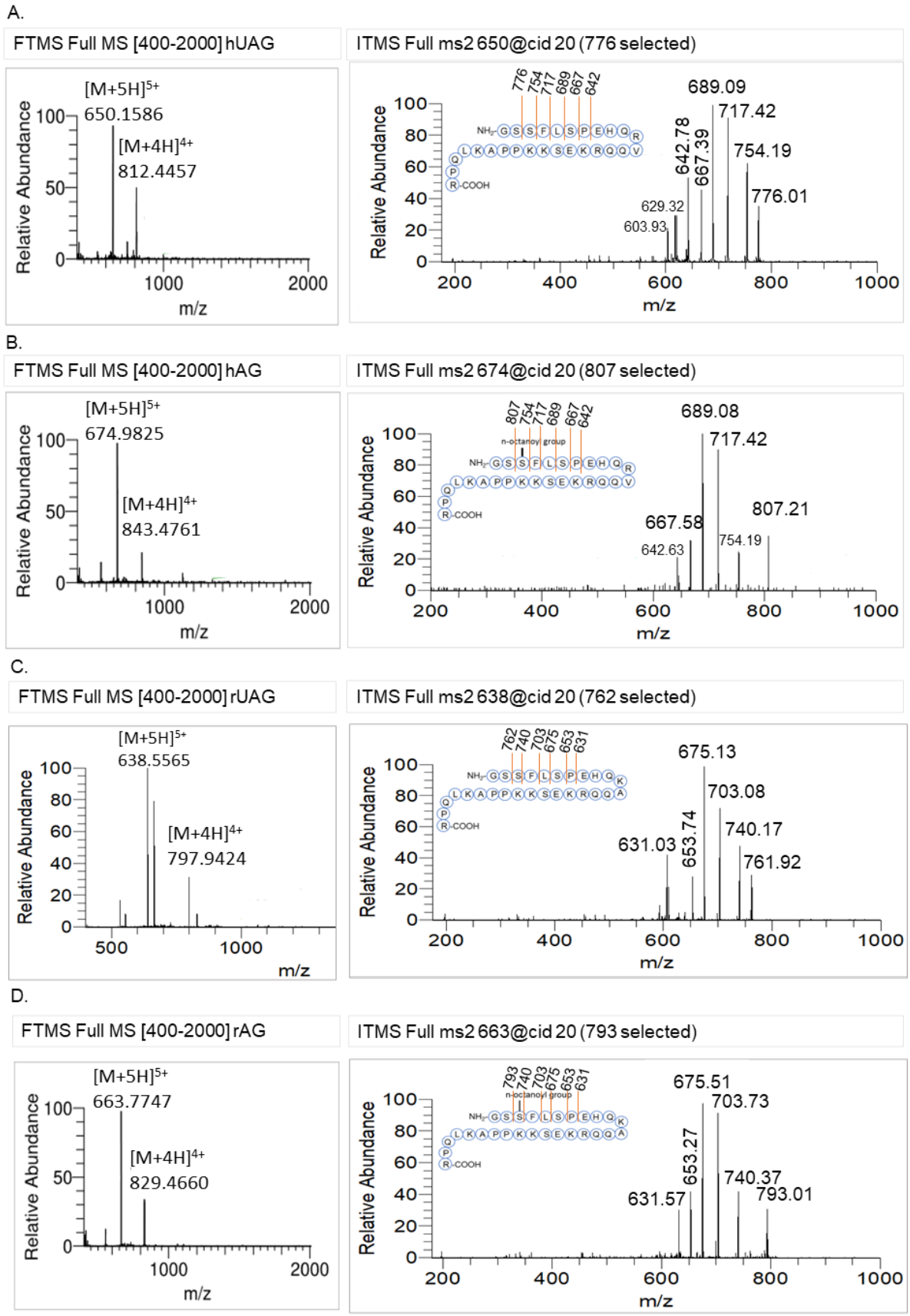

Figure 4.5 NanoESI with FTMS of chosen ghrelin charge state followed by MS/MS in ITMS mode to identify product ions. A. hUAG. B. hAG. C. rUAG. D. rAG. 10 scan events were taken and merged.

Ghrelin species	Amino acid sequence	Collision energy	Precursor or 'Parent' ion (m/z)	Product or 'Daughter' ion of interest (m/z)	MS/MS included in the MRM
Human UAG	GSSFLSPEHQRVQQRKESKKPPAKLQPR	20	650 ($[M+5H]^{5+}$)	776.25	650 / 775-777
Human AG	GSS(n-octanoyl)FLSPEHQRVQQRKESKKPPAKLQPR	20	674 ($[M+5H]^{5+}$)	807.21	674 / 806-808
Rat UAG	GSSFLSPEHQKAQQRKESKKPPAKLQPR	20	638 ($[M+5H]^{5+}$)	762.00	638 / 761-763
Rat AG	GSS(n-octanoyl)FLSPEHQKAQQRKESKKPPAKLQPR	20	663 ($[M+5H]^{5+}$)	793.58	663 / 792-794

Table 4.2 Peptide sequence and basic mass spectrometer parameters.

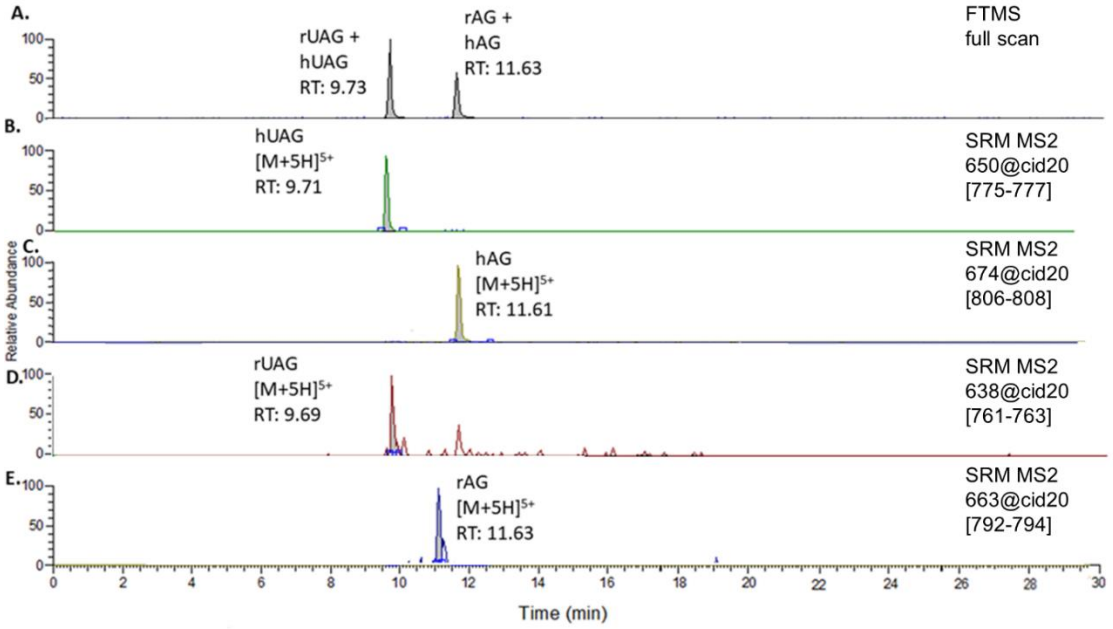

Figure 4.6 LC Chromatograms for the 40-minute run.

A. Full MS scan 400-1700 m/z, showing the overall FTMS LC trace for hUAG and rUAG at RT: 9.73 and hAG and rAG at RT: 11.63, respectively. B. SRM MS2 scan event for hUAG $[M+5H]^{5+}$ (RT:9.71). C. SRM MS2 scan event for hAG $[M+5H]^{5+}$ (RT:11.61). D. SRM MS2 scan event for rUAG $[M+5H]^{5+}$ (RT:9.69). E. SRM MS2 scan event for rAG $[M+5H]^{5+}$ (RT:11.63). Using MS/MS transitions as described in table 4.2 RT: Retention time.

To assess the performance and sensitivity of the LC-MS/MS method, calibration curves for human acylated and unacylated ghrelin were generated using synthetic standards diluted in 0.01% plasma in HPLC-grade water. An initial calibration curve was prepared over a broad concentration range (0.4–40 ng/mL), reflecting the dynamic range used in previous MALDI-TOF analysis. The peak area was plotted against ghrelin concentration, and to improve the linearity of the resulting calibration curves, one high-concentration point was excluded. This adjustment substantially improved the correlation, with final R^2 values of 0.92 for human unacylated ghrelin and 0.88 for human acyl ghrelin (Figure 4.7). The excluded point corresponded to the highest concentration and may suggest partial detector saturation or signal suppression, potentially due to column or source overloading at elevated analyte levels.

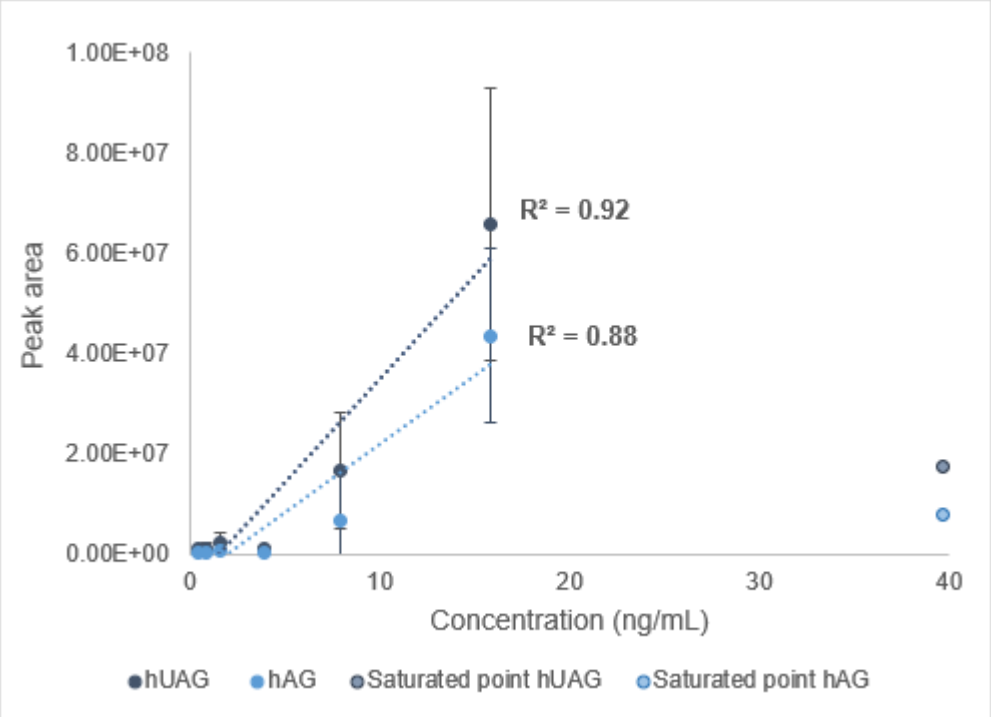

Figure 4.7 Calibration for hAG and hUAG ranged from 0.4-40 ng/mL.

Analysed by LC-MS/MS. N=3, average mean plotted with SEM. One high-concentration point excluded to improve linearity. The final plotted point is the mean of these three-run means, and error bars represent the standard deviation across runs, reflecting inter-run variability. Trendlines represent linear regression fits, and R^2 values are reported to indicate goodness of fit.

To further refine the method, a second calibration curve was generated within a lower concentration range (0.08–8 ng/mL), more reflective of physiological levels. In this

case, two data points were excluded to achieve acceptable linearity, resulting in improved R^2 values of 0.98 for human unacylated ghrelin and 0.88 for human acyl ghrelin (Figure 4.8). While system overloading is less likely at these concentrations, the need to exclude additional points raises the possibility of analyte instability during longer analytical runs. This may reflect gradual degradation of ghrelin in the autosampler or carry-over effects and will be discussed further within this chapter. Alternatively, the observed variability may simply reflect that the LC-MS/MS conditions were not yet fully optimised at the time of analysis. This possibility will be considered in more detail in the following section.

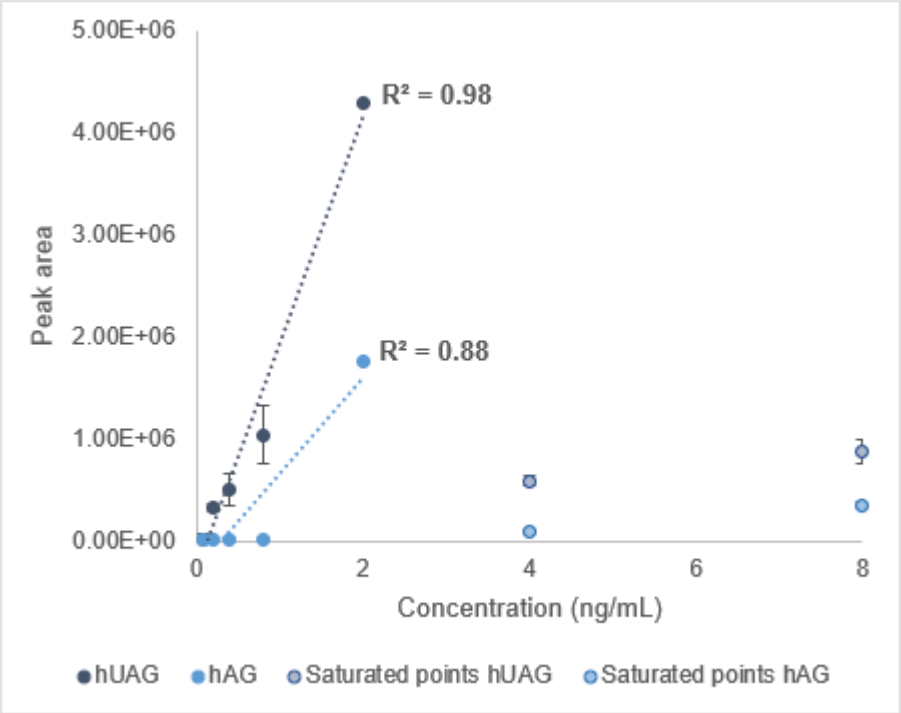

Figure 4.8 Calibration curve of hUAG and hAG ranging from 0.08-8 ng/mL.
Analysed by LC-MS/MS. N=3, average mean plotted with SEM. Two points excluded to improve linearity. The final plotted point is the mean of these three-run means, and error bars represent the standard deviation across runs, reflecting inter-run variability. Trendlines represent linear regression fits, and R^2 values are reported to indicate goodness of fit.

As the current method used a 40-minute run time, reducing the run time was evaluated, which would increase sample throughput and allow optimisation steps to be performed at a quicker rate. The calibration curve was repeated using a new shortened run time of 14 minutes with an equimolar mixture of human and rat, unacylated and acyl ghrelin, ranging from 0.08-8 ng/mL. All time points of the 14-minute run were visually inspected for the presence of unacylated ghrelin and/or acyl

ghrelin, particularly at retention time points 5.50 and 8.20, which are the times at which the percentage of the mobile phase B (20%) is at the point where ghrelin would usually elute during the 40-minute run. However, ghrelin was not identified (Figure 4.9). Thus, all further analysis and method development was continued using the 40-minute run.

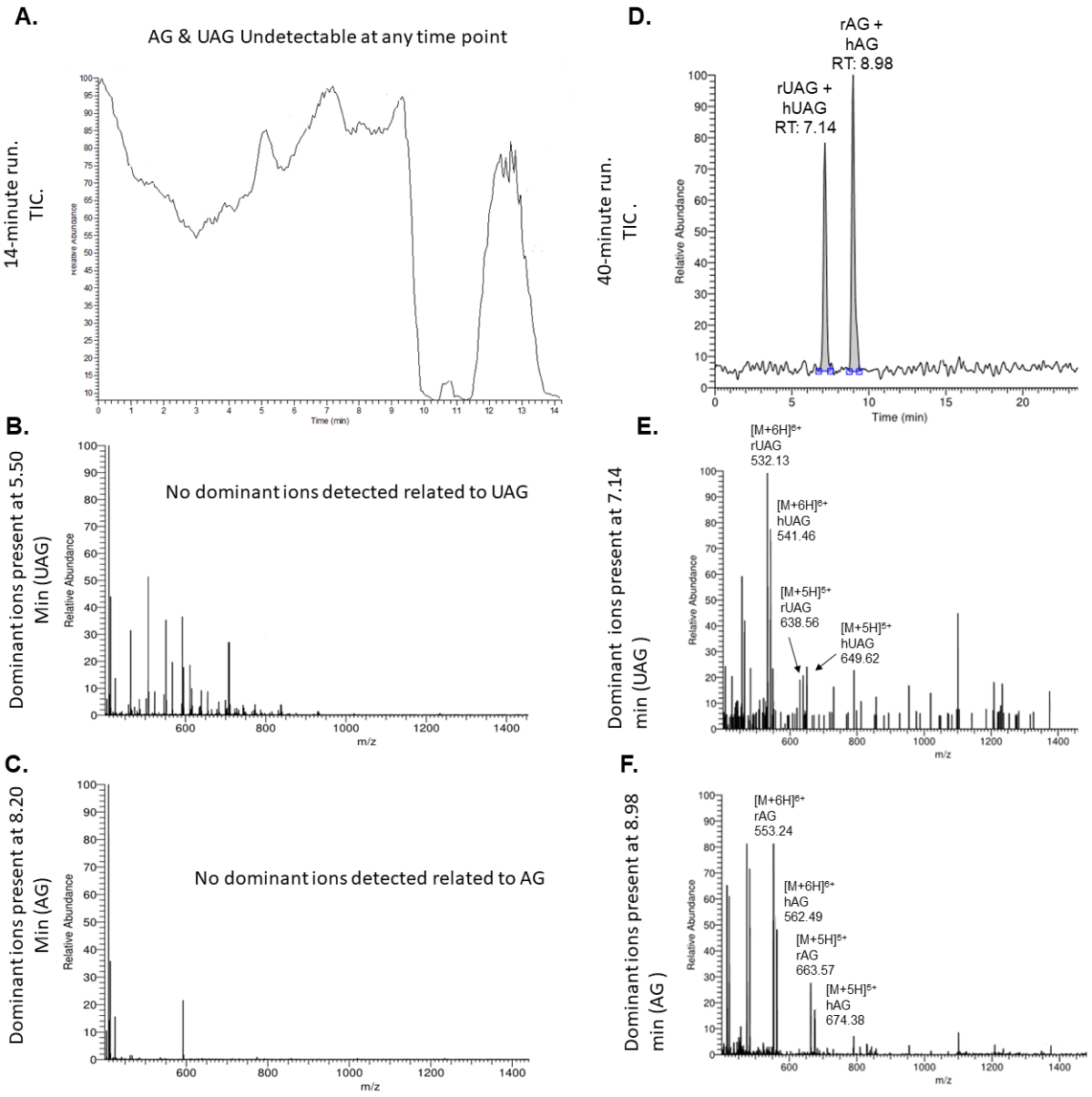

Figure 4.9 Spectra from ghrelin in a 14-minute run versus a 40-minute run analysed by LC-MS/MS.

Human and rat acyl and unacylated ghrelin standards varying from 0.08-8 ng/mL were prepared and analysed using either a run time of 14 minutes (A) or 40 minutes (D). B. Ions present at 5.50 mins (20% of mobile phase B). C. Ions present at 8.20 mins (20% of mobile phase B). E. Ions present at 7.34 mins (20% of mobile phase B), hUAG and rUAG present. F. Ions present at 8.98 mins (20% of mobile phase B), hAG and rAG present.

4.3.2 Exploring Appropriate Diluent for Ghrelin Peptide

To stabilise the ghrelin signal throughout the range of analysed concentrations, particularly at lower concentrations, the choice of solvent(s) most suitable for the dilution of samples prior to LC-MS/MS analysis of ghrelin was explored. More specifically, the effect of using plasma diluted to 0.01% using HPLC grade water or different percentages of acetonitrile on the detection of human and rat, unacylated, and acyl ghrelin species at a final concentration of 20 ng/mL was investigated. Human unacylated ghrelin showed no significant differences in peak area after diluting in different solvents (Figure 4.10A). However, human acyl ghrelin had a significantly higher peak area when diluting in 20% acetonitrile compared to any other solvents (Figure 4.10B). For rat unacylated ghrelin, dilution in water resulted in a significantly higher peak area than any of the other solvents (Figure 4.10C). Lastly, for rat acyl ghrelin, dilution in 20% acetonitrile resulted in a significantly higher peak area than any of the other solvents (Figure 4.10D). Overall, apart from rat unacylated ghrelin where water appeared to be the best solvent, 20% acetonitrile generally gave the best results. Thus, based on these results, 20% acetonitrile was used thereafter to dilute ghrelin whilst preparing the standards for the calibration curve. The calibration curve was re-run, human and rat acyl and unacylated ghrelin were prepared at 0.08-80 ng/mL (Figure 4.11). The calibration curves for rat unacylated and acyl ghrelin obtained R^2 values of 0.98 and 0.89, respectively, whilst both the human unacylated and acyl ghrelin obtained an R^2 value of 0.99. Although the R^2 values were very much improved (when comparing to Figure 4.8) for the human acyl and unacylated ghrelin, a large standard error was observed demonstrating a need for improvement in terms of stability. Additionally, samples at the lower concentration range of the curve, <1 ng/mL, were either undetectable or obtained very small peak areas. The absence of detection at lower concentration ranges poses a potential issue since endogenous ghrelin levels typically fall within the range of 0.03-2 ng/mL. Hence, it is crucial to ensure a reliable linear detection of ghrelin across these regions of the calibration curve.

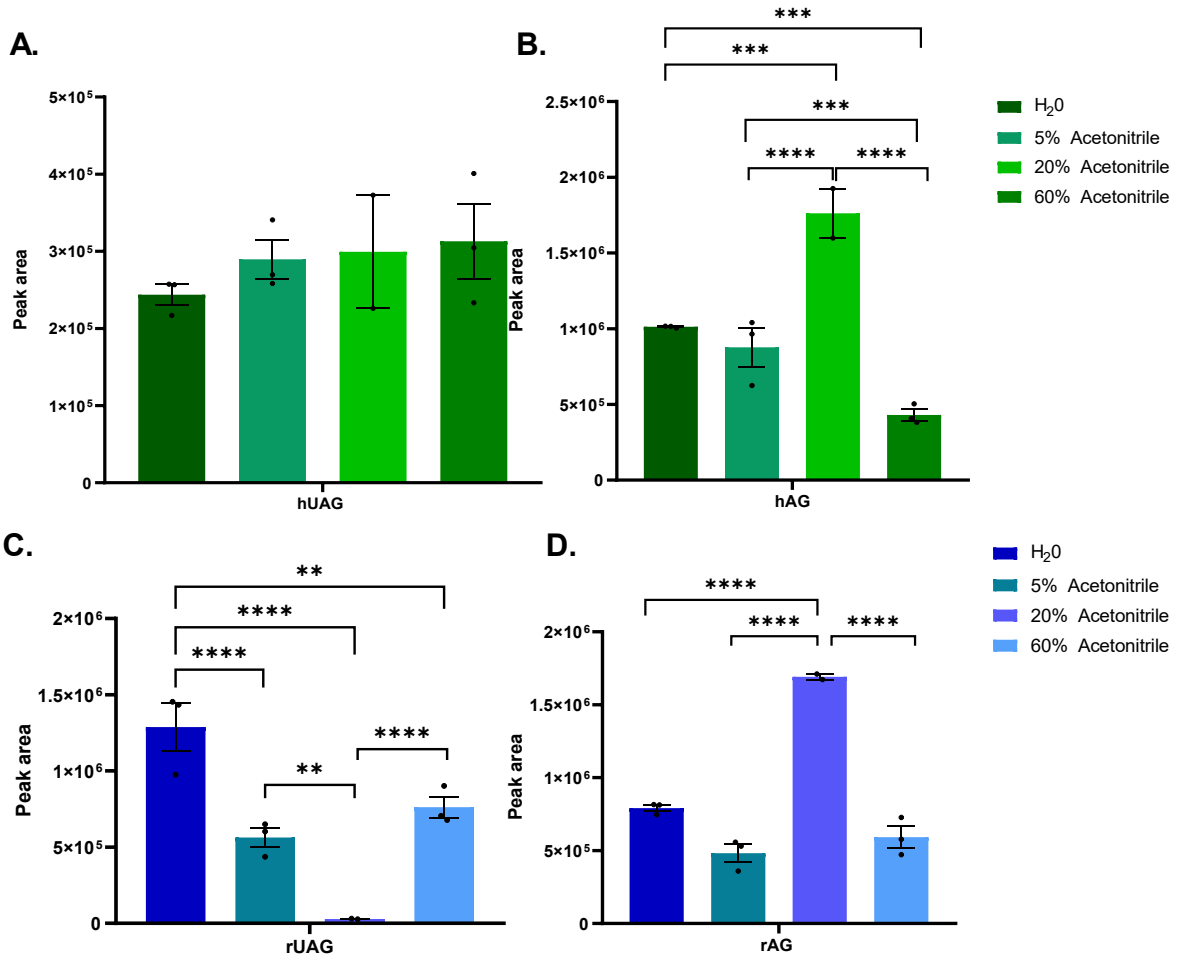

Figure 4.10 Comparison of using water and different percentages of acetonitrile during sample preparation on the peak area of ghrelin species.

Samples analysed by LC-MS/MS. A. hUAG. B. hAG. C. rUAG D. rAG. Two-way ANOVA was performed with Tukey corrections. P<0.05 is considered statistically significant. **** P<0.0001, *** P<0.001, **P<0.01. N=3, average mean plotted with SEM.

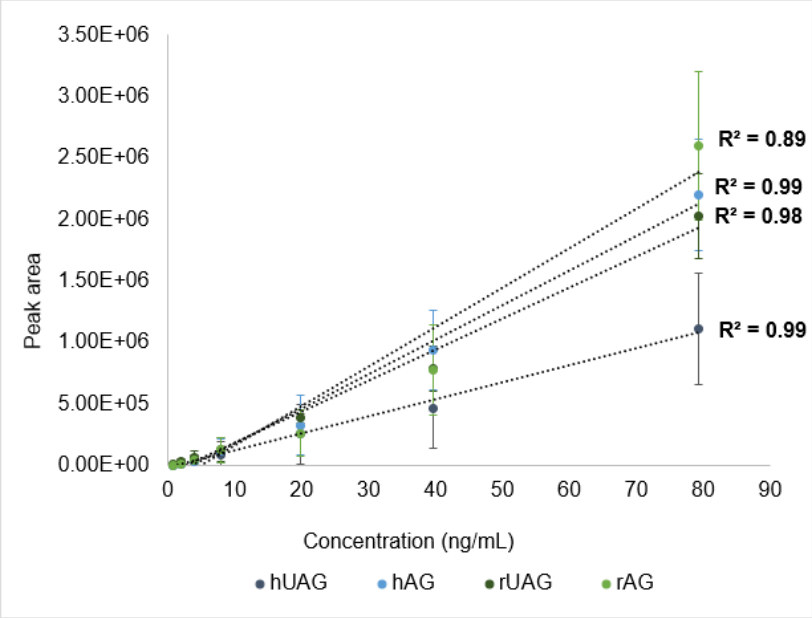

Figure 4.11 Calibration curve of hUAG, hAG, rUAG and rAG ranging from 0.08-80 ng/mL, diluted using 20% Acetonitrile.

Analysed by LC-MS/MS. N=3, average mean plotted with SEM. The final plotted point is the mean of these three-run means, and error bars represent the standard deviation across runs, reflecting inter-run variability. Trendlines represent linear regression fits, and R^2 values are reported to indicate goodness of fit.

4.3.3 Alteration of Initial Sample Volume

To enhance signal intensity at the lower concentration range of the calibration curve, the injection volume was increased from 1 µL to 2.5 µL. Both curves were prepared using identical concentration ranges (0.8–80 ng/mL), with stock solutions diluted accordingly to ensure that final injected concentrations remained consistent. Although only a single run (n=1) was performed due to limited instrument availability and the lengthy run time per sample (~40 minutes), a visual increase in peak area was observed in the 2.5 µL injections compared to the 1 µL injections. Based on this apparent improvement, and in the absence of contradictory data, a 2.5 µL injection volume was adopted for all subsequent experiments (Figure 4.12).

However, this increase in volume was insufficient to produce detectable peaks at the lowest calibration points (0.8 and 2 ng/mL). Despite achieving strong linearity (R^2 = 0.99) across all ghrelin species in both rat and human plasma (Figure 4.13), further method optimisation was necessary to improve detection sensitivity, particularly at the low end of the curve.

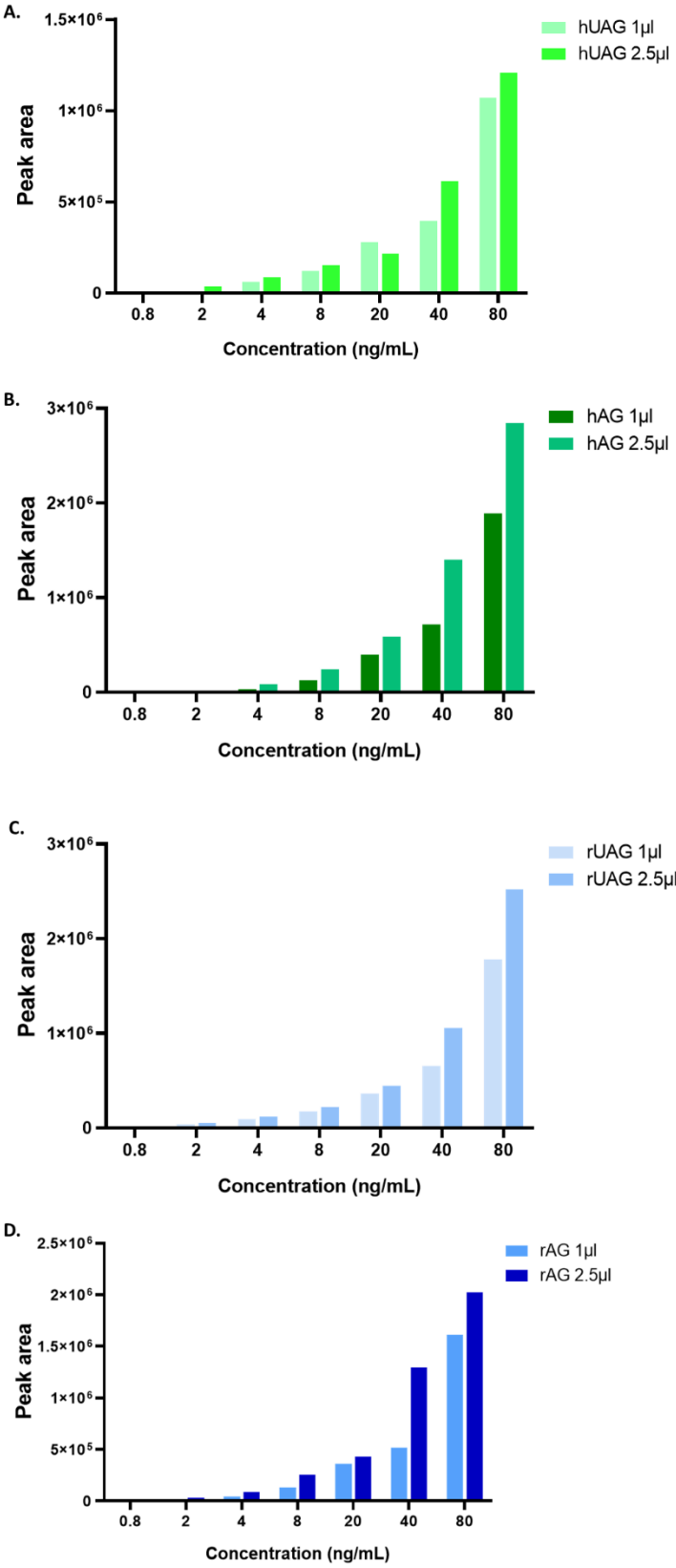

Figure 4.12 Comparison of altering the injection volume from 1 µL to 2.5 µL on the peak area of ghrelin species following LC-MS/MS analysis.

A. hUAG. B. hAG. C. rUAG. D. rAG. N=1.

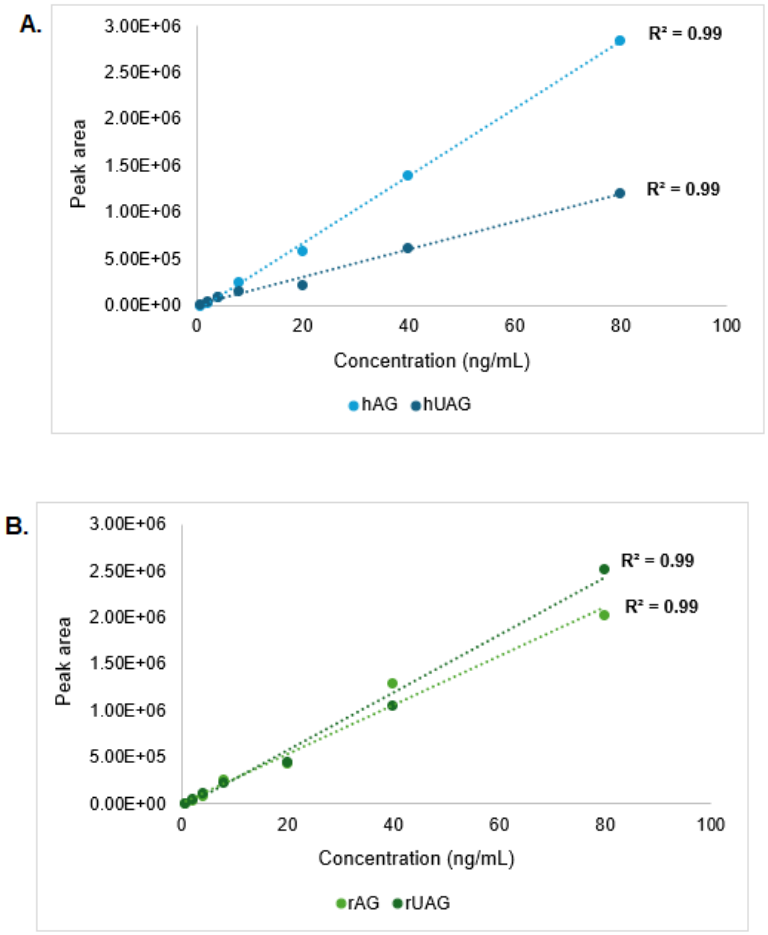

Figure 4.13 Calibration curve of ghrelin species using an injection volume of 2.5 µL.
A. hUAG and hAG. B. rUAG and rAG ranging from 0.8-80 ng/mL. Analysed by LC-MS/MS. N=1, average mean plotted. Trend lines represent linear regression fits, and R^2 values are reported to indicate goodness of fit.

4.3.4 Charge State Optimisation Following the Inclusion of Different Additives in the Mobile Phase During LC-MS/MS Analysis

At this point of the study, the Agilent 1100 HPLC system failed and was beyond repair, thus the HPLC system was changed to a Dionex Ultimate 3000 coupled with the same Thermo Orbitrap LTQ XL, as used above. During this alteration, a new HPLC-MS/MS method was developed with a reduced run time of 20 minutes with a 10-minute equilibration phase (Figure 4.14C,D). An additional benefit of using the Ultimate 3000 is that it has a cooling tray that can maintain the sample vials at 4˚C during analysis, reducing the potential for degradation of the peptides in the samples.

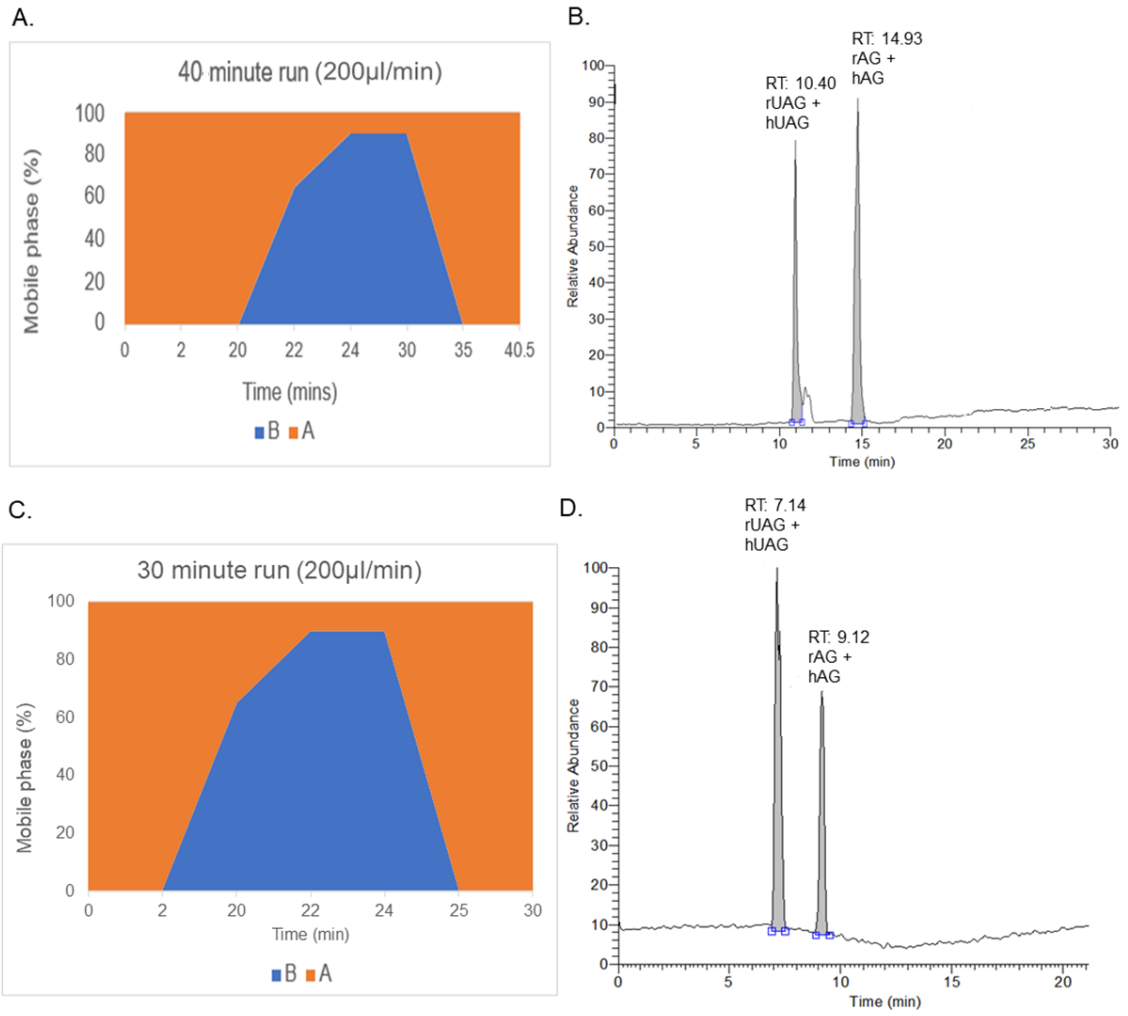

Figure 4.14 40-minute (A and B) versus 30-minute (C and D) LC-MS/MS run.

A and C HPLC % gradient trace of mobile phases A and B from the 40- or 30-minutes runs, respectively. B and D LC chromatogram of hUAG, hAG, rUAG, and rAG during both LC-MS/MS runs.

As noted in the introduction, the generation of multiple charged state ions is commonly reported for ghrelin during LC-MS/MS analysis. As the formation of an increased number of charged states can reduce the intensity of the peaks, I investigated whether modifying the mobile phase could reduce the scattering of charged state ions produced during the analysis. Reducing the overall distribution of charged states could increase the intensity of ghrelin at a particular charged state and thus improve the detection of ghrelin generally but also at the lower concentrations of the calibration curve.

4.3.4.1 Exploring the Use of Acids or Salts Within the Mobile Phase

Acids are commonly included in the mobile phase during LC-MS/MS analysis to help improve ionisation. Previously within this chapter, acetic acid has been used; however, formic acid is also commonly used in mobile phases for MS analysis. Therefore, formic acid was explored as an alternative to acetic acid, to assess whether it can reduce the number of charged state ions of ghrelin.

For this experiment, mobile phase A was prepared using HPLC grade water with 2% acetonitrile and either 0.1% acetic acid or 0.1% formic acid, whilst mobile phase B contained acetonitrile with either 0.1% acetic acid or 0.1% formic acid. An equimolar sample of all ghrelin species (20 ng/mL) was analysed by LC-MS/MS. No significant differences in peak area were seen between the peak areas for any of the ghrelin species following the use of acetic or formic acid in the mobile phases (Figure 4.15).

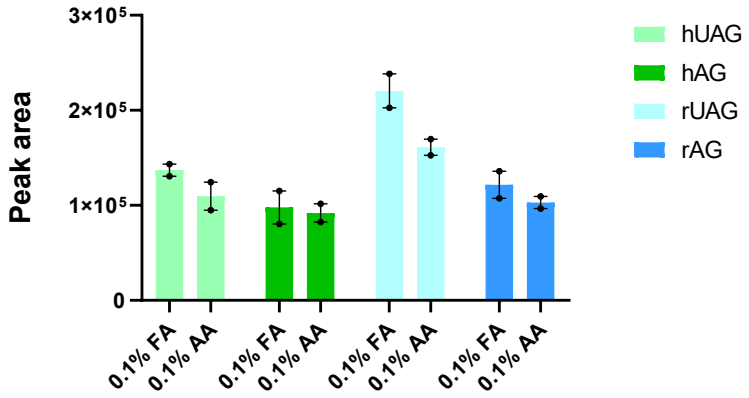

Figure 4.15 Comparison of acetic acid or formic acid on the peak area of ghrelin species $[M+5H]^{5+}$ (20 ng/mL) following LC-MS/MS analysis.

Two-way ANOVA was performed with Tukey corrections. P<0.05 is considered statistically significant. N=3, average mean plotted with SEM. Acetic Acid = AA; Formic Acid (FA).

The distribution of charged state ions for the ghrelin species did not differ greatly when using formic or acetic acid in the mobile phase (Figure 4.16). As a result, it was concluded that the switch from acetic acid to formic acid alone did not reduce the spread of charged state ions or improve peak areas of ghrelin during the analysis of the $[M+5H]^{5+}$ parent ion.

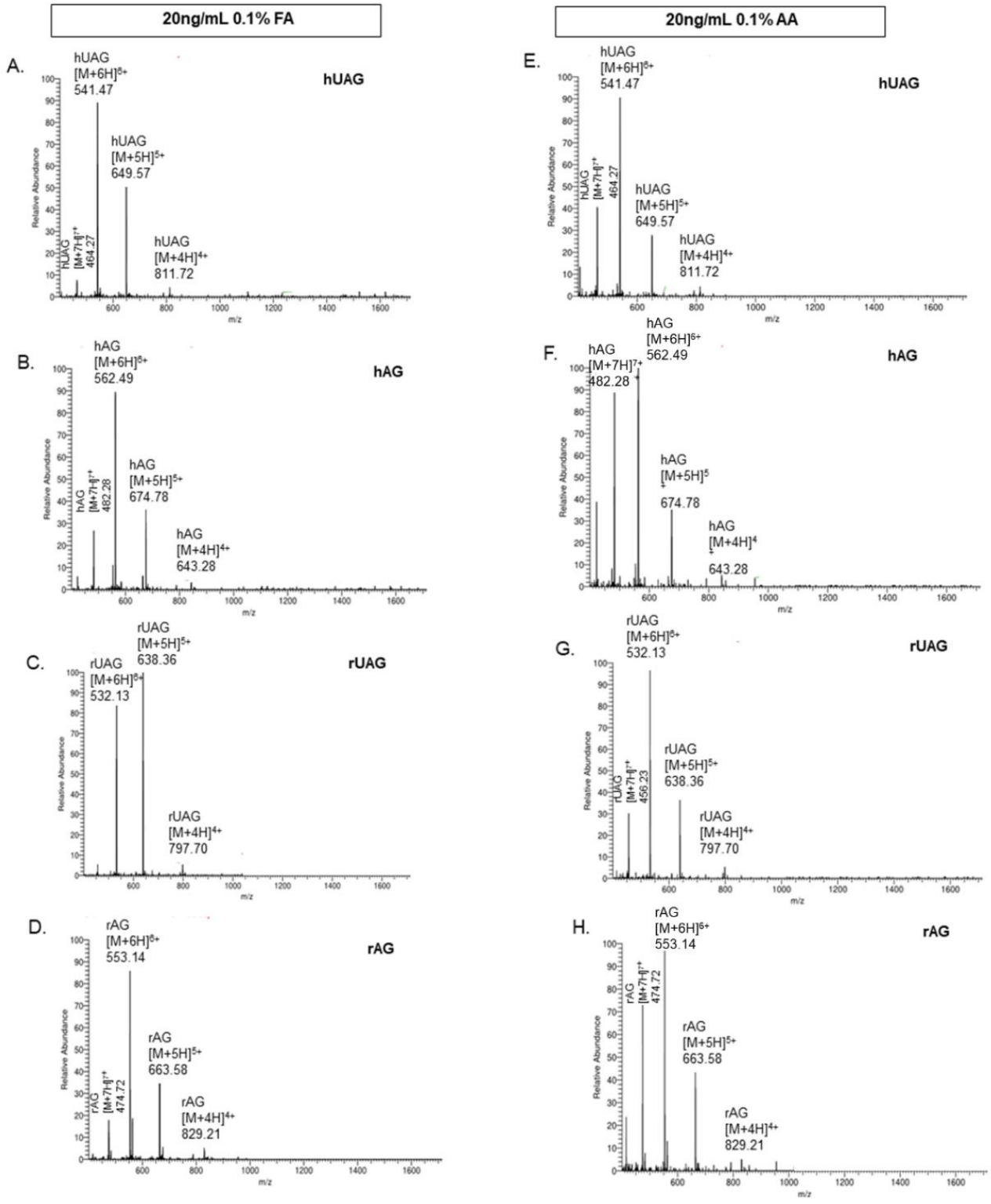

Figure 4.16 The distribution of different charged state ions of ghrelin ions after including either FA or AA in the mobile phase.

MS spectra of ghrelin species (20 ng/mL) when using mobile phases containing 0.1% FA (A, B, C, D) or AA (E, F, G, H). Acetic Acid = AA; Formic Acid (FA). 10 scans merged into 1.

An alternative method for increasing the ionisation of a peptide is to introduce buffer salts into the mobile phase. Buffer salts containing ammonia such as ammonium acetate and ammonium formate are often used to help the ionization of polar neutral compounds to increase their ionization and are commonly used with LC-MS/MS (Lupo et al. 2017). Thus, I investigated the inclusion of both salts in the mobile phases alongside the inclusion of formic acid or acetic acid. Firstly, ammonium acetate was included in mobile phase A consisting of 2% acetonitrile, 0.1% acetic acid, and 50 mM ammonium acetate. Mobile phase B was composed of 90% acetonitrile, 10% water, 0.1% acetic acid, and 50 mM ammonium acetate. In this instance, mobile phase B 10% water as ammonium acetate is not soluble in acetonitrile alone. In an alternative experiment, ammonium formate was also added to mobile phases containing formic acid. Mobile phase A contained 2% acetonitrile, 0.1% formic acid, and 50 mM ammonium formate, whilst mobile phase B contained 90% acetonitrile, 10% H_2O, 0.1% formic acid, and 50 mM ammonium formate.

The addition of the buffer salts to the mobile phases had an impact on the distribution of multiple charge states of ghrelin (Figure 4.17). The addition of ammonium acetate or ammonium formate to buffers containing either acetic acid or formic acid respectively caused an increase in the abundance of $[M+3H]^{3+}$ and $[M+4H]^{4+}$ ghrelin ions whilst causing a notable decrease in the $[M+6H]^{6+}$ ion. However, the inclusion of the ammonium acetate or ammonium formate in the mobile phases did not result in any significant alterations when comparing the peak areas of the $[M+5H]^{5+}$ ions for ghrelin (Figure 4.18). Thus, we can conclude that the addition of salts into the mobile phases did not help improve ghrelin detection, likely because it did not reduce the distribution of ghrelin-charged states but rather shifted the dominant peak state from $[M+5H]^{5+}$ to $[M+4H]^{4+}$.

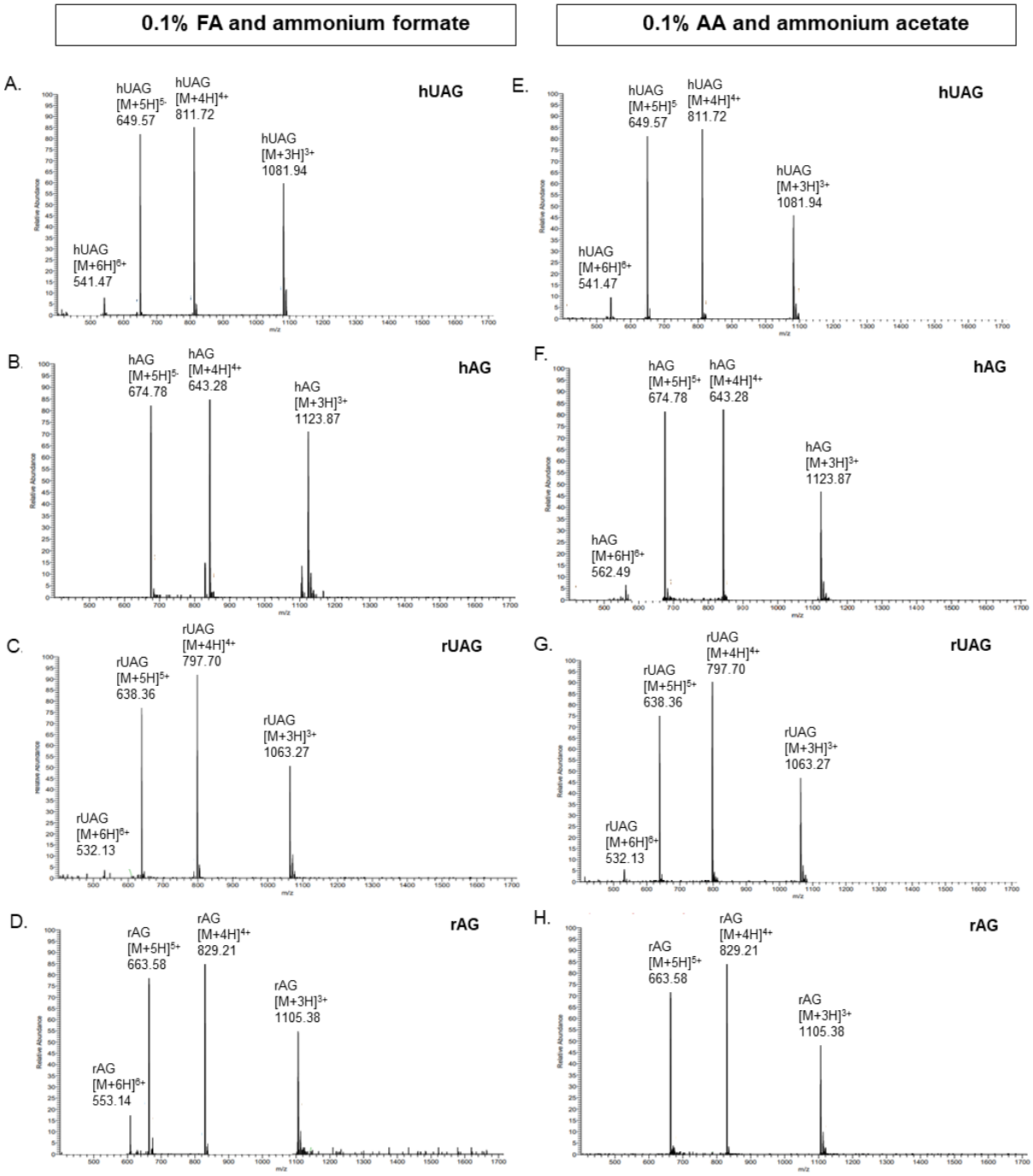

Figure 4.17 The distribution of different charged states ions of ghrelin when analysed by LC-MS using either FA or AA in the mobile phase.

MS spectra of ghrelin species (20 ng/mL) following the inclusion of 50 mM ammonium formate within the mobile phases containing 0.1% Formic acid (A, B, C, D) or 50 nM ammonium acetate within the mobile phases containing 0.1% Acetic acid (E, F, G, H). Acetic Acid = AA; Formic Acid (FA).

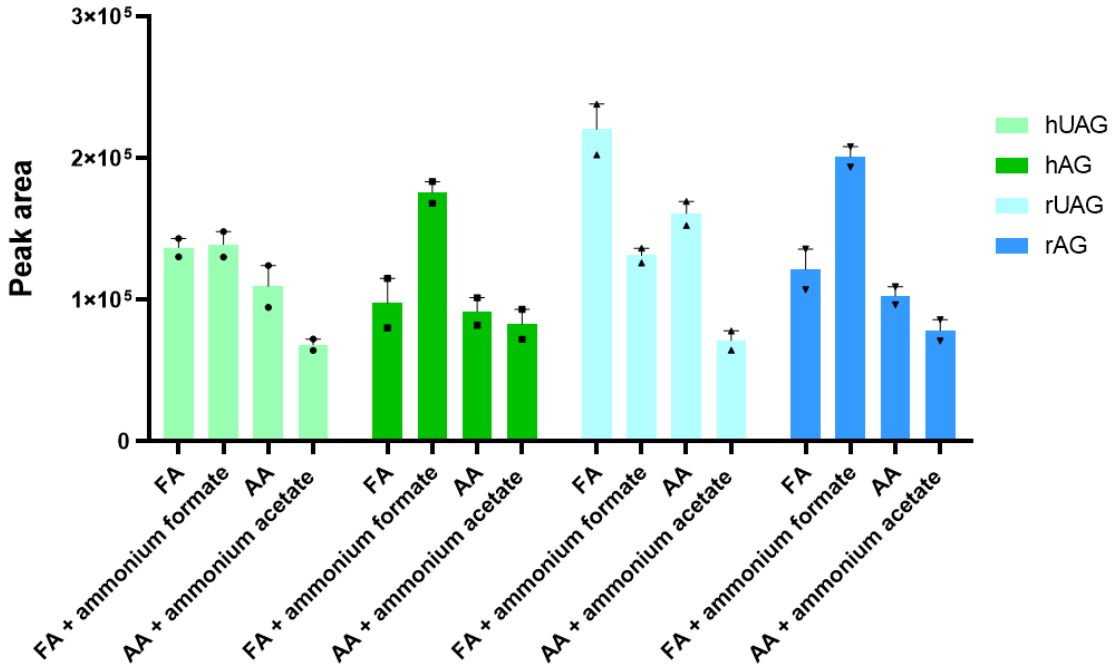

Figure 4.18 Comparison of different combinations of acids and/or salts in the mobile phase on peak areas of the ghrelin species $[M+5H]^{5+}$ (20 ng/mL) following LC-MS/MS analysis.

Two-way ANOVA was performed with Tukey corrections. $P<0.05$ is considered statistically significant. N=2, average mean peak area plotted with SEM. Acetic Acid = AA; Formic Acid (FA).

4.3.4.2 Exploring the Inclusion of DMSO in Mobile Phase

Recently, the use of DMSO within LC solvents has been explored for proteomics. Studies have found that the addition of a low percentage of DMSO increases the sensitivity of protein identification through the enhancement of electrospray ionisation of peptides (Thomas et al., 2021) Thus, I explored the addition of 1% DMSO in both mobile phase A (water, 2% acetonitrile and 0.1% acetic acid + 1% DMSO) and mobile phase B (acetonitrile and 0.1% acetic acid + 1% DMSO) when analysing ghrelin at concentrations of both 20 ng/mL and 80 ng/mL. These concentrations were selected where sensitivity or detection limits posed no concern. Following the addition of DMSO, the scattering of charged state ions shifted. In MS spectra where no DMSO was included the $[M+6H]^{6+}$, $[M+7H]^{7+}$, $[M+5H]^{5+}$ and $[M+4H]^{4+}$ species were present (Figure 4.19A-D), whilst following the inclusion of DMSO the most dominant species shifted to predominantly the $[M+5H]^{5+}$ charged state ion (Figure 4.19E-H). The inclusion of DMSO also led to a significant increase ($P<0.0001$) in the peak areas of the $[M+5H]^{5+}$ ions for ghrelin (at both 20 and 80 ng/mL) (Figure 4.20). As the $[M+6H]^{6+}$ charged state of ghrelin was looking to be as dominant if not more dominant than the $[M+5H]^{5+}$ charged states, the next step was to re-optimise the MS/MS parameters for monitoring ghrelin and compare MRMs set to analyse both the $[M+5H]^{5+}$ and $[M+6H]^{6+}$ charged state of ghrelin. However, before this, a series of PEG species were detected in the total ion count spectra (a broad scan of all events that occur during the MS1) following the use of DMSO within the mobile phase (for both 20 ng/mL and 80 ng/mL samples) (Figure 4.21). The peaks corresponding to these PEG species were not present in the spectra observed when using the mobile phase without DMSO. While the PEG peaks do not directly interfere with the detection of ghrelin species (as the elution time of PEGs from the column occurs after that of the ghrelin species), an accumulation of PEG could pose a risk to the integrity of the LC instrumentation and potentially result in column blockage over time.

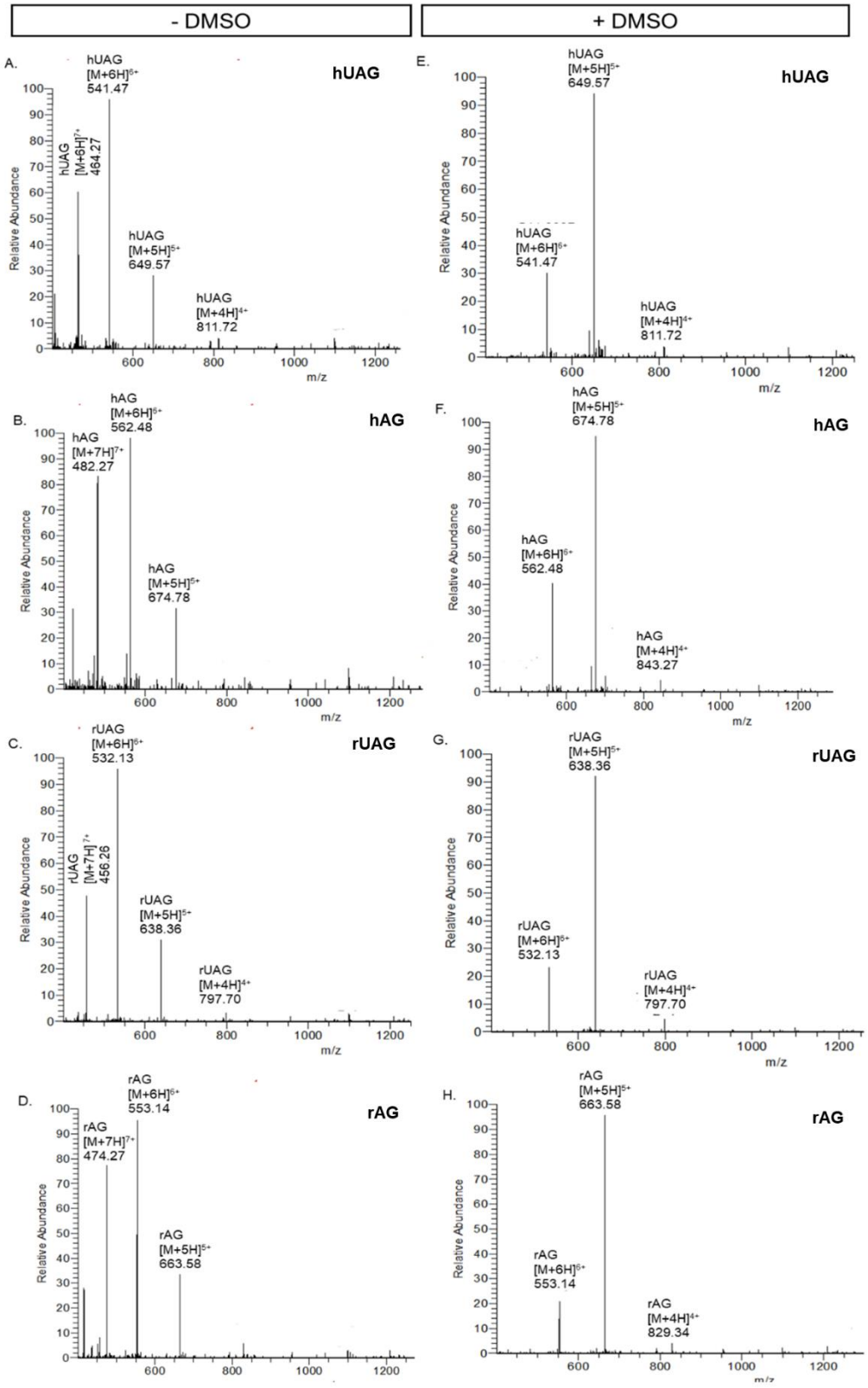

Figure 4.19 The distribution of different charged states of ghrelin ions when analysed by LC-MS, following the use of mobile phase with or without the inclusion of DMSO.

MS spectra of ghrelin species (20 ng/mL) following the use of mobile phase either with (A, B, C, D) or without DMSO (E, F, G, H). 10 scan events combined into 1.

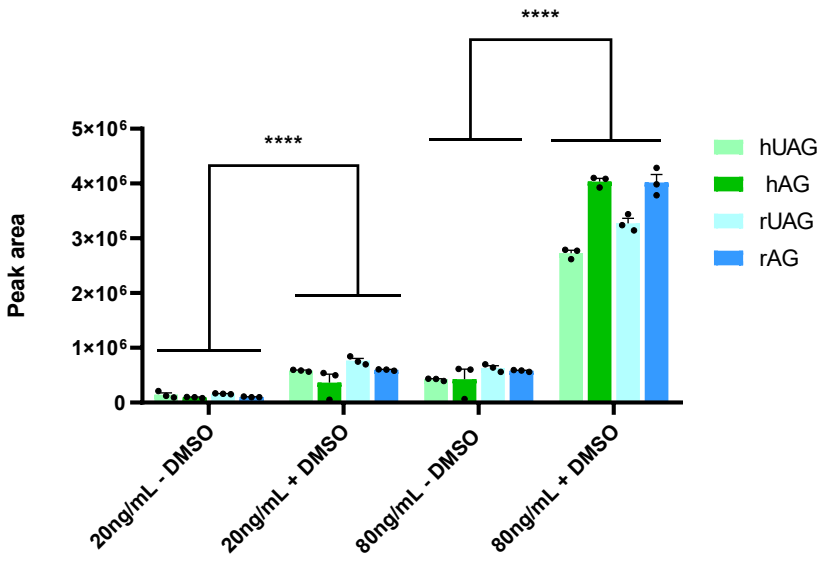

Figure 4.20 Comparison of the inclusion of DMSO within the mobile phase on the peak areas of the ghrelin species $[M+5H]^{5+}$ (20 and 80 ng/mL) following LC-MS/MS analysis.

Two-way ANOVA was performed with Tukey corrections. P<0.05 is considered statistically significant. ****P<0.0001. N=3, average mean area plotted with SEM.

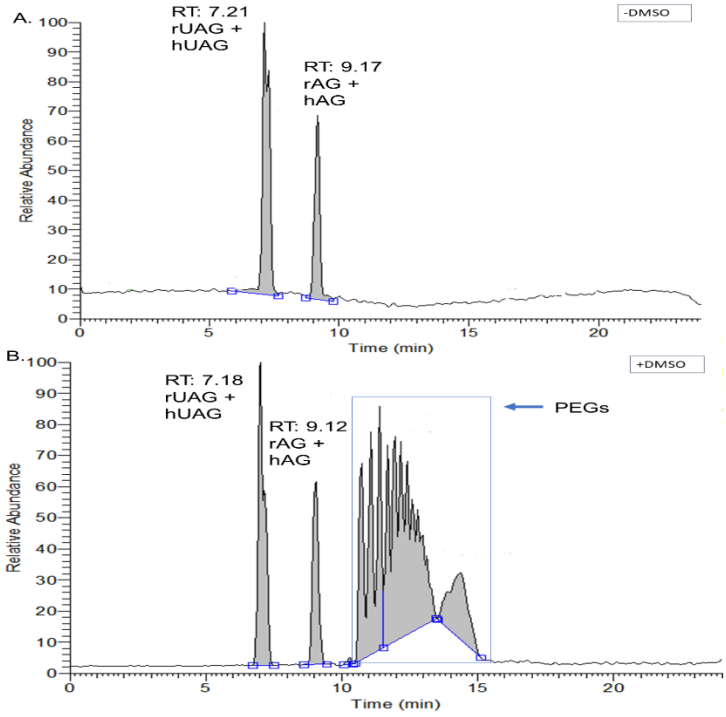

Figure 4.21 Example of PEG contamination during LC-MS/MS analysis of ghrelin (20 ng/mL).

The LC-MS/MS traces are shown for the Total Ion Count monitored after using the mobile phase where DMSO was absent (A) or present (B).

As this contamination may have been due to the DMSO itself, the investigation was repeated using a mobile phase containing a new DMSO. As shown in figure 4.22, the

PEG contamination was absent from the chromatogram resulting after the use of the mobile phase with 'new' DMSO, suggesting that the PEG contamination was due to the previous stock of DMSO.

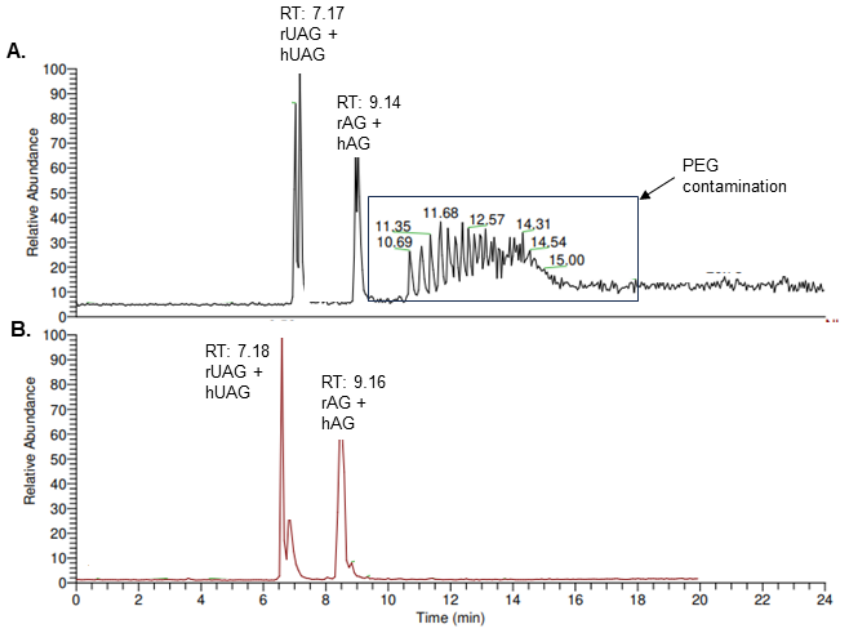

Figure 4.22 Presence of PEG during LC-MS/MS analysis of ghrelin (20 ng/mL).
The LC-MS/MS traces are shown for the Total Ion Count monitored after using the mobile phase that included the 'old' DMSO (A) (as used in Figure 4.20) and 'new' DMSO (B).

Having resolved the PEG contamination, I now continued with optimising additional MRM MS/MS transitions monitoring for the $[M+6H]^{6+}$ charged state of ghrelin, which was seen to be the most dominant in the spectra when DMSO was not included (Table 4.3). Additionally, for comparison purposes, new multiple reaction monitoring (MRM) methods were developed to include the $[M+5H]^{5+}$ precursor ion alongside the previously used $[M+6H]^{6+}$ ion. Both charge states were analysed by selecting their respective parent m/z values (i.e., the mass-to-charge ratios of the intact precursor ions) and fragmenting them to monitor the two most dominant product ions observed during MS/MS analysis. This approach differs from previous methods, which used a specific 'diagnostic ion' for quantification. Instead, the revised method aims to improve sensitivity and comparability by focusing on the most intense and consistently observed fragment ions (Figure 4.23). The most intense ion upon fragmentation was used for quantification purposes, the second ion was only included as a secondary means of confirming/supporting the identity of the correct peak belonging to ghrelin. The most intense ion upon fragmentation was chosen as the quantifier ion, used to

determine the analyte response whilst the other ion selected was chosen as the qualifier ion, which is used to identify the analyte. Two new methods were created, each containing 8 MRM transitions (Table 4.3).

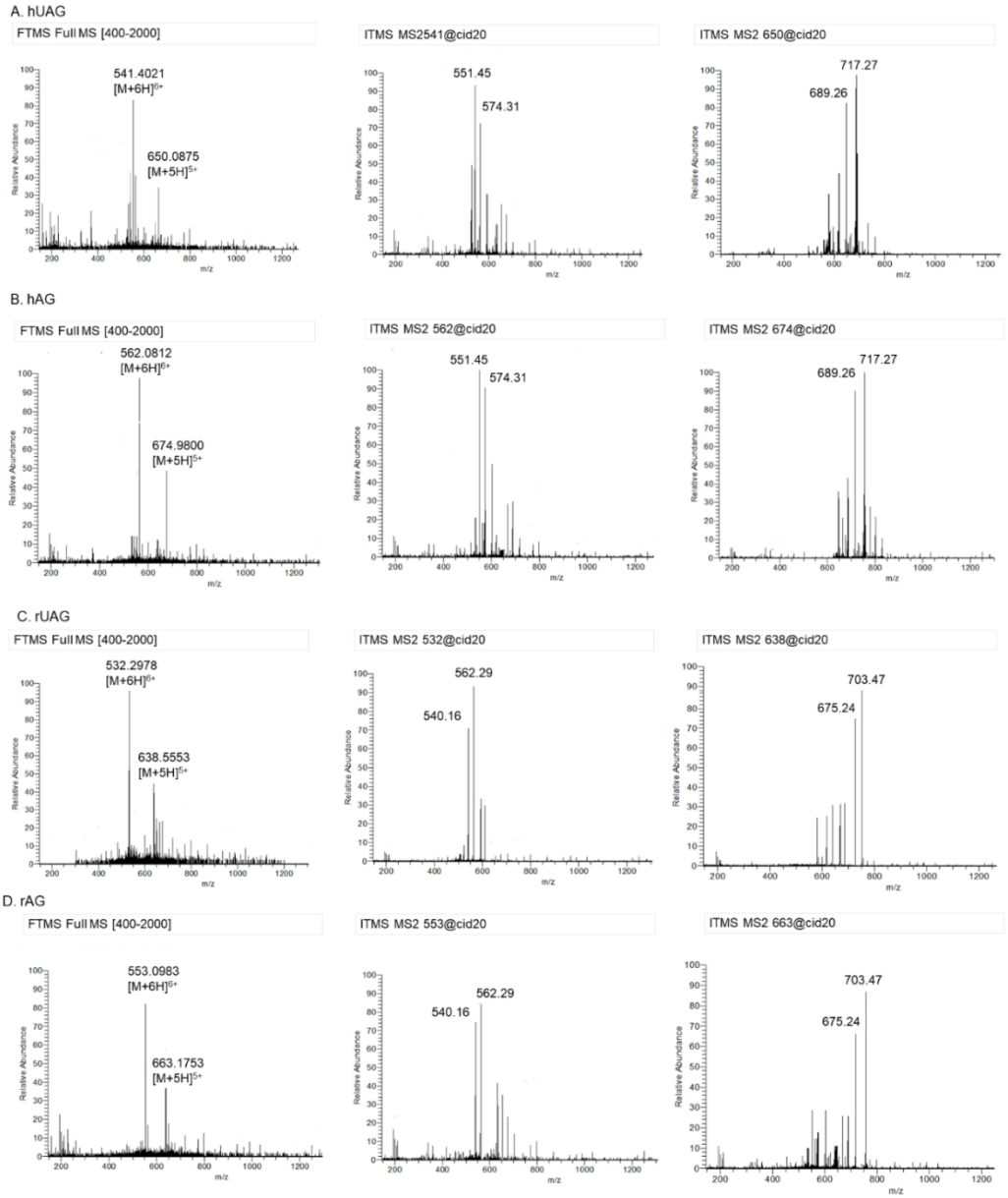

Figure 4.23 MS and MS/MS spectra of the $[M+6H]^{6+}$ and $[M+5H]^{5+}$ charged state ion.

A. hUAG at m/z 541 and B. hAG at m/z 562 with the most abundant product ions at 551 and 574 for $[M+6H]^{6+}$ and 689 and 717 for the $[M+5H]^{5+}$. C. rUAG at m/z 532 and D. rAG at m/z 553 with the most abundant product ions at 540 and 562 for the $[M+6H]^{6+}$ and 675 and 703 for the $[M+5H]^{5+}$. (All ghrelin species were analysed at 20 ng/mL, 10 scan events).

Ghrelin species	Amino acid sequence	Collision energy	Precursor or 'Parent' ion (m/z)	Product or 'Daughter' ion of interest (m/z)	MS/MS included in the MRM
Human UAG	GSSFLSPEHQRVQQRKESKKPPAKLQPR	20	650 ($[M+5H]^{5+}$)	Quantifier ion: 717 689	650/ 715-718 650/ 688-690
			541 ($[M+6H]^{6+}$)	Quantifier ion: 551 574	541/ 573-575 541/ 550-552
Human AG	GSS(n-octanoyl)FLSPEHQRVQQRKESKKPPAKLQPR	20	675 ($[M+5H]^{5+}$)	Quantifier ion: 717 689	675/ 715-718 675/ 688-690
			562 ($[M+6H]^{6+}$)	Quantifier ion: 551 574	562/ 573-575 562/ 550-552
Rat UAG	GSSFLSPEHQKAQQRKESKKPPAKLQPR	20	638 ($[M+5H]^{5+}$)	Quantifier ion: 703 675	638/ 702-704 638/ 673-675
			532 ($[M+6H]^{6+}$)	Quantifier ion: 562 540	532/ 561-563 532/ 539-541
Rat AG	GSS(n-octanoyl)FLSPEHQKAQQRKESKKPPAKLQPR	20	663 ($[M+5H]^{5+}$)	Quantifier ion: 703 675	663/ 702-704 663/ 673-675
			553 ($[M+6H]^{6+}$)	Quantifier ion: 562 675	553/ 561-563 553/ 539-541

Table 4.3 New 8 MS/MS MRM transitions to monitor rat and human ghrelin species either focusing on $[M+5H]^{5+}$ or $[M+6H]^{6+}$ charged state ion.

MS/MS transition in black: used for quantifying peak areas of ghrelin, MS/MS transition in grey: used for identification purposes to confirm the correct peak of ghrelin.

The new MRM methods were tested using a 20 ng/mL equimolar mixture of human and rat unacylated and acyl ghrelin. This was carried out either with or without the inclusion of DMSO in the mobile phase. Overall, in the absence of DMSO, the peak areas seen for the $[M+6H]^{6+}$ charged states of human acyl ghrelin and rat unacylated and acyl ghrelin were significantly higher than the peak areas seen using the original MRM method for the $[M+5H]^{5+}$ charged state of ghrelin (Figure 4.24). However, there was no difference in the peak areas when comparing the $[M+6H]^{6+}$ MRM method and the original method analysing the $[M+5H]^{5+}$ charged state of human unacylated ghrelin. For the 'new' MRM method using the $[M+5H]^{5+}$ charged state (refer to table 4.3), peak

areas for all the ghrelin species were significantly higher than what was seen using the original $[M+5H]^{5+}$ method (refer to table 4.2) (Figure 4.24).

As such, for the mobile phase including DMSO, the MRM methods following the $[M+5H]^{5+}$ charged state ion of ghrelin (using 717 and 675 as the product ions for the human and rat ghrelin species respectively) were used for further analysis. When using the mobile phase without the inclusion of DMSO, the new MRM method following the $[M+6H]^{6+}$ charged state ion of ghrelin was used (using 551 and 562 as the product ions for the human and rat ghrelin species, respectively). The effect of DMSO on the generation and distribution of different charged states of ghrelin was assessed using the new MRM methods. In the absence of DMSO, an increase in ghrelin-charged states was seen with the most dominant being the $[M+6H]^{6+}$ ion and overall scattering ranging from $[M+4H]^{4+}$ to $[M+7H]^{7+}$ (Figure 4.25). In the presence of DMSO, the $[M+5H]^{5+}$ ion dominated with a lesser presence of the $[M+6H]^{6+}$ and lesser amounts of the $[M+4H]^{4+}$ (Figure 4.25). For both human and rat unacylated and acyl ghrelin, the overall peak area was significantly higher in the presence of DMSO (Figure 4.26A-B).

Considering the results from 4.25 and 4.26, it was decided that the most effective method for monitoring ghrelin was by using the ‘new’ $[M+5H]^{5+}$ charged state (as described in table 4.3), alongside the inclusion of DMSO in the mobile phase.

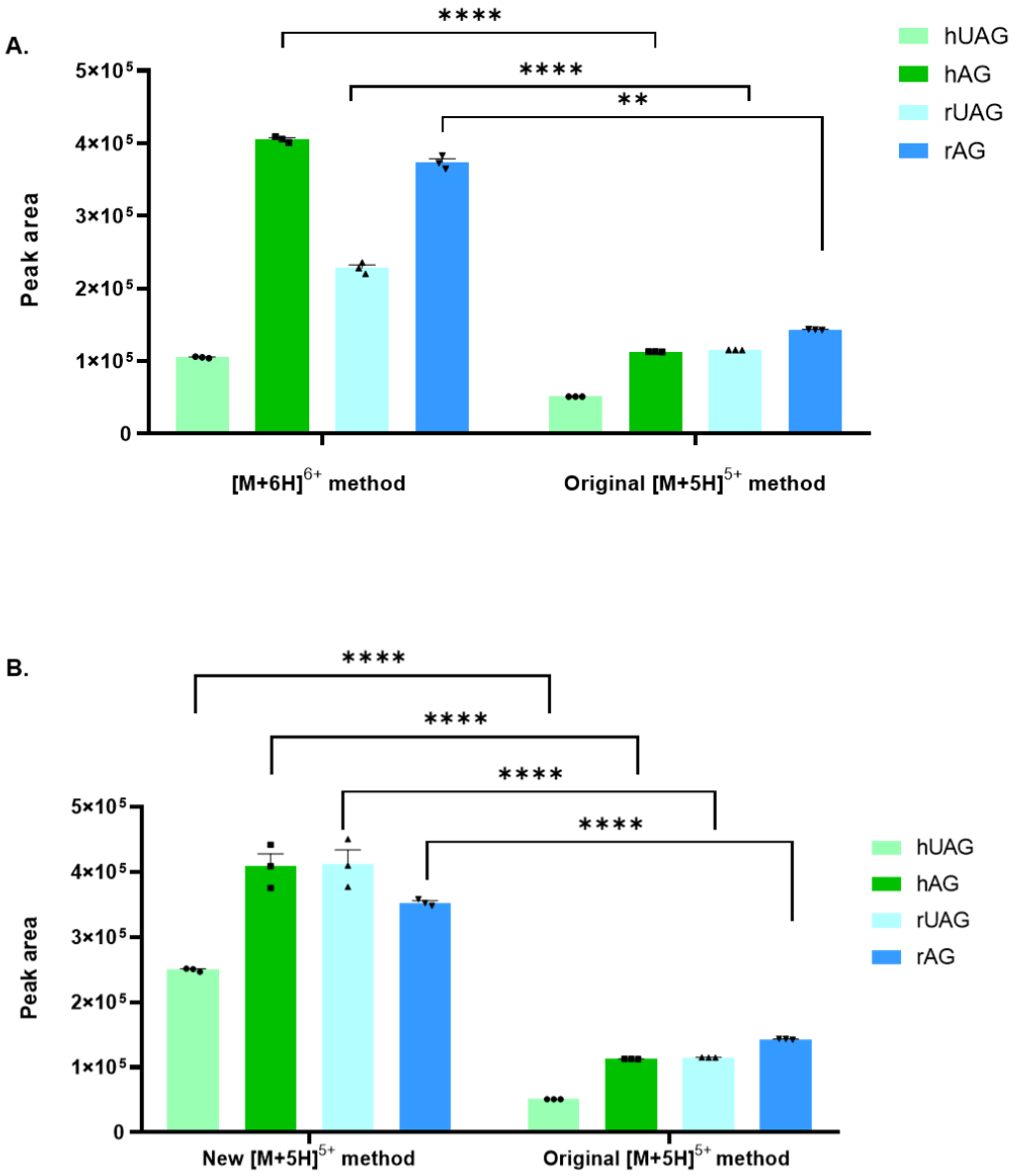

Figure 4.24 Comparison of peak areas of ghrelin after analysis using LC-MS/MS parameters monitoring the $[M+6H]^{6+}$ and $[M+5H]^{5+}$ charged states of ghrelin (analysed at 20 ng/mL) (no inclusion of DMSO).

A. Comparison of the new MRM monitoring the $[M+6H]^{6+}$ charged state parent ions and the most dominant product ions to the original $[M+5H]^{5+}$ MRM method. B. Comparison of the new MRM monitoring the $[M+5H]^{5+}$ charged state parent ions and the most dominant product ions to the original $[M+5H]^{5+}$ MRM method. Two-way ANOVA was performed with Tukey corrections. $P<0.05$ is considered statistically significant. **$P<0.01$. ****$P<0.0001$. N=3, with the average mean plotted and SEM.

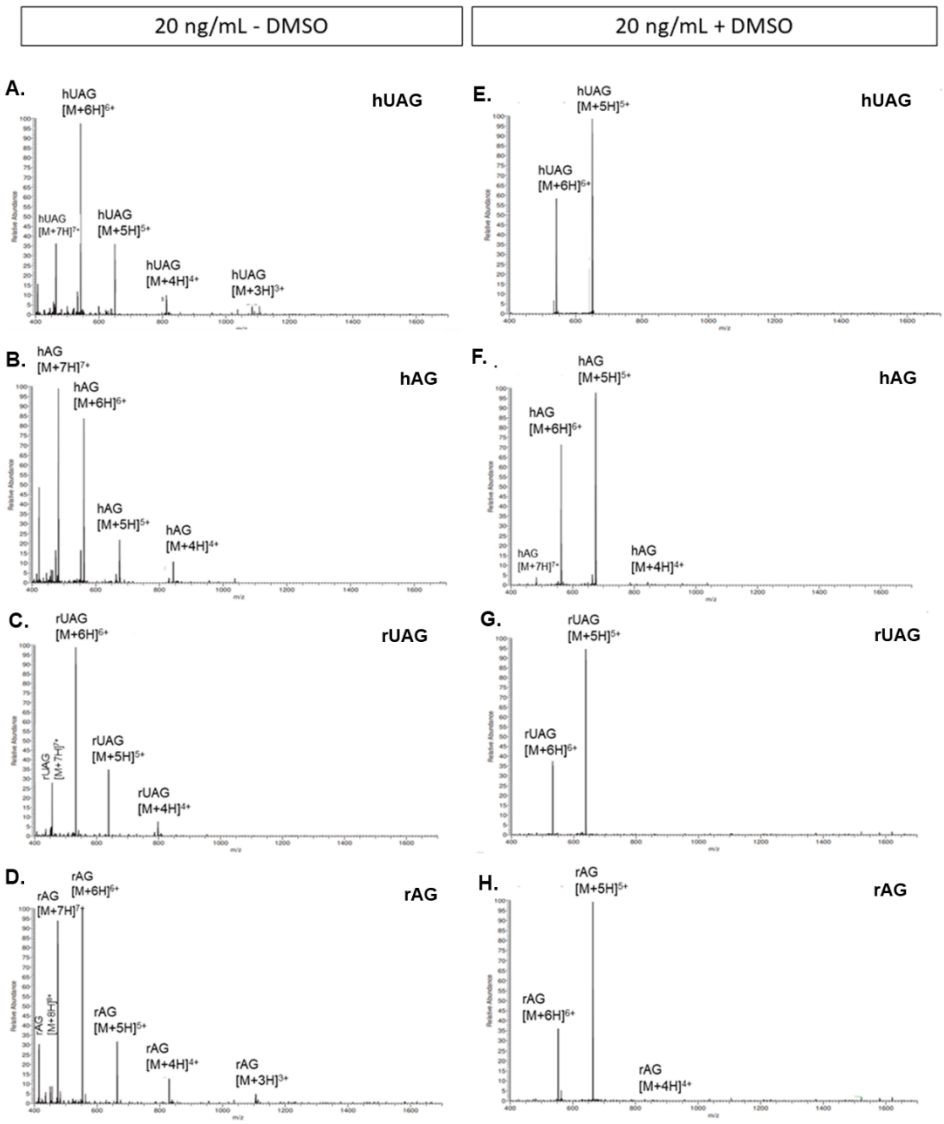

Figure 4.25 The distribution of different charged states of ghrelin ions when analysed by LC-MS, following the use of mobile phase with or without the inclusion of DMSO.

MS spectra of ghrelin species (20 ng/mL) following the use of mobile phase either without (A, B, C, D) or with DMSO (E, F, G, H). 10 scan events combined.

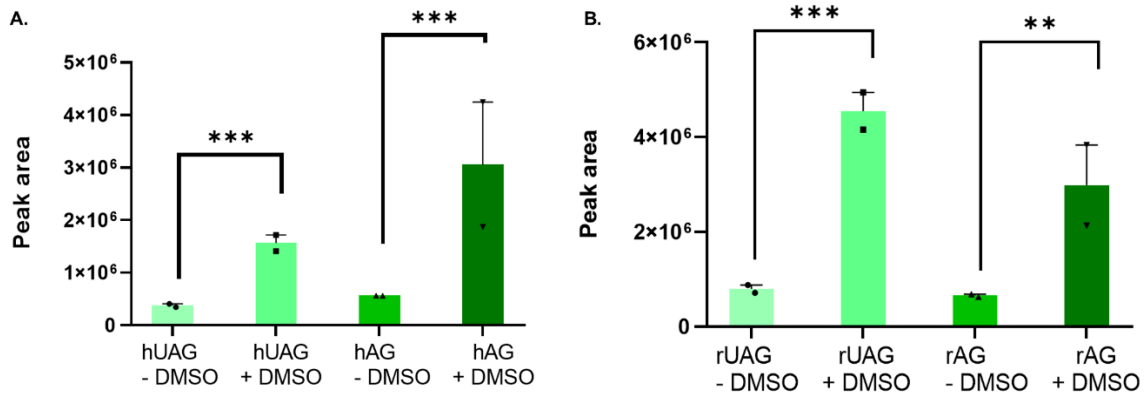

Figure 4.26 Assessing the effect of DMSO on ghrelin peak area (analysed at 20 ng/mL).

A. hUAG and hAG. B. rUAG and rAG. Two-way ANOVA performed with Tukey corrections. $P<0.05$ considered statistically significant. **$P<0.01$, ***$P<0.001$. N=3, with average mean peak area plotted and SEM.

Following on from these promising results of increased intensity after the inclusion of DMSO in the mobile phase, a new calibration curve was established to test the limit of detection. The calibration curve consisted of human and rat, acyl, and unacylated ghrelin within an equimolar mixture ranging from 0.4-40 ng/mL (Figure 4.27). For the first time, ghrelin species were detected at levels as low as 0.4 ng/mL, demonstrating an improved method for sensitivity.

To improve linearity and reduce visual complexity, the highest concentration point (40 ng/mL) was excluded from the calibration curve. This decision was based on a consistent deviation from linearity observed at this concentration, which may reflect partial signal suppression, column overloading, or possible ghrelin degradation under prolonged LC-MS/MS conditions. The underlying cause will be explored further in the later sections of this chapter.

The resulting data were presented across two panels (Figure 4.27A and 4.27B) to aid clarity and interpretation. Figure 4.27A displays the calibration curves for unacylated ghrelin species, demonstrating strong linearity with R^2 values of 0.98 for human unacylated ghrelin and 0.92 for rat unacylated ghrelin. Figure 4.27B presents the acyl ghrelin calibration curves, where both human and rat acyl ghrelin achieved excellent linearity, each with an R^2 value of 0.99.

Despite the promising new lower limit of detection achieved, the R^2 values for some analytes remained below the ideal threshold of 0.95, and peak intensities at the lower end of the concentration range were relatively small. Given that this top-down approach has now been explored extensively, a bottom-up strategy was pursued next as an alternative method for the analysis of ghrelin.

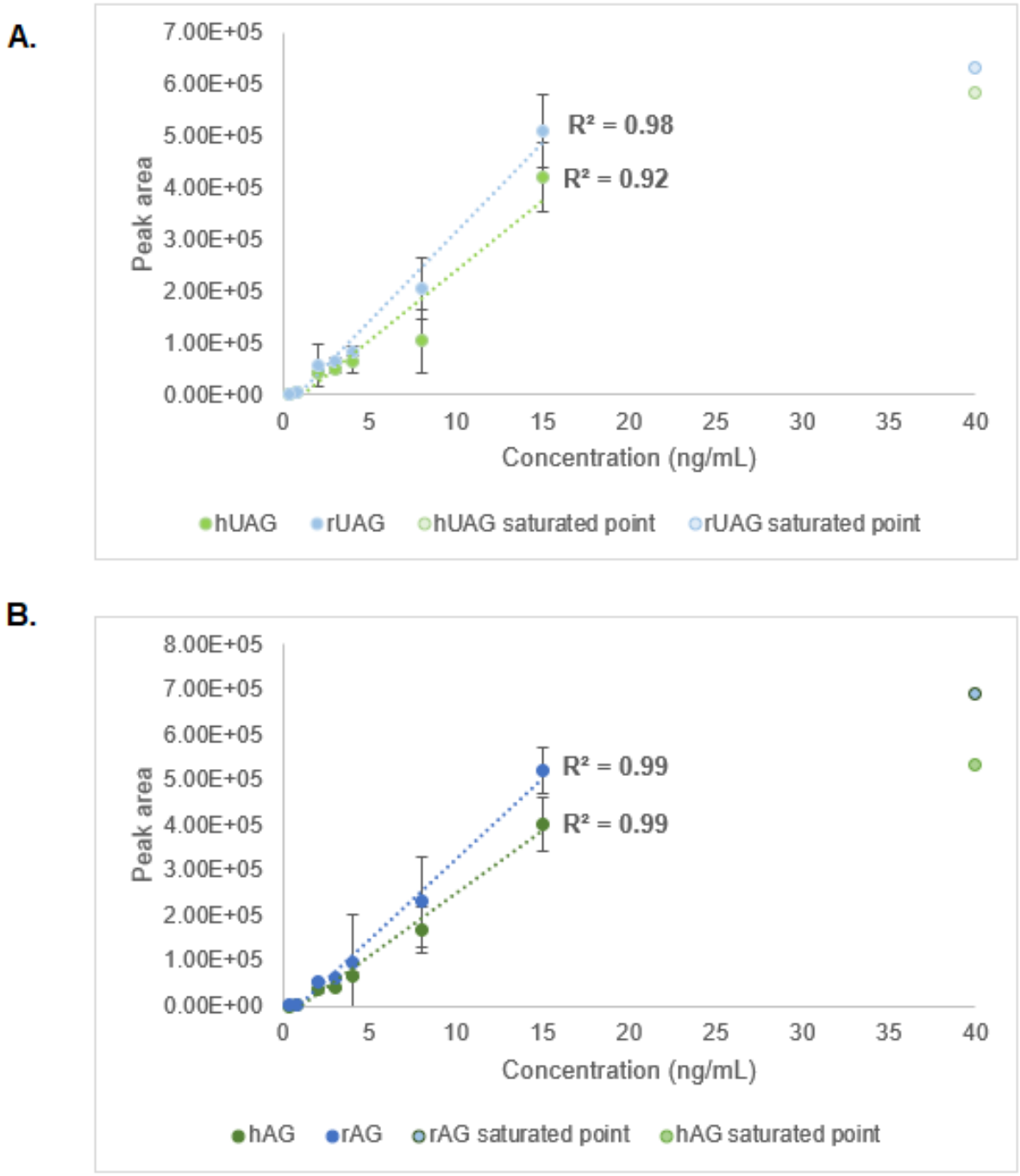

Figure 4.27 Calibration curve of hUAG, hAG, rUAG, and rAG ranging from 0.4-40 ng/mL. Analysed by LC-MS/MS, MRM transitions as described in $[M+5H]^{5+}$ new method (Table 4.3) with the inclusion of DMSO. N=3. The final plotted point is the mean of these three-run means, and error bars represent the standard deviation across runs, reflecting inter-run variability. Trendlines represent linear regression fits, and R^2 values are reported to indicate goodness of fit.

4.3.5 Trypsin Digestion of Ghrelin Prior to MS Analysis

Here, a bottom-up approach is explored which entails, enzymatically digesting a protein of interest into peptides before analysis by LC-MS/MS. Thomas et al. 2021 used this method successfully for identifying ghrelin. Trypsin, a serine protease is commonly used for protein digestion (Laskay et al., 2013). It functions by cutting at the carboxyl side of lysine and arginine residues. As such, tryptic digestion of ghrelin was tested. The tryptic digestion results in the production of an 11 amino acid fragment of ghrelin and as such the (1-11) peptide still includes the acyl-modification at the serine 3 residue (Figure 4.2).

Following tryptic digestion of ghrelin, the products were analysed by MS where product ion scans of the dominant parent ions were carried out. The parent and product ions seen for the human ghrelin following trypsin digestion were consistent with what was previously reported by Thomas et al (2021), using the same bottom-up approach. The diagnostic product ions of human unacylated ghrelin ($_{1\text{-}11}$) and human acyl ghrelin ($_{1\text{-}11}$) were obtained from their $[M+2H]^{2+}$ charge state, parent ions seen at m/z 622 and m/z 685 respectively (Figure 4.28). For rat acyl and unacylated ghrelin, the $[M+2H]^{2+}$ charged state parent ions can be seen at m/z 608 and 671 respectively (Figure 4.28). The most appropriate collision energies and instrument parameters for each MS/MS were determined by analysing the samples using the Nanomate by direct injection before analysing by LC-MS/MS. For the new MRM transitions the product ions with the highest intensity were chosen to quantify the peak areas.

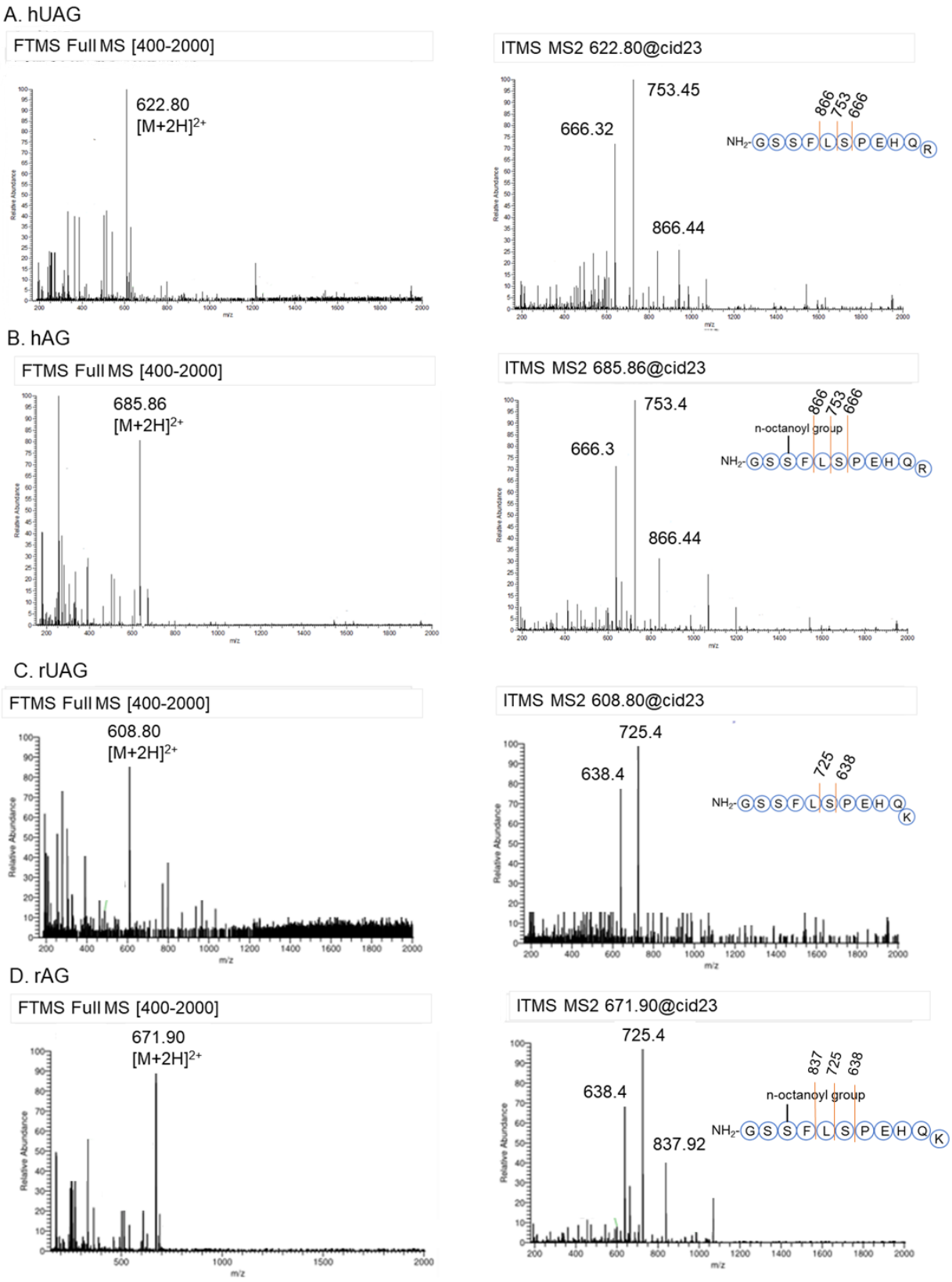

Figure 4.28 MS and MS/MS spectra of the trypsin digested product.

A hUAG (t1-11) at m/z 622 and B. hAG (t1-11) at m/z 685 with the most abundant product ions being at 666 and 753. C. rUAG (t1-11) at m/z 608 and D. rAG(t1-11) at m/z 671 with the most abundant product ions being at 638 and 725.

To summarise, the new mass spectrometer parameters for the bottom-up approach of the tryptic ghrelin peptides are highlighted in Table 4.4 below.

Ghrelin species	Amino acid sequence	Collision energy	Precursor or 'Parent' ion (m/z)	Product or 'Daughter' ion of interest (m/z)	MS/MS for use in MRM
Human UAG	GSSFLSPEHQR	23	622.80 ($[M+2H]^{2+}$)	Quantifier ion:753.4 666.3	622/ 752-754 622/ 665-667
Human AG	GSS(n-octanoyl)FLSPEHQR	23	685.86 ($[M+2H]^{2+}$)	Quantifier ion: 753.4 666.3	685/ 752-754 685/ 665-667
Rat UAG	GSSFLSPEHQK	23	608.80 ($[M+2H]^{2+}$)	Quantifier ion: 725.4, 638.4	608/ 724-726 608/ 637-639
Rat AG	GSS(n-octanoyl)FLSPEHQK	23	671.40 ($[M+2H]^{2+}$)	Quantifier ion: 725.4, 638.4	671/ 724-726 671/ 637-639

Table 4.4 New 4 LC-MS/MS MRM transitions to monitor rat and human ghrelin species focusing on $[M+2H]^{2+}$ charged state following digestion using Trypsin.

MS/MS transitions in black: used for quantifying peak areas of ghrelin, MS/MS transition in grey: used for identification purposes to confirm correct peak of ghrelin.

Following the MS characterization, the ratio of trypsin to ghrelin was tested using either a 1:20 or 1:100 (w/w) as recommended by suppliers. The 1:20 or 1:100 (w/w) trypsin ghrelin ratio was mixed and incubated overnight at 37°C on a rotor mixer set at 500 rpm. The reaction was quenched using 2% acetic acid followed by centrifugation at 9000xg for 2 minutes. Overall, no significant differences were seen for the peak areas of the $[M+2H]^{2+}$ charged state of ghrelin following treatment with trypsin at the ratio of 1:20 or 1:100 (trypsin to ghrelin) (Figure 4.29).

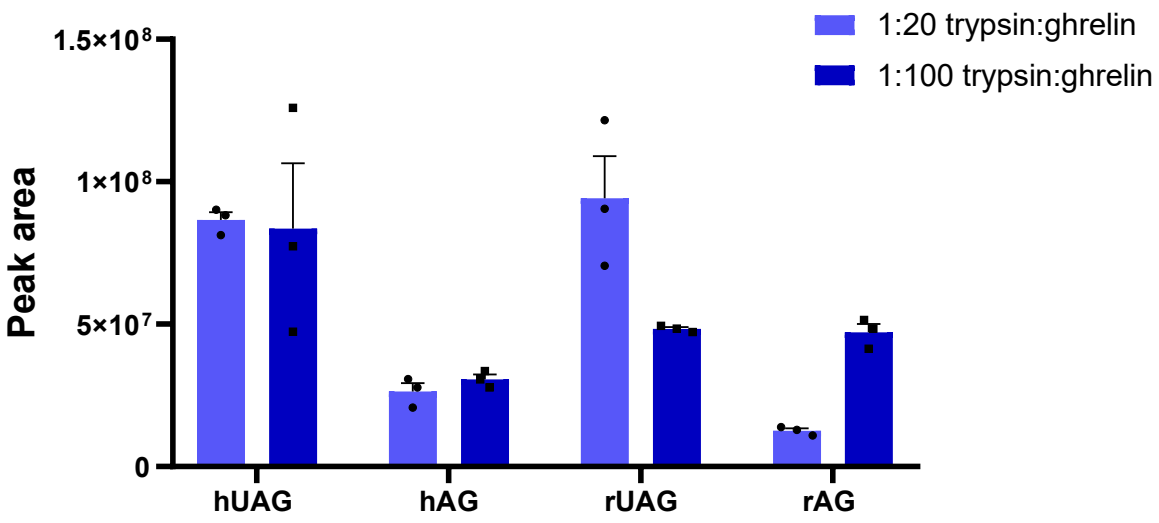

Figure 4.29 Comparison of 1:20 or 1:100 (w/w) of trypsin to ghrelin on peak areas of ghrelin ($[M+2H]^{2+}$ charged stated) following LC-MS/MS analysis.

Two-way ANOVA was performed with Tukey corrections. P<0.05 is considered statistically significant. N=3, average mean peak area plotted with SEM.

During LC-MS/MS analysis of the acyl ghrelin samples (both human and rat), a continual presence of a peak that corresponded to the same retention time as unacylated ghrelin (RT:8.60 and RT:8.68 for rat and human unacylated ghrelin respectively) was noticed (Figure 4.30). The presence of unacylated ghrelin in the samples of acyl ghrelin that had undergone tryptic digestion was confirmed by carrying out MS/MS product ion spectra of those peaks at 8.68 and 8.76 minutes which contained product ions diagnostic of unacylated ghrelin (m/z/ 608 and 622 for rat and human unacylated ghrelin respectively) (Figure 4.30). This was not believed to be associated with the ratio of the trypsin ghrelin treatment as there was no correlation between the amount of trypsin used and the peak area of the 'contaminating' unacylated ghrelin. It was considered whether this degradation of acyl ghrelin in samples could be due to a 'natural' degradation/ loss of the acyl group in response to samples being incubated overnight at 37°C for the digestion process. Therefore, the samples were re-analysed after being stored for an additional 24 hours at 4°C, to see whether the presence of unacylated ghrelin increased further in the acyl ghrelin samples. However, no significant differences were observed between the peak areas of the 'contaminating' unacylated ghrelin when the samples were analysed either immediately after trypsin digestion or after being stored for an additional 24 hours at 4°C (figure 4.31).

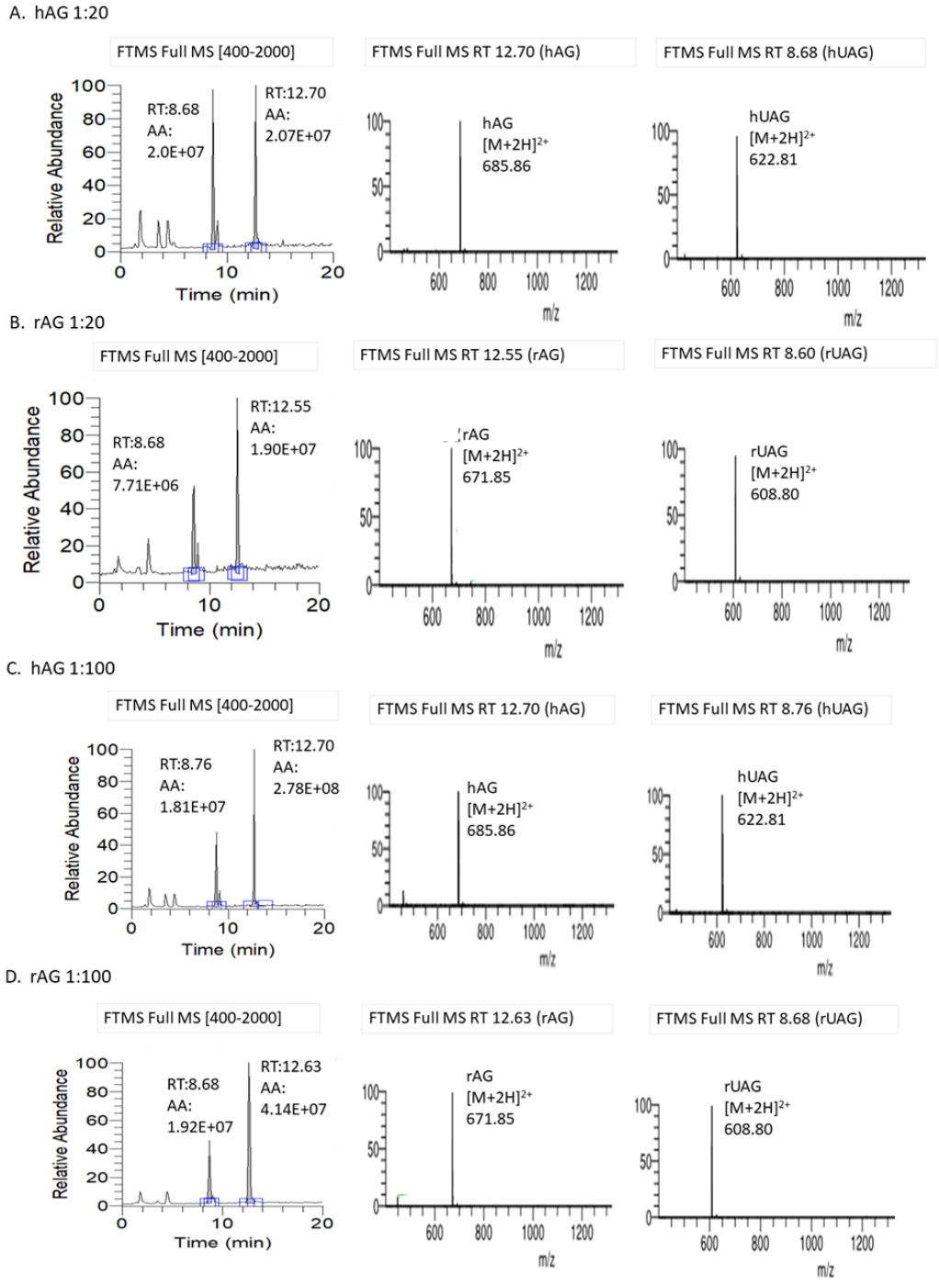

Figure 4.30 MS Chromatograms and spectra of acyl ghrelin samples following digestion with trypsin suggest the presence of unacylated ghrelin at 8.6 or 8.7 minutes.

A. hAG 1:20 digestion with the presence of hAG (RT 12.70) and hUAG (RT 8.68) followed by spectra of the dominant ion present at 12.55, diagnostic of hAG and spectra of the dominant ion present at 8.68, diagnostic of hUAG. B. hAG 1:20 digestion with the presence of hAG (12.70) and hUAG (8.68). C. rAG 1:100 digestion with the presence of rAG (RT 12.55) and rUAG (RT 8.76). D. rAG 1:100 digestion with the presence of rAG (12.63) and rUAG (8.68). AA: peak area. RT: retention time.

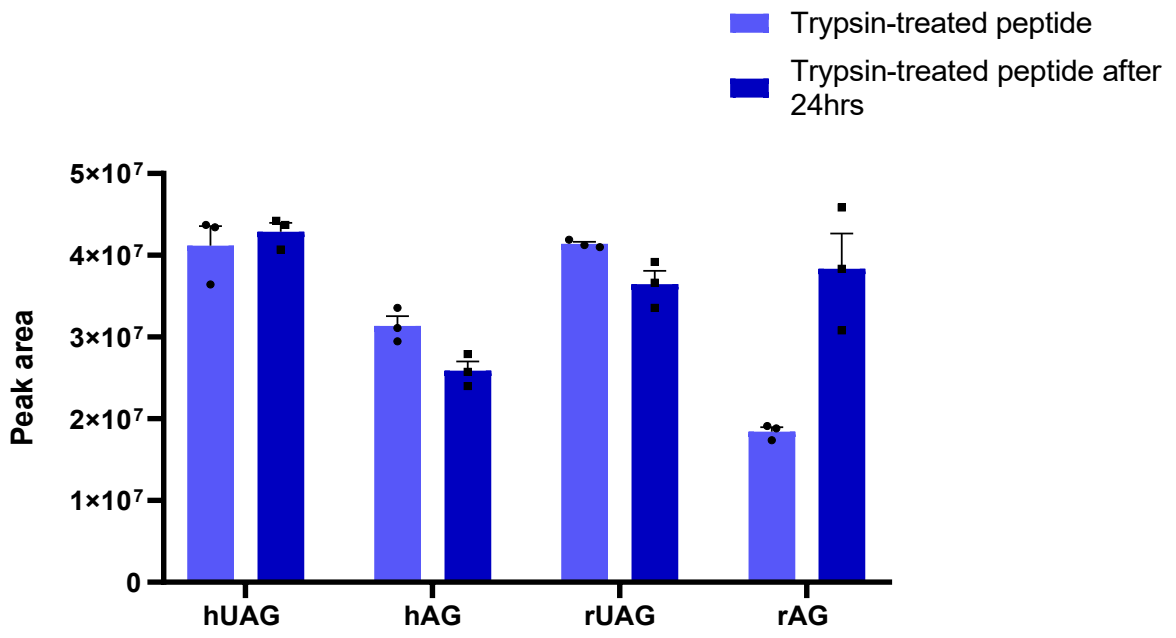

Figure 4.31 Comparison of trypsin digested ghrelin peptides (1:20) analysed immediately or after 24 hours storage at 4°C.

Analysed by LC-MS/MS analysis (Following the ($[M+2H]^{2+}$ charged stated). Two-way ANOVA was performed with Tukey corrections. $P<0.05$ is considered statistically significant. N=3, average mean peak area plotted with SEM.

To investigate whether degradation of the acyl ghrelin in samples could be due to a 'natural' degradation/loss of the acyl group, individual preparations of both rat and human acyl ghrelin standards of intact (non-digested) ghrelin were analysed immediately after preparation (time 0) by LC-MS/MS then stored for 24 hours at 4°C before being re-analysed by LC-MS/MS. The presence of unacylated ghrelin in the samples of acyl ghrelin was confirmed by analysing the spectra of chromatogram peaks at 8.68 and 8.6 minutes (the presence of m/z 622 and 608 indicating the presence of human and rat unacylated ghrelin, respectively) (Figure 4.32). Overall, a significant decrease was seen in the peak areas for all ghrelin species after being stored for 24 hours (Figure 4.33). This suggests that there is a potential degradation of ghrelin in samples at 24 hours. The results suggest degradation of both acyl and unacylated ghrelin species in samples at 24 hours, suggesting that the peptide is potentially unstable during storage at 4°C.

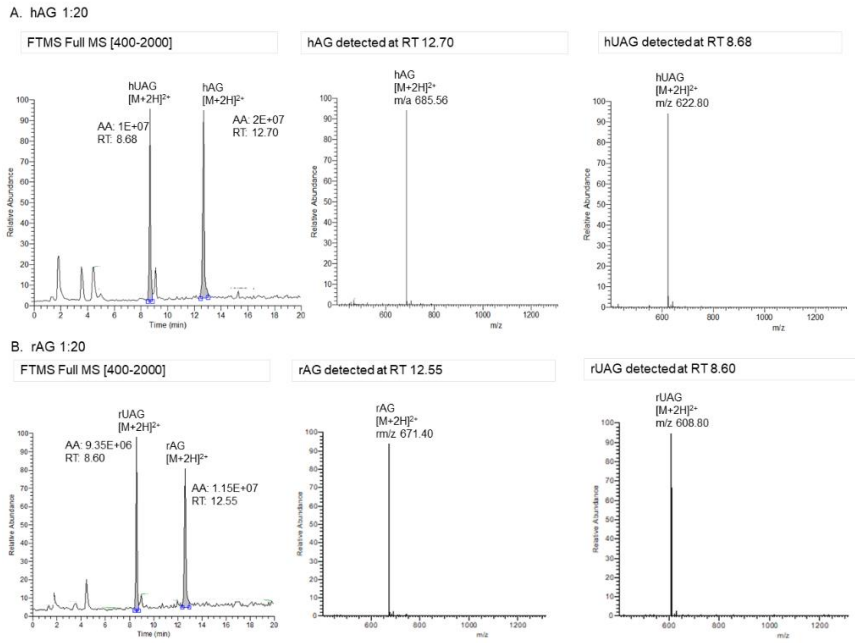

Figure 4.32 MS Chromatograms and spectra of intact ghrelin after being stored for 24 hours at 4°C.

A. LC-MS chromatogram of hAG (12.70) with spectra of peaks at 8.68 minutes supporting the presence of hUAG. B. LC-MS chromatogram of rAG (12.55) with spectra of peaks at 8.60 minutes supporting the presence of rUAG. AA: peak area. RT: retention time.

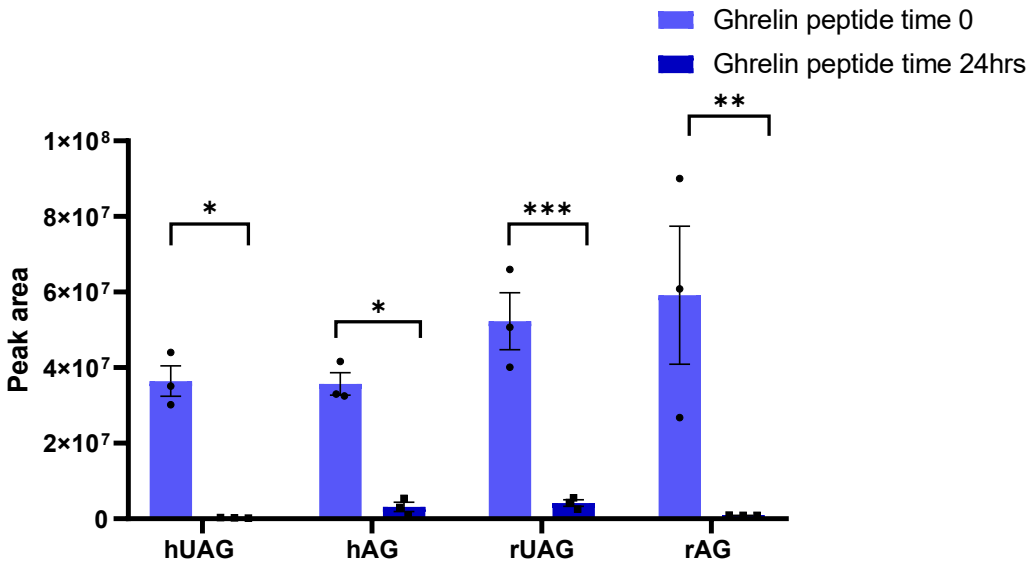

Figure 4.33 Comparison of the peak areas of intact ghrelin analysed after immediate preparation (time 0) and after 24 hours of storage at 4°C.

Sample analysed by LC-MS/MS analysis (following $[M+5H]^{5+}$ charged state as described in table 4.3). Two-way ANOVA was performed with Tukey corrections. P<0.05 is considered statistically significant. *P>0.05, ** P<0.01, ***P<0.001. N=3, average mean peak area plotted with SEM.

The LC-MS/MS chromatograms of acyl ghrelin (enzymatically digested and intact) after being stored for 24 hours at 4°C were compared to gain further insights into the presence of the unacylated ghrelin species within the acyl ghrelin samples. As before, unacylated ghrelin was present within all acyl ghrelin samples (Figure 4.34). No significant differences were observed between the peak areas of the unacylated ghrelin observed within the trypsin acyl ghrelin samples when analysed immediately via LC-MS/MS in comparison to storing the samples at 4°C for 24 hours (Figure 4.35A). However, significant changes were observed in the peak areas of intact ghrelin species over 24 hours (Figure 4.35B). Specifically, human unacylated ghrelin and rat acyl ghrelin both showed a significant decrease in signal intensity from time 0 to 24 hours ($P<0.0001$ and $P<0.05$, respectively), indicating potential degradation or instability under the storage conditions. Interestingly, a significant increase in the human acyl ghrelin peak area was observed after 24 hours of storage at 4°C ($P < 0.05$), which contrasts with the expected pattern of degradation. The reason for this unexpected rise is unclear and may reflect delayed ionisation efficiency, sample variability, or possible artefactual changes during storage or analysis. These findings suggest that, while degradation of some ghrelin species is evident over time, the dynamics are complex and may not follow a uniform pattern across species or isoforms.

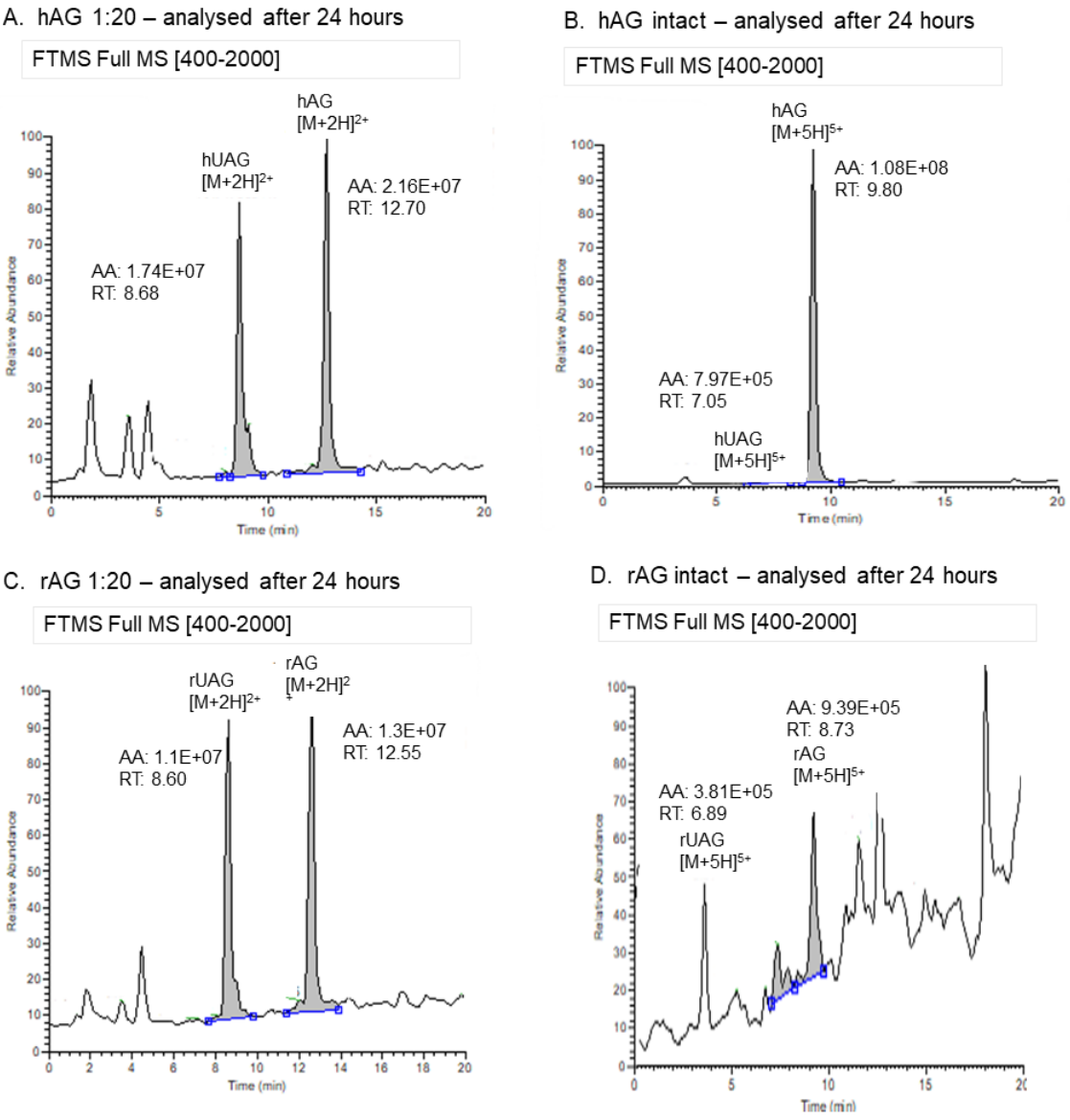

Figure 4.34 LC-MS chromatograms for human and rat ghrelin after being stored for 24 hours at 4°C - with and without trypsin digestion.

A. hAG treated with trypsin and 24 hours storage (1:20) B. intact hAG stored for 24 hours. C. rAG treated with trypsin (1:20) and 24 hours storage. D. intact rAG stored for 24 hours.

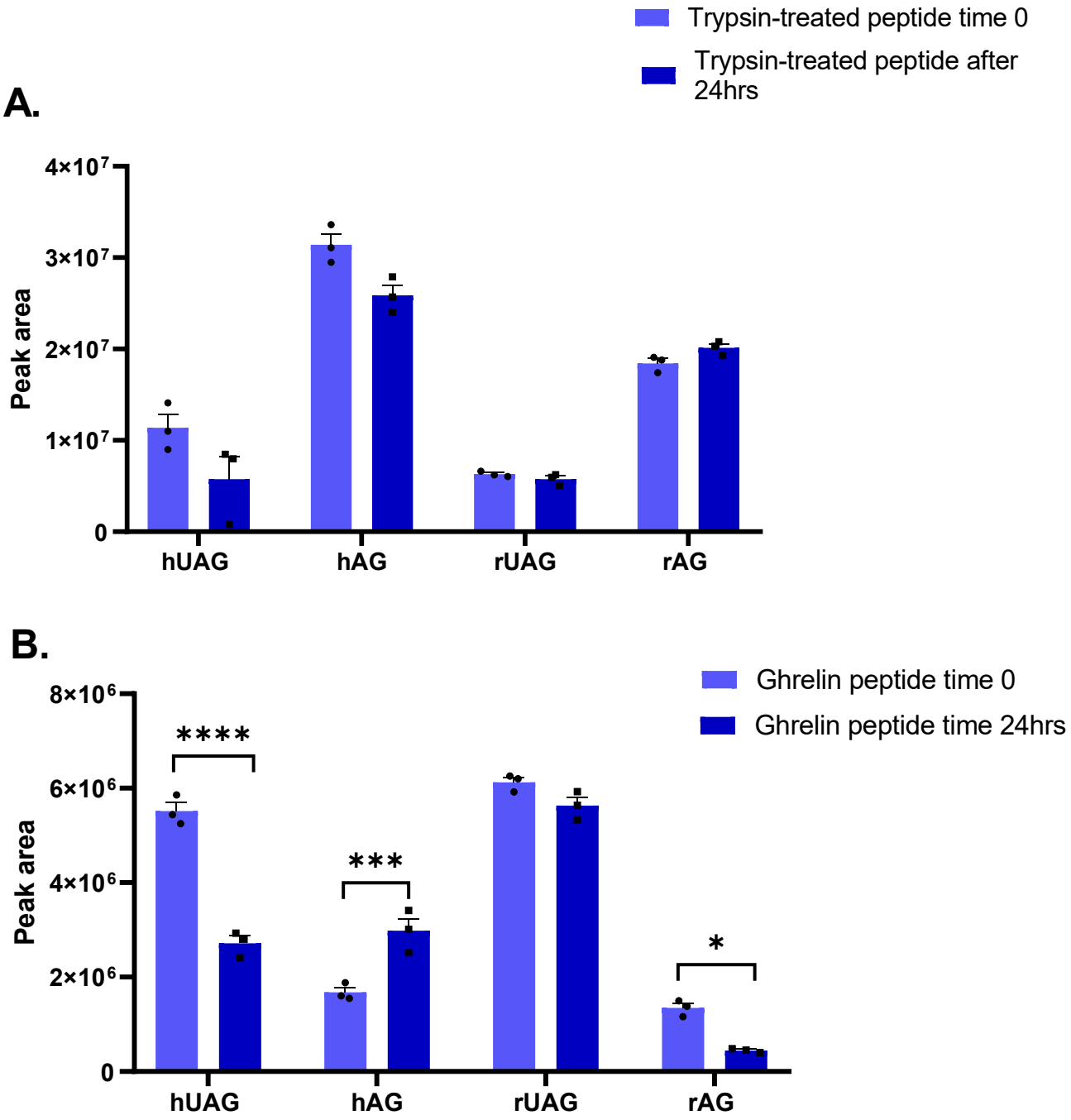

Figure 4.35 The presence of UAG within AG samples treated with and without trypsin was analysed at 0 and 24 hours post storage at 4°C.

Peak areas of ghrelin analysed by LC-MS/MS. A. Trypsin-treated ghrelin ($[M+2H]^{2+}$, refer to table 4.4 for MS/MS transitions). B. Intact ghrelin ($[M+5H]^{5+}$ refer to table 4.3 for MS/MS transitions). Two-way ANOVA was performed with Tukey corrections. $P<0.05$ is considered statistically significant. N=6, average mean peak area plotted with SEM.

To reduce the likelihood of ghrelin degradation during treatment with trypsin, two adaptations to the method were explored A. the implementation of a one-hour incubation step for the trypsin digestion instead of being carried out overnight, or B. following an overnight incubation with trypsin, as described in the original method, the quenching reaction would be carried out by freezing the samples at -20°C instead of using acetic acid. No other steps within the protocol were changed. However, no change in the peak areas of the ghrelin species was seen after either alteration compared to the original protocol (Figure 4.36).

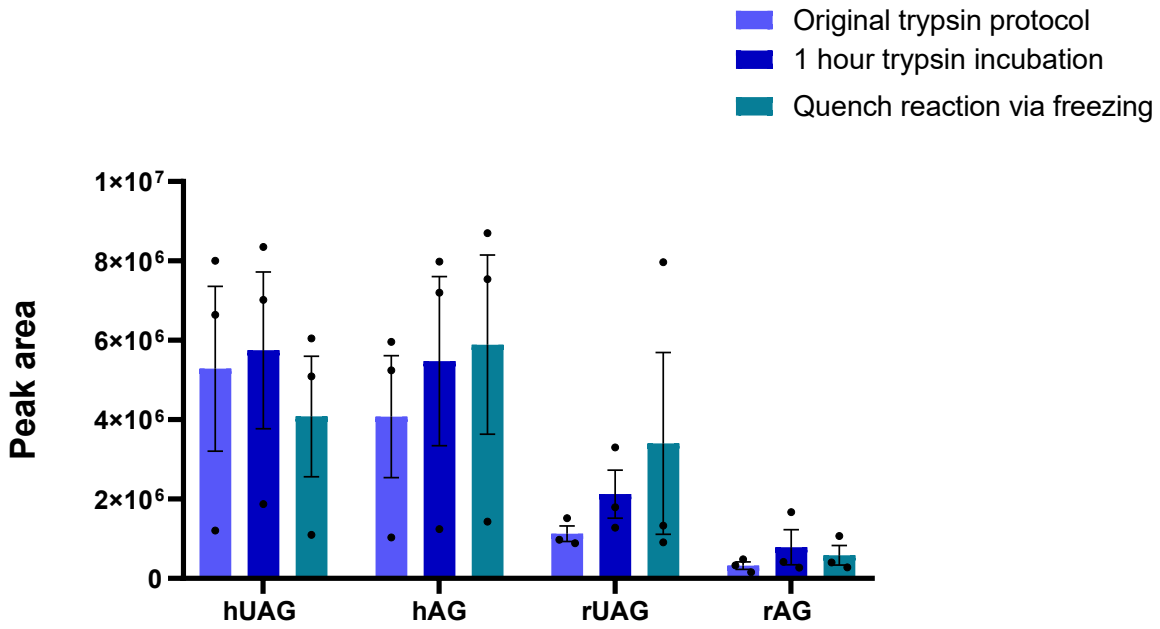

Figure 4.36 Comparison of alternating the trypsin digestion protocol; the original method was altered to include either a 1-hour trypsin incubation step or the use of freezing to quench the reaction.

Samples analysed by LC-MS/MS analysis ($[M+2H]^{2+}$ charged stated). Two-way ANOVA was performed with Tukey corrections. $P<0.05$ is considered statistically significant. N=6, average mean peak area plotted with SEM.

Given that the one-hour treatment of acyl ghrelin with trypsin gave results that were comparable to the overnight treatment with trypsin, allowing for quicker sample preparation, this alteration in the method was included as a permanent adaptation of the protocol. Further optimisation of the MS method included re-testing the initial HPLC injection volume with the comparison between a partial loop injection set at 1 µL, 10 µL or 20 µL versus a full-loop injection at 20 µL. For the Ultimate 3000 LC system, the full-loop provides better reproducibility however, for the partial-loop injection, less

sample is required which could be better when analysing precious samples with small initial starting volumes. As the unacylated ghrelin species appear to be the most stable in terms of peak areas produced, the tests were carried out using rat and human unacylated ghrelin. The amount of ghrelin per mL was altered to ensure that whatever the starting injection volume, the same amount of ghrelin would be injected onto the HPLC column itself (20 ng). For both the rat and human unacylated ghrelin, the 20 µL volume (partial and full loop) resulted in the biggest peak areas, which were significantly higher than those seen for the 1 µL and 10 µL injections (Figure 4.37). No significant differences were seen between the partial injection at 20 µL volume or the full loop injection at 20 µL. As such, a 20 µL partial loop injection was chosen as the preferred method for future sample analysis as it uses a smaller volume of sample overall compared to the full loop.

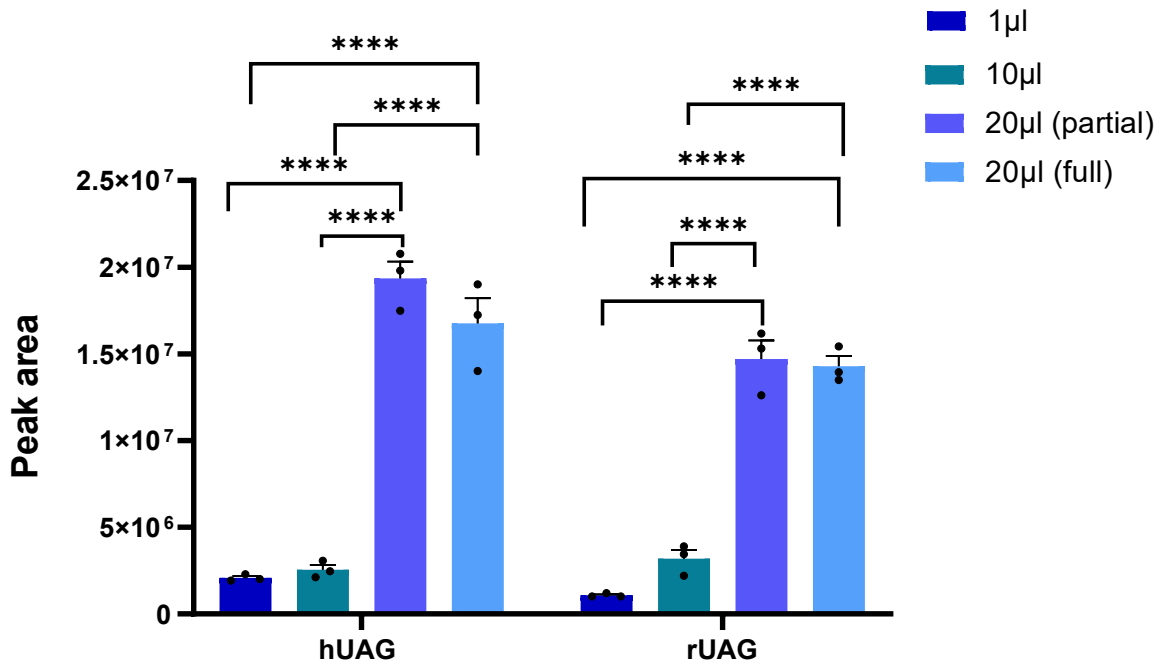

Figure 4.37 Comparison of different loop volumes on the peak areas of unacylated tryptic ghrelin, 20 ng of ghrelin was injected onto the HPLC column in either 1 µL, 10 µL, 20 µL (partial), or 20 µL (full) starting injection volume.

Samples were analysed by LC-MS/MS (trypsin UAG: $[M+2H]^{2+}$ charged stated). Two-way ANOVA was performed with Tukey corrections. P<0.05 is considered statistically significant. ****P<0.0001. N=3, average mean peak area plotted with SEM.

With the new method of a one-hour trypsin digestion incubation and 20 µL partial loop injection, a calibration curve for the human and rat, acyl and unacylated ghrelin species was prepared to see whether a lower limit of detection could be obtained in

comparison to what was achieved by the analysis of intact ghrelin. A calibration curve was prepared in the range of 0.04 to 40 ng/mL. To summarise the method, each sample underwent digestion for 1 hour with trypsin, quenching using AA then analysis by LC-MS/MS. Both rat and human unacylated ghrelin were detectable down to 0.2 ng/mL, whilst the acyl species were still undetectable until 0.4 ng/mL. Overall, an improvement was seen using the bottom-up approach with higher R^2 values in comparison to the top-down approach analysing intact ghrelin (Figure 4.27), despite these improvements, achieving a lower limit of detection remains difficult (Figure 4.38).

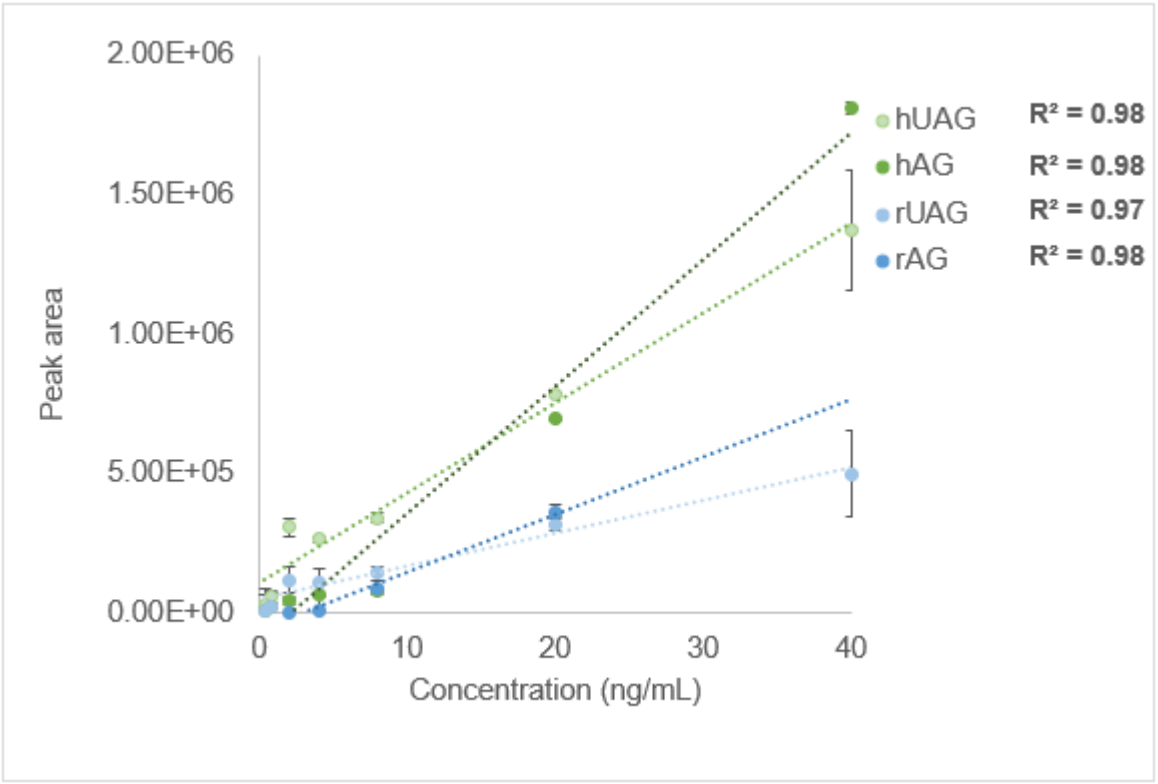

Figure 4.38 Calibration curve of hUAG, hAG, rUAG, and rAG ranging from 0.4-40 ng/mL post-treatment with trypsin for 1 hour.

Analysed by LC-MS/MS ($[M+2H]^{2+}$ charged stated). N=3, average mean plotted with SEM.

To generate a calibration curve where rat ghrelin is used as an internal standard, a calibration curve was prepared with human unacylated ghrelin concentrations varying from 0.2-40 ng/mL and with rat unacylated ghrelin fixed at 16 ng/mL (Figure 4.39A). The R^2 from the curve is shown at 0.99, suggesting a reproducible and reliable method. A similar calibration curve was prepared for acyl ghrelin with human acyl ghrelin varying from 0.2-40 ng/mL whilst rat acyl ghrelin was fixed at 16 ng/mL (Figure 4.39B). An R^2 of 0.97 was obtained.

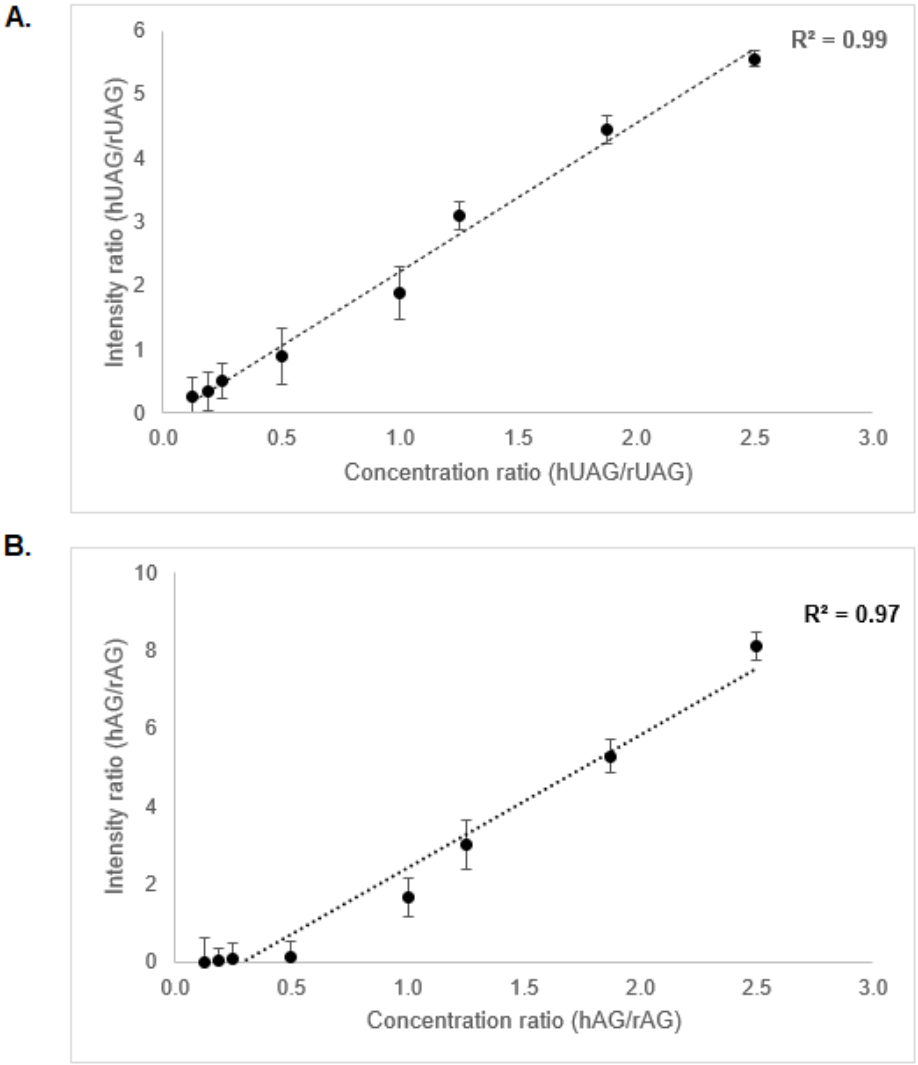

Figure 4.39 Calibration of human AG and UAG, using rat AG and UAG as internal standards, following digestion with trypsin.

A. hUAG ghrelin varying concentration from 0.2-40 ng/mL and rUAG fixed at 16 ng/mL. B. hAG ghrelin varying concentration from 0.2-40 ng/mL and rAG fixed at 16 ng/mL. Analysed by LC-MS/MS ($[M+2H]^{2+}$ charged stated). N=3, average mean plotted with SEM.

From this, we can conclude that the method works well and is optimised within the range of 0.4-40 ng/mL for acyl ghrelin species and 0.2-40 ng/mL for unacylated ghrelin. However, the method is unable to reach the lower levels of detection needed to observe endogenous ghrelin successfully, which is expected to be in the range of 0.3-1.2 ng/mL. As such the final optimised method for ghrelin detection consisted of the bottom-down approach following digestion of the ghrelin with trypsin, detecting the $[M+2H]^{2+}$ species by LC-MS/MS.

4.4 Discussion

This chapter aimed to develop and optimise a liquid chromatography-tandem mass spectrometry (LC-MS/MS) protocol for the detection of both exogenous and endogenous ghrelin within the physiological range expected in human plasma. While this work was largely methodological, it yielded important insights into the capabilities and limitations of LC-MS/MS for ghrelin quantification, especially in preparation for more targeted approaches, such as BAMS, explored in subsequent chapters.

During the development and optimisation, one section focused on determining the optimal diluent for the ghrelin species and assessing how various solvents might affect ghrelin. Upon purchasing lyophilised ghrelin, manufacturers recommend diluting ghrelin in water for storage and future work. Despite this, previous studies have reported the ghrelin peptide remaining more stable within acidic conditions (Staes et al., 2010). As such, ghrelin peptides diluted in HPLC grade water or 5, 20, and 60% acetonitrile were tested. Overall, my results showed that 20% acetonitrile was the most effective for ghrelin stability, apart from rat unacylated ghrelin which favoured water. Similar results were reported by Staes et al. 2010 where stability tests of ghrelin under acidic to basic conditions were tested. They reported that unacylated ghrelin remained stable under all conditions, whilst acyl ghrelin was most stable under acidic conditions (~pH 4) and became unstable at pH 7. In support of this, Hosoda et al., 2004 also reported higher acyl ghrelin stability at lower pH (~pH 3-4). Thus, my results were consistent with what has been noted in the literature.

One of the key factors during the process of LC-MS/MS is the chromatographic approach. Within this thesis, HPLC was utilised to separate the ghrelin species. For successful HPLC separation, choosing the most appropriate mobile and stationary phase is key. In the case of ghrelin, its octanoyl modification confers a hydrophobic property. As such, reversed-phase columns have previously been reported as the best for ghrelin separation. In 2010, Staes et al. reported an optimised RP-HPLC/UV method using a TSK-gel ODS column with mobile phase A consisting of water and 0.1% TFA and mobile phase B consisting of acetonitrile with 0.1% TFA. In this case, the separation of ghrelin was achieved; however, the lower limit of detection was determined to be 6236.35 ng/mL. Moving beyond this, monolithic columns such as the C18 (Rauh et al., 2007) were considered due to the application of acidic mobile phases to protect the acyl modification. Throughout this thesis, the C18 column was utilised

with an optimised method of a 30-minute run time with retention times of 8.70 for unacylated ghrelin and 12.70 for acyl ghrelin. Similarly, Date et al. 2000, reported a 40-minute run time with unacylated ghrelin and acyl ghrelin obtaining retention times of 11.4 and 21 minutes, respectively. The success of a shorter run time has been previously reported for ghrelin analysis. More recently, Thomas et al 2021. reported a 14-minute run time but here ultra-performance liquid chromatography (UHPLC) was used, and a lower limit of detection was reported at 30 pg/mL. Reducing the run time would be beneficial for increasing sample throughput. I attempted to reduce the run time to 14 minutes but in this case, the ghrelin was not successfully retained or separated on the column and as such, the 30-minute run time was retained. Using a UHPLC system similar to the approach described by Thomas et al. (2021) could potentially accomplish both shorter run times and sustained sensitivity with a lowered limit of detection. UHPLC can produce results up to ten times faster than HPLC as it works at higher pressures and smaller particle sizes.

Another key consideration for HPLC is the mobile phase as this impacts how an analyte is retained on the column. The original method described within this chapter included mobile phase A with HPLC grade water, 2% acetonitrile, and 0.1% acetic acid whilst mobile phase B contained acetonitrile with 0.2% acetic acid. In comparison, Sidibe et al. 2014, who also used a C18 column, used 0.2% formic acid, 0.01% TFA in water for mobile phase A, and 0.2% FA, 0.01% TFA in acetonitrile for mobile phase B. Likewise, Zemenova et al., included 0.1% formic acid in water as mobile phase A with 0.1% FA in acetonitrile for mobile phase B. Despite these reports using formic acid instead of acetic acid, both work in the same manner of reducing the overall pH of the mobile phase. Additionally, my results showed no significant change in the ghrelin signal between 0.1% AA and 0.1% formic acid. For 0.1% acetic acid multiple charged states between $[M+4H]^{4+}$ to $[M+8H]^{8+}$ were detected, with the highest signal intensity observed for the $[M+6H]^{6+}$ ion. For 0.1% formic acid, charged states between $[M+3H]^{3+}$ to $[M+6H]^{6+}$ were observed, with $[M+4H]^{4+}$ and $[M+5H]^{5+}$ detected having the highest signal intensities. In comparison, Sidibe et al., observed the molecular ion of $[M+7H]^{7+}$ as the most intense, whilst Zemenova et al., monitored the $[M+6H]^{6+}$ ion. Overall, my method and previously stated methods describe a scattering of charged states for the ghrelin species, with the most intense molecular ion being picked for subsequent analysis. As the scattering of charged states also results in the scattering

of signal intensity and is therefore likely to be lower overall, work was carried out to reduce this scattering of charge states and 'push' the ghrelin to a smaller number of charged states that were more intense. As such, the addition of ammonium buffers to the mobile phases was tested. Previously, Rauh et al., 2007, reported using ammonium acetate buffer (10 mmol/L): methanol (97:3) containing 1 mL acetic acid (17M) as the mobile phase A whilst mobile phase B contained ammonium acetate (2 mmol/L): methanol (5:95) with 0.1 mmol/L formic acid. Although success was seen within ghrelin retention, separation, and detection, the lower limit of detection was determined at 20 ng/L. For my investigations, ammonium acetate and ammonium formate were tested and resulted in a slight reduction in the number of charged state scattering compared to without the ammonium salts. Despite this, no significant increase in the overall signal intensity was observed.

In 2021, Thomas et al. reported ghrelin detection down to 50-100 pg/mL, and here, 1% DMSO was used within the mobile phase, and the $[M+5H]^{5+}$ molecular ion was reported as the most intense signal. As such, I investigated the addition of 1% DMSO within the mobile phase. Using this method, I observed a reduction in the number of charged state ions to be between $[M+4H]^{4+}$ and $[M+6H]^{6+}$. I also observed the $[M+5H]^{5+}$ as having the most intense signal. Notably, the overall signal intensity was significantly increased ($P<0.001$) following the addition of DMSO. Similarly, Hahne et al. (2013) reported that the addition of DMSO resulted in improved electrospray ionization of peptides, leading to an enhancement in ghrelin detection of up to ten-fold. Although the presence of DMSO significantly increased the signal intensity of ghrelin, a lower limit of detection was observed at 0.4 ng/mL, which is insufficient to detect endogenous ghrelin. My analysis for both the intact ghrelin and ghrelin enzymatically digested with trypsin suggests degradation and instability of both acyl and unacylated ghrelin. Previously, ghrelin was shown to remain stable at 4°C, and ghrelin instability has been reported from anything above this temperature (Hosoda et al., 2004). The utilisation of 37°C during the tryptic digestion procedure might account for the observed degradation. Previous studies have also reported peptide degradation following trypsin digestion. More specifically, Shufrod and Grant (2023) reported that trypsin digestion for longer than 4 hours caused peptide degradation. Toth, Kuklenyik, and Barr 2018, developed an online trypsin digestion method aimed at reducing

peptide degradation. My results showed no significant decrease in ghrelin intensity when comparing the 1-hour and overnight trypsin treatment.

There is a possibility that our current LC system was not sensitive enough to detect low ghrelin levels and therefore, future work using a UHPLC which offers improved resolution due to reduced band broadening of the peaks may allow successful detection. Additionally, exploring routes such as online trypsin digestion and SPE, alongside the use of a new column such as the hydrophilic interaction liquid chromatography (HILIC) column could aid in enhanced LC-MS/MS detection. The HILIC column contains a polar stationary phase with the partitioning of the analytes between the hydrophilic layer of the stationary phase and the less polar mobile phase. As such, the HILIC may be a desirable choice of column for more polar analytes such as the acyl ghrelin group. Additionally, it has been previously shown that HILIC-MS more readily removes acetonitrile compared to reverse phase-HPLC-MS (which is used throughout this chapter) (Periat et al., 2014). Therefore, using UHPLC whilst employing the HILIC column could be a new method for ghrelin analysis via LC-MS/MS.

An important theoretical consideration emerged from the use of 0.1% plasma as a diluent during sample preparation. This approach was selected to simulate a more physiological matrix and to incorporate internal standards, introducing a consistent background for more realistic recovery assessments. Although no dedicated experiments were performed to isolate the effects of plasma components, it is hypothesised that albumin within the plasma may contribute to reduced recovery of acyl ghrelin due to its strong binding affinity. The octanoyl (C8) fatty acid on acyl ghrelin imparts hydrophobicity, promoting binding to serum albumin, particularly problematic in matrices with endogenous proteins. This binding may contribute to a distorted AG:UAG ratio and could become more pronounced with longer chain fatty acids (C10–C16), which have even stronger albumin binding properties (Heppner et al., 2012). As LC-MS lacks an immuno-affinity step to dissociate these complexes, sample preparation must either use organic solvents or low pH conditions, both of which carry the risk of promoting ghrelin degradation.

These challenges underscore how the LC setup influences the MS readout and ultimately impacts quantitative performance. Despite observed improvements in signal intensity and charge state control, the LC-MS/MS method remained insufficiently

sensitive for the detection of endogenous ghrelin within the physiological range. Sensitivity remained above 200 pg/mL, and matrix interference was still detectable, even when samples were diluted in 0.1% plasma. These methodological constraints provided the rationale for pursuing BAMS (Bead-Assisted Mass Spectrometry), discussed in the following chapter. BAMS offers a promising upstream enrichment strategy, enabling immunocapture of ghrelin (or GOAT) prior to MS analysis, thereby overcoming many of the technical and biological challenges encountered here.

Further work could be made on identifying ghrelin bound by different fatty acids. Work in this chapter concentrated on identifying human acyl C8 ghrelin at m/z of 3371 (the most common form of ghrelin). However, ghrelin can bind to a range of fatty acids varying from C2 to C16 (Heppner et al., 2012). Although the presence of short-chain variants like C2-acyl ghrelin in vivo remains speculative and has not been confirmed in plasma, such forms are theoretically possible. However, their biological relevance is questionable due to limited hydrophobicity and likely poor binding affinity to the GHS-R1a receptor. The impact of different ghrelin species on the brain is currently unknown and there is no method suitable to detect or quantify them. LC-MS/MS holds great promise for this aim. A change in the fatty acid group attached to the serine would result in a m/z change, for example, human acyl C6 ghrelin would lead to a m/z of 3343. Appropriate MRM transitions accounting for these different m/z could be included in the method. As yet, no standards for these alternative forms of ghrelin are available commercially. Thus, an alternative method of confirming correct peak identity would have been to run sample extracts collected from cells such as RAW cells (that have genes for both ghrelin and GOAT) that have been incubated with a range of different fatty acids and therefore ‘encouraged‘ to generate different species of ghrelin. Additional approaches, such as co-expression of acyl-CoA synthetases, inhibition of β-oxidation, or delivery of fatty acids via albumin-bound or liposomal systems, may further enhance the incorporation of specific acyl chains. With MS fragmentation using ESI-MS/MS, we can identify these fatty acids. Using the plasma sample preparation from Chapter 3, there is a possibility to detect distinct fatty acids that are attached to ghrelin. Since capturing sufficient ghrelin from plasma proved challenging in Chapter 3, a novel technique called BAMS was introduced and tested in the subsequent chapter. Initially associated with MALDI-TOF capture, this concept could potentially be

adapted for future work, enabling measurement via LC-MS/MS in addition to MALDI-TOF.

To summarise the various LC-MS/MS method optimisation parameters trialled throughout this chapter, Table 4.5 presents a summary of the experimental conditions tested and their impact on ghrelin signal intensity, charge state distribution, and limit of detection. This table highlights both the incremental improvements and the persistent limitations encountered in the development of a robust detection protocol for ghrelin species.

Optimisation Parameter	Outcome	Effect on Detection	Notes
Solvent (Water vs ACN)	20% ACN improved AG stability	Improved peptide recovery	UAG stable in water
Acid (FA vs AA)	Minor variation	Similar intensity profiles	Charge states varied slightly
Ammonium Salts	Reduced charge scatter	No intensity gain	Limited impact
DMSO Addition	Significantly improved signal intensity	Best performance with $[M+5H]^{5+}$	Detection down to 0.4 ng/mL
Tryptic Digestion	No benefit to AG, benefit to UAG	UAG detected to 0.2 ng/mL	AG degradation likely
0.1% Plasma Dilution	Physiological background	Albumin binding of AG	Potential AG loss

Table 4.5 Summary of LC-MS Optimisation Strategies and Outcomes

4.5 Conclusion

In conclusion, while LC-MS/MS holds substantial potential for ghrelin isoform analysis, the method developed here was limited by sample degradation, binding effects, matrix interference, and sensitivity thresholds. These findings justify the transition toward immuno-enriched techniques like BAMS, which will be discussed in the following chapter.

Chapter

5. Developing a BAMS Assay to Analyse Ghrelin

5.1 Introduction

Over the last few decades, mass spectrometry has evolved into a powerful tool within the realm of proteomics, owing to the continual advancements in instrumentation, fragmentation methodologies, and analytical strategies (Han et al., 2008). Chapters 3 and 4 have explored the use of MALDI-TOF and LC-MS in the detection and (semi-) quantification of ghrelin species. However, these chapters have also unveiled some difficulties with the exclusive use of mass spectrometry in detecting endogenous ghrelin in biological samples. The difficulty arises from ghrelin being a small peptide (~3000 Da), that can bind to larger proteins such as albumin (Thomas et al., 2021). Furthermore, the addition of the fatty acid component to ghrelin alters its chemical properties therefore both acyl and unacylated ghrelin behave differently during the SPE extraction process.

Considering these complexities, this chapter explores the use of immunoprecipitation mass spectrometry (IP-MS) to detect and quantify ghrelin. IP-MS offers several advantages compared to conventional MS. It involves the enrichment of target proteins via the use of specific antibodies, thereby enhancing sensitivity and detection efficiency. This technique is particularly beneficial for low-abundance species, such as ghrelin, within complex biological samples. By selectively amplifying the protein of interest, background noise is minimised, thus resulting in improved precision, reproducibility, and consistency (Have et al., 2011). Despite the advantages of IP-MS, caveats include issues of specificity, antibody quality, potential loss of low-affinity interactions, and increased background noise due to improper antibody binding or sample contamination (Have et al., 2011). Moreover, IP-MS may face restrictions with only a few antibodies available for a specific target and protein denaturation with the acyl group falling below limits of detection and may require specialised and expensive equipment such as magnetic beads. In summary, while IP-MS holds promise of being a valuable tool in proteomics, its efficacious application is accompanied by its challenges.

Previously, Guiterrez et al. (2005) reported the use of IP-MS to detect ghrelin, which involved magnetic beads but also entailed a labour-intensive sample preparation. The protocol involved ‘spiking’ blood samples with a stable isotope ISTD (labelled with both ^{13}C and ^{15}N) of synthetic unacylated or acyl ghrelin, followed by protein precipitation for two hours and centrifugation for an hour. The peptide precipitate was then dried

under nitrogen gas and solubilised in 1 mL of tris-Hepes buffer. Following this, magnetic beads with 1 µg of an anti-ghrelin antibody were added to the suspension and incubated for two hours at 4°C with gentle rotation. The beads now conjugated with ghrelin, were washed at room temperature, twice in 50 mM ammonium bicarbonate, once in 0.1% SDS in ammonium bicarbonate, followed by another wash in 50 mM ammonium bicarbonate, and finally once in distilled water. The bound ghrelin was eluted from the antibody beads via acidification with 0.1% TFA and concentrated using a C18 ziptips. Ghrelin peptides were eluted from the C18 ziptips and spotted directly onto the target to be analysed using MALDI-TOF MS. Herein, the concept of BAMS is explored to identify unacylated and acyl ghrelin and undertaken in collaboration with Adeptrix (USA), the developers of the BAMS technology. BAMS involves incubating antibody-conjugated magnetic beads (created by Adeptrix) in a biological sample such as plasma, to capture the target analytes of interest, which for this work are unacylated and acyl ghrelin. Post-incubation, the beads are washed to remove any molecules that have bound non-specifically and added onto a BAMS microwell array slide that consists of an elastomer gasket, containing a square grid array of 88x26 through-holes (microwells) attached to a gold microscope slide (Figure 5.1).

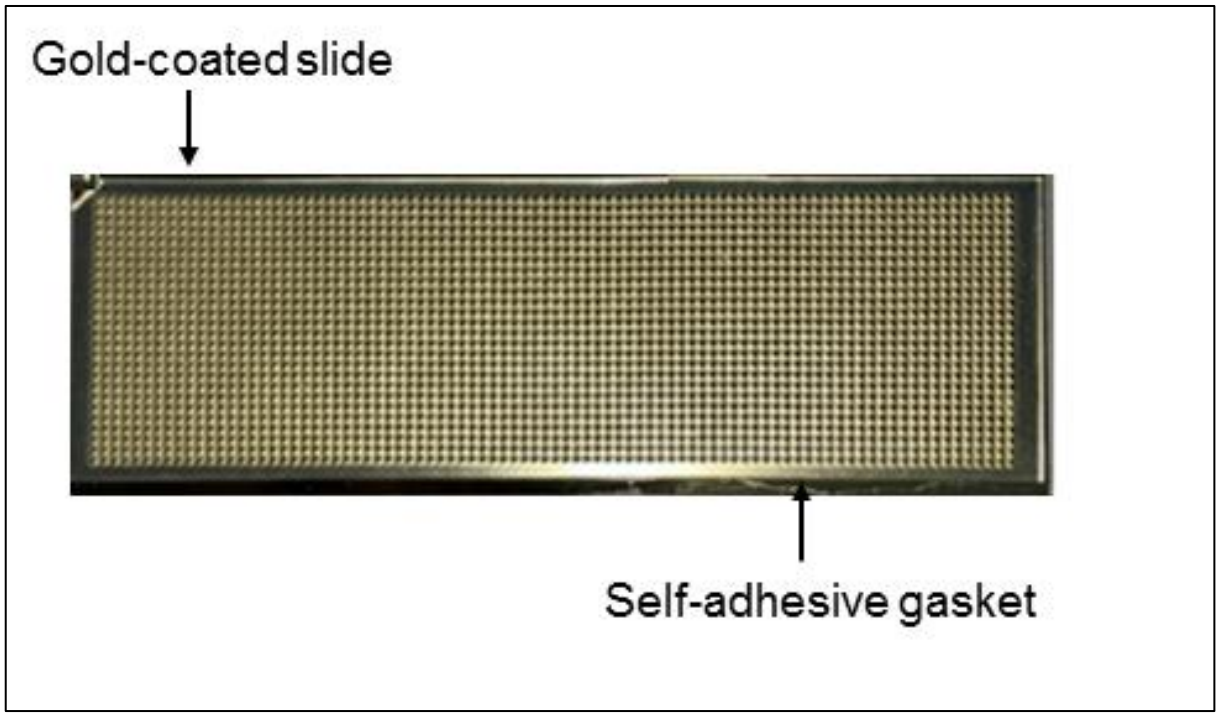

Figure 5.1 BAMS microwell array slide that contains a gold-coated microscope slide attached to a silicone gasket.

The bead array is exposed to an aerosol-containing matrix for MALDI-TOF MS. The captured analytes are eluted from beads into individual microwells. The gasket alongside the beads is removed, resulting in an array of spots containing concentrated and purified analytes incorporated into the matrix. Individual spots in the array are measured by MALDI-MS. BAMS supports both single-plex and multiplex assays integrated with MALDI-TOF analysis. The multiplex assay is achieved by combining different BAMS assay beads, each containing different antibodies. In addition, on-bead multiplexing can be achieved using an antibody that recognises a common protein sequence for a target that allows MALDI-TOF-based detection of protein variants and/or post-translational modifications for example, phosphorylated and non-phosphorylated proteins.

The potential of BAMS to improve upon alternative assay formats, such as ELISA, is evident due to its capacity to simultaneously measure an extensive array of proteins within a single assay. When compared to other assays such as Luminex, which is also able to analyse multiple analytes, BAMS has an additional advantage due to its ability to detect the analytes through the means of MS instead of using detection antibodies. As BAMS detection uses MS to detect analytes rather than secondary detection antibodies, it avoids the problem of antibody cross-reactivity as seen in assays such as the Luminex, ELISA, and WB. During MS detection, the analytes are separated based on mass and thus allow identification of different analyte species, for example, ghrelin bound by distinct fatty acid species. Furthermore, in comparison to LC-MS, BAMS does not need the more labour-intensive and time-consuming chromatographic separation, thus increasing the potential of high sample throughput. In comparison to MALDI-TOF alone, BAMS has better specificity and sensitivity (by decreasing background ‘noise’) and the potential for direct quantification of analytes. Therefore, in this chapter, I explored the use of BAMS as a method to detect and quantify ghrelin species in plasma samples.

5.1.1 Aims

The primary research objectives are to.

- Develop an innovative BAMS assay capable of detecting both unacylated and acyl ghrelin species in a single assay.

- Compare the analysis of the BAMS assay against the established unacylated and acyl ghrelin ELISAs.

5.2 Materials and Methods

An in-depth description of the material and methods for the BAMS assay are provided in Chapter 2.7.

Briefly, a BAMS array kit with magnetic beads coated in antibodies for unacylated and acyl ghrelin was generated by our collaborators at Adeptrix and sent to our laboratory for validation. One antibody kit included a 96-well plate, with each well containing three magnetic antibody-coated beads that bind to a sequence common to all ghrelin peptides. One well, containing three beads was used per 250 µL sample.

Two commercially available antibodies raised against ghrelin (ADX086 and ADX088) were tested and included in the assay development process. As this was a collaborative effort, with Adeptrix providing the antibodies, details of antigen recognition were not disclosed.

5.2.1 Sample Preparation

For ‘neat’ samples, 250 µL of plasma was defrosted and pipetted into an Eppendorf tube. For ‘spiked’ samples, recombinant ghrelin was added to the plasma at a concentration of 2.5 ng per 250 µL of plasma.

5.2.2 Preparation of the BAMS Beads and their Addition to Samples

To accumulate the antibody-coated beads to the bottom of the well, the 96-well ghrelin BAMS assay kit was centrifuged at 4°C, 500xg for 3 minutes. Once centrifuged, all three antibody-coated beads were transferred using the QuickPick (magnetic pipette) into 500 µL of 1X PBS wash solution and were mixed on a shaker mixer for 1 minute at 1100 rpm. Following the wash stage, the antibody-coated beads were added to the prepared plasma sample and were incubated overnight at 4°C, 1100 rpm in an Eppendorf Thermomixer.

5.2.3 Washing Ghrelin Bound Beads

After overnight incubation (section 5.2.2), ghrelin-bound beads underwent washing to remove molecules that had bound non-specifically. The wash tubes were prepared by adding 750 µL of wash buffer A into a new 1.2 mL Eppendorf tube. The ghrelin-bound

beads were transferred into this new Eppendorf and centrifuged for 10 minutes at 500xg at RT. Next, the beads were transferred into tubes containing wash buffer B and centrifuged for 10 minutes, followed by transfer into tubes containing buffer C and centrifugation for 10 minutes (500xg). The beads were transferred into tubes containing wash buffer D and centrifuged for 5 minutes (500xg). The beads were subsequently transferred to buffer E-containing tubes before centrifugation for 2 minutes. Finally, this process was repeated with tubes containing buffer F.

5.2.4 BAMS Array Assembly

The assembly of the BAMS array occurred during one of the wash steps in 5.2.3. A silicone gasket was placed onto the BAMS gold-coated slide, with both the silicone gasket and slide being aligned correctly. On top of the silicone gasket, a multi-chamber frame consisting of 16 chambers was placed, creating the BAMS array. The BAMS array was held in place via stainless-steel clips at the top and bottom of the multi-chamber. The BAMS array was inserted into a centrifuge slide adapter and deionised water was dispensed into each chamber to cover the microwells with a depth of 0.5 cm of water (~150 µL). Next, the BAMS array was centrifuged for three minutes at 500xg to hydrate the microwells. In the meantime, the matrix sprayer was set up and ready for section 5.2.5. Once centrifuged, the slide adapter and stainless-steel clips were removed. The washed beads were transferred using the QuickPick pipette to the designated BAMS array chamber. The side of the BAMS array was gently tapped to disperse all three beads into individual microwells inside the sample chamber. Once transferred, a magnet is placed beneath the BAMS array to collect the beads at the bottom of the microwell. The BAMS array containing magnetic beads was inverted and gently tapped to remove any excess water. The next section proceeded immediately to prevent BAMS beads from drying out, which would result in inefficient elution of target analytes.

5.2.5 Eluting Ghrelin from BAMS Reagent Beads

Next, elution of the ghrelin analyte from the bead was carried out by incubating it with an acidic matrix solution, which gradually replaced the deionised water in the microwells. To provide the acidic matrix solution, a matrix sprayer was used which generates aerosol-containing microdroplets of the MALDI matrix over the microwell array. Once the solvent evaporates, the ghrelin analyte is incorporated into the MALDI

matrix and localised in distinct spots at the bottom of the microwell. To achieve this, the following protocol was used.

The BAMS array assembly from 5.2.4 was placed into the Matrix sprayer (HDX sprayer) and 5 mL of CHCA matrix was loaded. The sprayer was turned on and set to a program with the following conditions:

Temperature: 30°C.

Velocity: 1350

Tracking spacing (mm): 1

Pattern: W

Pressure (psi):19

Drying time: 0

Nozzle height (mm): 65

Number of spray cycles: 10

Flow rate: 145 µL/min.

After matrix application, the slide was removed from the HDX sprayer, and the residual matrix was left to evaporate to dryness before continuing. Using compressed air, the beads were ejected from the microwells into an appropriate chemical waste. The silicon gasket was removed, and it was ensured that all beads were successfully removed during the compressed air stage. To calibrate the MALDI-TOF instrument, 1 µL of caesium iodide was mixed with 1 µL of CHCA matrix and spotted onto a corner of the slide that has no bead-eluted analyte spots. Spots were left to completely dry before inserting into the MALDI-TOF instrument.

5.2.6 Data Collection of Ghrelin BAMS

Once dried, the slide was placed into an adapter suitable for the MALDI instrument and an image of the slide was obtained using the Epson Perfection V600 photo. Once obtained, the slide was inserted into the MALDI-TOF instrument. The following MS conditions on the MALDI-TOF were used: Linear positive mode, laser power = 60%, 'limit diameter' = 600 µM, shot frequency = 1000, number of laser shots = 25,000, sampling was set to partial, mass range = 700-7000m/z.

5.2.7 Analysing BAMS MS Data

All analysis was carried out using flex Analysis. The 'subtract baseline mass spectrum' and 'smooth mass spectra' were carried out on all spectra. The following method parameters were used: Peak detection algorithm was centroid, signal to noise threshold = 1.5, relative intensity threshold = 0. minimum intensity threshold = 0, maximal number of peaks = 2000, peak width = 1000 m/z, height = 10%, baseline subtraction=median, flatness=0.1, median level = 0.5. A Mass list was generated via the ‘perform a find mass list’ function. The m/z of interest were exported into Excel for further analysis.

5.2.8 Collection of Plasma Samples

Five healthy donors were chosen, ranging between 20-40 years old with two females and three males (Swansea University Medical School (SUSM) Research Ethics Committee (RESC). All donors underwent an overnight 12-hour fast before donating blood. AEBSF was added to blood upon collection to avoid degradation of the acyl group, and the blood was centrifuged to collect plasma. Plasma was stored as 500 µL aliquots and stored at -80°C until use. The same donors were bled on three separate occasions, resulting in three different withdrawal data sets.

5.2.9 ELISA

Plasma concentrations of acyl and unacylated ghrelin were quantified using commercial competitive ELISA kits (Bertin Bioreagent, France; Cat. No. A05106 for acyl ghrelin and A05119 for unacylated ghrelin), according to the manufacturer’s instructions. Samples and standards were prepared in duplicates, with all reagents and samples equilibrated to room temperature prior to assay. Absorbance was measured at 405 nm using a microplate reader, and concentrations were calculated using a four-parameter logistic (4-PL) standard curve. Sample concentrations were interpolated and expressed in pg/mL. The intra- and inter-assay coefficients of variation were within the acceptable range as specified by the manufacturer.

5.3 Results

5.3.1 HDX Sprayer Optimisation

Before introducing the BAMS procedure, the HDX sprayer parameters were optimised using BAMS training samples provided by Adeptrix. For the optimisation of the

sprayer, magnetic beads with no antibody bound were used. Optimisation of the sprayer involved ensuring the bead size after spraying the MALDI-TOF matrix was optimal. An image of the ideal bead size was provided by Adeptrix (Figure 5.2A) and close collaboration with Dr Tamil Selvan at Adeptrix ensured optimal spot characteristics were achieved. Four rounds of optimisation were performed before finding the most appropriate settings for our HDX sprayer that created the optimal bead size. The first optimisation conditions consisted of 10 spraying cycles, with a flow rate of 175 µL/min and a temperature of 30°C, while maintaining the conditions described in Section 5.2.5. The initial attempt exhibited flooding within the microwells which resulted in the bead size being too large (Figure 5.2B). The second optimisation explored alterations to both the flow and operational cycles of the speed sprayer. Therefore, a method of 15 spraying cycles, a flow rate of 115 µL/min, and a temperature of 30°C was tested. In the second attempt, the spot size remained unchanged compared to the starting size of the bead, which is likely the consequence of a high flow rate and shorter cycle needed (Figure 5.2C). As a result, due to the high flow rate, the third optimisation involved a lower flow rate of 110 µL/min, 10 spraying cycles, and an elevated temperature of 40°C (Figure 5.2D). Although the third attempt showed an improvement, a slight under sizing of the spots was noted. Considering this observation, the fourth attempt included an increased flow rate at 145 µL/min, 10 spraying cycles, and a temperature of 30°C. The fourth method and the final optimisation demonstrated promising results with adequate spot dimensions, indicating optimal sprayer conditions (Figure 5.2E).

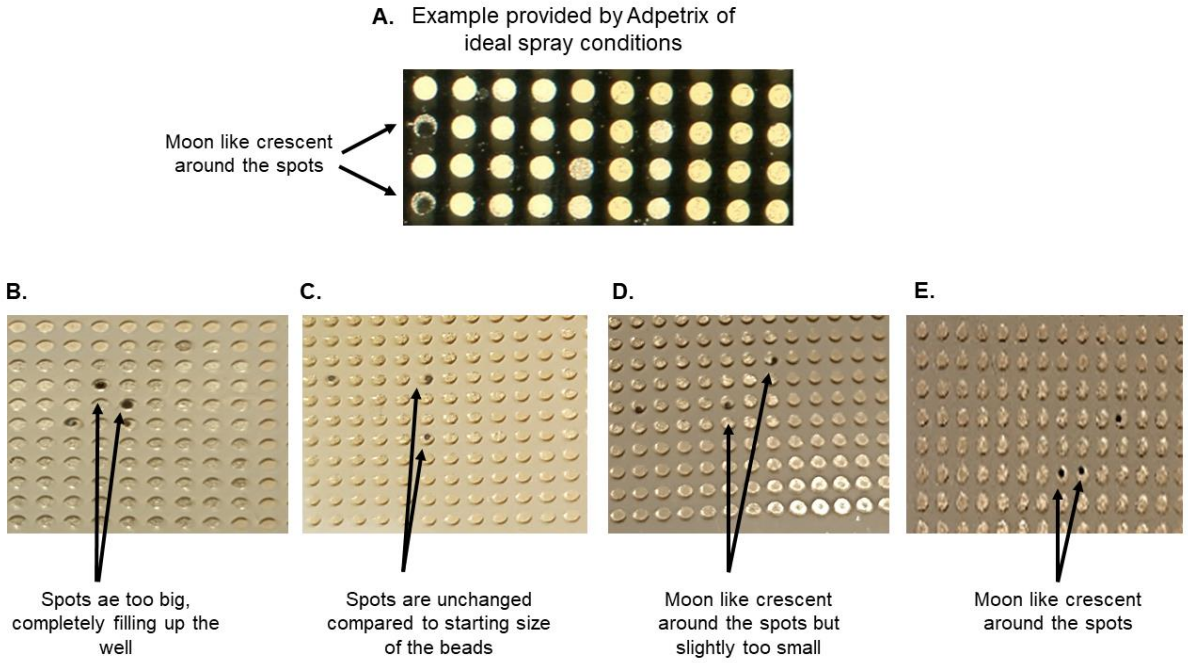

Figure 5.2 Optimization of HDX sprayer conditions.

A. Example provided by Adeptrix of spot appearance at optimal conditions. B. Sprayer conditions: 10 spray cycles, flow rate of 175 µL/min and 30°C. C. 15 spray cycle, the flow rate of 115 µL/min and 30°C. D. 10 spray cycles, the flow rate of 110 µL/min, and 40°C. E. 10 spray cycles, the flow rate of 145 µL/min and 30°C.

After the successful optimisation of the sprayer conditions for the HDX sprayer, the full protocol was tested using the reference protein kit. The training sample included magnetic beads with antibodies for four different synthetic peptides in digested BSA, which were:

1. ATK1 (amino acid 2330249).
   m/z of 2457, amino acid sequence: gTTAIQTVADGLKKQEEEEmDF.
2. RPS6 (acid 233-249).
   m/z of 2070, amino acid sequence: gRLssLRASTSKSESSQK.
3. ATK1 (amino acid 466-480).
   m/z of 1790, amino acid sequence: gRPHFPQFsYSASGTA
4. ATK1/2 (amino acid 468-480).
   m/z pf 1678, amino acid sequence: gTHFPQFsYSASIR.

To the protein reference, 15 magnetic antibody beads (each bead with a different antibody for the synthetic peptides) were added and incubated overnight. The BAMS protocol for MALDI-TOF setup analysis was followed as described in section 5.2. The

visualisation of the BAMS array using the MALDI-TOF provides a clear indication of the location of the analyte, against the spots containing the matrix only (Figure 5.3).

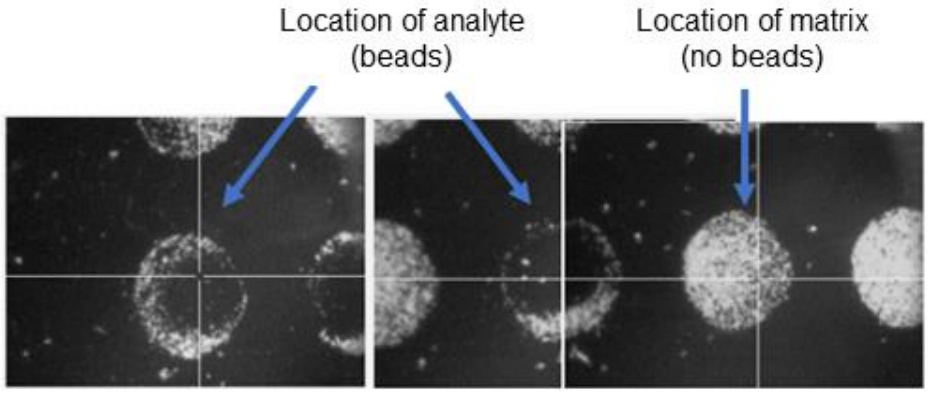

Figure 5.3 Visualisation of the BAMS array during MALDI-TOF analysis.

Areas where the analytes of interest (the beads) are located and areas that did not include any beads can be seen.

Upon MALDI-TOF analysis, successful capture of the reference protein beads was achieved with the identification of each of the four peptides (Figure 5.4).

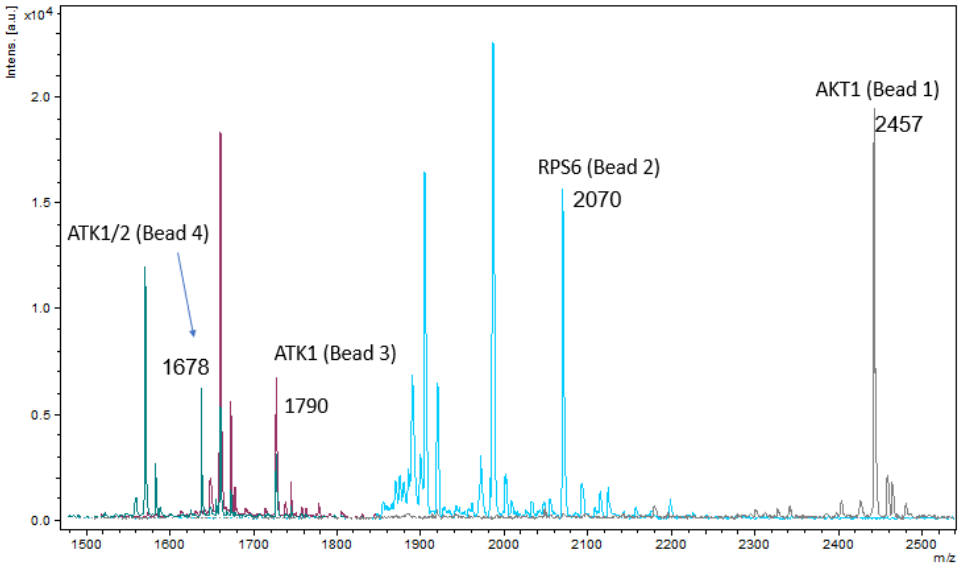

Figure 5.4 BAMS spectra of the protein reference.

Four spectra overlapped, demonstrating four peptides overall. Unlabelled peaks demonstrate background noise.

The identification of the correct reference peptide peaks that were consistent with what should reportedly be seen suggested that the procedure was working effectively with the laboratory protocol. Thus, I continued with the use of the BAMS ghrelin peptide detection kit.

5.3.2 Comparison and Selection of Antibody Kits

Throughout the following section, as detailed in Section 5.3.2, two different antibody kits, designated Antibody 86, and Antibody 88, were used in the following comparative analysis. Both antibody kits were used to analyse donor plasma with and without the introduction of exogenous human acyl and unacylated ghrelin. ‘Neat’ plasma samples, refer to samples that contain endogenous ghrelin only, whereas ‘spiked’ plasma refers to samples containing additional exogenously added ghrelin.

5.3.2.1 The Use of Rat Ghrelin as an Internal Standard to Quantify Human Ghrelin

Within mass spectrometry, the use of ISTD is important for accurate quantification. An ISTD of known concentration is introduced to samples, blanks, and calibration curves. Its purpose is to compensate for the potential loss of analytes during the sample preparation and ionisation processes.

In previous chapters dedicated to LC-MS/MS and MALDI-TOF analyses, rat ghrelin species was frequently used as an ISTD. This choice was made based on their similarity in amino acid sequence to human ghrelin. Whilst we would ideally use deuterated human ghrelin as an internal standard for MS work, this was financially not viable at the time. Thus, the approach of using rat ghrelin as an ISTD in human samples offers an economical alternative to the use of deuterated human ghrelin, if it is kept in mind that their ionisation and extraction efficiencies may vary. Hence, we explored the feasibility of using rat ghrelin as an ISTD during ghrelin BAMS. Due to the limitations of the number of beads, the tests were carried out on the plasma of two different donors, donor 1, and donor 2. The selection rationale was derived from the different levels of endogenous ghrelin in these donors that had previously been identified by ELISA analysis. Donor 1, a 23-year-old female, had lower levels of endogenous ghrelin (0.1 ng/mL for unacylated ghrelin and 0.01 ng/mL for acyl ghrelin) while donor 2, a male approximately 40 years old had higher levels of endogenous ghrelin (0.6 ng/mL for unacylated ghrelin and 0.06 ng/mL for acyl ghrelin).

Firstly, for the ADX086 antibody kit (antibody 86) the following conditions were tested using a volume of 250 µL; ‘neat’ plasma, plasma with the addition of exogenous human ghrelin (both unacylated and acyl ghrelin) in an equimolar mix of 1 ng/100 µL, plasma with exogenous rat ghrelin (both unacylated and acyl ghrelin) in an equimolar mix of 1 ng/100 µL, and plasma containing all four exogenous ghrelin species (human and rat,

both unacylated and acyl ghrelin) in an equimolar mix of 1 ng/100 µL. After preparation with the BAMS kit, the samples were analysed by MALDI-TOF. The 1-28 amino acid sequence of ghrelin $[M+H]^+$ was monitored, with m/z 3244 for human unacylated ghrelin, m/z 3188 for the rat unacylated ghrelin, m/z 3370 for the human acyl ghrelin and m/z 3314 for the rat acyl ghrelin.

No exogenous rat acyl ghrelin was detected in any of the plasma samples, however, unacylated rat ghrelin was detectable (Figure 5.5). In addition, for donor 1, human acyl ghrelin was also undetectable. As expected, the samples ‘spiked’ with exogenous human ghrelin observed a significant increase in mean intensity for human unacylated ghrelin ($P<0.05$) compared with the ‘neat’ plasma. However, upon the inclusion of exogenous rat ghrelin alongside the human unacylated and acyl ghrelin spike, a significant decrease in the human unacylated ghrelin ($P<0.0001$) was seen in comparison to the plasma ‘spiked’ with human ghrelin alone (Figure 5.5). This suggests that rat ghrelin may have a negative impact on the human ghrelin species. For donor 2, in comparison to the ‘neat’ plasma samples, both human unacylated and acyl ghrelin show a significant increase ($P<0.0001$) in samples ‘spiked’ with the exogenous human unacylated and acyl ghrelin. Likewise, a significant increase ($P<0.0001$) in intensity was reported for human unacylated and acyl ghrelin in the four-way ghrelin ‘spiked’ plasma versus the ‘neat’ plasma (not shown on the graph). For the samples ‘spiked’ with exogenous rat acyl and unacylated ghrelin alone, very low human unacylated and acyl ghrelin levels were observed alongside low rat unacylated ghrelin. However, in samples ‘spiked’ with the four ghrelin species, the rat unacylated ghrelin and human acyl and unacylated ghrelin were detected at higher levels (Figure 5.3.4). Upon addition of exogenous rat ghrelin (unacylated and acyl) and human ghrelin (unacylated and acyl), the human unacylated ghrelin was significantly lower ($P<0.0001$) relative to the ‘spiked’ human acyl and unacylated ghrelin (Figure 5.5).

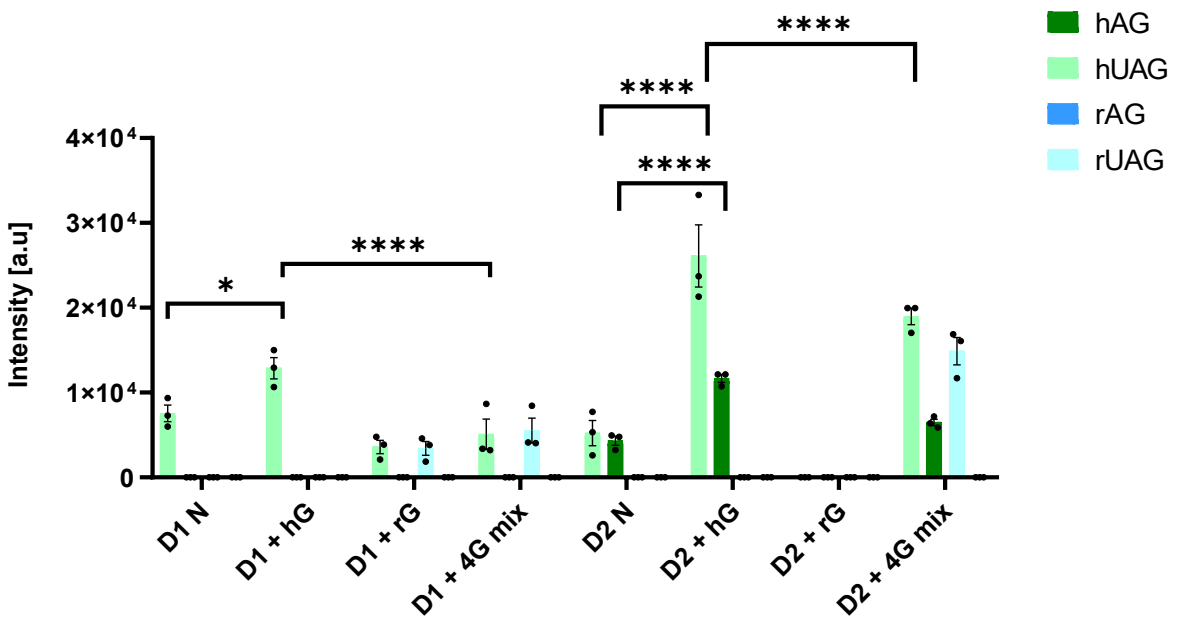

Figure 5.5 Detection of human and rat ghrelin using BAMS-antibody 86.

D1 – donor 1. D2 – donor 2. N – 'neat' plasma sample (no exogenous ghrelin). + hG – the addition of exogenous human ghrelin (both unacylated and acyl) to plasma. + rG – the addition of rat exogenous ghrelin (both unacylated and acyl) to plasma. + 4G mix – equimolar mixture of exogenous human and rat, unacylated, and acyl ghrelin to plasma. Two-way ANOVA was performed with Tukey corrections. P<0.05 is considered statistically significant. N = 3, mean average plotted with SEM. ****P<0.0001. *P<0.05.

To determine whether the lack of detectable rat acyl ghrelin was a problem with the BAMS procedure or an issue with the peptide mix, the exogenous 'spiked' human and rat ghrelin four-way equimolar mixture was re-analysed by MALDI-TOF before repeating the BAMS procedure with Antibody 88. As such 1 ng/100 µL of human and rat ghrelin equimolar mixture was spotted directly onto a MALDI-TOF target (as previously described in Chapter 3, section 3.2.5). All four ghrelin species within the exogenous 'spiked' mixture were detectable (Figure 5.6), suggesting that the original 'spiked' mixture added to the plasma samples contained the four ghrelin species and should have been detectable by BAMS. A possible loss of rat acyl ghrelin could be explained by issues during the antibody-based capture process of ghrelin species. Thus, given the inability to detect rat acyl ghrelin and due to a limited number of beads available to conduct further tests, it was ruled out as a possible internal standard in the detection of human ghrelin.

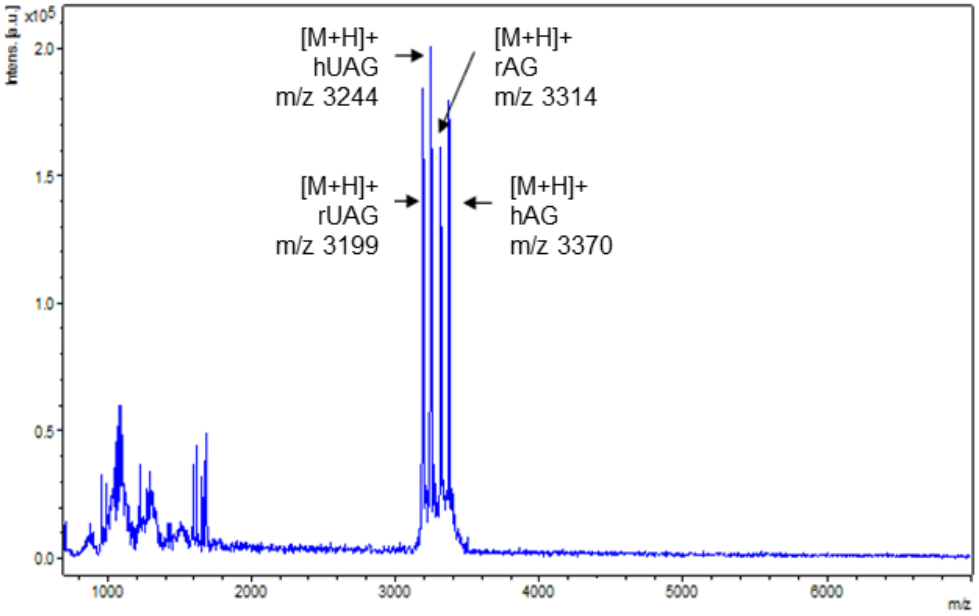

Figure 5.6 MALDI-TOF analysis of an equimolar mixture of the exogenous human and rat ghrelin species.

Thus, for the ADX088 (antibody 88) kit, the rat unacylated ghrelin was explored as an ISTD. As such, for antibody 88 the samples were as follows: 'neat' plasma, the addition of exogenous acyl and unacylated human ghrelin in an equimolar mixture of 1 ng/100 µL, the addition of exogenous rat unacylated ghrelin at 1 ng/100 µL, and the addition of exogenous human acyl and unacylated ghrelin with exogenous rat unacylated ghrelin in an equimolar mix at 1 ng/100 µL (Figure 5.7). For donor 1 a significant increase ($P<0.01$) in both human unacylated and acyl ghrelin was seen in plasma 'spiked' with exogenous human unacylated and acyl ghrelin compared to the 'neat' plasma. Both human unacylated and acyl ghrelin were significantly reduced ($P<0.05$ and $P<0.01$, respectively) upon the inclusion of rat exogenous unacylated ghrelin alongside the human exogenous unacylated and acyl ghrelin in the 'spiked' mix compared to when plasma was 'spiked' with only exogenous human acyl and unacylated ghrelin (Figure 5.7). The same trends were observed in donor 2, with human acyl and unacylated ghrelin showing a significant increase ($P<0.001$) within the plasma 'spiked' with exogenous human acyl and unacylated ghrelin compared to the 'neat' plasma. Additionally, human acyl and unacylated ghrelin were significantly reduced ($P<0.001$) upon the addition of rat unacylated ghrelin to the human

exogenous ‘spiked’ mix compared to the plasma ‘spiked’ with only exogenous human acyl and unacylated ghrelin (Figure 5.7).

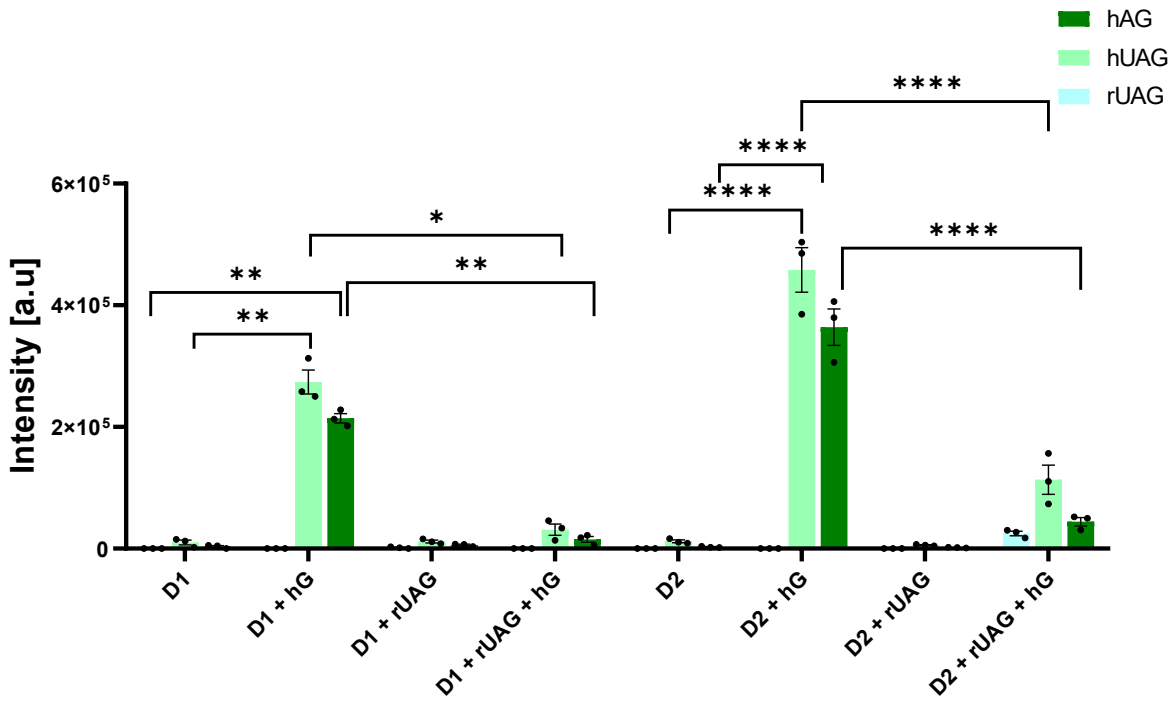

Figure 5.7 Detection of human acyl and unacylated ghrelin and rat unacylated ghrelin using BAMS antibody 88.

(N) – ‘neat’ plasma sample (no exogenous ghrelin). +hG – the addition of exogenous human ghrelin (both acyl and unacylated) to plasma. +rUAG – the addition of exogenous rat unacylated ghrelin to plasma. + rUAG + hG – an equimolar mixture of human acyl and unacylated exogenous ghrelin along with rat unacylated ghrelin to plasma. Two-way ANOVA was performed with Tukey corrections. P<0.05 is considered statistically significant. N = 3, mean average plotted with SEM. ****P<0.0001, **P<0.01. *P<0.05.

These data demonstrate a reduction in human acyl and unacylated ghrelin levels upon the addition of exogenous rat ghrelin in both ADX086 and ADX088 assays. As a result, my experiments demonstrate that rat ghrelin was not a viable ISTD and was no longer used in subsequent experiments. Our collaborators at Adeptrix, explored the viability of ISTD for BAMS further whilst I carried out further investigations in the meantime.

5.3.3 Limit of Detection of the BAMS Assay

Due to the challenges encountered while employing exogenous rat ghrelin as an ISTD, initial calibration curves were constructed exclusively using exogenous human ghrelin standards. This mainly aimed to test the limits of detection of the BAMS kit. The

intention was to revisit this calibration approach following further refinements involving rat ISTD or after purchasing deuterated human ghrelin. However, in this section, only exogenous human ghrelin was tested. A standard curve to determine the lower limit of detection was established on exogenous human ghrelin standards for both antibody 86 (Figure 5.8A, C) and 88 (Figure 5.8B, D) BAMS kit. The highest concentration of the curve was 10 ng/mL for human acyl and unacylated ghrelin. This was subjected to a serial dilution in a 1:2 ratio. This dilution process continued until concentrations of 0.02 ng/mL were reached, creating an eight-point curve. For antibody 86, an R^2 value of 0.82 was obtained for the human acyl ghrelin curve (Figure 5.8A). Here, human acyl ghrelin's lower limit of detection was determined at 0.31 ng/mL. For antibody 88, human acyl ghrelin's lower limit of detection was established at 0.04 ng/mL with an R^2 value of 0.89 obtained for the standard curve (Figure 5.8B). The lower limit of detection for human unacylated ghrelin was established at 0.02 ng/mL for both antibody 86 and antibody 88. Antibody 86 obtained an R^2 value of 0.71 (Figure 5.8C), whilst antibody 88 obtained an R^2 value of 0.99 (Figure 5.8D).

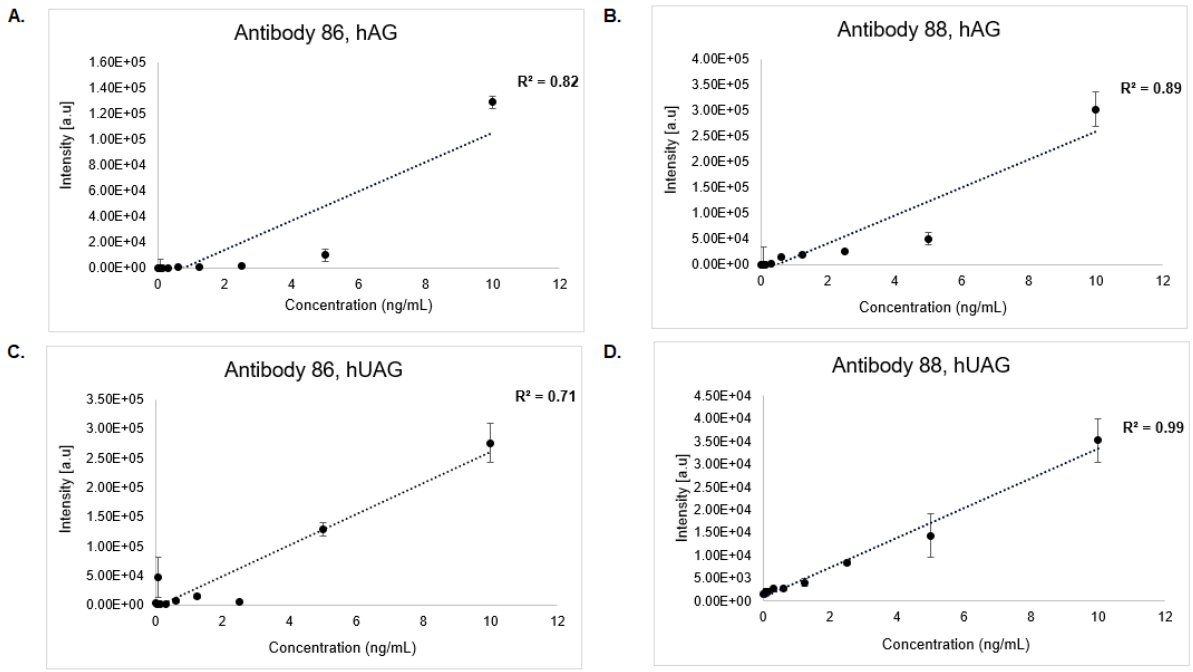

Figure 5.8 Standard curve from 0.02-10 ng/mL to establish limits of detection of both human acyl and unacylated ghrelin using either antibody 86 or antibody 88.

A. Antibody 86, hAG B. Antibody 88, hAG. C. Antibody 86, hUAG. D. Antibody 88, hUAG. The final plotted point is the mean of these three-run means, and error bars represent the standard deviation across runs, reflecting inter-run variability. Trendlines represent linear regression fits, and R^2 values are reported to indicate goodness of fit.

Upon determining the lower limit of detection, a standard curve using human acyl ghrelin as an ISTD set at 2.5 ng/mL and human unacylated ghrelin varying from 0.02-10 ng/mL was generated (Figure 5.9). Antibody 86 obtained a good R^2 value of 0.88 (Figure 5.9A), whilst antibody 88 demonstrated an excellent R^2 value of 0.98 (Figure 5.9B). Thus, suggesting that overall, antibody 88 outperforms antibody 86.

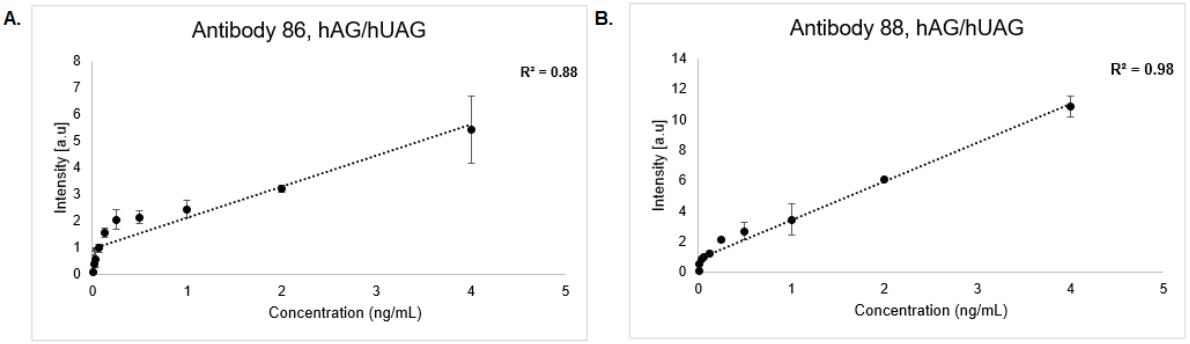

Figure 5.9 Assessing the limit of detection via a standard curve with hUAG varying from 0.2-10 ng/mL and hAG as an ISTD at 2.5 pg/mL. A. Antibody kit 86. B. Antibody kit 88. The mean intensity ratio and mean concentration ratio of hAG/hUAG is plotted. The final plotted point is the mean of these three-run means, and error bars represent the standard deviation across runs, reflecting inter-run variability. Trendlines represent linear regression fits, and R^2 values are reported to indicate goodness of fit.

5.3.4 Performance Tests of BAMS Antibody Assays

Two forms of variability tests were performed to test the reproducibility and reliability of the kits. The first evaluated the variation between distinct beads sourced from the same sample. The second form evaluated the variation resulting from multiple analyses of the same sample. Both antibody kits were used to analyse both ‘neat’ and ‘spiked’ plasma samples. Here, the 'spiked' samples contained an equimolar mixture of human acyl ghrelin and human unacylated ghrelin, each at a concentration of 2.5 ng within 250 µL of plasma.

5.3.4.1 Spiked Plasma Analysis

This first analysis assesses the variability of antibody 86 versus antibody 88 in ‘spiked’ plasma among all donors (D1-D5) and across two different blood withdrawals from the same donor (W1-2). The data set, which includes bead averages of three analyses of the same plasma sample, was subjected to an ANOVA test. Here, there were no statistically significant differences reported in the intensity ratio of AG:UAG when

comparing antibody 86 and antibody 88 values from the same withdrawals (Figure 5.10). These data suggest that both antibodies 86 and 88 perform at a similar level.

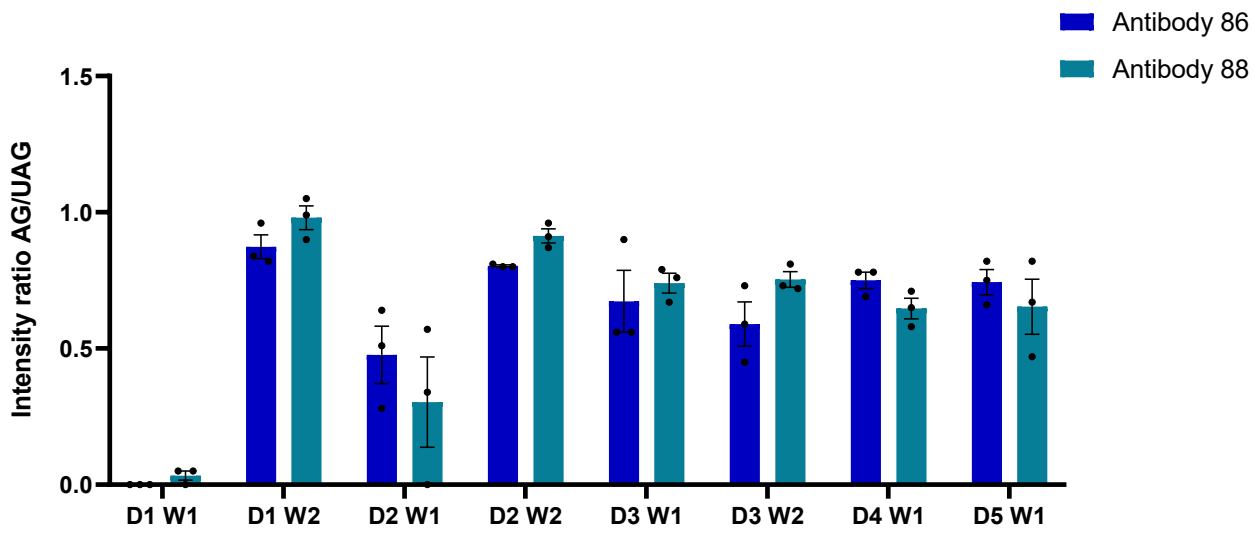

Figure 5.10 Comparison of antibody 86 versus antibody 88 from five different donors with 'spiked' plasma.

The samples were spiked with an equimolar mixture of human acyl and unacylated ghrelin (2.5 ng each per 250 µL plasma) from five different donors (D1–D5) with two withdrawals each (W1–W2). Data represent N = 3, mean ± SEM. Two-way ANOVA with Tukey correction was applied; $P < 0.05$ was considered statistically significant. D1 = donor 1, D2 = donor 2, D3 = donor 3, D4 = donor 4, D5= donor 5. W1 – withdrawal 1, W2 = withdrawal 2.

To evaluate the performance characteristics of the antibodies, intra-assay variability tests were performed using donor plasma samples. Each sample was mixed in a well containing three antibody-coated beads, and the reproducibility of ghrelin quantification was assessed by comparing the signal intensities across these beads

(Bead 1, Bead 2, and Bead 3) within the same analytical run (Figure 5.11). Intra-assay variation was expressed as %CV across triplicate bead measurements.

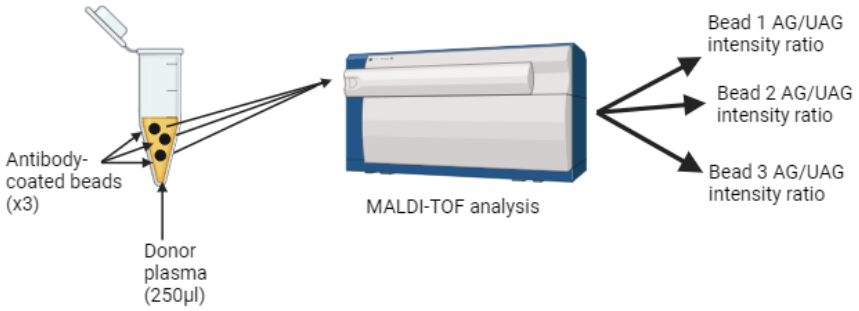

Figure 5.11 Schematic demonstrating three ghrelin antibody-coated beads after incubation in donor plasma subjected to MADLI-TOF analysis, producing an intensity ratio of AG:UAG for each bead.

The intra-assay precision of Antibody 86 and Antibody 88 was evaluated across 21 and 24 replicate runs, respectively, following spiking. Results were categorised based on %CV thresholds: excellent (<10%), acceptable (11–20%), and poor (>21%), as shown in Figure 5.12A–B. Additional intra-assay variability analysis based on bead-to-bead regression is presented in Supplementary Figure S2. Antibody 86 (spiked) demonstrated strong intra-assay reproducibility, with 89.95% of runs classified as excellent, 9.5% as acceptable, and 9.5% as poor. The distribution was consistent with a low median %CV of 6.0%, and most values fell within acceptable precision limits. Two runs exceeded the 15% threshold, with maximum variability reaching 31%. Antibody 88 (spiked) showed comparable performance, with 83.3% of runs rated excellent, 12.5% acceptable, and only 4.1% poor. The median %CV was slightly lower at 4.0%, and overall variability remained tightly constrained, except for a single outlier at 32%.

These findings confirm that both antibodies provide high intra-assay precision when spiked into plasma, with Antibody 88 exhibiting slightly lower overall variability and fewer poor-performing runs. This supports their suitability for sensitive and

reproducible quantitative analysis under controlled spiking conditions.

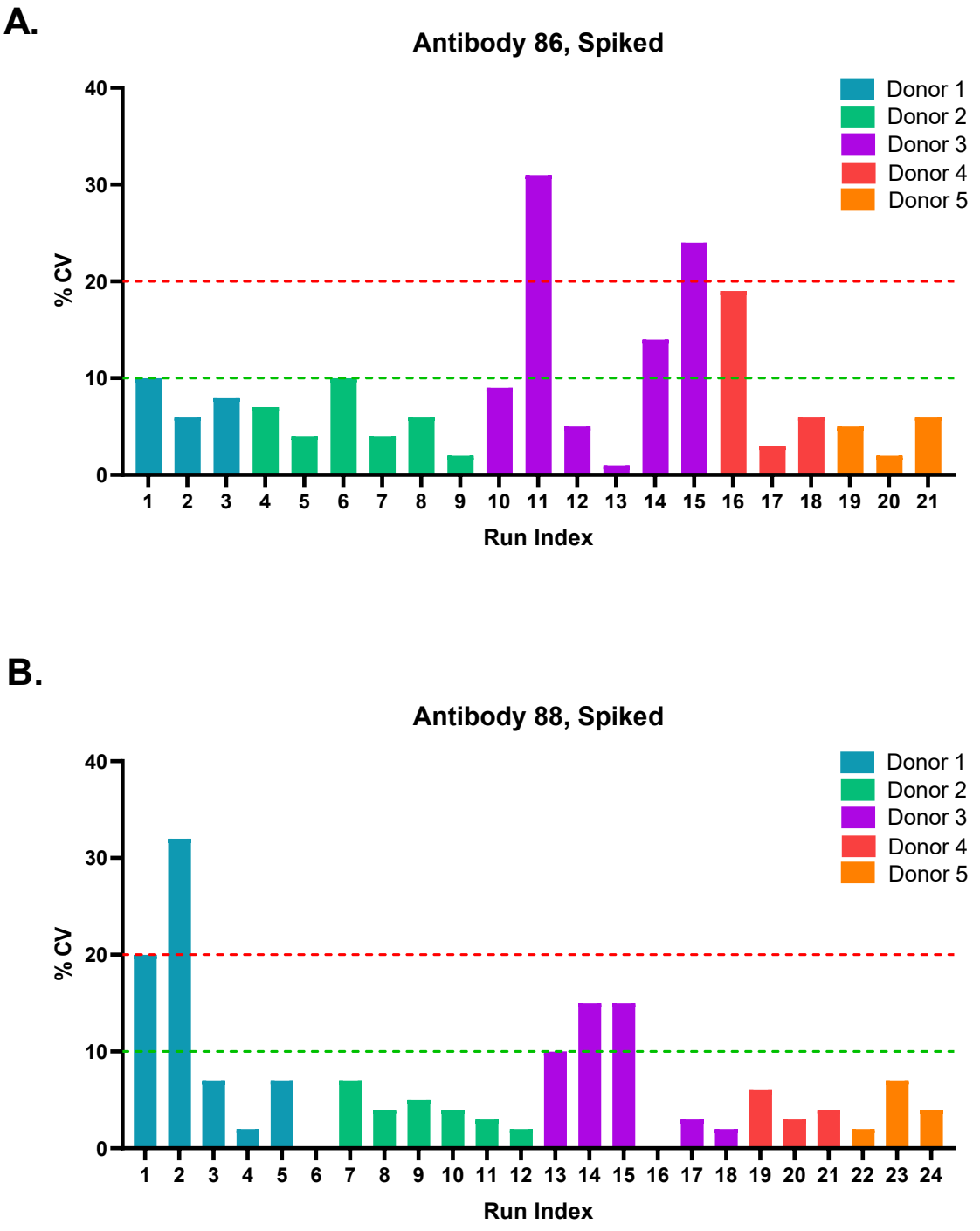

Figure 5.12 Intra-assay variability shows the reproducibility between antibody-coated beads used to quantify ghrelin levels in the same donor 'spiked' plasma sample. Each run represents triplicate measurements (Bead 1–3) for a single withdrawal. Thresholds of 10% and 20% are marked to denote good and acceptable precision, respectively. Runs exceeding 20% CV were considered to have poor repeatability. For additional intra-assay reproducibility based on bead-wise regression analysis, see Supplementary Figure S2. A. Antibody 86. B. Antibody 88.

Inter-assay variability was assessed by measuring reproducibility across independent assay runs of the same donor's spiked plasma, collected from a single withdrawal. For each donor–withdrawal combination, the mean AG:UAG ratio was calculated from triplicate bead measurements within each run. The %CV across these runs was then used to evaluate inter-assay precision (Figure 5.13A–B). Supplementary Figure S3 provides additional regression-based comparisons between experimental runs to further illustrate inter-assay reproducibility.

Antibody 86 (Figure 5.13A) demonstrated moderate inter-assay performance, with 42.9% of runs classified as excellent, 14.3% acceptable, and 42.9% poor. While several timepoints showed low CVs (1–8%), variability was notably higher in other runs, with CVs reaching 29%, 37%, and 24%, indicating day-to-day inconsistencies in assay performance.

Antibody 88 (Figure 5.13B), by comparison, showed improved inter-assay reproducibility, with 75% of runs falling within the excellent range, and 25% classified as poor. No runs fell into the intermediate acceptable range. Most CV values remained well below 10%, with the exception of two elevated timepoints (22% and 26%).

Taken together, these results suggest that Antibody 88 provides more stable inter-assay precision when compared to Antibody 86 under spiked conditions. The reduced frequency of poor-performing runs supports its suitability for longitudinal applications where reproducibility over time is critical. Supplementary Table S1 details the raw AG:UAG intensity ratios from each run, highlighting specific run-to-run inconsistencies, including potential outliers that may account for elevated CVs. These differences in peak detection are further illustrated in Supplementary Figure S4, which shows MALDI-TOF spectra where acyl ghrelin signal variability may explain inter-assay precision differences due to signal-to-noise threshold effects.

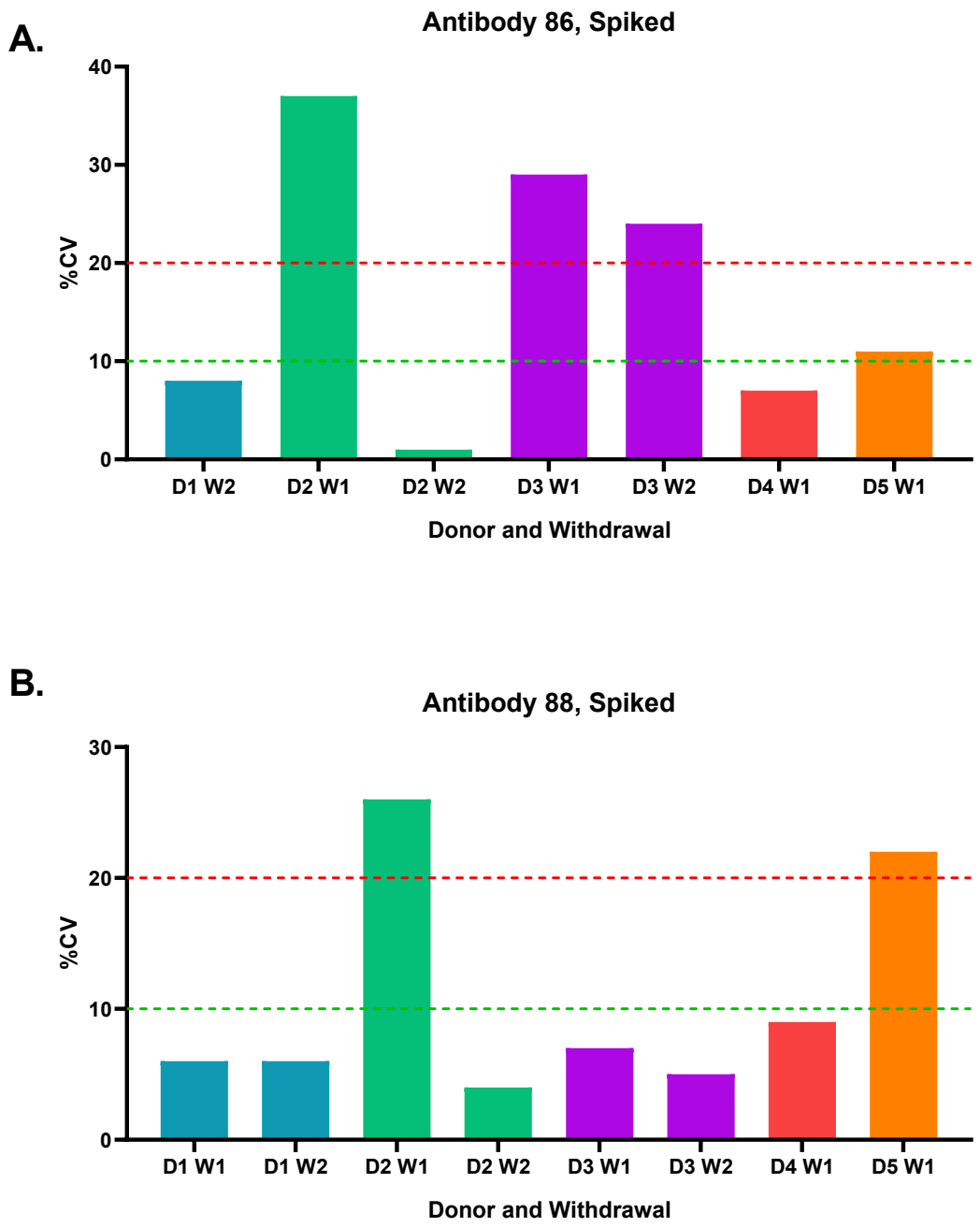

Figure 5.13 Inter-assay variability. Reproducibility across independent assay runs of the same donor's spiked plasma from a single withdrawal. For each donor–withdrawal pair, the mean UAG/AG ratio from triplicate bead measurements was calculated per run, and the CV% across runs was used to assess inter-assay precision. Thresholds of 10% (good precision) and 20% (acceptable precision) are indicated by dashed lines. CV values exceeding 20% denote poor reproducibility between runs. For additional run-to-run comparisons using regression analysis, see Supplementary Figure S3.A. Antibody 86, B. Antibody 88.

The precision and reproducibility of antibody 86 and antibody 88 spiked assays were evaluated by comparing mean intra-assay and inter-assay CV% across five donors (Figure 5.14). Intra-assay CV% reflects consistency within a single assay run, whereas inter-assay CV% captures reproducibility across multiple independent runs using the same sample.

For antibody 86 (Figure 5.14A), intra-assay CV% ranged from 4.3% to 14%, with the lowest variability observed in Donor 5 (4.3%) and the highest in Donor 3 (14%). Inter-assay variability exhibited a wider spread, ranging from 7% (Donor 4) to 26.5% (Donor 3), indicating greater inconsistency across runs for certain samples. The elevated inter-assay CV% in Donor 3 suggests potential procedural or sample-handling variability requiring attention.

In contrast, antibody 88 (Figure 5.14B) demonstrated overall lower inter-assay variability across most donors. Intra-assay CV% values ranged from 4.2% to 11.4%, while inter-assay CV% ranged from 5.9% to 22%. The highest inter-assay variability was noted in Donor 5 (22%), while the lowest occurred in Donor 1 (5.99%), reflecting improved reproducibility relative to antibody 86. Notably, most donors using antibody 88 fell below the 20% threshold for inter-assay CV%, indicating enhanced stability and potential suitability for longitudinal sample comparisons.

These findings show that both antibodies exhibit acceptable intra-assay precision; however, antibody 88 offers comparatively improved inter-assay reproducibility across the donor set, supporting its potential for more consistent application in repeated measurements. To further visualise assay robustness, Supplementary Figure S5 plots the relationship between intra-assay (%CV beads) and inter-assay (%CV run) variability for each donor.

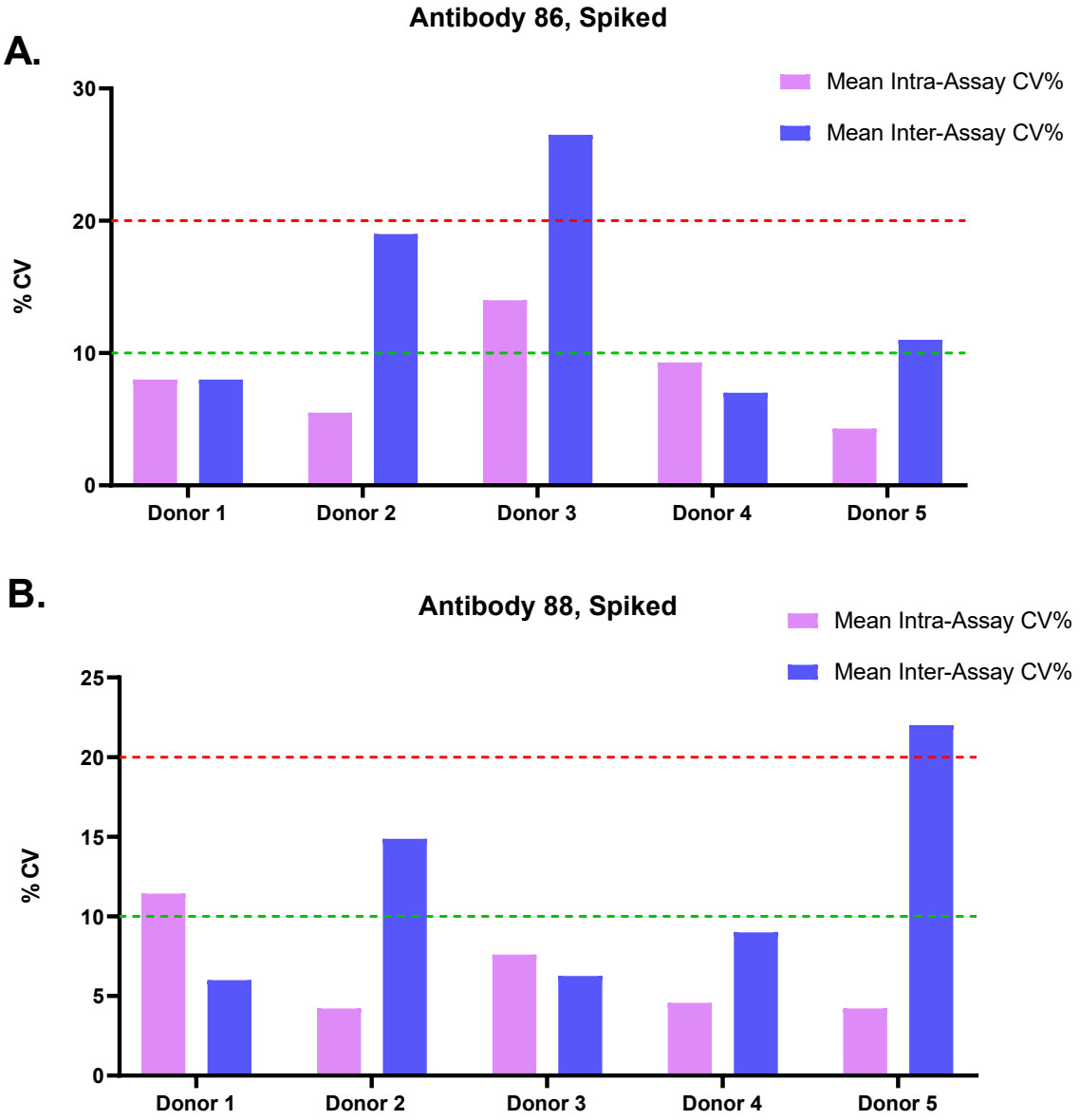

Figure 5.14 Comparison of mean intra-assay CV% and inter-assay CV% for each donor. Intra-assay variability reflects bead-to-bead consistency within a single run, while inter-assay variability reflects reproducibility across multiple runs for the same sample. Donors with high inter-assay CVs (>40%) indicate a need for protocol standardisation or improved control of sample handling and processing. See Supplementary Figure S5 for detailed comparison of intra- versus inter-assay CVs across individual donors. A. Antibody 86, B. Antibody 88.

5.3.4.2 Neat Plasma Results

Next, antibodies 86 and 88 were used to measure AG:UAG intensity in the 'neat' plasma samples from different donors. The evaluation of the 'neat' plasma was limited due to the availability of beads. As a result, only three donors out of the five were analysed for both antibodies 86 and 88 and only two blood withdrawals of each were analysed, apart from donor 2, which only had one withdrawal analysed for antibody 86.

For donor 1, antibody 86 was unsuccessful at measuring acyl ghrelin, and therefore the AG:UAG ratio was 0. As a result, antibody 88 AG:UAG intensity ratio was significantly better for donor 1 ($P<0.001$ for donor 1, withdrawal 1 and $P<0.01$ for donor 1, withdrawal 2) (Figure 5.15). For donor 2, no statistically significant differences were observed between antibody 86 and antibody 88 in the intensity ratio of AG:UAG when comparing values from the same withdrawals. For donor 3, antibody 88 significantly outperformed antibody 86 ($P<0.001$) in terms of AG:UAG intensity.

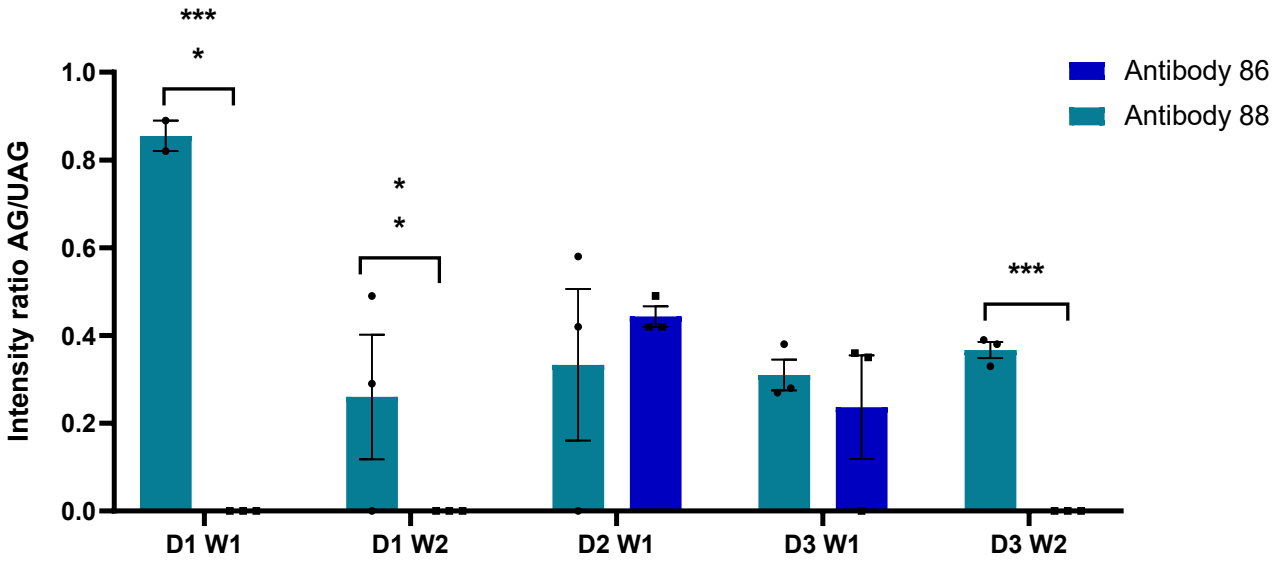

Figure 5.15 Comparison of antibody 86 versus antibody 88 for the analysis of AG:UAG intensity in 'neat' plasma samples from three different donors.

Two-way ANOVA was performed with Tukey corrections. $P<0.05$ is considered statistically significant. N = 3, mean plotted with SEM. $P<0.0001$ = ****, $P<0.001$ = ***, $P<0.01$= **D1 = donor 1, D2 = donor 2, D3 = donor 3.. W1 – withdrawal 1, W2 = withdrawal 2.

The intra-assay precision of Antibody 86 and Antibody 88 was further assessed using neat (unspiked) plasma samples across 5 and 16 replicate runs, respectively, as shown in Figure 5.16A–B. Additional intra-assay variability analysis based on bead-to-bead regression is presented in Supplementary Figure S6.

Antibody 86 (neat) exhibited moderate reproducibility, with 20% of runs rated as excellent, 60% as acceptable, and 20% as poor. The median %CV was 11.0%, suggesting overall acceptable performance; however, one run showed high variability at 33%, potentially indicating instability or inconsistent binding in neat matrix conditions.

In contrast, Antibody 88 (neat) showed a broader distribution of variability. Only 18.8% of runs met the excellent threshold, while 25.0% were acceptable and the majority (56.3%) fell into the poor precision category. The median %CV was 17.0%, reflecting higher variability under neat conditions. Notably, the highest %CV reached 37%, further highlighting reduced consistency without prior spiking.

These results indicate that both antibodies demonstrate diminished intra-assay precision when used directly in neat plasma, with Antibody 88 showing greater variability overall. The findings underscore the impact of matrix complexity on assay performance and reinforce the importance of optimising assay conditions for consistent quantification.

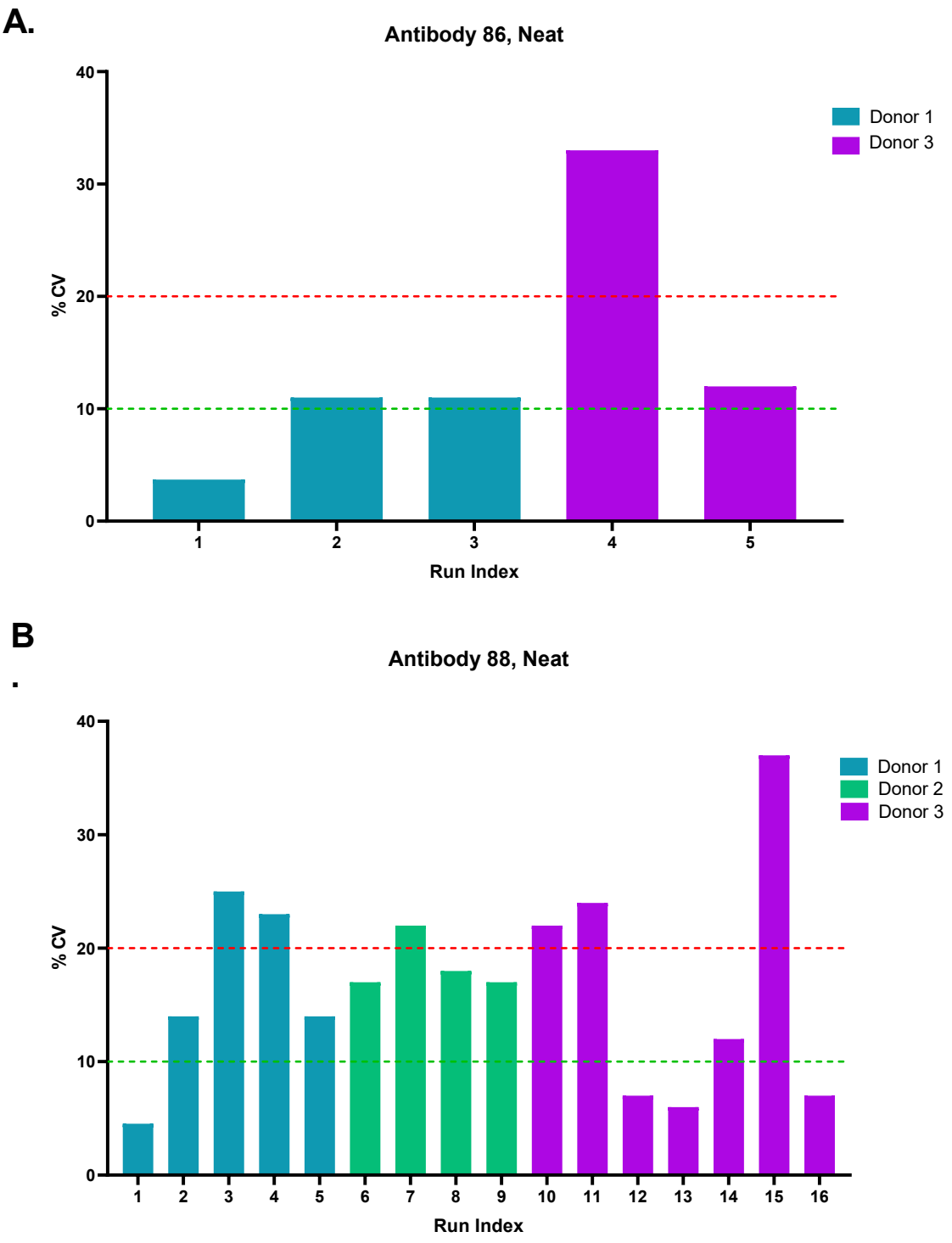

Figure 5.16 Intra-assay variability. Reproducibility between three beads was used to quantify ghrelin levels in the same donor 'neat' plasma sample. Each run represents triplicate measurements (Bead 1–3) for a single withdrawal. Thresholds of 10% and 20% are marked to denote good and acceptable precision, respectively. Runs exceeding 20% CV were considered to have poor repeatability. For additional intra-assay reproducibility based on bead-wise regression analysis, see Supplementary Figure S6. A. Antibody 86. B. Antibody 88.

Inter-assay variability was assessed by evaluating reproducibility across independent assay runs using neat plasma samples from the same donor and withdrawal event (Figure 5.17A–B). Supplementary Figure S7 provides additional regression-based comparisons between experimental runs to further illustrate inter-assay reproducibility.

Antibody 86 (Figure 5.17A) demonstrated excellent inter-assay precision, with a single run (D2 W1) showing a %CV of 8%, thus classified as good. Although only one data point was available, the result suggests high reproducibility under neat conditions in this instance. In contrast, Antibody 88 (Figure 5.17B) showed considerable inter-assay variability, with only 1 of 5 runs (D3 W2) achieving excellent precision (%CV = 9%). One run (D3 W1, 20%) fell at the threshold for acceptable performance, while the remaining three runs (D1 W1, D1 W2, and D2 W1) were classified as poor, with CVs ranging from 29% to 44%.

These findings indicate that while Antibody 86 maintained strong inter-assay reproducibility in neat plasma (albeit with limited data), Antibody 88 exhibited substantial variability between runs. This reinforces the need for further optimisation when using Antibody 88 in longitudinal or repeated measures designs involving unspiked samples.

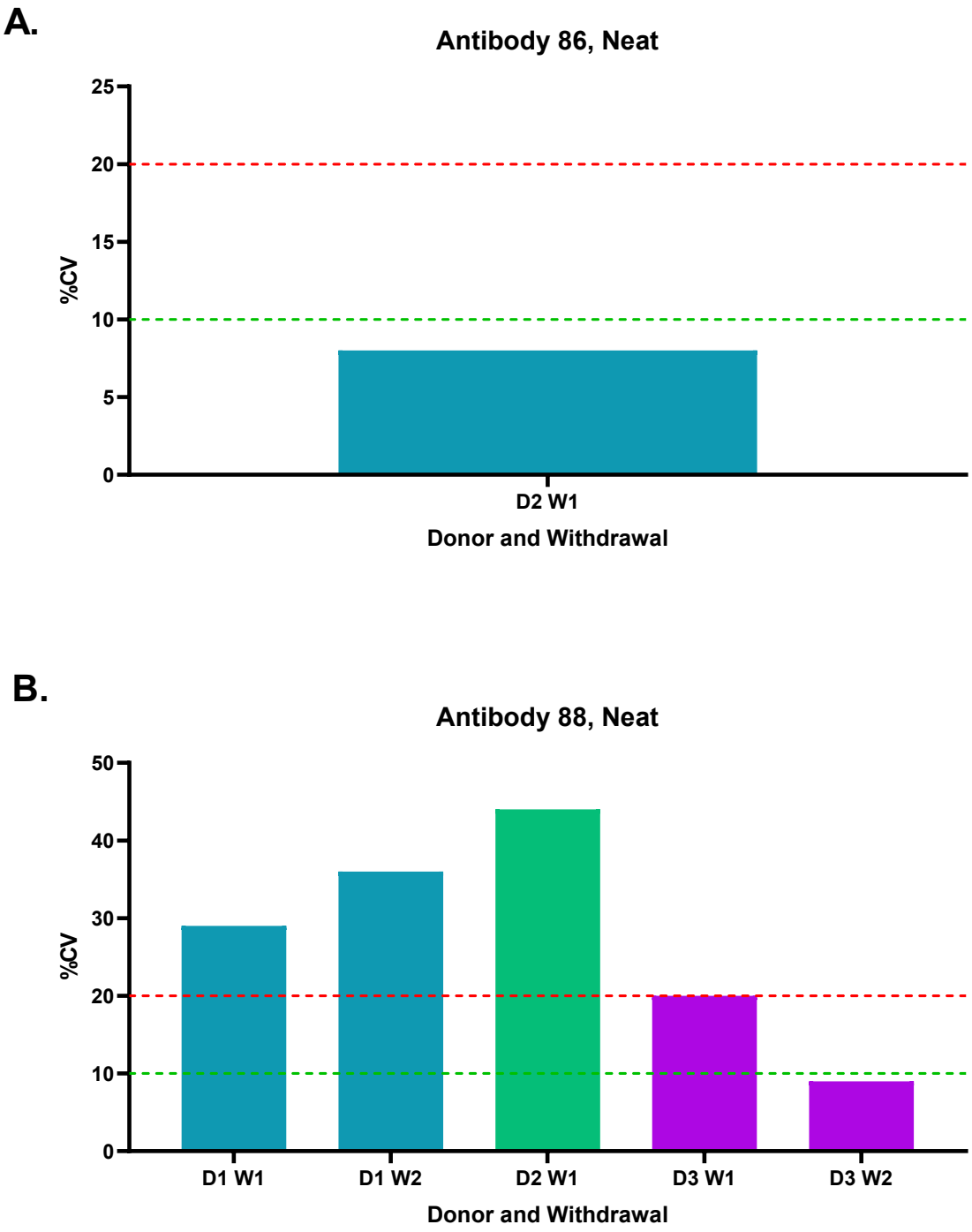

Figure 5.17 Inter-assay variability. Reproducibility across independent assay runs of the same donor's spiked plasma from a single withdrawal. For each donor–withdrawal pair, the mean AG:UAG ratio from triplicate bead measurements was calculated per run, and the CV% across runs was used to assess inter-assay precision. Thresholds of 10% (good precision) and 20% (acceptable precision) are indicated by dashed lines. CV values exceeding 20% denote poor reproducibility between runs. For additional inter-assay reproducibility based on bead-wise regression analysis, see Supplementary Figure S7. A. Antibody 86, B. Antibody 88.

The precision and reproducibility of Antibody 86 and Antibody 88 assays were evaluated by comparing mean intra-assay and inter-assay CV% across donors, as shown in Figure 5.18. Intra-assay CV% indicates consistency within individual assay runs, while inter-assay CV% reflects reproducibility across independent runs of the same samples. To further visualise assay robustness, Supplementary Figure S8 plots the relationship between intra-assay (%CV beads) and inter-assay (%CV run) variability for each donor.

For Antibody 86 (Figure 5.18A), both intra-assay and inter-assay CV% were consistent for Donor 2, with mean values of 8% each. It should be noted that this observation is based on a single donor dataset, limiting broader conclusions. Nonetheless, the data suggest stable performance of Antibody 86 under neat conditions with minimal variability both within and between assay runs.

In contrast, Antibody 88 (Figure 5.18B) displayed greater variability. Mean intra-assay CV% ranged from 16% to 18.5% across donors, while inter-assay CV% showed a wider spread, from 14.2% (Donor 3) up to 44% (Donor 2). Notably, Donor 2 exhibited particularly high inter-assay variability, indicating inconsistent assay reproducibility across runs for this donor’s neat sample. Donor 3, however, showed relatively better inter-assay precision (14.2%) despite intra-assay CVs in the mid-teens.

These results demonstrate that Antibody 86 provides more stable and reproducible performance in neat plasma across both intra- and inter-assay conditions, though the limited data available warrants cautious interpretation. By comparison, Antibody 88 shows increased variability, particularly in inter-assay precision, which may impact its reliability for longitudinal studies without further optimisation.

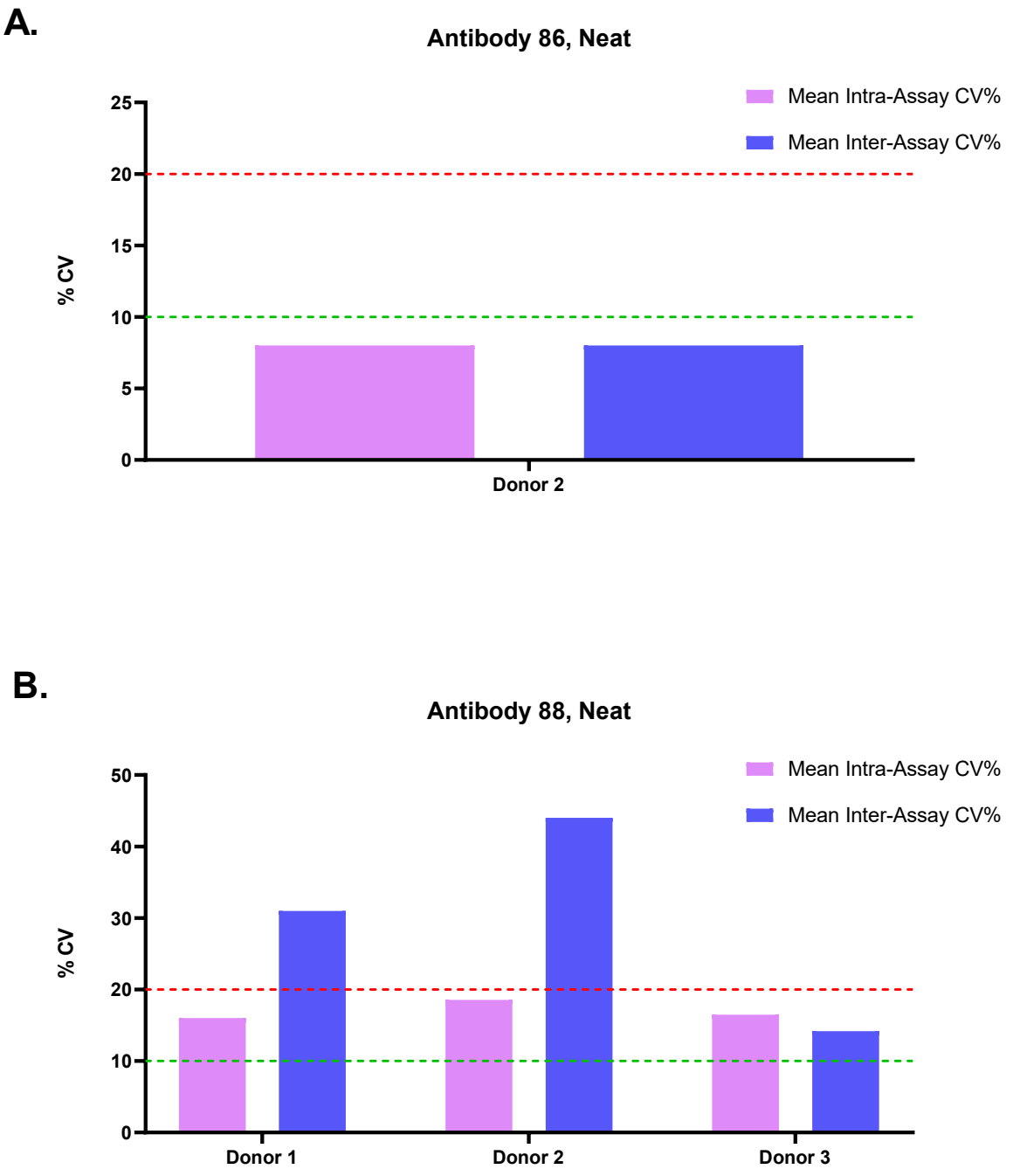

Figure 5.18 Comparison of mean intra-assay CV% and inter-assay CV% for each donor. Intra-assay variability reflects bead-to-bead consistency within a single run, while inter-assay variability reflects reproducibility across multiple runs for the same sample. Donors with high inter-assay CVs (>40%) indicate a need for protocol standardisation or improved control of sample handling and processing. See Supplementary Figure S8 for detailed comparison of intra- versus inter-assay CVs across individual donors. A. Antibody 86, B. Antibody 88.

Performance testing of the BAMS antibody assays demonstrated that both antibodies 86 and 88 exhibit strong intra-assay precision when quantifying ghrelin levels in spiked plasma, with antibody 88 showing slightly better overall reproducibility and inter-assay stability. However, in neat plasma samples, both antibodies showed reduced precision, with antibody 86 generally outperforming antibody 88 in inter-assay reproducibility. Supplementary Figure S9 illustrates this contrast through a boxplot comparison of %CV distributions between spiked and neat samples across both antibodies. These results highlight the importance of assay conditions on antibody performance and suggest antibody 88's suitability for controlled, spiked samples, while antibody 86 may be more reliable for unspiked plasma. Due to limited bead availability, the full performance characteristics could not be established, particularly for unspiked plasma; however, given time constraints, the available BAMS antibody assay data were compared with ELISA results to evaluate their relative strengths and suitability for ghrelin quantification.

5.3.5 Comparison Between the Ghrelin BAMS and ELISA

The main aim of my thesis is to develop a novel approach for identifying acyl and unacylated ghrelin within the same plasma sample that improves on the current reliance on two distinct ELISA kits, one for unacylated ghrelin and one for acyl ghrelin. To do so, I compared the reproducibility and sensitivity of the new approach of BAMS with ELISA kits that have been validated and used widely within our research group.

5.3.5.1 Reproducibility of ELISA

To assess the reproducibility of unacylated and acyl ghrelin detection using ELISA kits (A05119 and A05106, Bertin), standard curves were generated and analysed across three independent experimental runs. This allowed evaluation of both intra-assay variation (between replicate wells within the same kit) and inter-assay variation (between different kits). Intra-assay variability was calculated using duplicate well measurements per donor sample (n = 23). For BAMS, intra-assay precision was assessed by comparing signal intensities across three analytical beads prepared from the same plasma sample. CVs were calculated for each condition using either Antibody 86 or 88 in spiked (n = 21 and n = 24, respectively) or neat plasma (n = 5 and n = 16, respectively). Additional intra-assay variability analysis for the ELISA, based on bead-to-bead regression is presented in Supplementary Figure S10.

The ELISA platform showed moderate reproducibility (Figure 5.19), with 39.13% of runs classified as excellent, and the remaining equally split between acceptable (30.43%) and poor (30.43%). In contrast, BAMS demonstrated substantially improved precision, particularly in spiked plasma. Antibody 86 (spiked) achieved 80.95% excellent, 9.5% acceptable, and 9.5% poor runs. Antibody 88 (spiked) performed similarly, with 83.3% of runs falling into the excellent category, 12.5% acceptable, and only 4.1% poor.

In neat plasma, BAMS performance varied. Antibody 86 maintained good reproducibility (60% excellent, 20% acceptable, 20% poor), while Antibody 88 showed greater variability, with only 18.75% of runs classified as excellent, 37.5% acceptable, and 43.75% poor.

Overall, these findings demonstrate that BAMS offers superior intra-assay reproducibility compared to ELISA, particularly when applied to spiked samples. The reduced precision observed with Antibody 88 in neat plasma suggests an influence of matrix effects or endogenous analyte variability on assay performance. See Supplementary Table S2 for further comparison between ELISA and BAMS variability.

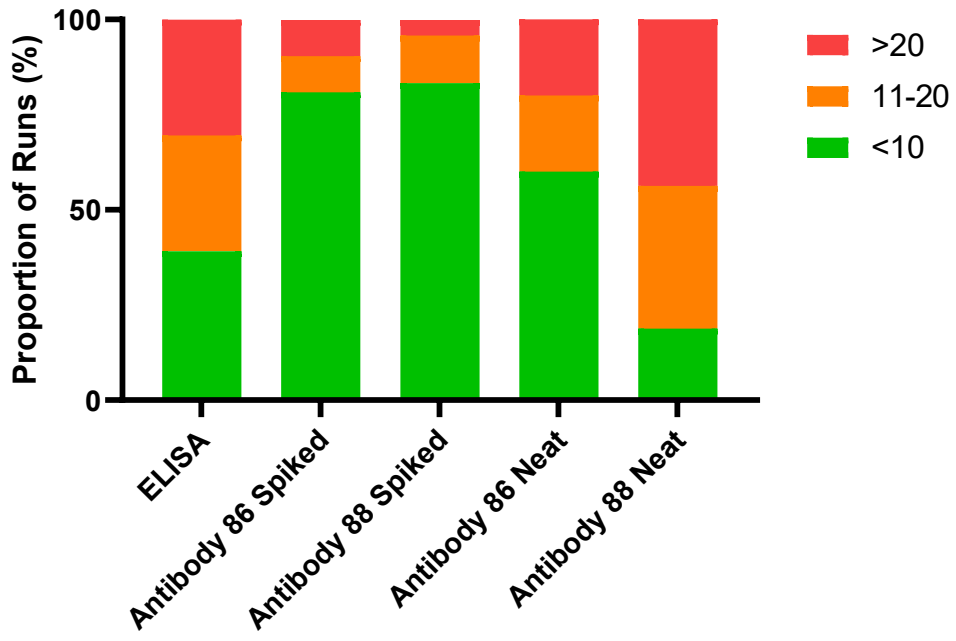

Figure 5.19 Intra-assay variability comparison across ELISA and BAMS methods.
Each method's replicate runs were categorised by %CV into three quality thresholds: ≤10% (excellent), 11–20% (acceptable), and >20% (poor). For each category, the percentage was calculated by dividing the number of runs falling within that %CV range by the total number of intra-assay runs for that method. For additional intra-assay reproducibility based on bead-wise regression analysis, see Supplementary Figure S10 and Supplementary Table S2.

Following the intra-assay evaluation, inter-assay variability was assessed to determine the consistency of each method across multiple experimental runs (Figure 5.20). Supplementary Figure S11 provides additional regression-based comparisons between experimental runs to further illustrate inter-assay reproducibility. The proportion of CVs within each category was expressed as a percentage of the total inter-assay values per method. In total, ELISA contributed 8 CV values, Antibody 86 (spiked) had 7, Antibody 88 (spiked) had 8, and Antibody 88 (neat) had 5. Antibody 86 (neat) was excluded from this analysis due to insufficient data (n = 1). ELISA again showed the highest degree of variability across runs, with only 12.5% of measurements classified as excellent, 25% acceptable, and 62.5% exceeding the 20% threshold. In contrast, BAMS methods displayed better inter-assay precision. Antibody 86 (spiked) achieved 42.86% excellent, with the remaining results split evenly between acceptable and poor categories (14.29% each). BAMS with Antibody 88 (spiked) demonstrated the most consistent performance, with 75% of values falling within the excellent range and only 25% in the poor category. Conversely, Antibody 88 (neat) showed lower reproducibility across runs, with just 20% excellent, 20% acceptable, and 60% poor. These results reinforce the superior reproducibility of BAMS, particularly in spiked formats, over ELISA, while also highlighting the reduced stability and increased variability observed in neat plasma preparations, especially with Antibody 88.

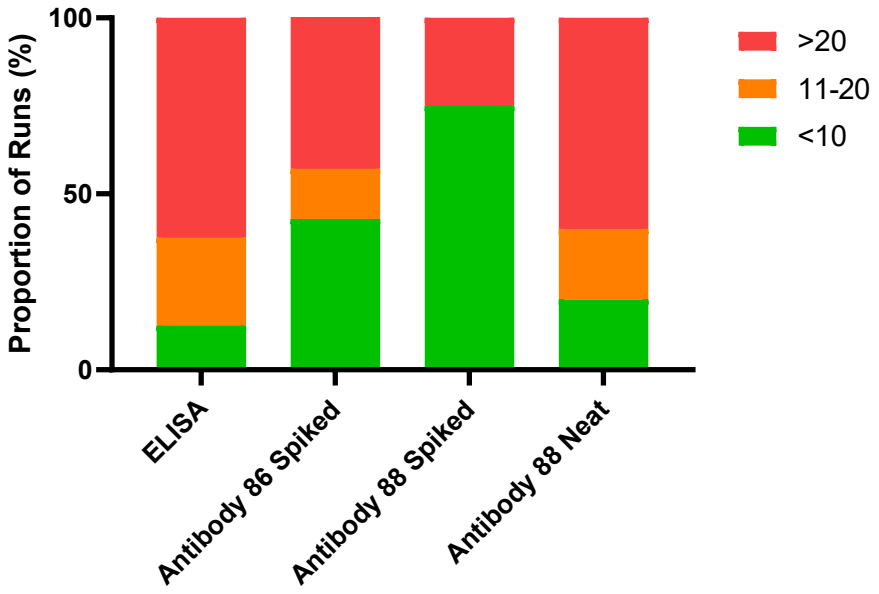

Figure 5.20 Inter-assay variability comparison across ELISA and BAMS methods. Each method's runs were categorised by %CV into three quality thresholds: ≤10% (excellent), 11–20% (acceptable), and >20% (poor). For additional run-to-run comparisons using regression analysis, see Supplementary Figure S11.

Together, these results demonstrate that both intra- and inter-assay variability were lowest for the BAMS approaches, particularly when using Antibody 88. The improved consistency suggests that BAMS may offer a more robust and reliable method for quantifying ghrelin isoforms in plasma compared to traditional ELISA-based assays.

5.3.5.2 Comparison of the Reproducibility of ELISA and BAMS Using Plasma from the Same Donors

To directly compare assay reproducibility under matched biological conditions, intra-assay %CVs were evaluated for five healthy donors across both ELISA and BAMS platforms using the same plasma samples. Each donor provided plasma from three independent blood withdrawals. While ELISA was performed on all withdrawals, BAMS analysis was limited to the spiked conditions due to bead availability, with neat data excluded from this comparison because of incomplete donor coverage. ELISA analysis was performed three months after BAMS analysis.

As shown in Figure 5.21, ELISA displayed substantially greater intra-assay variability across donors. The %CVs ranged from 7.85% to 94.18%, with Donor 5 exhibiting the

poorest reproducibility. In contrast, BAMS using Antibody 86 yielded more consistent results (%CVs: 4.3%–14%), and Antibody 88 offered the highest precision across all donors (%CVs: 4.2%–11.4%). Notably, for Donor 5, the most variable ELISA case, BAMS reduced intra-assay variability by more than 20-fold. This side-by-side comparison demonstrates that BAMS, particularly when paired with Antibody 88 in spiked samples, delivers markedly improved reproducibility relative to ELISA when analysing matched donor plasma under standardised conditions. Additional intra-assay variability analysis based on bead-to-bead regression is presented in Supplementary Figure S12.

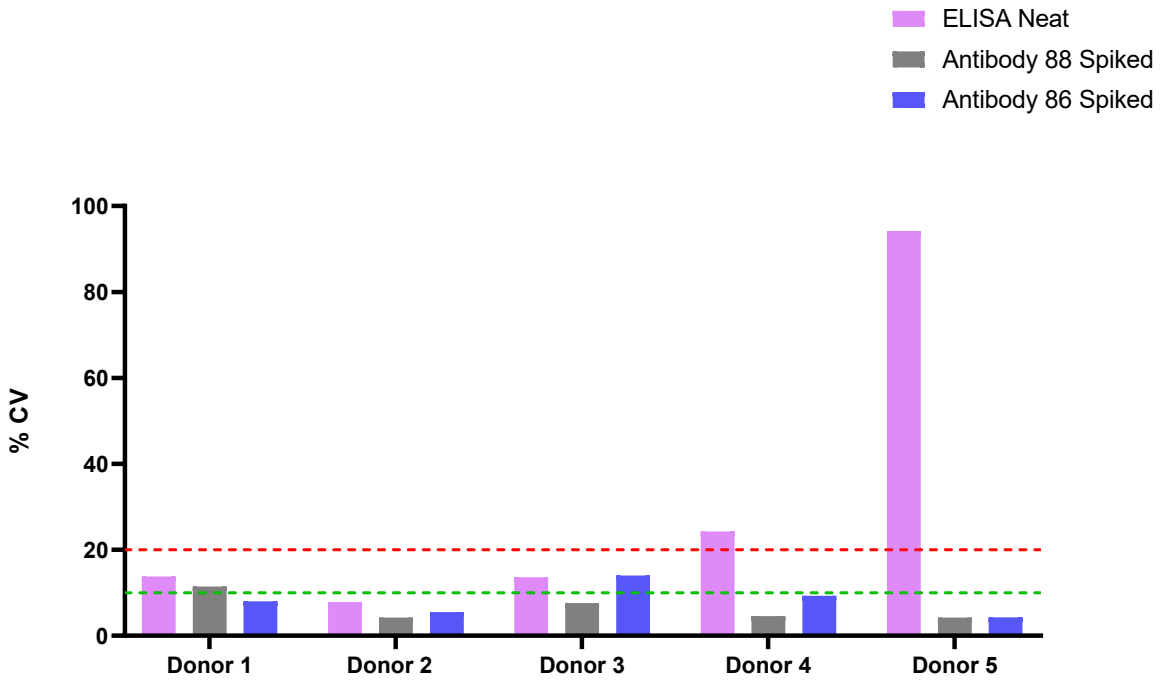

Figure 5.21 Comparison of intra-assay %CV across different detection platforms (ELISA, BAMS using Antibody 86 spiked, and BAMS using Antibody 88 spiked) for five individual donors. Median %CVs per donor were used to summarise the intra-assay variability within each platform. For additional intra-assay reproducibility based on bead-wise regression analysis, see Supplementary Figure S12.

To provide a broader perspective on intra-assay reproducibility across all datasets, including partially complete neat BAMS measurements, replicate runs from each platform were grouped into three predefined %CV categories: ≤10% (excellent), 11–20% (acceptable), and >20% (poor). The proportion of replicate runs within each

category was then calculated to facilitate direct cross-platform comparison of assay precision (Figure 5.22).

Consistent with earlier observations, ELISA exhibited the highest intra-assay variability, with only 40% of runs achieving excellent precision and a substantial proportion (40%) falling into the poor reproducibility range. In contrast, BAMS demonstrated markedly improved consistency, particularly in the spiked plasma formats, where over 80% of runs met the excellent threshold for both Antibody 86 and 88. Neat BAMS samples showed more variability; while Antibody 86 maintained generally good reproducibility, Antibody 88 neat runs exhibited a notable decline in precision, reflecting potential influences from sample matrix complexity or limited replicate data.

These results reinforce the superior intra-assay performance of BAMS relative to ELISA, especially when employing spiked antibody protocols. They also highlight the challenges posed by neat plasma samples, where matrix effects and lower analyte levels may reduce assay consistency.

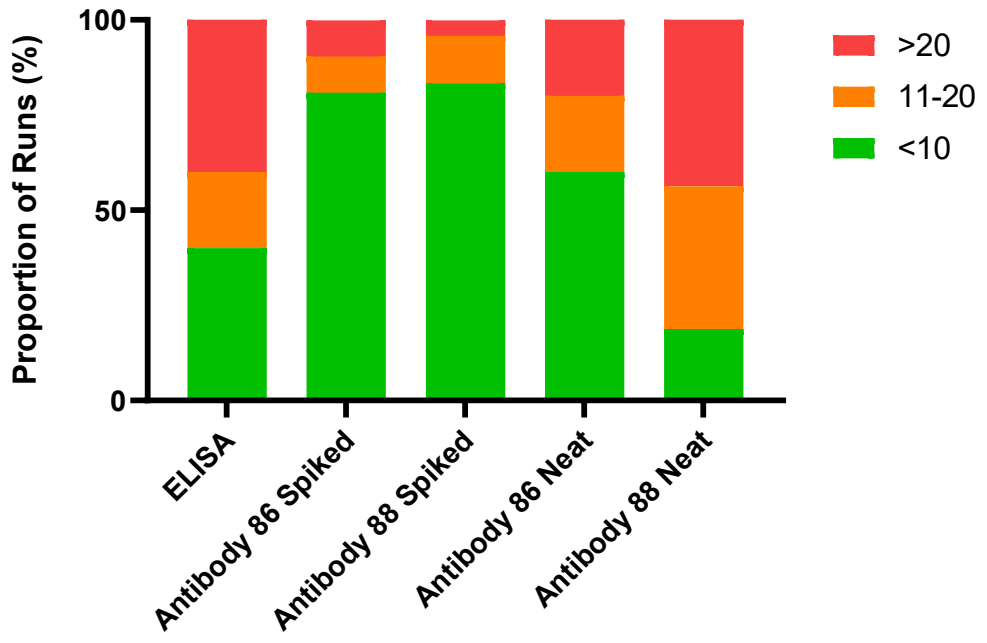

Figure 5.22 Intra-Assay variability comparison across ELISA and BAMS methods. Intra-assay variability comparison across ELISA and BAMS methods.

Each method's replicate runs were categorised by %CV into three quality thresholds: ≤10% (excellent), 11–20% (acceptable), and >20% (poor). For each category, the percentage was calculated by dividing the number of runs falling within that %CV range by the total number of intra-assay runs for that method.

Overall, the data indicate that BAMS assays, particularly when using spiked plasma samples with Antibody 88, offer superior intra-assay reproducibility compared to conventional ELISA. BAMS maintained higher precision, underscoring its potential as a more reliable platform for detecting ghrelin species in human plasma. However, the reduced consistency observed in neat plasma BAMS assays highlights the need to consider sample matrix effects and assay conditions when interpreting results. These findings support prioritising BAMS with spiked antibody formats for robust and reproducible ghrelin quantification in future studies.

5.3.6 Plasma Volume Reduction

All patient-derived plasma samples that we analyse in our laboratory are valuable resources. However, even more valuable, and difficult to obtain are samples that we receive from the central PD clinics, thus reducing the sample volume used per experiment would have a substantial impact on the analyses that we can perform. In the process of validating the use of BAMS, we chose to compare the well-established and widely used ELISA. Currently, the BAMS assay uses 250 µL per sample to analyse both acyl and unacylated ghrelin, whilst the ELISA kit uses 140 µL overall for both acyl and unacylated ghrelin. Thus, I attempted to validate the use of BAMS with a lower starting plasma volume. As such, plasma samples with and without exogenous ghrelin at a volume of 150 µL or 250 µL were compared. In the same manner as before, exogenous ghrelin was added at a concentration of 1 ng/100µL. No endogenous ghrelin was detected within the 150 µL sample volume, whilst endogenous ghrelin was detectable when using a sample volume of 250 µL (Figure 5.23). In the plasma ‘spiked’ with exogenous human ghrelin, there was a significant increase ($P<0.05$) in human acyl ghrelin in the 250 µL compared to the 150 µL volume.

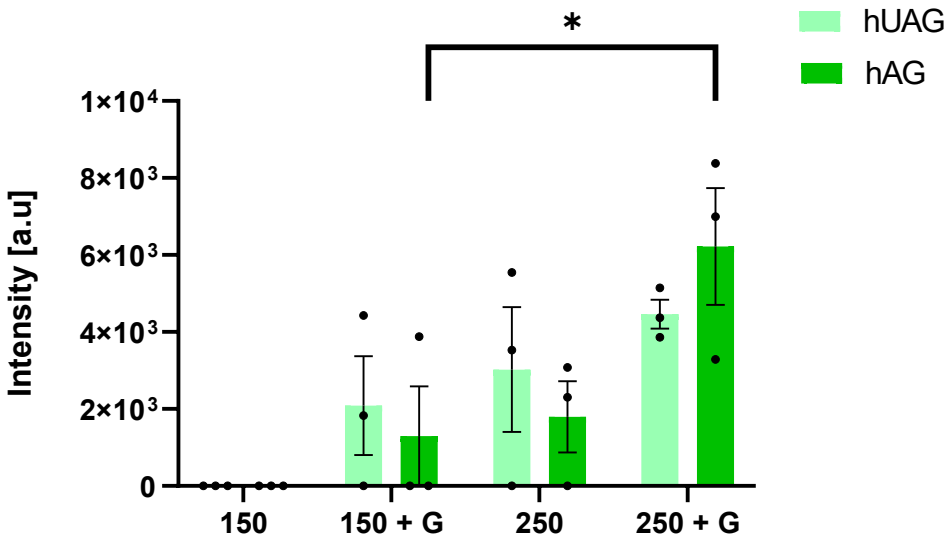

Figure 5.23 A comparison of the detection of ghrelin using different initial plasma volumes. 150 µL or 250 µL plasma volumes were analysed by BAMS (Antibody 88) either within 'neat' or 'spiked' plasma which included the addition of human ghrelin (+hG) at 1 ng/100 µL. Two-way ANOVA was performed with Tukey corrections. P<0.05 is considered statistically significant. N = 3, mean average plotted with SEM. *P<0. 05.

5.4 Discussion and Conclusion

This chapter aimed to 1) optimise a BAMS method that can detect endogenous human ghrelin and 2) assess the performance between the BAMS assay and the ELISA. The results of this study showed that BAMS could successfully detect endogenous human ghrelin with good reproducibility, although there is a current limit of detection. Furthermore, from the results, it was observed that the reproducibility of BAMS was on par with the ELISA kit, although ELISA sensitivity was greater overall. It is important to note that, in line with the manufacturer's recommendations and standard practice, ELISA measurements were performed in duplicate (such as, two wells per sample). In contrast, the BAMS assay utilised three beads per sample for comparative analysis. While a three-bead setup allows for more stringent reproducibility assessment, the two-well format used in ELISA inherently leaves slightly more room for variability. However, given that the ELISA is a well-established, validated method and two wells per sample is the widely accepted and published standard, this format was used to enable a fair and representative comparison between the established ELISA and the novel BAMS approach. The main limitation of these studies was the availability of

beads, which hindered testing larger sample sizes and further optimisation steps, which will be discussed below.

The introduction of an ISTD proved challenging, with the use of rat ISTD in some cases having a negative impact on the BAMS assay by hindering the signal of human ghrelin during MS analysis. In other cases, the rat ISTD was not detectable, suggesting a lack of binding to the antibody. Ghrelin has previously been analysed by IP-MS on MALDI-TOF, where human stable isotope-labelled and unlabelled peptides were used as an ISTD for rat plasma (Gutierrez et al., 2005). This concept is like the one tested herein, although in our case, the difficulties of binding both rat and human to the same antibody proved difficult. In Gutierrez et al., 2005, antibodies with specificity for the carboxyl terminus of the ghrelin peptide were used, which were bound to Dynal magnetic beads. Unfortunately, the exact binding mechanism of the antibody selected by Adeptrix was not disclosed to us. A deeper understanding of how antibodies were selected for the ghrelin BAMS kit would help to improve our understanding regarding the lack of binding to rat ghrelin and how to address and/or pursue alternative antibodies that may bind to different areas of the peptide. However, the use of a deuterated labelled human ISTD would be the best option for an ISTD (Thomas et al., 2021). As the deuterated human ghrelin standard would be closer in structure to the human ghrelin, it is likely to have fewer problems in terms of anybody binding. In addition, studies have previously shown that deuterated standards reduce ion suppression and increase methods precision, accuracy and repeatability compared to a structural analogue internal standard (Lanckmans, K., Sarre, S., Smolders, I., and Michotte, Y. 2007; Stokvis, Rosing, and Beijen 2005; Piórkowska, Musijowski, J., Buś-Kwaśnik, K., and Rudzki 2017).

Standard curves were generated using one human species against the other as an ISTD, to assess the limit of detection of ghrelin in the BAMS assay. Using this approach, the limit of detection for human acyl ghrelin was 312 pg/mL for antibody kit 86, whilst the limit of detection for antibody kit 88 was 40 pg/mL. Both antibodies 86 and 88 successfully detected human unacylated ghrelin down to levels of 20 pg/mL. In comparison, working levels for ghrelin IP-MS have previously been reported at 375 to 3750 pg/mL for acyl ghrelin, while unacylated ghrelin was reported at 211-2109 pg/mL (Gutierrez et al., 2005). As such, my project successfully detected unacylated and acyl ghrelin at levels lower than previously described for a similar immune-based

assay. In an alternative non-immune-based assay that used LC-MS/MS, the limit of detection level was observed at 30 pg/mL for unacylated and acyl ghrelin, with a signal-to-noise ratio (S/N) of 3, while quantification levels were 50 pg/ml with an S/N of 10 (Thomas et al., 2021). In healthy human patient samples, acyl ghrelin levels range from 0 to 200 pg/ml, while unacylated ghrelin ranges from 100 to 1500 pg/mL (Tong J, Dave N, Mugundu GM et al. and Eslami et al., 2016). As such, the current BAMS method needs optimisation to increase sensitivity to be able to compete with assays such as the ELISA, which can detect down to 2 pg/mL.

Another area that needs further optimisation is the volume of plasma that is being used. In my studies, 250 µL of plasma was used, allowing the successful identification of both acyl and unacylated ghrelin. While in the Bertin ELISA kits used in our laboratory for acyl and unacylated ghrelin require 180 µL of plasma. Hence, to enhance the efficacy of the BAMS kit, reducing plasma usage to 150 µL would prove advantageous. Although briefly explored in this chapter, the investigation involved assessing ghrelin levels using a reduced plasma volume of 150 µL compared to 250 µL. When analysing plasma volumes of 150 µL 'spiked' with exogenous human ghrelin (1 ng/100µL concentration), both human ghrelin species were detectable. However, human acyl ghrelin exhibited a significant decrease ($P<0.05$) in the 150 µL volume compared to the 250 µL volume of plasma. Since both volumes contained the same concentration of 'spiked' exogenous ghrelin (1 ng/100µL), the disparity observed is likely attributed to higher levels of endogenous ghrelin in 250 µL of plasma. Following discussions with our collaborators at Adeptrix, they suggested that using a plasma volume as low as 100 µL would be feasible if the number of beads used per sample was increased to 6. This is important to test, however, a delay in the supply of additional beads meant that there was no time to explore this further. Despite the lack of an effective ISTD, investigatory tests of antibody kits were performed.

The implementation of an ISTD is to correct for variability in dilutions, improve method validation, and assess instrument performance. In our case, the addition of an available ISTD (rat ghrelin) caused suppression of the human ghrelin species and in some cases the ISTD was undetectable, likely due to differential antibody binding or matrix interference. Likewise, a study by Stokvis et al. analysed the usage of different ISTD for a tubulin inhibitor (D-24851) and discovered that the quantification without ISTD resulted in improved results. Implementing an internal standard in their case

caused problems with accuracy and precision which was caused by ion suppression (Stokvis et al., 2004). This highlights the crucial role of collaborative academic-industry efforts, especially when working with proprietary reagents like the Adeptrix antibodies, whose binding sites are not disclosed. Such opacity limits the ability to rationally design ISTDs or interpret unexpected assay performance. A deuterated human ghrelin peptide would represent the gold standard, allowing for precise quantification and correction for sample loss or matrix effects. Moving forward, the development of fully characterised, epitope-mapped antibodies and peptide standards must be prioritised if BAMS is to be adopted as a clinically viable biomarker assay. This also underscores a broader translational lesson: for biomarker development to bridge discovery and diagnostics, full assay transparency and joint validation pipelines are essential.

The MALDI-TOF performance was tested every day with calibration before analysis. Also, a known amount of exogenous human acyl and unacylated ghrelin was tested every time to check performance.

For the BAMS assay, our collaborators provided us with two potential antibody kits, antibody 86 and antibody 88. We performed a comparative analysis of both antibody kits to select the most appropriate antibody. Overall, the assessment revealed that both antibodies exhibited comparable results for the intensity readings of AG:UAG. However, antibody 88 consistently demonstrated better reproducibility and precision. The evaluation of the 'spiked' plasma samples highlighted the consistency and reproducibility of antibody 88 compared to antibody 86. One trend shown in the reproducibility between the extraction of different donors for 'spiked' antibodies 88 and 86 (see Supplementary Table S1 and Figure S4), was a reduced R^2 value for run 3. Supplementary Table S1 highlighted that the reduced value of R^2 was obtained from donors 1 and 2, withdrawal 1. Here, runs 1 and 2 obtained similar values whilst run 3 was different. Investigations into the dates these runs were performed highlighted that the first two runs for donor 1 and 2, withdrawal 1 were performed in February 2023 while run 3 and the rest of the experiments were performed in late April-June 2023. During this period, a slight adjustment was made within the protocol due to concerns about the dehydration of the beads. It is plausible that this adjustment influenced the lower ratio values observed in runs 1 and 2 from donor 1, withdrawal 1. Lastly, considering that this is a new protocol, it is conceivable that improvements in technique between the February and April time frames might account for the improved bead

performance observed in the later runs. It was also observed that acyl ghrelin was occasionally detected at levels close to the signal-to-noise ratio (Supplementary Figure S4), which altered the readings of the AG:UAG ratio and resulted in reduced CV values. The signal-to-noise ratio was determined following the company's established protocol, using a threshold of 1.5. However, adjusting the signal-to-noise ratio threshold to 3 (Thomas et al., 2021) could prevent such instances as it increases the meaningfulness of a signal.

As highlighted in the introduction to this chapter, IP-based techniques often face reproducibility and specificity challenges due to antibody variability. In this study, we attempted to address this by evaluating two different antibody kits (antibody 86 and 88) for their performance in capturing human ghrelin species using an in vitro approach, a standard strategy in biomarker development. These comparative assessments are crucial in validating both the sensitivity and specificity of antibodies prior to clinical translation. Such in vitro validation steps align with biomarker qualification frameworks used in both academic and industrial settings, wherein specificity, reproducibility, and signal-to-noise ratio must be rigorously assessed before progressing to larger cohort studies or clinical validation trials. Here, antibody 88 demonstrated superior reproducibility, suggesting better epitope targeting or binding affinity, though the undisclosed epitope details remain a limitation to full mechanistic insight.

Overall, ‘spiked’ plasma samples analysing the AG:UAG ratio, had lower CV values compared to 'neat' plasma samples. The ‘spiked’ plasma samples contain an additional variable for human error during preparation or the addition of the exogenous ghrelin to create the ‘spiked’ sample. Despite this, the lower CV values within the ‘spiked’ plasma samples suggest minimal human error throughout the protocol. Higher CV values in the 'neat' plasma sample are an issue of sensitivity when ghrelin levels fall near or below the detection limit, resulting in poor CV values or unreadable values.

Comparison between the BAMS assay and a commercial ELISA kit showed the potential of the BAMS assay to perform to the same standard when peptide levels were not low. The BAMS assay demonstrated comparable, and sometimes better, reproducibility in capturing ghrelin, particularly in ‘spiked’ samples. One noteworthy aspect is that the ELISA kit can successfully detect acyl ghrelin at low levels of 2 pg/mL

and be able to detect acyl ghrelin levels in all donors. This contrasts with the BAMS assay, which did not achieve the same level of sensitivity. Optimising the BAMS assay to attain an improved lower limit of detection would enable a more direct comparison of both assays.

Additionally, it should be noted that the ELISA assay was conducted approximately three months after the BAMS experiments. While both assays used plasma samples stored under identical conditions, the delay in analysis may introduce temporal or storage-related variability. Nonetheless, this reflects a realistic scenario in research workflows where batch processing and equipment availability often impose temporal separation between assays. Despite this, the ELISA results still aligned well with expected concentrations in endogenous plasma, suggesting sample integrity was largely maintained. Importantly, any comparison between the two platforms should consider these temporal factors, particularly in relation to peptide degradation and assay reproducibility over time. While ELISA remains the gold standard for measuring ghrelin due to its sensitivity (down to 2 pg/mL), it is limited in multiplexing capability and often requires larger plasma volumes. The BAMS assay, while currently less sensitive, showed comparable reproducibility in spiked samples and offers the potential for multiplex analysis from a single sample, an advantage in biomarker panels. For acyl ghrelin detection, which is particularly labile, the reduced pre-analytical handling and direct MALDI-MS readout offer reduced degradation risks compared to ELISA. However, until the lower detection threshold of BAMS approaches that of ELISA, its utility as a standalone diagnostic tool remains constrained. To become a viable alternative, BAMS workflows must undergo sensitivity improvements, potentially through increased bead count, deuterated ISTD integration, and improved antibody selection.

The BAMS technique has previously assessed site-specific phosphorylation of eukaryotic initiation factor 4E-binding 1 and ribosomal protein S6 in response to stimulatory treatments such as kinase inhibitor effects. It has also been used to profile select cytokine-regulated transduction factors and histone H3 protein modifications (Hamza et al., 2020). Unlike my method of BAMS, which captures proteins from plasma, in these published studies the proteins were captured from cell lysates. This method shows success in capturing and identifying all proteins but to note the proteins extracted from cell lysates were 100-200 µg in comparison our lower limit of detection

is 0.32 µg for acyl ghrelin or 0.04 µg for unacylated ghrelin. This demonstrates the success of the BAMS at a higher concentration.

Other than the BAMS technique, analytical methods to measure plasma AD biomarkers have been developed in the past few decades, to offer alternatives to the ELISA. One of the first technologies to offer an alternative was the use of multiple analyte profiling (xMAP) technologies which, similar to the BAMS, could simultaneously measure Aβ40, Aβ42, total tau, and pTau isoforms (Herskovtis, Locascio, Peskind and Hyman 2013). The semi-automated Luminex xMAP assays successfully obtained a higher sensitivity than the ELISA but poor reproducibility of the assay across different laboratories was reported (Song, Poljak, Valenzuela, Mayeux, Smythe and Sachdev 2011). In addition, a SIMOA was developed to detect AD biomarkers. SIMOA can detect protein concentrations at femtogram concentrations compared to ELISA which can detect at picogram concentrations (Wilson et al., 2016; Kuhle et al., 2016). Despite its success, the SIMOA is costly and therefore not currently a viable option for many laboratory groups. In terms of using IP-MS to quantify plasma biomarkers, success has been shown with reliable protein quantification for Aβ and pTau when interfaced with LC-MS (Janelidze et al., 2022; Hu et al., 2022). Additionally, some of these assays have been used as Laboratory Developed Tests (LDT) in the United States (Janelidze et al., 2021, Quest Diagnostics). Janelidze et al. used an IP-MS-based method developed at Washington University (IP-MS-WashU). This method involves spiking plasma samples with 1 ng of ^{15}N-labelled recombinant 2N4R tau as ISTD, followed by a sample preparation of precipitating the protein, SPE, and lyophilisation by SpedVac. After sample preparation, the samples were immunoprecipitated with Tau1 and Hj8.5 antibodies and digested with trypsin. The digests were ‘spiked’ with 50 and 5 fmol of unphosphorylated and phosphorylated peptide and purified by a further SPE. The eluate was lyophilised and resuspended in 25 µL of 2% acetonitrile and 0.1% formic acid in MS-grade water, before nano-LC-MS analysis (Barthelemy et al., 2020). Despite the success of IP-MS interfaced with LC-MS, these methods still require a labour-intensive sample preparation protocol, highlighting the need for an IP-MS assay that reduces burdensome steps, such as BAMS.

The decision to utilise the BAMS-MALDI format over a BAMS-LC/MS workflow was based on several practical and methodological considerations. Firstly, the BAMS-

MALDI platform provided direct compatibility with the Adeptrix BAMS technology without the need for extensive LC optimisation or sample dilution, which could compromise low-abundance peptides like acyl ghrelin. Secondly, MALDI-TOF provides rapid acquisition and robustness in high-throughput environments, a critical consideration for potential diagnostic implementation. While LC-MS/MS offers superior sensitivity and dynamic range, it typically requires more complex sample preparation, extended runtime, and technical expertise, which limit its scalability for routine clinical diagnostics. Given the trade-off between simplicity and sensitivity, BAMS-MALDI presents a pragmatic midpoint that, with further optimisation, could bridge research and diagnostic workflows.

Looking forward, the integration of IP with MS presents a promising avenue for diagnostic biomarker development. While traditional IP-MS methods are labour-intensive, BAMS offers a streamlined, semi-automated platform with multiplex capacity and reduced sample handling. However, for it to serve as a translational diagnostic tool, several challenges must be addressed: antibody specificity and disclosure, standardisation of internal controls, and assay reproducibility across labs. In the context of neurodegenerative diseases, where multi-analyte panels (e.g., ghrelin, Aβ, tau, NfL) are increasingly necessary, a multiplexed BAMS platform with optimised sensitivity could provide a scalable and robust diagnostic solution. Future work should involve testing BAMS in larger cohorts, assessing its reproducibility across different sites, and refining the workflow to reduce plasma volume and increase throughput, ultimately setting the stage for regulatory approval and clinical adoption.

In summary, the BAMS assay provides a promising approach for analysing ghrelin in plasma samples that has the potential to surpass current methods. Additionally, the BAMS technology has multiplexing capabilities that would allow the analysis of additional biomarkers (for example, AB, Tau, NfL) from a single plasma sample. Future BAMS protocols should consider including these established biomarkers alongside ghrelin to provide a better understanding of the disease.

Chapter

6. General Discussion

6.1 Conclusions and Discussion

Throughout my doctoral work, my objective has been to optimise a mass spectrometry method with sensitivity to detect endogenous ghrelin peptides. The method optimisation for each distinct MS technique, MALDI-TOF, LC-MS (Inoue et al., 2023) and BAMS was lengthy; methods were developed that successfully identified exogenous peptides however, they fell short in detecting endogenous ghrelin peptides, either due to complications in sample preparation or due to issues with the limit of detection and/or sensitivity.

The LC-MS chapter (chapter 4) focused solely on the development and optimisation of a sensitive method for detecting endogenous ghrelin using both bottom-up and top-down approaches. The top-down approach detected intact ghrelin peptides. Top-down MS has advanced rapidly over the past decade and has helped to understand biological functions (Melby et al., 2021; Tucholski et al., 2020) and disease mechanisms (Melby et al., 2021; Ntai et al., 2018), along with the discovery of new biomarkers such as discovering new and unique protein S-thiolation switch (Melby et al., 2021; Ansong et al., 2013). One complication with using a top-down method to detect ghrelin is that ghrelin generates multiple charge states during ESI, which decreases assay sensitivity. Decreasing the number of ghrelin charged states via the addition of DMSO in the mobile phase increased the sensitivity of the assay, which is consistent with previous studies (Thomas et al., 2021; Meyer, JG, Komives EA 2012). Despite this, we could not detect exogenous ghrelin at concentrations below 0.4 pg/mL. Top-down MS methods of identifying intact proteins is approximately 100-fold less sensitive than bottom-up MS approaches, which include enzymatic digestion of the proteins (Timp and Timp 2020). Thus, we used trypsin to digest ghrelin peptides before LC-MS analysis which led to the generation of a dominant [M+2H]2+ charged state. However, the use of trypsin on ghrelin peptides highlighted the instability of both the intact and enzymatically digested ghrelin peptides. In support of this, it has previously been reported that ghrelin peptides can become unstable easily, depending on the acidity of the solution (Hosoda and Kangawa et al., 2004). As discussed in Chapter 4, ‘online’ tryptic digestion may offer a more stable and sensitive method for future consideration.

Using LC-MS/MS as a technique for identifying blood-based biomarkers has shown in some cases, great success. For example, an AHEAD 3-45 study (double-blind,

placebo-controlled, parallel-treatment arm study in participants with preclinical AD and elevated amyloid (A45 Trial) and participants with early preclinical AD and Aβi (A3 Trial)) supported the use of plasma pTau217/novel pTau217 as a screening test for preclinical AD using an LC-MS/MS method which involved a Waters Acquity M-class UPLC coupled to a Thermo Scientific Fusion Lumos Tribrid MS (Rissman et al., 2023). Beyond this, Inoue et al. developed an LC-MS/MS method to identify 45 plasma proteins as biomarkers for MCI and AD (Inoue et al., 2023). They used a bottom-up approach whereby plasma underwent tryptic digestion, where a 1:5 trypsin:peptide ratio was used, compared to the method described within this thesis where a 1:20 trypsin:peptide was used. LC-MS/MS analysis was conducted using a triple quadrupole mass spectrometer LC-MS-8060 system with an Aeris PEPTIDE XB-C18 column, similar to the method used herein where a C18 column was used for ghrelin separation. Using this method, they identified eight plasma protein biomarkers (albumin, APOC1, complement component 3, complement component 4 gamma chain, alpha-2-antiplasmin, alpha-2-macroglobulin, hemopexin, alpha-1-B-Glycoprotein) that could distinguish between MCI and AD with the clinical potential assessed using receiver operating characteristic (ROC) analysis, which yielded 0.83 for males and 0.71 for females (Inoue et al., 2023). Another LC-MS/MS method developed analysed tryptophan metabolites using the top-down approach in the urine of patients with PD (Chung et al., 2023). Here, a UPLC-MS/MS system was used coupled to an API 3200 triple quadrupole mass spectrometer where urine samples were injected onto a C18 column after protein precipitation and concentration by drying under Nitrogen. For the first time, indole-3-acetic acid was reported as a potential biomarker for PD due to its aberrantly high urinary levels in PD compared to healthy controls. Watson et al. (2023) reported an SRM-MS method that can quantify CSF protein biomarkers which were mainly neuronal proteins (VGF, NPTX2, NPTXR and SCG2) across stages of AD. Here, the peptides were analysed using a triple quadrupole mass spectrometer coupled to a 1290 Infinity II UHPLC system, with the UHPLC system having better resolution than the HPLC system used in this thesis. The mass spectrometer described throughout this thesis can perform both SRM and MRM at a resolution of 0.15-3 full width at half maximum (FWHM), whilst the mass spectrometer described within the paper can only perform SRM but still at a good resolution of 0.2-2 FWHM. The sensitivity of the MS instrument used herein is comparable if not better than some of the instruments described above. Thus, the lack

of sensitivity and LOD seen during the analysis of ghrelin should not be an instrumental factor.

Using MALDI-TOF we detected exogenous ghrelin at 0.08-80 ng/mL levels, R2 = 0.99. However, signal suppression due to contamination of PEGs prevented reliable detection of endogenous ghrelin. Although ghrelin detection by MALDI-TOF is well documented (Satou et al., 2010, Schopfer et al., 2015, Bender et al., 2019), in general, MALDI-TOF is used more effectively alongside IP-MS for blood-based biomarkers, which will be discussed below. In 2020, Abe et al. detected four new peptide biomarkers in serum (Fibrinogen β chain, α2-HS-glycoprotein, fibrinogen α chain and plasma protease C1 inhibitor) that can discriminate between control, MCI, and AD patients, with 87% sensitivity and 65% specificity. The peptide sequences were analysed using the ultrafleXtreme TOF/TOF, which is the same instrument used as described in Chapter 3 of this thesis. Thus, despite the problems described herein, MALDI-TOF can still be used effectively to detect serum-based biomarkers.

As described in Chapter 5, I optimised the use of BAMS, which removes multiple stages of sample preparation, to immuno-capture ghrelin peptides. Although BAMS itself is novel with little supporting literature, IP-MS, in general, has risen in popularity. Several IP-MS methods coupled either to LC-MS or MALDI-TOF have been developed to assess biomarkers for dementia, examples of which are discussed below. IP-MS has been used for the isolation of Aβ peptides from plasma with some studies focusing on IP-MS coupled to MALDI-TOF (such as Kaneko et al (2014) and Nakamura et al. (2018)), while others couple IP-MS with LC-MS/MS (such as Ovod et al. (2017) and Keshavan et al. (2021)). One study by Pannee et al. (2014) used MALDI-TOF followed by LC-MS/MS to confirm the identification of the Aβ peptides. Nakamura et al. (2018) measured amyloid-β precursor protein (APP)669-711/amyloid-β (Aβ)1-42 and Aβ1-40/Aβ1-42 ratios, and their composites through IP-MS LC-MS and demonstrated high AUC (94-96%) alongside an accuracy of 80% when compared against PET scanning (Nakamura et al., 2018). In support of IP-MS being used alongside LC-MS effectively, Keshavan et al measured plasma amyloid-β1-42/1-40 with an AUC of 0.82, using a Dionex Ultimate LC system and a Thermo Scientific Q Exactive Quadrupole-Orbitrap, which both perform similarly in terms of sensitivity and resolution compared to the instruments used within Chapter 4.

In a head-to-head comparison, the LC-MS-IP-MS measurements of pTau217 provided the highest accuracy for assessing the presence of Aβ pathology compared to other immunoassays such as the SIMOA and the Lumipulse (Janelidze et al., 2022). For IP-MS coupled to MALDI-TOF, Hirtz et al. (2023) compared the IP-MS technique developed by Shimadzu (IMPS_Shim Aβ42, Aβ40) against the SIMOA Human Neurology 3-PLEX A assay (Aβ42, Aβ40). They reported that the IP-MS method can detect the decrease in plasma Aβ42 that is specific to AD patients when comparing the Aβ40/Aβ42 ratios to those with MCI (AUC 0.78), subjective cognitive impairments (AUC 0.91), other neurodegenerative disease (AUC 0.89) and other neurological disorders (AUC 0.89). The SIMOA performed modestly with AUC ranging from 0.60-0.84 (Hirtz et al., 2023). As of yet, there is no literature on the use of BAMS in the analysis of analytes in patient samples, and thus it is difficult to assess the true effectiveness of the technique. These findings underline the evolving role of mass spectrometry-based methods and immunoassays for blood-based biomarker detection, each with distinct advantages and limitations. To provide a clear overview of the relative strengths and weaknesses of each platform evaluated in this thesis, Table 6.1 summarises the key analytical and practical features of ELISA, BAMS, and LC-MS/MS for ghrelin detection in plasma.

Feature	ELISA	BAMS	LC-MS/MS
Sample Volume	180 µL	250 µL	Variable
Limit of Detection (Acyl Ghrelin)	~2 pg/mL	40 pg/mL	~30 pg/mL
Reproducibility	High (low conc.)	Comparable to ELISA	High
Sensitivity	Highest	Moderate	High
ISTD Use	N/A	Challenging (rat ISTD issues)	Rat ghrelin standards effective
Multiplex Capability	Limited	High potential	Moderate
Sample Preparation Complexity	Low	Moderate	High
Cost	Moderate	Potentially low to mid	High

Table 6.1 Comparative summary of ghrelin detection platforms evaluated in this thesis. Parameters include sample volume, analytical sensitivity, reproducibility, cost, and overall utility for plasma biomarker quantification.

Beyond the mass spectrometry techniques described throughout this thesis, there has been a rise in the development of new platforms and immunoassays for measuring blood-based biomarkers. One such development is the next generation ELISAs, specifically the EUROIMMUN ELISA which uses C-terminal and N-terminal antibodies, whilst most previous ELISA do not. A head-to-head comparison of the EUROIMMUN ELISA to the SIMOA for the accuracy of Aβ40/ Aβ42 measurements within plasma as well as the Aβ42/tau ratio was carried out. The measurement of the Aβ40/ Aβ42 ratio was similar and methods correlated to the same extent with amyloid PET and CSF Aβ42/tTau (De Meyer et al., 2020). The EUROIMMUN ELISA is still new with more head-to-head tests needed for blood-based biomarkers. Outside of this, the EUROIMMUN ELISA has been studied for CSF Aβ42 and Aβ40/Aβ42 ratio within large studies of clinically heterogeneous cohorts. These studies demonstrated that CSF Aβ42 predicts amyloid PET positivity with a higher degree of accuracy with AUCs of 0.81-0.89, additionally, the Aβ40/Aβ42 ratio showed improvement performance with AUCs of 0.87-0.96 (Janelidze et al., 2016, Janelidze et al., 2017).

Another assay is the SIMOA. In terms of blood Aβ, it was first reported that there were no or weak correlations between plasma Aβ40 and Aβ42 biomarkers, between controls, AD and MCI patients (Janelidz et al., 2016, Verberk et al., 2020). To distinguish between Aβ+ and Aβ- patients identified by PET scanning, Janelidze et al. reported a modest AUC of 0.60-0.62 for plasma Aβ, while Verberk et al. reported 0.66-0.79. More recently, Thijssen et al. reported discrimination between Aβ+ and Aβ- patients with AUC 0.95 vs 0.85 and reported a strong correlation between plasma Aβ40/Aβ42 ratio and CSF Aβ42 (r=0.71 vs r=0.53) (Thijssen et al,. 2020). In terms of using SIMOA in the identification of tau variants, Bayoumy et al. reported high analytical and clinical performance alongside correlations in six different SIMOA assays for three different tau variants using plasma. These included three assays for pTau181 (Eli Lilly, ADx, Quantrix), one for pTau217 (Eli Lilly), and two for pTau231 (ADx, Gothenburg) (Bayoumy et al., 2021). In addition, Ashton et al. reported diagnostic accuracy of plasma pTau217 whilst using SIMOA. The study involved 786 participants, and they reported high accuracy in identifying tau pathology (AUC 0.93-0.97) alongside elevated Aβ (AUC 0.92-0.96) with the accuracies being comparable to CSF biomarkers (Aβ42/40, pTau, and tTau) in determining abnormal PET signals (Ashton et al., 2023). In a comparison of SIMOA with LC-MS analysis, pTau217

diagnostic performances between the both were highly comparable, whilst pTau181 and pTau231 had lower performance in the LC-MS method compared with SIMAO (Therriault et al., 2024). In general, the SIMOA assay presents certain limitations, notably in terms of cost, as the kits are more expensive than traditional ELISA kits. Additionally, the detection instrument is costly and limited to SIMOA analysis and needs specialised training, thus it may be difficult introduce into a clinical laboratory. In contrast, while mass spectrometry also entails expensive instrumentation, these instruments are often accessible within institutes and hospitals and are not restricted to a single type of assay.

Another form of immunoassay is the Meso Scale Discovery platform (MSD) which allows multiplexing. The MSD plate is a working electrode surface where capture antibodies are immobilised on well-defined spots. Vogelgsang et al. showed a moderate correlation between CSF and plasma Aβ40/Aβ42 ratio (Vogelgsang et al., 2018). A head-to-head comparison of SIMOA versus MSD when analysing pTau217, pTau181, and pTau231 was conducted using 200 participants with 177 being cognitively unimpaired and 23 had MCI. For samples from cognitively unimpaired patients, both pTau217 and pTau181 MSD (AUC0.80-0.81) outperformed the SIMOA (AUC 0.70) (Mielke et al., 2021). Janelidze et al also showed success of the MSD in measuring plasma pTau181. In their study, plasma pTau181 was measured in three cohorts with a total of 589 individuals including cognitively unimpaired, MCI, AD, and non-AD neurodegenerative disorders. Plasma pTau181 was reported to increase in preclinical AD and further increased at the MCI and dementia stages. It also showed a good correlation with CSF pTau181, with an AUC of 0.87-0.91 for different brain regions. Additionally, plasma pTau181 was able to differentiate between AD dementia and non-AD neurodegenerative disease with an accuracy similar to that of Tau PET and CSF pTau181 (AUC 0.94-0.98) analysis (Janelidze et al., 2020).

Multiplexed ELISA platforms are increasingly being utilised in clinical laboratory environments, particularly for applications in oncology, infectious diseases, and autoimmune disorders, where multiple analytes can be quantified simultaneously from minimal sample volume (Ellington et al., 2010; Bjerner et al., 2015). In the context of neurodegenerative disease diagnostics, platforms such as Luminex xMAP and MSD have been adopted in research and reference laboratories to measure panels of biomarkers, Aβ, total tau, and phosphorylated tau in cerebrospinal fluid. Although

these multiplex immunoassays are CE-marked (meets European standards) and have demonstrated clinical utility in specialist centres, they are not yet widely deployed in routine NHS diagnostics for dementia. However, initiatives such as the UK's Blood Biomarker Challenge are actively piloting the use of multiplex blood tests for early dementia detection, suggesting that broader clinical implementation is imminent (Alzheimer's Society, 2025). These developments align with a shift in diagnostic strategy, favouring biomarker panels over single-analyte assays to capture the multifactorial nature of neurodegenerative conditions. Thus, multiplex ELISA and related platforms are positioned to play a central role in future clinical screening, provided issues of standardisation, regulatory approval, and integration into NHS workflows are addressed.

Cournut et al. (2024) recently published a new technique to compete with IP-MS, coined surface-assisted MALDI (SALDI-MS). Here, they investigated whether SALDI-MS can monitor the Aβ40/Aβ42 ratio without any prior sample treatment. Although the other IP-MS techniques described previously show success in terms of sensitivity for detecting the Aβ40/Aβ42 ratio, the drawbacks include time-consuming preparatory procedures and the potential loss of biomarkers due to the non-direct two-step procedure (IP followed by MS). SALDI-MS involves samples being deposited onto an inert material. Despite their success in detecting Aβ40 and Aβ42 without aggregation, their detection limit remained too high for a meaningful determination of the Aβ40/Aβ42 ratio (Cournut et al., 2024) but brings to light another new technique for identifying biomarkers with a reduced workflow.

As described, the development of new ultrasensitive, high throughput assays has led to discoveries and potential clinical applications for promising biomarkers that can discriminate between different dementias and neurodegenerative disorders. However, there is still a need to do more direct comparisons of assay performance, conduct further studies with larger cohorts from diverse backgrounds, and evaluate the use of multi-marker panels.

6.2 Limitations of Body Fluid-Based Biomarkers

Several body fluid biomarkers for neurodegeneration have emerged, with plasma biomarkers being well-researched as a practical source due to its ease of collection. However, there can be disadvantages in some contexts; for example, some biomarkers are only present at low levels in the blood. This has driven the development of increasingly sensitive and selective assays, yet challenges remain in balancing sensitivity with assay reproducibility and scalability for clinical use. Many blood-based assays still require validation in large, diverse cohorts before being considered clinically actionable. Here we discuss and compare the range of biomarkers currently being developed in the context of dementia and the advantages and disadvantages of targeting analytes within CSF, plasma, serum, and urine.

The plasma Aβ40/Aβ42 ratio has a good correlation with Aβ deposition identified by PET scans (AUC 0.84) and with CSF measurements (AUC 0.85) (Li et al., 2021). It has been shown using different platforms of analysis such as immunoassays and IP-MS. As discussed above, the plasma Aβ40/Aβ42 ratio is lower in Aβ+ groups than Aβ-negative groups, regardless of the cognitive status of the cohort; however, individual Aβ40 and Aβ42 are reduced in AD dementia (Janelidze et al., 2016; Ovod et al., 2017; Nakamura et al., 2018). Despite this, a limitation arises from the variation of the Aβ40/Aβ42 ratio across the different assay platforms. For example, IP-MS assays detected Aβ pathology with an AUC of 0.84–0.87, while other immunoassays fell short of acceptable performance (AUC 0.64–0.69) (Janelidze et al., 2021). This discrepancy highlights a core limitation in assay development: platform-to-platform variability. Differences in antibody specificity, sample preparation protocols, detection sensitivity, and calibration strategies significantly impact inter-assay agreement. As such, standardisation and harmonisation efforts are urgently needed if these assays are to be widely adopted in routine diagnostics.

Different pTau isoforms in plasma including pTau181, pTau217, and pTau231 have also shown reliable detection of AD (Mielke et al., 2018; Palmqvist et al., 2020; Ashton et al., 2021). Head-to-head comparisons of the pTau isoforms demonstrated that pTau217 is a better detector of AD pathology and future development of AD; however, these results are only based on three studies (Mielke et al., 2021; Janelidze et al., 2022; Ashton et al., 2022). In a study by Janelidze et al., they reported a high correlation between plasma and CSF levels of pTau217 (Janelidze et al., 2022). Both

pTau217 and pTau181 showed a correlation with Aβ plaques and tau tangles, with pTau217 again showing a stronger correlation between pathologies (Mattson-Carlgren et al., 2022). Whilst Aβ plaque load seems to be associated with pTau231, with increases seen at small Aβ plaque levels, Aβ plaque load does not seem to be associated with levels of pTau217 and pTau181 (Therriault et al., 2022). Currently, there are no specific plasma-based tau tangle biomarkers; however, there are potential biomarkers in CSF for measuring the microtubule-binding region of tau (Horie et al., 2021). The development of tau tangle-specific assays remains technically complex, especially in plasma, due to both low abundance and the need for highly selective reagents capable of distinguishing structurally similar isoforms. These limitations underscore the need for high-fidelity antibody development and improvements in signal amplification methods.

As both Aβ and tau can be cleared by the kidneys, another route for detecting these proteins is within the urine (Tian et al., 2021), an ideal biomarker source for those who are afraid of needles. Despite this, research on urine biomarkers is still limited. Upon testing for Aβ monomers by ELISA and Aβ oligomers using western blotting, it was discovered that the Aβ oligomer concentrations in both plasma and urine correlated negatively with cognitive function, and both were able to differentiate between AD patients and controls (Zhou et al., 2012). In another study, both Aβ40 and Aβ42 alongside pTau levels were tested in exosomes isolated from clinical urine samples using ELISA. Here, it was shown that exosomes were significantly increased with Aβ42 and pTau concentration detected in AD patients; however, the relationship between exosome levels and AD pathology was not determined (Sun et al., 2019). More recently, a chemoresistive platform based on a polypyrrole bioelectrode was developed, which successfully detected Aβ40 and Aβ42 at concentrations as low as 5.71 fg/mL and 9.09 fg/mL, respectively, but was only tested using synthetic samples in PBS/plasma (Supraja et al., 2021). While these results demonstrate promising analytical sensitivity, the lack of validation in clinical samples limits translational relevance. Furthermore, newer detection modalities often lack scalability, robustness, and reproducibility across laboratories—key hurdles that must be addressed before clinical deployment. As such, there is still a need to test this assay on urine samples and assess how it compares to PET scans and CSF measurements. Given the ease of obtaining urine samples, there is a need for more research in this area.

Using both SIMOA and ELISA, tTau, pTau, and Aβ42 levels were tested using the saliva, plasma, and urine of AD patients and healthy controls. Although tTau and pTau levels were significantly higher in AD patients compared to controls, the levels in urine (96.76, 118.68, and 16.88 pg/mL for Aβ42, tTau441, and pTau181 respectively) were much lower than in plasma (340.07, 669.44, and 493.79 pg/mL for Aβ42, tTau441, and pTau181 respectively) (Chan et al., 2017). As a result, the biomarkers for tau have focused on blood-based biomarkers. Despite this, more recent research by Rutledge et al. compared 4,877 CSF, blood plasma, and urine samples for PD biomarkers. Here, hundreds of proteins were found to be upregulated in the CSF, blood, or urine of PD patients, with one promising biomarker for early PD being DOPA decarboxylase (DCC). DCC catalyses the final step in dopamine synthesis and was seen particularly to be upregulated in the CSF and urine of PD patients, making it a promising diagnostic and prognostic marker (Rutledge et al., 2024). However, translating such proteomic findings into robust, high-throughput assays suitable for clinical use involves extensive optimisation, including selection of detection antibodies, reduction of background interference, and establishment of clinically meaningful thresholds. Therefore, despite the difficulties in using these particular biofluids, there are still some very recent successes through their use.

Plasma neurofilament light chain (NfL) has also shown promise with a good correlation to CSF measurements (Gisslen et al., 2016). Despite NfL levels being associated with neurodegeneration in AD, the association is weaker with plasma than with CSF. Serum levels of NfL also showed a strong association with CSF levels ($P < 0.001$) (Disanto et al., 2017) and plasma levels. More specifically, it was reported that the median levels of NfL were significantly higher in serum compared to plasma (Kwon et al., 2023). This discrepancy highlights the importance of matrix selection in assay development. Serum and plasma differ in protein content, clotting factors, and pre-analytical stability—all of which influence assay output. Developers must consider these variables to optimise sensitivity, specificity, and reproducibility.

Plasma glial fibrillary acidic protein (GFAP) levels have also shown a good correlation with Aβ pathologies alongside the prediction of cognitive decline and conversion to AD dementia in cognitively impaired individuals and patients with mild cognitive impairment (Benedet et al., 2021; Verberk et al., 2021; Cicognola et al., 2021). In a comparison of all the biomarkers discussed, using the SIMOA platform, Sanchez et al.

investigated GFAP, NfL, pTau181, and Aβ40/Aβ42 in 44 healthy controls and 480 participants diagnosed with AD/MCI, Parkinson's disease, frontotemporal dementia, or cerebrovascular disease (Sanchez et al., 2023). It was reported that GFAP, NfL, and/or pTau181 were elevated among all diseases compared to controls, whilst pTau181 was specific to the AD/MCI patients, and sparse associations were found in the frontotemporal dementia and cerebrovascular disease cohorts for the Aβ40/Aβ42 ratio. Additionally, Mattson-Carlgren et al. used SIMOA to measure plasma pTau181, pTau231, NfL, GFAP, and N-terminal tau within their study to evaluate plasma biomarkers for identifying Aβ positivity and stage of tau accumulation. It was reported that pTau217 was most strongly associated with Aβ positivity (AUC 0.94) (Mattson-Carlgren et al., 2024). Despite these successes, current ultra-sensitive platforms such as SIMOA are costly and require specialised infrastructure. Multiplex assay development must also account for cross-reactivity between analytes, potential signal interference, and technical variability between batches and operators. These factors collectively challenge assay reproducibility and broader clinical adoption.

In conclusion, while body fluid biomarkers, particularly plasma-based ones, offer promising avenues for detecting neurodegenerative diseases like AD, challenges such as low analyte levels, assay variability, and limited correlations with gold-standard measurements like PET scans and CSF analyses underscore the need for further research and refinement in this field. Future efforts should focus on assay harmonisation across platforms, expansion of validation studies in preclinical and prodromal populations, and technological innovations that enable high-throughput, low-cost, and reproducible measurements in routine clinical settings.

6.3 Limitations of the Work

One of the limitations of the thesis was the instrumentation used for mass spectrometry analysis. Limitations included instrument malfunction which created delays in the progress of the project. However, it was rare for all instrumentation to be unusable at the same time, and therefore during the periods when either the LC-MS or MALDI-TOF were being investigated, progress could still be made on the instrument that was not 'broken'. Another limitation in the instrumentation was the availability of only an HPLC system rather than a UHPLC system. The UHPLC system has been shown to increase the sensitivity of ghrelin detection, increase chromatographic resolution, and obtain shorter analytical run times, which would not only reduce the cost of the analysis but also allow faster progress within optimisation (Behnoush et al., 2015 and Thomas et al., 2021). Additionally, the current detectors within the MS were old and were waiting for an upgrade, which also could have potentially resulted in a decreased sensitivity.

One of the major limitations of the BAMS assay was the limited availability of beads, which ceased further optimisation and left the studies incomplete. The limited availability of beads also led to the measurement of ghrelin in only a small pool of healthy donors (5 in total). In addition to this, no correct internal standard was used to quantify ghrelin within the assay and as such the inclusion of an appropriate ISTD should be assessed. Due to the collaboration with Adeptrix, we were also unaware of the specific antibody being used, and therefore, we could not gain insight as to which terminal the antibody was binding. Information as such may have aided in the optimisation of using rat ghrelin as an internal standard in place of a costly isotope labelled human ghrelin standard. Another limitation within the chapter while comparing the BAMS and ELISA assays is that the ELISA using healthy donor samples was only carried out once due to time constraints and the availability of the ELISA kit. This allowed us to make a direct comparison with the sensitivity of the kit and the intra-assay variation but requires further repeats for a more robust comparison. Although not carried out three times in total, as a laboratory group we have used the ghrelin ELISA kits extensively and, therefore, to obtain information on the inter-assay variation, the standard curves of the kits across three different occasions were measured instead.

The exploration into differentiating the fatty acids linked to ghrelin, forming acyl ghrelin, remains difficult due to the absence of commercially available synthetic ghrelin variants with a range of fatty acids present as the acyl chain. Consequently, to analyse the various forms of acyl ghrelin, these variants must initially be synthesised in-house. In 2005, Nishi et al. investigated whether ingested medium-chain fatty acids were directly utilised for the acyl modification of ghrelin. The study involved Male C57BL/6J mice fed a standard laboratory chow supplemented with medium-chain fatty acids C6, C8, and C10. To evaluate the ghrelin peptides modified by different acyl groups, stomach peptides were extracted using a Sep-Pak Plus C18 cartridge, subjected to C18 RP-HPLC, and their ghrelin content measured in each fraction via ghrelin C- and N-radioimmunoassay. By adapting the described method, we could potentially generate C4, C6, C8, C10, C12, C14 and C16 variants of ghrelin for analysis via mass spectrometry using Nanomate. Subsequently, an LC-MS/MS method could be developed for their routine identification. Following this, (and after optimising ghrelin extraction from plasma) the presence of these variants could be investigated in patient samples, particularly from people with neurodegenerative disorders. The method established by Nishi et al. requires the use of mice, which may not be the most cost-effective or practical approach. However, a similar method could possibly be carried out using a cell line that can produce both ghrelin and GOAT. For example, Bando et al. (2016) developed a gastric cell line MGN3-1, which harbours GOAT and expresses large amounts of ghrelin. In their study, they introduced C5, C11, C12, and C16 fatty acids into the culture media of the MGN3-1 cells. They successfully managed to measure intracellular acylcarnitine levels, which should correlate with acyl-CoA (fatty acid associated with CoA) levels, through tandem mass spectrometry. However, they encountered instability issues with measuring the different acyl-CoA analytes by LC-ESI-MS/MS, likely due to the instability of acyl-CoA. Thus, the utilisation of a cell line presents a more accessible and alternative approach for generating different species of acyl ghrelin as ‘standards’ to build a method for their analysis by mass spectrometry. However, further research is also required on the stability of the acyl ghrelin species for/during analysis via mass spectrometry.

In summary, despite the limitations posed by instrumentation malfunctions, limited bead availability, and constraints on assay repetition, efforts were made to maximise progress and draw insights from available data. Moving forward, addressing these

limitations through improved instrumentation, expanded sample pools and rigorous assay validation will enhance the reliability and robustness of future studies in this area.

6.4 Future Directions

This work has highlighted the importance of blood-based biomarkers for detecting dementia and the difficulty in extracting small peptides such as ghrelin from plasma. Overall, BAMS has been demonstrated as a novel and promising assay for the detection of blood-based biomarkers. Once the BAMS assay is successfully optimised for the analysis of ghrelin, it should be used to analyse plasma that has already been analysed by ELISA. For example, in 2020 our group published a paper in which the plasma AG:UAG ratio was quantified in PDD, cognitively intact PD, and controls patients using ELISA kits. We identified reduced AG:UAG as a circulating diagnostic biomarker of dementia in people with PDD (Hornsby et al., 2020). An advantage of BAMS is that multiplexing the assay with other potential biomarkers is possible, in addition to the simultaneous identification of different species of human acyl ghrelin. For example, the combined detection of ghrelin, Aβ, NfL, and tau in a single sample would allow quick analysis of several biomarkers across dementia groups. This should aid in stratifying disease sub-types for participation in clinical trials and, in future, therapies. Outside of the world of neurodegeneration, the analysis of ghrelin by BAMS could also be employed to help research other conditions that currently rely heavily on immunoassays. These include diabetes (Hörber et al 2020), anorexia (Tezenas du Montcel et al., 2022) and obesity (Muñoz-Prieto et al., 2019), inflammatory disorders (Molina et al., 2020), sleep (Kennaway et al., 2020), and cardiovascular disease (Radha et al., 2021). Thus, ghrelin has potential relevance in a very wide variety of disorders.

To summarise the translational trajectory of this work, from the underlying biological rationale through to the development and optimisation of detection methods and clinical application, Figure 6.1 presents an overview of the thesis structure and future outlook.

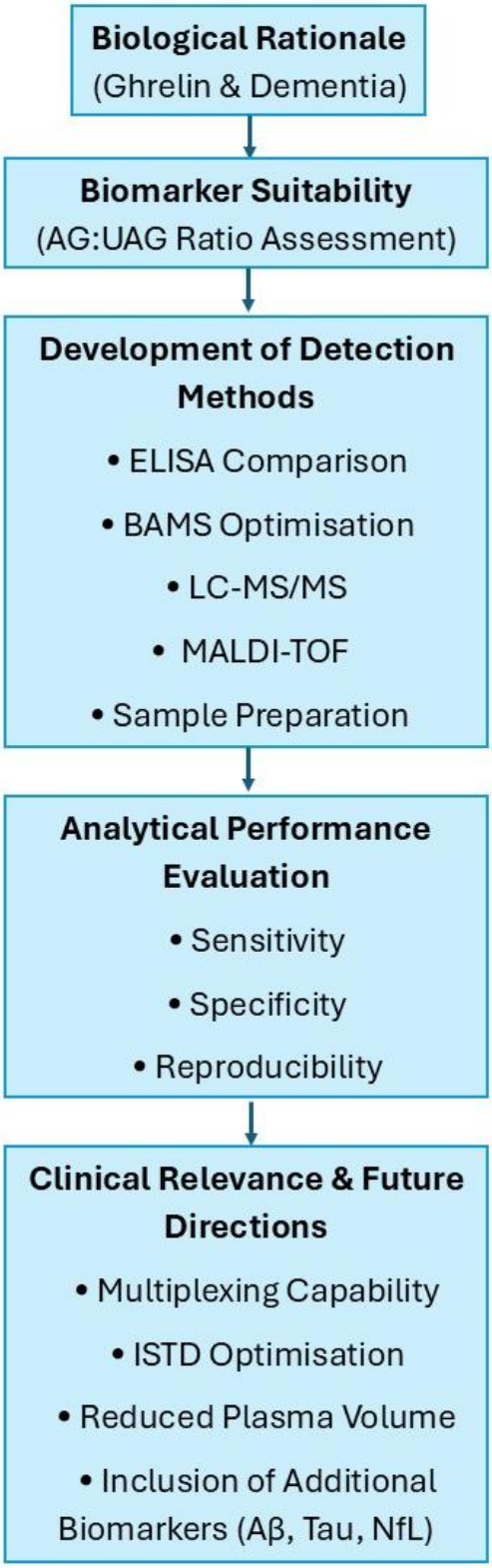

Figure 6.1. Overview of the thesis workflow, outlining the progression from the biological rationale for ghrelin as a dementia biomarker to method development and optimisation, analytical validation, and clinical translation. Future directions include multiplexed biomarker detection, internal standard (ISTD) optimisation, reduced plasma volume requirements, and the inclusion of additional dementia biomarkers.

6.5 Translating Ghrelin Detection to Clinical Application: Future Prospects for Biomarker Screening

Ghrelin has been increasingly implicated in neurodegenerative conditions such as AD and PD. At the research level, mass spectrometry platforms such as LC–MS/MS have demonstrated high analytical performance for detecting ghrelin isoforms, particularly acyl ghrelin unacylated ghrelin with sub-picogram sensitivity and high specificity (Rauh et al., 2007; Eslami et al., 2017). These approaches, however, require tightly controlled pre-analytical conditions, such as the use of EDTA tubes, serine protease inhibitors, and immediate acidification to prevent ghrelin deacylation (Hosoda et al., 2004, Blatnik et al., 2010). While effective in experimental contexts, such stringent protocols are unsuitable for widespread clinical implementation. Consequently, translational efforts have begun to focus on technologies capable of balancing analytical sensitivity with practical feasibility.

In contrast to laboratory-based MS, immunoassays offer a more accessible path toward clinical utility. Conventional ELISAs and radioimmunoassay have been widely used to measure circulating ghrelin levels, though they can vary significantly in their sensitivity and specificity (Foster-Schubert et al., 2010). Newer digital immunoassays, such as SIMOA and MSD, have improved detection limits into the femtogram per millilitre range, making them viable for low-abundance biomarkers in plasma (Rissin et al., 2010). However, these platforms may still face limitations in specificity due to antibody cross-reactivity, which remains a critical consideration when distinguishing between acyl and unacylated ghrelin isoforms.

A future clinical assay for ghrelin would need to address several core criteria to function effectively as a screening tool within the NHS. First, the sample type must be compatible with standard clinical practice. Although acidified plasma with protease inhibitors is ideal for preserving acyl ghrelin, it is not practical in routine diagnostics. Thus, either pre-analytical stabilisation buffers or dried blood spot (DBS) methodologies could be explored to simplify sample handling while preserving analyte integrity (Lim et al., 2010. Huner et al., 2024). The assay must also be analytically robust and maintain high sensitivity within the physiological range of ghrelin, typically between 50–150 pg/mL in fasting plasma (Foster-Schubert et al., 2010). Platforms like SIMOA and MSD are capable of this level of sensitivity and are already used for other neurodegenerative biomarkers (Li et al., 2019, Pais et al,. 2023)

Multiplexing is another crucial feature. Diagnostic strategies are increasingly moving towards biomarker panels rather than single analyte tests, given the multifactorial nature of neurodegenerative disease. For instance, studies have shown that combinations of p-tau181, p-tau217, NfL, and GFAP provide strong predictive value for dementia (Zhu et al., 2021, Rabl et al., 2024). The inclusion of metabolic peptides such as ghrelin could augment these panels by adding complementary information about disease-modifying pathways, particularly given ghrelin's neuroprotective properties (Beuker et al., 2025, Buntwal et al., 2019).

Another critical requirement is turnaround time. Point-of-care (POC) devices should ideally deliver results within 30 minutes to facilitate immediate clinical decisions. While conventional ELISAs may require several hours, advances in microfluidics and lab-on-a-chip technologies offer promising solutions for rapid immunoassay implementation. Simplified MS-based devices, such as immunoaffinity MALDI-TOF are also under exploration for rapid, multiplexed protein detection with minimal sample preparation (Montoliu-Gaya et al., 2023). A related translational strategy explored in this thesis involved BAMS, which combines antibody-based enrichment with direct MALDI-TOF detection. This approach enabled the detection of human acyl ghrelin at a limit of 40 pg/mL using antibody kit 88, and unacylated ghrelin at 20 pg/mL, which fall within the physiological concentration range. Although the method required 250 µL of plasma, which is higher than ideal for large-scale screening, the assay demonstrated strong reproducibility. Notably, antibody interference from the internal standard was observed, highlighting the need for improved reagent specificity. Nevertheless, BAMS represents a promising bridge between high-performance mass spectrometry and clinically adaptable workflows. With further refinement, it could be suitable for use in diagnostic laboratories or even in decentralised point-of-care environments.

Interpretability of the results is essential for clinicians. This includes clear reference intervals and risk stratification tools. For example, In dementia diagnostics, blood-based biomarkers are increasingly being adopted as pre-screening tools to identify patients who may benefit from more definitive but invasive or costly procedures, such as CSF or PET imaging (Hansson et al., 2022; Hampel et al., 2018). This approach gained further momentum with the recent U.S. Food and Drug Administration (FDA) clearance of the first blood-based test for AD in May 2025, marking a major regulatory milestone in the shift toward minimally invasive diagnostics (U.S. Food and Drug Administration [FDA], 2025). It is

planned that such blood-based biomarker tests will soon be pilot implemented in NHS memory clinics and potentially rolled out within primary care settings over the coming years, as part of the UK-wide Blood Biomarker Challenge. This initiative has begun recruiting over 3,100 participants across 28 NHS sites to evaluate whether a panel of tests can complement existing diagnostic pathways and could lead to routine use within the NHS within five years (Alzheimer's Society, 2025; Oxford Health NHS Foundation Trust, 2025). In terms of regulatory compliance, any clinical assay must adhere to the UKCA or CE-IVDR standards for in vitro diagnostics. This requires evidence of both analytical and clinical validation, quality control under ISO 13485, and oversight from a notified body for moderate- to high-risk tests. NHS protocols also mandate that POC devices be assessed by accredited pathology services under UKAS guidelines (NHS England, 2021).

Economic feasibility is another critical consideration. Although high-end MS and digital immunoassays carry significant upfront costs, these may be offset by reductions in downstream healthcare use, such as fewer unnecessary specialist referrals or imaging procedures. Systematic reviews suggest that point-of-care diagnostics can be cost-effective when implemented strategically (Lingervelder et al., 2021).

Finally, successful translation of a ghrelin-based assay into NHS workflows depends on seamless integration into existing diagnostic pathways. For neurodegenerative screening, this may involve deploying the test at the GP level or in memory clinics as a complement to cognitive assessments. Ongoing initiatives such as the Blood Biomarker Challenge and the Cambridge READ-OUT study are already piloting the use of multi-biomarker blood tests in NHS settings, with early results suggesting potential to enhance early detection and streamline patient care (Cambridgeshire and Peterborough NHS Foundation Trust, 2024).

From a fundamental analytical perspective, BAMS bridges the sensitivity and selectivity of mass spectrometry with the specificity of antibody capture, representing a hybrid approach that is well suited for isoform-level discrimination of ghrelin. Compared to conventional LC–MS/MS, BAMS offers a shorter run time, reduced chromatographic complexity, and potential for higher throughput. These advantages position BAMS as a promising candidate for translational applications where laboratory infrastructure or time constraints limit the use of more complex MS workflows.

Looking ahead, future biomarker screening platforms are expected to move toward rapid, multiplexed formats capable of detecting panels of neurodegenerative and metabolic markers in a single test. In this context, BAMS could be developed into a modular system for multi-peptide detection, where ghrelin isoforms are analysed alongside established biomarkers such as pTau, NfL, or GFAP. This vision would require further technical refinement, including miniaturisation of sample input, integration with automated spotting platforms, and validation against clinical reference standards.

With these advancements, a future BAMS-based diagnostic tool could take the form of a cartridge-based device, operated within clinical laboratories or decentralised settings such as memory clinics or general practice. Such a system would ideally require minimal hands-on time, return results within 30 to 60 minutes, and integrate with electronic health records for streamlined interpretation and triage. While current limitations remain, the results of this thesis support the continued development of BAMS as a feasible intermediate step between research-grade mass spectrometry and routine biomarker testing in clinical care.

In summary, a clinically viable ghrelin biomarker assay will need to balance the precision of mass spectrometry with the operational simplicity of immunoassays, while aligning with evolving trends in neurodegeneration diagnostics, including panel-based testing, POC delivery, and NHS integration. Translational success will require interdisciplinary coordination across analytical science, clinical neurology, and healthcare policy.

Appendix A: Supplementary Figure and Tables.

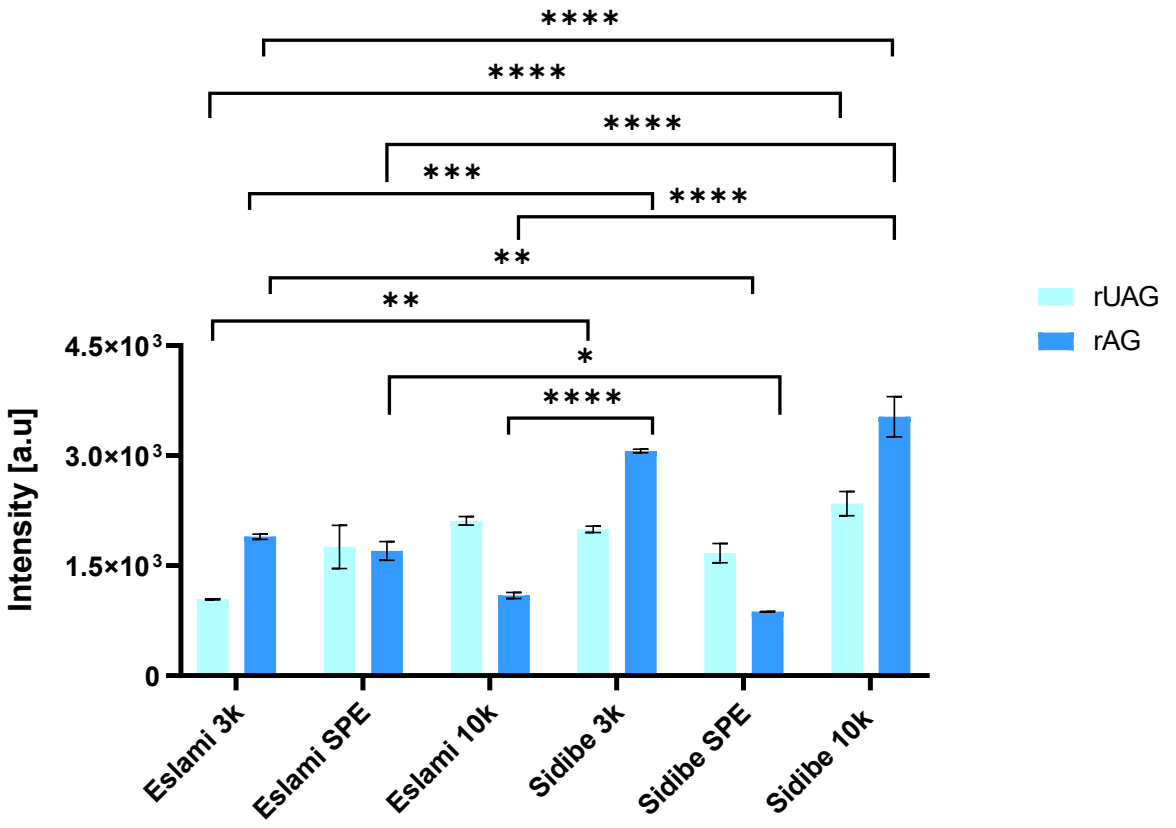

Supplementary Figure S1: Extended statistical comparisons of 3kDa and 10kDa centrifugal filters following protein precipitation (Eslami et al. and Sidibe et al.) and SPE protocols. This figure provides additional pairwise comparisons not shown in Figure 3.14 for visual clarity, including significant differences between Eslami and Sidibe protocols. Two-way ANOVA with Tukey's post hoc test was used for all analyses $P < 0.05$ was considered statistically significant. ****$P < 0.0001$, ***$P < 0.001$, **$P < 0.01$, *$P < 0.05$. Data are presented as mean ± SEM (N=3). See Results section for full statistical interpretation.

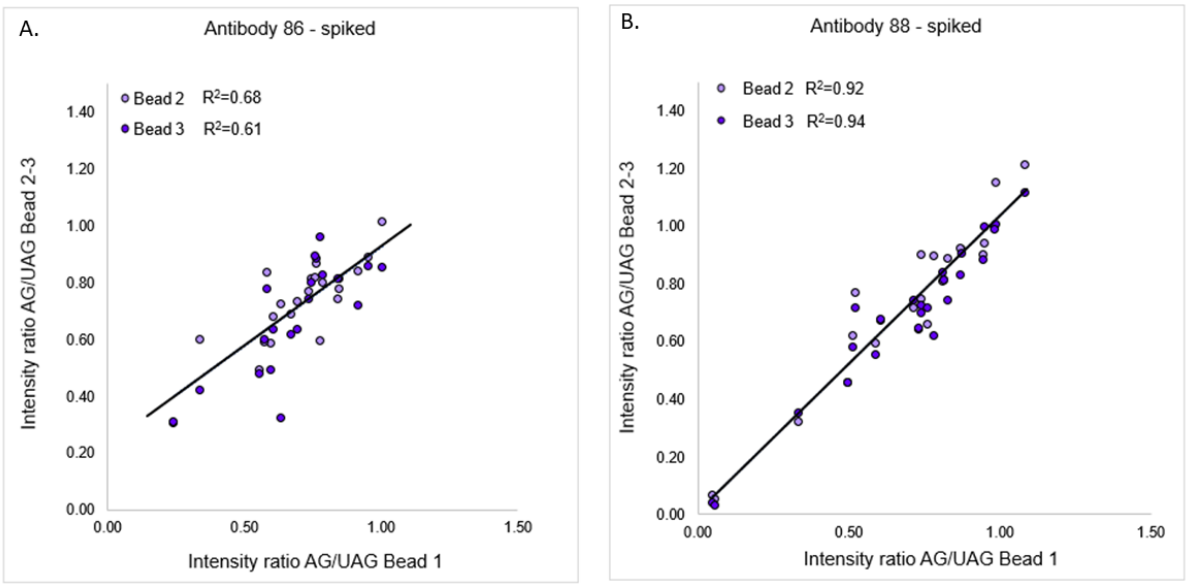

Supplementary Figure S2: Intra-assay variability of BAMS assay for antibodies 86 and 88. This figure illustrates the reproducibility of antibody-coated magnetic beads used to quantify ghrelin levels in the same donor 'spiked' plasma sample. For each antibody, the intensities of hAG:UAG from one bead were compared with those from the other two beads, and the results were fitted using a linear regression model ($y = mx + b$) with R^2 values calculated in Microsoft Excel. Panel A shows data for antibody 86, which yielded an R^2 value of ~0.6 for both bead comparisons, indicating a substantial degree of intra-assay variability. In contrast, panel B shows antibody 88, which produced R^2 values exceeding 0.9, reflecting high reproducibility and acceptable intra-assay performance. These additional variability tests, as reported by Nielsen et al. (2020), further support antibody 88's superior performance within the same experimental run.

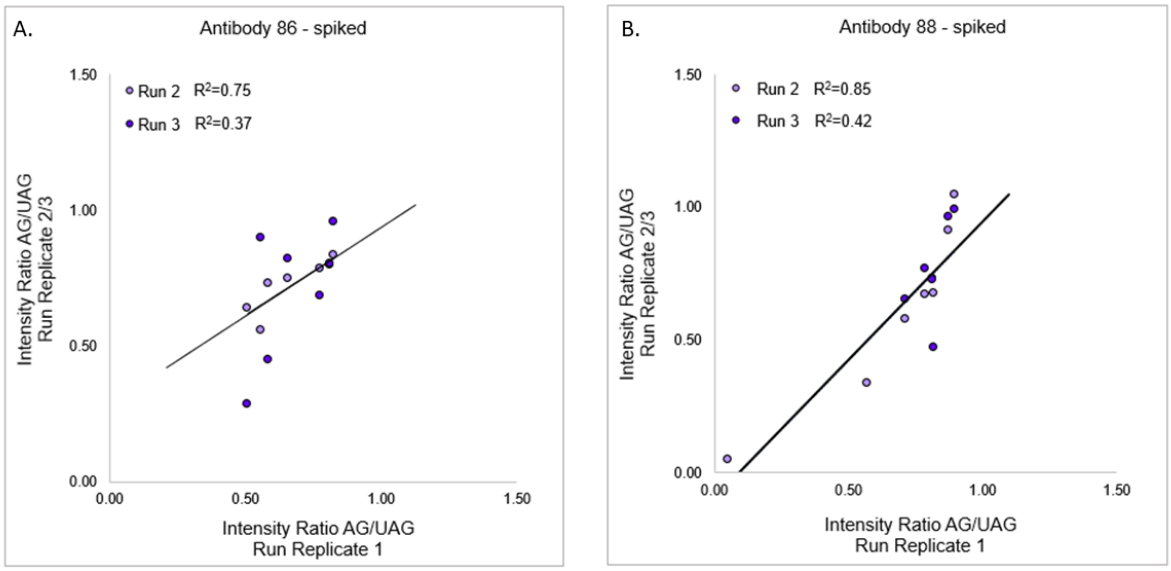

Supplementary Figure S3 Inter-assay variability assessing reproducibility between experimental runs using 'spiked' plasma samples from the same donor. To further evaluate reproducibility, the BAMS protocol was performed on the identical plasma sample across three separate experimental runs to assess inter-assay variability for each antibody. The analysis approach parallels that used in Supplementary Figure S2, where the average intensity ratio of AG to UAG from run 1 was compared against those from runs 2 and 3. Panel (A) shows results for antibody 86, and panel (B) for antibody 88. Linear regression fits (ordinary least squares) were applied, and R^2 values calculated using Microsoft Excel. Antibody 88 consistently demonstrated superior reproducibility over antibody 86, with run 2 R^2 values of 0.85 and 0.75 respectively, relative to run 1. Both antibodies showed decreased reproducibility in run 3, with R^2 values dropping to 0.42 for antibody 88 and 0.37 for antibody 86, potentially reflecting human or instrument-related errors. These findings align with previously observed variability within beads (Supplementary Figure S2).

Antibody 88			Ratio AG:UAG					
Sample	Withdrawal	Run	Intensity					
			Bead 1	Bead 2	Bead 3	Mean	SD	CV
Donor 1 (spiked)	1	1	0.05	0.07	0.04	0.05	0.01	20
		2	0.06	0.05	0.03	0.05	0.02	32
		3	0.83	0.88	0.74	0.82	0.06	7
Donor 1 (spiked)	2	1	0.88	0.92	0.90	0.90	0.02	2
		2	0.99	1.15	1.00	1.05	0.07	7
		3	0.99	0.99	0.99	0.99	0.00	0
Donor 2 (spiked)	1	1	0.52	0.62	0.58	0.57	0.04	7
		2	0.34	0.32	0.35	0.34	0.01	4
		3	1.09	1.21	1.11	1.14	0.05	5
Donor 2 (spiked)	2	1	0.87	0.92	0.83	0.87	0.04	4
		2	0.95	0.90	0.88	0.91	0.03	3
		3	0.95	0.94	0.99	0.96	0.02	2
Donor 3 (spiked)	1	1	0.74	0.90	0.72	0.79	0.08	10
		2	0.53	0.77	0.71	0.67	0.10	15
		3	0.78	0.90	0.62	0.76	0.12	15
Donor 3 (spiked)	2	1	0.82	0.81	0.81	0.81	0.00	0
		2	0.74	0.74	0.70	0.73	0.02	3
		3	0.72	0.71	0.74	0.72	0.01	2
Donor 4 (spiked)	1	1	0.77	0.66	0.71	0.71	0.04	6
		2	0.59	0.59	0.55	0.58	0.02	3
		3	0.61	0.67	0.67	0.65	0.03	4
Donor 5 (spiked)	1	1	0.81	0.81	0.84	0.82	0.01	2
		2	0.74	0.64	0.65	0.67	0.04	7
		3	0.50	0.46	0.45	0.47	0.02	4

Supplementary Table S1 Human AG:UAG intensity ratios for each donor and withdrawal across three experimental runs using antibody 88 in 'spiked' plasma samples. To investigate the reproducibility decline observed in experimental run 3 (Supplementary Figure S3), individual mean intensity values for runs 1, 2, and 3 were analysed. For donor 1, withdrawal 1, run 3 exhibited an outlier mean intensity ratio of 0.8, compared to runs 1 and 2, which averaged approximately 0.05. However, donor 1 withdrawal 2 showed all three runs with mean intensity ratios between 0.9 and 1, suggesting that runs 1 and 2 in withdrawal 1 are potential outliers. This conclusion is supported by CV values, where runs 1 and 2 had elevated CVs of 20 and 32, respectively, relative to run 3's CV of 7. A comparable trend was observed for donor 2, withdrawal 1, where run 3 initially appeared as an outlier (mean 1.14) against runs 1 and 2 (means 0.57 and 0.34). Yet, in donor 2 withdrawal 2, all runs ranged narrowly between 0.87 and 0.96, indicating that runs 1 and 2 in withdrawal 1 are outliers. Notably, donor 2 withdrawal 1 runs 1 and 2 coincided with the same day anomalies were detected for donor 1, suggesting a potential shared source of experimental variation. Cells highlighted in red indicate potential anomalous values within withdrawals.

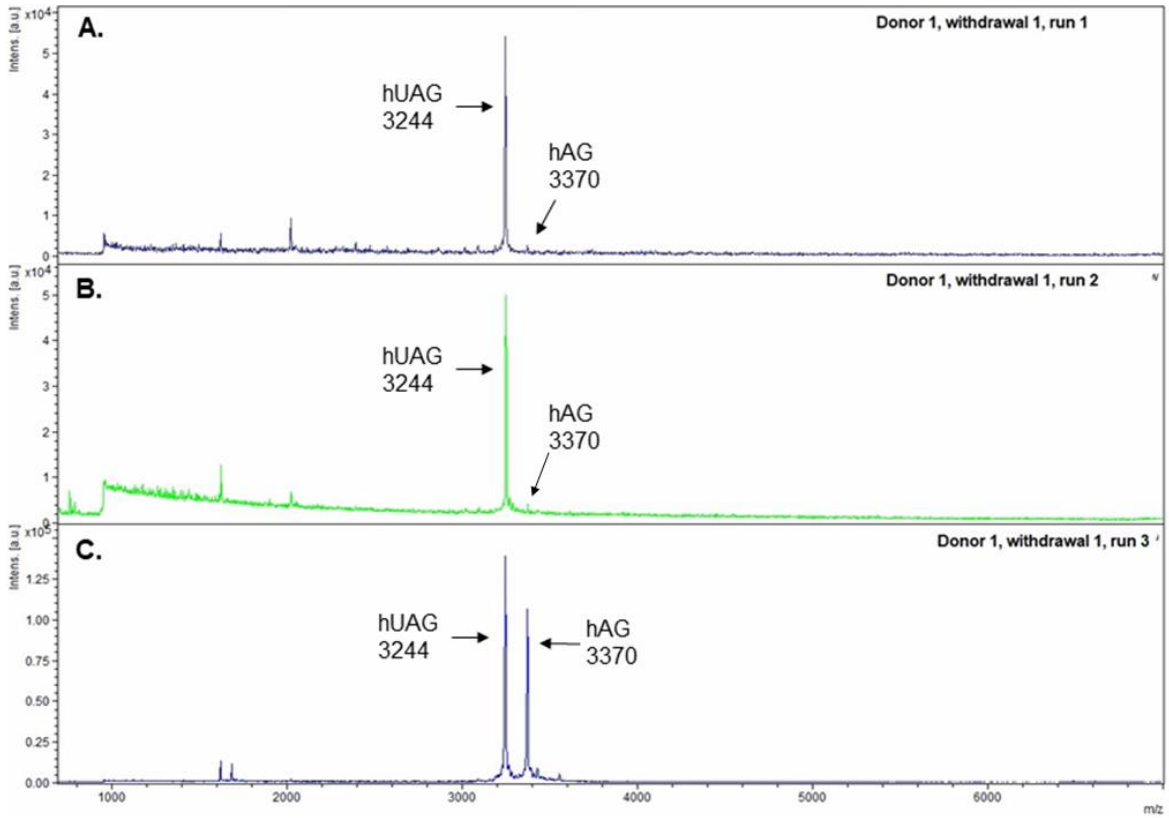

Supplementary Figure S4 MALDI-TOF spectra from donor 1 across three experimental runs, illustrating variability in acyl ghrelin detectability. An additional observation throughout this analysis was that CV values were often impacted by the human acyl ghrelin signal falling below the signal-to-noise ratio threshold. Spectra from runs 1 and 2 of donor 1, withdrawal 1 show a prominent unacylated ghrelin peak, whereas the acyl ghrelin peak is barely detectable (Panels A and B). Conversely, in run 3 of donor 1, withdrawal 1, the acyl ghrelin peak is clearly visible and well above the signal-to-noise threshold (Panel C). This difference in acyl ghrelin detectability highlights how signal-to-noise ratio thresholds can influence measurement accuracy and contribute to elevated CV values.

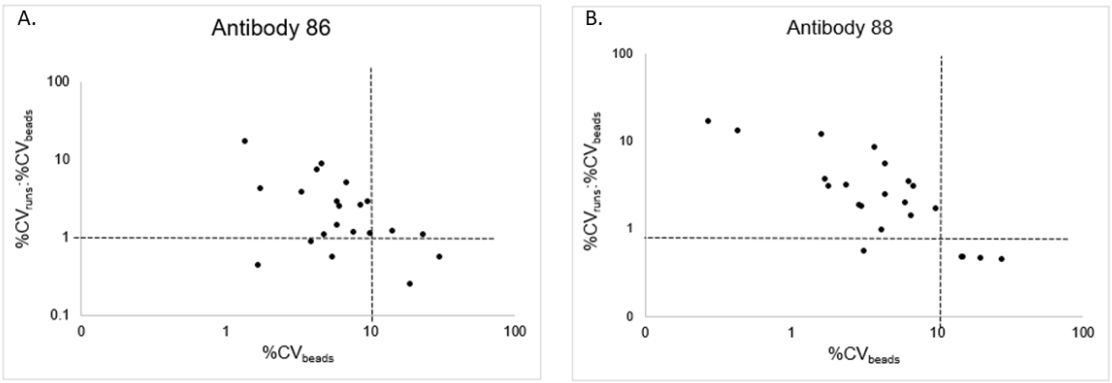

Supplementary Figure S5. The percentage of CV run /% CV beads was determined for individual donors 'spiked' plasma plotted against the corresponding values of %CV beads. The final variability test evaluated the %CV related to variation between beads within the same sample (%CV beads, x-axis) and across different experimental runs (%CV run, y-axis). Desired performance is represented by %CV beads values below 10% and %CV run values below 1%. Data points positioned below both these thresholds indicate high precision and reproducibility. For both antibody 86 (Panel A) and antibody 88 (Panel B), the majority of data points cluster in the upper left quadrant, indicating good assay performance. Specifically, %CV beads values generally remain under 10%, while %CV run values tend to exceed 1% but stay within the 1–10% range, reflecting acceptable inter-run variability.

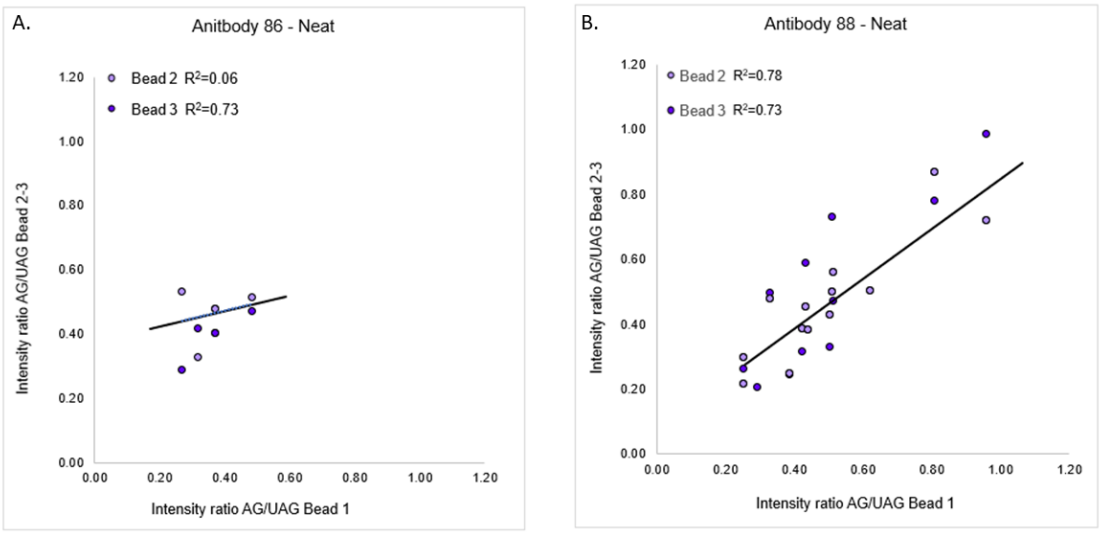

Supplementary Figure S6 Intra-assay variability assessing reproducibility between three beads quantifying human AG:UAG ratios in the same donor 'neat' plasma sample. To evaluate intra-assay variability in 'neat' plasma samples, the intensity ratio of AG to UAG measured by one bead was plotted against the corresponding ratios from the other two beads from the same donor. For antibody 86 (Panel A), bead 2 versus bead 1 showed a low R^2 value of 0.06, whereas bead 3 versus bead 1 yielded a higher R^2 of 0.73. Antibody 88 (Panel B) demonstrated R^2 values of 0.78 and 0.73 for bead 2 versus bead 1 and bead 3 versus bead 1, respectively. However, the limited number of data points for antibody 86 in the 'neat' samples restricts definitive interpretation of these results. Linear regression fits were calculated using ordinary least squares in Microsoft Excel.

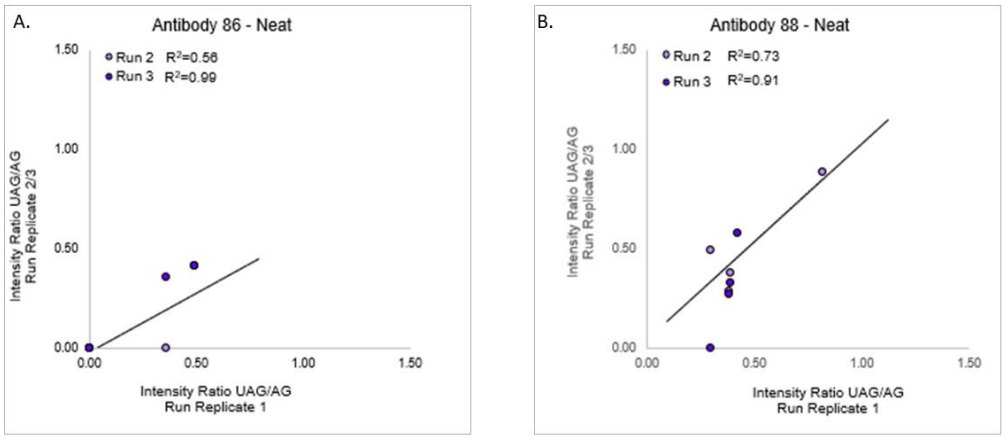

Supplementary Figure S7 Inter-assay variability assessing reproducibility between experimental runs using 'neat' plasma samples from the same donor. Variation between sample runs was analysed by plotting the average AG:UAG intensity ratio from run 1 against those from runs 2 and 3. Both antibodies 86 (Panel A) and 88 (Panel B) exhibited similar performance with high R^2 values of 0.99 and 0.91, respectively, when comparing run 1 to run 3. However, lower R^2 values were observed for run 1 versus run 2, 0.56 for antibody 86 and 0.73 for antibody 88, likely reflecting run 2 as an outlier with reduced AG:UAG ratios. Compared to 'spiked' plasma samples (Supplementary Figure S3), reproducibility in 'neat' samples was reduced, with the latter showing R^2 values of 0.56 and 0.73 for run 1 versus run 2, versus 0.75 and 0.85 in 'spiked' samples, respectively. For run 3, both antibodies achieved acceptable R^2 values above 0.9 in 'neat' samples (this figure, Supplementary Figure S7). Overall, better reproducibility was noted in 'spiked' samples, likely due to elevated acyl ghrelin levels improving AG:UAG ratio detection. Linear regression fits were calculated using ordinary least squares in Microsoft Excel.

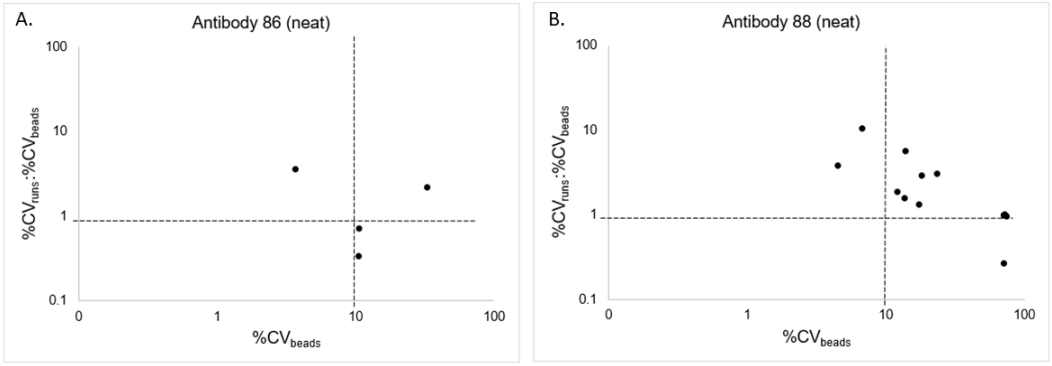

Supplementary Figure S8 Variability assessment of human AG:UAG quantification in 'neat' plasma samples from individual donors. The %CV values for individual beads (%CV beads) and replicates across runs (%CV run) were plotted to evaluate variability. Both antibodies 86 and 88 exhibited similar trends, with a substantial number of data points showing elevated %CV beads and %CV run:%CV beads ratios. For antibody 86, the mean %CV run:%CV beads ratio was 1.7, with %CV beads values frequently exceeding 10%. Antibody 88 demonstrated a higher mean %CV run:%CV beads ratio of 2.1 and %CV beads values often surpassing 20%. These findings suggest notable variability for both antibodies, potentially arising from sensitivity limitations, especially when peptide concentrations are low.

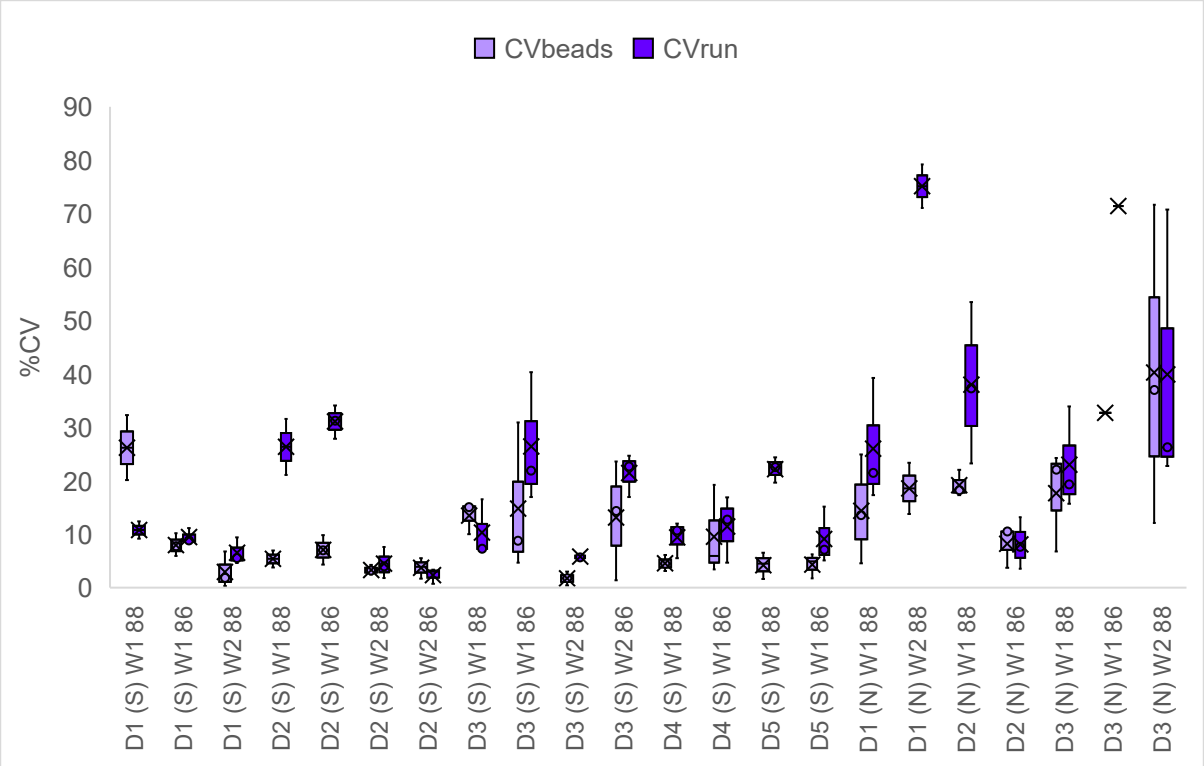

Supplementary Figure S9 Box plot illustrating the distribution of %CV values for 'neat' and 'spiked' plasma samples using antibodies 86 and 88. The box plot represents %CV values calculated from quantification data across different donors, comparing variability within beads (%CV beads) and between runs (%CV run). Notably, %CV values are consistently higher in 'neat' samples compared to 'spiked' samples. This increased variability in 'neat' samples is likely due to sensitivity limitations inherent in the assay protocol. Donor identifications: D1 = donor 1, D2 = donor 2, D3 = donor 3, D4 = donor 4, D5 = donor 5. Sample types: S = 'spiked', N = 'neat'. Withdrawals: W1 = withdrawal 1, W2 = withdrawal 2, W3 = withdrawal 3.

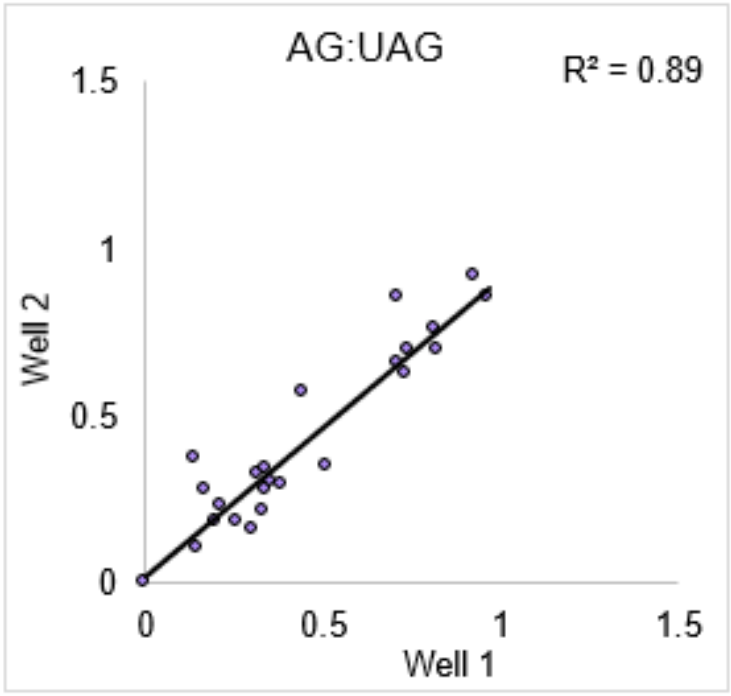

Supplementary Figure S10 ELISA intra-assay variation assessing reproducibility between wells within the same donor plasma sample. Standard curves were generated across three experimental runs to evaluate intra-assay variation within ELISA kits for unacylated (A05106) and acyl ghrelin (A05119) detection (Bertin). Intra-assay variation was quantified by comparing intensity ratios of hAG:UAG between two wells from the same ELISA kit. A linear regression fit was applied, yielding an R^2 value of 0.88. For comparison, the BAMS assay's intra-assay variability was evaluated through intensity comparisons across three beads within a sample. BAMS showed R^2 values above 0.9 for antibody 88 in 'spiked' plasma (Supplementary Figure S2B), demonstrating comparable or superior reproducibility to ELISA. However, antibody 86 in 'spiked' plasma showed lower BAMS reproducibility (R^2 = 0.6, Supplementary Figure S2A). In 'neat' samples, ELISA reproducibility outperformed BAMS, with ELISA showing higher R^2 values compared to antibody 86 (R^2 = 0.06 and 0.73) and antibody 88 (R^2 > 0.7) in BAMS (Supplementary Figures S6A and S6B). Linear regression was calculated using ordinary least squares in Microsoft Excel.

Bertin AG/UAG						
Concentration	Run	Well 1 AG/	Well 2 AG/	Mean	SD	CV
2	1	0.166667	0.28125	0.224	0.081	36
	2	0.333333	0.217391	0.275	0.082	30
	3	0.139535	0.37037	0.255	0.163	64
3.9	1	0.196262	0.182796	0.190	0.010	5
	2	0.142857	0.108108	0.125	0.025	20
	3	0.383333	0.298246	0.341	0.060	18
7.8	1	0.211382	0.234848	0.223	0.017	7
	2	0.354167	0.305085	0.330	0.035	11
	3	0.506667	0.349398	0.428	0.111	26
15.6	1	0.304813	0.15942	0.232	0.103	44
	2					
	3	0.731343	0.623932	0.678	0.076	11
31.3	1	0.259819	0.184524	0.222	0.053	24
	2	0.443925	0.570707	0.507	0.090	18
	3	0.738739	0.693617	0.716	0.032	4
62.5	1	0.339383	0.277477	0.308	0.044	14
	2	0.710692	0.659459	0.685	0.036	5
	3	0.814815	0.758929	0.787	0.040	5
125	1	0.315043	0.32948	0.322	0.010	3
	2	0.711429	0.854197	0.783	0.101	13
	3	0.963357	0.853795	0.909	0.077	9
250	1	0.338599	0.342162	0.340	0.003	1
	2	0.824742	0.699507	0.762	0.089	12
	3	0.923122	0.919204	0.921	0.003	0

Antibody 88			Ratio AG/UAG					
Sample	Withdraw	Run	Intensity					
			Bead 1	Bead 2	Bead 3	Mean	SD	CV
Donor 1 (spiked)	1	1	0.05	0.07	0.04	0.05	0.01	20
		2	0.06	0.05	0.03	0.05	0.01	28
		3	0.83	0.88	0.74	0.82	0.06	7
Donor 1 (spiked)	2	1	0.88	0.92	0.90	0.90	0.02	2
		2	0.99	1.15	1.00	1.05	0.07	7
		3	0.99	0.99	0.99	0.99	0.00	0
Donor 2 (spiked)	1	1	0.52	0.62	0.58	0.57	0.04	7
		2	0.34	0.32	0.35	0.34	0.01	4
		3	1.09	1.21	1.11	1.14	0.05	5
Donor 2 (spiked)	2	1	0.87	0.92	0.83	0.87	0.04	4
		2	0.95	0.90	0.88	0.91	0.03	3
		3	0.95	0.94	0.99	0.96	0.02	2
Donor 3 (spiked)	1	1	0.74	0.90	0.72	0.79	0.08	10
		2	0.53	0.77	0.71	0.67	0.10	15
		3	0.78	0.90	0.62	0.76	0.12	15
Donor 3 (spiked)	2	1	0.82	0.81	0.81	0.81	0.00	0
		2	0.74	0.74	0.70	0.73	0.02	3
		3	0.72	0.71	0.74	0.72	0.01	2
Donor 4 (spiked)	1	1	0.77	0.66	0.71	0.71	0.04	6
		2	0.59	0.59	0.55	0.58	0.02	3
		3	0.61	0.67	0.67	0.65	0.03	4
Donor 5 (spiked)	1	1	0.81	0.81	0.84	0.82	0.01	2
		2	0.74	0.64	0.65	0.67	0.04	7
		3	0.50	0.46	0.45	0.47	0.02	4

Supplementary Table S0.1 Comparison of intra-assay variability between ELISA and BAMS assays using antibody 88 in 'spiked' plasma samples. CV values from 24 samples analysed by both ELISA and BAMS assays are compared to assess intra-assay variability. The BAMS assay demonstrated less variation, with only two CV values exceeding 20, whereas the ELISA had seven CV values above this threshold. According to Reed, Lynn, and Meade (2002), CV values below 20 are considered acceptable, values below 10 are good, and values below 5 are excellent.

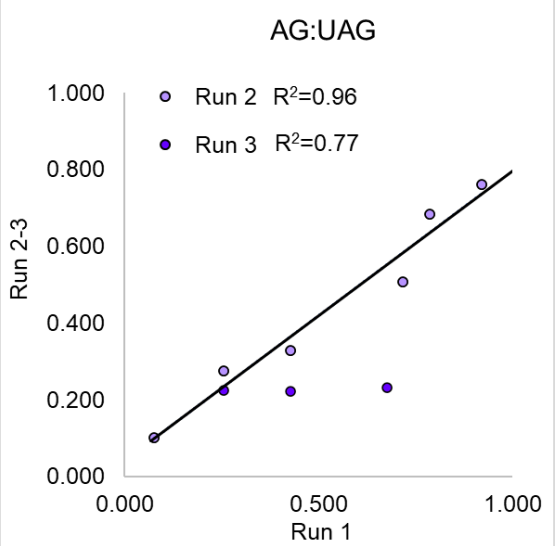

Supplementary Figure S11 ELISA inter-assay variability assessing reproducibility between samples of the same donor across different kits (N=3). The inter-assay variation for the human ghrelin ELISA was evaluated by comparing measurements from multiple kits across three experimental runs. Results indicate similar performance to the intra-assay variability, with the ELISA showing consistent reproducibility. Notably, the ELISA exhibited more CV values outside the acceptable range compared to the BAMS assay, which only had two CV values above the threshold, highlighting the relative robustness of the BAMS assay.

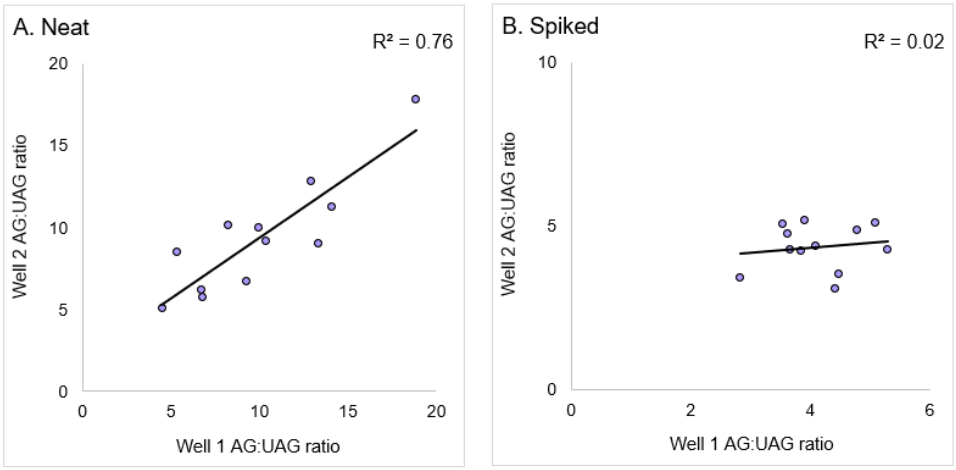

Supplementary Figure S12 AG:UAG ratio is used to determine the intra-assay variation of the ELISA kit using plasma from 5 healthy donors. Plasma samples were obtained from the same donors and blood withdrawals as those analysed by the BAMS assay. Both 'neat' and 'spiked' plasma samples were assessed. Unlike BAMS, where some withdrawals were excluded due to bead availability, the ELISA was performed on all samples. Intra-assay variation was evaluated separately for 'neat' plasma (Panel A) and 'spiked' plasma (Panel B). This data highlight differences in assay reproducibility between ELISA and BAMS across plasma sample types.

References

Alzheimer's Society. (2025, January 30). *Trial for blood tests to diagnose dementia accepts first participants* [Press release]. Retrieved from https://www.alzheimers.org.uk/news/2025-01-30/trial-blood-tests-diagnose-dementia-accepts-first-participants

Andrews, Z. B., Erion, D., Beiler, R., Liu, Z. W., Abizaid, A., Zigman, J., … & Horvath, T. L. (2009). Ghrelin promotes and protects nigrostriatal dopamine function via a UCP2-dependent mitochondrial mechanism. *Journal of Neuroscience, 29*(45), 14057–14065. https://doi.org/10.1523/JNEUROSCI.4190-09.2009

Akamizu, T., Takaya, K., Irako, T., Hosoda, H., Teramukai, S., Matsuyama, A., Tada, H., Miura, K., Shimizu, A., Fukushima, M., Yokode, M., Tanaka, K., and Kangawa, K. (2004). Pharmacokinetics, safety, and endocrine and appetite effects of ghrelin administration in young healthy subjects. European journal of endocrinology, 150(4), 447–455. https://doi.org/10.1530/eje.0.1500447

Alnasser, S., et al. (2020). Diagnostic value of serum ghrelin levels in inflammatory diseases: A systematic review. The Journal of International Medical Research, 48(7), 0300060520920441. https://doi.org/10.1177/0300060520920441

Andrews Z. B., Erion D. M., Beiler R., Choi C. S., Shulman G. I., Horvath T. L., et al. (2009). Ghrelin Promotes and Protects Nigrostriatal Dopamine Function via a UCP2-Dependent Mitochondrial Mechanism. J. Neurosci. 29 (45), 14057–14065. doi:10.1523/JNEUROSCI.3890-09.2009

Ansong, C.; Wu, S.; Meng, D.; Liu, X.; Brewer, H. M.; Kaiser, B. L. D.; Nakayasu, E. S.; Cort, J. R.; Pevzner, P.; Smith, R. D.; Heffron, F.; Adkins, J. N.; Paša-Tolić, L. Top-down Proteomics Reveals a Unique Protein S-Thiolation Switch in Salmonella Typhimurium in Response to Infection-like Conditions. Proc. Natl. Acad. Sci. U. S. A. 2013, 110 (25), 10153– 10158, DOI: 10.1073/pnas.1221210110

Ashton, N. J., Brum, W. S., Di Molfetta, G., Benedet, A. L., Arslan, B., Jonaitis, E., Langhough, R. E., Cody, K., Wilson, R., Carlsson, C. M., Vanmechelen, E., Montoliu-Gaya, L., Lantero-Rodriguez, J., Rahmouni, N., Tissot, C., Stevenson, J., Servaes, S., Therriault, J., Pascoal, T., Lleó, A., … Zetterberg, H. (2024). Diagnostic Accuracy of a

Plasma Phosphorylated Tau 217 Immunoprawf for Alzheimer Disease Pathology. JAMA neurology, 81(3), 255–263. https://doi.org/10.1001/jamaneurol.2023.5319

Bando, M., Iwakura, H., Koyama, H., Hosoda, H., Shigematsu, Y., Ariyasu, H., Akamizu, T., Kangawa, K., & Nakao, K. (2016). High incorporation of long-chain fatty acids contributes to the efficient production of acylated ghrelin in ghrelin-producing cells. FEBS letters, 590(7), 992–1001. https://doi.org/10.1002/1873-3468.12132

Banks, W. A., Tschöp, M., Robinson, S. M., and Heiman, M. L. (2002). Extent and direction of ghrelin transport across the blood-brain barrier is determined by its unique primary structure. The Journal of pharmacology and experimental therapeutics, 302(2), 822–827. https://doi.org/10.1124/jpet.102.034827

Barthélemy, N. R., Horie, K., Sato, C., and Bateman, R. J. (2020). Blood plasma phosphorylated-tau isoforms track CNS change in Alzheimer's disease. The Journal of experimental medicine, 217(11), e20200861. https://doi.org/10.1084/jem.20200861

Bateman, R. J., Barthélemy, N. R., and Horie, K. (2020, March 1). Another step forward in blood-based diagnostics for Alzheimer’s disease. Nature Medicine, Vol. 26, pp. 314–316. https://doi.org/10.1038/s41591-020-0797-4

Bayliss, J. A., & Andrews, Z. B. (2013). Ghrelin is neuroprotective in Parkinson’s disease: Molecular mechanisms of metabolic neuroprotection. Therapeutic Advances in Endocrinology and Metabolism, 4(1), 25–36. https://doi.org/10.1177/2042018813479645

Bayliss, J. A., Lemus, M. B., Ding, C., Rose, C., & Andrews, Z. B. (2016). Central ghrelin-AMPK signaling mediates the neuroprotective effects of ghrelin in Parkinson’s disease. *Molecular Neurodegeneration*, 11, 30.

Bayliss, J. A., Lemus, M. B., Stark, R., Santos, V. V., Thompson, A., Rees, D. J., Galic, S., Elsworth, J. D., Kemp, B. E., Davies, J. S., and Andrews, Z. B. (2016). Ghrelin-AMPK Signaling Mediates the Neuroprotective Effects of Calorie Restriction in Parkinson's Disease. The Journal of neuroscience : the official journal of the Society for Neuroscience, 36(10), 3049–3063. https://doi.org/10.1523/JNEUROSCI.4373-15.2016

Bayoumy S, Verberk IMW, den Dulk B, Hussainali Z, Zwan M, van der Flier WM, Ashton NJ, Zetterberg H, Blennow K, Vanbrabant J, Stoops E, Vanmechelen E, Dage JL, Teunissen CE. Clinical and analytical comparison of six Simoa prawfs for plasma P-tau isoforms P-tau181, P-tau217, and P-tau231. Alzheimers Res Ther. 2021 Dec 4;13(1):198. doi: 10.1186/s13195-021-00939-9. PMID: 34863295; PMCID: PMC8645090.

Beavis RC, Chaudhary T, Chait BT. α-Cyano-4-hydroxycinnamic acid as a matrix for matrixassisted laser desorption mass spectrometry. Org Mass Spectrom 1992;27:156–158

Bednarek, M. A., Feighner, S. D., Pong, S. S., McKee, K. K., Hreniuk, D. L., Silva, M. V., Warren, V. A., Howard, A. D., Van Der Ploeg, L. H., and Heck, J. V. (2000). Structure-function studies on the new growth hormone-releasing peptide, ghrelin: minimal sequence of ghrelin necessary for activation of growth hormone secretagogue receptor 1a. Journal of medicinal chemistry, 43(23), 4370–4376. https://doi.org/10.1021/jm0001727

Behnoush, B., Sheikhazadi, A., Bazmi, E., Fattahi, A., Sheikhazadi, E., and Saberi Anary, S. H. (2015). Comparison of UHPLC and HPLC in benzodiazepines analysis of postmortem samples: a case-control study. Medicine, 94(14), e640. https://doi.org/10.1097/MD.0000000000000640

Benedet, A. L., Milà-Alomà, M., Vrillon, A., Ashton, N. J., Pascoal, T. A., Lussier, F., Karikari, T. K., Hourregue, C., Cognat, E., Dumurgier, J., Stevenson, J., Rahmouni, N., Pallen, V., Poltronetti, N. M., Salvadó, G., Shekari, M., Operto, G., Gispert, J. D., Minguillon, C., Fauria, K., … Translational Biomarkers in Aging and Dementia (TRIAD) study, Alzheimer's and Families (ALFA) study, and BioCogBank Paris Lariboisière cohort (2021). Differences Between Plasma and Cerebrospinal Fluid Glial Fibrillary Acidic Protein Levels Across the Alzheimer Disease Continuum. JAMA neurology, 78(12), 1471–1483. https://doi.org/10.1001/jamaneurol.2021.3671

Bender, B. J., Vortmeier, G., Ernicke, S., Bosse, M., Kaiser, A., Els-Heindl, S., Krug, U., Beck-Sickinger, A., Meiler, J., and Huster, D. (2019). Structural Model of Ghrelin Bound to its G Protein-Coupled Receptor. Structure (London, England : 1993), 27(3), 537–544.e4. https://doi.org/10.1016/j.str.2018.12.004

Bertram, L. and Tanzi, R.E. 2005. The Journal of Clinical Investigation The genetic epidemiology of neurodegenerative disease. The Journal of Clinical Investigation 115(6), pp. 1449–1457. Available at: http://www.jci.org.

Bjerner, J., Nustad, K., & Norum, L. F. (2015). Analytical performance of multiplex immunoassays: A comparative study of Luminex and other platforms. *Scandinavian Journal of Clinical and Laboratory Investigation*, 75(5), 397–404. https://doi.org/10.3109/00365513.2015.1039181

Beuker, C., Schreiner, U., Strecker, J. K., Altach, E., Rätzel, V., Schmidt-Pogoda, A., Wiendl, H., Minnerup, J., & Diederich, K. (2025). Ghrelin promotes neurologic recovery and neurogenesis in the chronic phase after experimental stroke. Neurological research and practice, 7(1), 14. https://doi.org/10.1186/s42466-025-00371-6

Bladergroen, M. R., and van der Burgt, Y. E. (2015). Solid-phase extraction strategies to surmount body fluid sample complexity in high-throughput mass spectrometry-based proteomics. Journal of analytical methods in chemistry, 2015, 250131. https://doi.org/10.1155/2015/250131

Blatnik, M. A., & Soderstrom, C. A. (2011). Pre-analytical considerations for ghrelin measurement. Journal of Clinical Endocrinology & Metabolism, 96(3), 740–748.

Blatnik M., Soderstrom C.I., Dysinger M., Fraser S.A. Prandial ghrelin attenuation provides evidence that des-acyl ghrelin may be an artifact of sample handling in human plasma. Bioanalysis. 2012;4:2447–2455. doi: 10.4155/bio.12.248.

Blatnik, M., and Soderstrom, C. I. (2011). A practical guide for the stabilization of acylghrelin in human blood collections. Clinical endocrinology, 74(3), 325–331. https://doi.org/10.1111/j.1365-2265.2010.03916.x

Blennow, K., Hampel, H., Weiner, M., and Zetterberg, H. (2010, March). Cerebrospinal fluid and plasma biomarkers in Alzheimer disease. Nature Reviews Neurology, Vol. 6, pp. 131–144. https://doi.org/10.1038/nrneurol.2010.4

Boer DEC, van Smeden J, Bouwstra JA, Aerts JMFG. Glucocerebrosidase: Functions in and Beyond the Lysosome. J Clin Med. 2020 Mar 9;9(3):736. doi: 10.3390/jcm9030736. PMID: 32182893; PMCID: PMC7141376.

Brandt, H., Ehmann, T., and Otto, M. (2010). Solvent selection for matrix-assisted laser desorption/ionization time-of-flight mass spectrometric analysis of synthetic polymers employing solubility parameters. Rapid communications in mass spectrometry : RCM, 24(16), 2439–2444. https://doi.org/10.1002/rcm.4668

Braak, H., de Vos, R. A., Bohl, J., & Del Tredici, K. (2003). Gastric α-synuclein immunoreactive inclusions in Meissner's and Auerbach's plexuses in cases staged for Parkinson's disease-related brain pathology. *Neuroscience Letters*, 396(1), 67–72.

Breijyeh, Z., and Karaman, R. (2020). Comprehensive Review on Alzheimer's Disease: Causes and Treatment. Molecules (Basel, Switzerland), 25(24), 5789. https://doi.org/10.3390/molecules25245789

Broglio F, Gottero C, Prodam F, Gauna C, Muccioli G, Papotti M, Abribat T, Van Der Lely AJ, Ghigo E. Non-acylated ghrelin counteracts the metabolic but not the neuroendocrine response to acylated ghrelin in humans. J Clin Endocrinol Metab. 2004 Jun;89(6):3062-5. doi: 10.1210/jc.2003-031964. PMID: 15181099.

Buntwal, L., Sassi, M., Morgan, A. H., Andrews, Z. B., and Davies, J. S. (2019). Ghrelin-Mediated Hippocampal Neurogenesis: Implications for Health and Disease. Trends in endocrinology and metabolism: TEM, 30(11), 844–859. https://doi.org/10.1016/j.tem.2019.07.001

Cabral, A., Fernandez, G., and Perello, M. (2013). Analysis of brain nuclei accessible to ghrelin present in the cerebrospinal fluid. Neuroscience, 253, 406–415. https://doi.org/10.1016/j.neuroscience.2013.09.008

Cao, X., et al. (2018). Serum acyl-ghrelin as a biomarker for mild cognitive impairment. Neurobiology of Aging, 65, 161–167.

Carabotti, M., Scirocco, A., Maselli, M. A., & Severi, C. (2015). The gut–brain axis: interactions between enteric microbiota, central and enteric nervous systems. *Annals of Gastroenterology*, 28(2), 203–209.

Castrillo, J. I., and Oliver, S. G. (2016). Alzheimer's as a Systems-Level Disease Involving the Interplay of Multiple Cellular Networks. Methods in Molecular Biology (Clifton, N.J.), Vol. 1303, pp. 3–48. https://doi.org/10.1007/978-1-4939-2627-5_1

Cambridgeshire and Peterborough NHS Foundation Trust. (2024). *READ-OUT: A feasibility study for blood biomarker-based dementia screening*. https://www.cpft.nhs.uk

Cicognola, C., Janelidze, S., Hertze, J., Zetterberg, H., Blennow, K., Mattsson-Carlgren, N., & Hansson, O. (2021). Plasma glial fibrillary acidic protein detects Alzheimer pathology and predicts future conversion to Alzheimer dementia in patients with mild cognitive impairment. Alzheimer's research & therapy, 13(1), 68. https://doi.org/10.1186/s13195-021-00804-9

Chamoun Z., Mann R. K., Nellen D., von Kessler D. P., Bellotto M., Beachy P. A., et al. (2001). Skinny Hedgehog, an Acyltransferase Required for Palmitoylation and Activity of the Hedgehog Signal. Science 293 (5537), 2080–2084. doi:10.1126/SCIENCE.1064437

Chan, H. N., Xu, D., Ho, S. L., Wong, M. S., & Li, H. W. (2017). Ultra-sensitive detection of protein biomarkers for diagnosis of Alzheimer's disease. Chemical science, 8(5), 4012–4018. https://doi.org/10.1039/c6sc05615f

Chen, V. P., Pang, Y.-P., Geng, L., Gao, Y., & Brimijoin, S. (2016). Physiological roles for butyrylcholinesterase: A BChE–ghrelin axis. Chemico-Biological Interactions, 259, 271–275.

Chen, B., Sun, Y., Niu, J., Jarugumilli, G. K., & Wu, X. (2022). Protein lipidation in cell signalling and diseases: Function, regulation, and therapeutic opportunities. *Signal Transduction and Targeted Therapy, 7*(1), 1–24. https://doi.org/10.1038/s41392-022-01245-y

Chen M.-H., Li Y.-J., Kawakami T., Xu S.-M., Chuang P.-T. (2004). Palmitoylation Is Required for the Production of a Soluble Multimeric Hedgehog Protein Complex and Long-Range Signaling in Vertebrates. Genes Dev. 18 (6), 641–659. doi:10.1101/gad.1185804

Christenson, J.L. Powers, L.M. Shaw, O. Hansson, J.D. Doecke, Q.X. Li, C. Teunissen, H. Tumani, K. Blennow. Elecsys® Total-Tau and Phospho-Tau (181P) CSF prawfs: Analytical performance of the novel, fully automated immunoprawfs for quantification of tau proteins in human cerebrospinal fluid

Clin. Biochem., 72 (2019), pp. 30-38, 10.1016/j.clinbiochem.2019.05.005

Chung, H., Li, E., Kim, Y., Kim, S., and Park, S. (2013). Multiple signaling pathways mediate ghrelin-induced proliferation of hippocampal neural stem cells. The Journal of endocrinology, 218(1), 49–59. https://doi.org/10.1530/JOE-13-0045

Chung, H., Choi, J., and Park, S. (2018). Ghrelin protects adult rat hippocampal neural stem cells from excessive autophagy during oxygen-glucose deprivation. Endocrine journal, 65(1), 63–73. https://doi.org/10.1507/endocrj.EJ17-0281

Chung, S. H., Yoo, D., Ahn, T., Lee, W., & Hong, J. (2023). Profiling Analysis of Tryptophan Metabolites in the Urine of Patients with Parkinson's Disease Using LC–MS/MS. Pharmaceuticals, 16(10), 1495. https://doi.org/10.3390/ph16101495

Cohen, S. L., and Chait, B. T. (1996). Influence of matrix solution conditions on the MALDI-MS analysis of peptides and proteins. Analytical Chemistry, 68(1), 31–37. https://doi.org/10.1021/ac9507956

Coombs G. S., Yu J., Canning C. A., Veltri C. A., Covey T. M., Cheong J. K., et al. (2010). WLS-Dependent Secretion of WNT3A Requires Ser209 Acylation and Vacuolar Acidification. J. Cell Sci. 123 (19), 3357–3367. doi:10.1242/JCS.072132

Cournut, A., Moustiez, P., Coffinier, Y., Enjalbal, C., & Bich, C. (2024). Innovative SALDI mass spectrometry analysis for Alzheimer's disease synthetic peptides detection. Talanta, 268, 125357. https://doi.org/10.1016/j.talanta.2023.125357

Covey, T. R., Thomson, B. A., and Schneider, B. B. (2009). Atmospheric pressure ion sources. Mass Spectrometry Reviews, 28(6), 870–897. https://doi.org/10.1002/mas.20246

Cowan, E., Burch, K. J., Green, B. D., & Grieve, D. J. (2016). Obestatin as a key regulator of metabolism and cardiovascular function with emerging therapeutic potential for diabetes. *British journal of pharmacology*, *173*(14), 2165–2181. https://doi.org/10.1111/bph.13502

Cowley, M. A., Smith, R. G., Diano, S., Tschöp, M., Pronchuk, N., Grove, K. L., Strasburger, C. J., Bidlingmaier, M., Esterman, M., Heiman, M. L., Garcia-Segura, L. M., Nillni, E. A., Mendez, P., Low, M. J., Sotonyi, P., Friedman, J. M., Liu, H., Pinto, S., Colmers, W. F., Cone, R. D., … Horvath, T. L. (2003). The distribution and mechanism of action of ghrelin in the CNS demonstrates a novel hypothalamic circuit

regulating energy homeostasis. Neuron, 37(4), 649–661. https://doi.org/10.1016/s0896-6273(03)00063-1

Darling J. E., Zhao F., Loftus R. J., Patton L. M., Gibbs R. A., Hougland J. L. (2015). Structure-Activity Analysis of Human Ghrelin O-Acyltransferase Reveals Chemical Determinants of Ghrelin Selectivity and Acyl Group Recognition. Biochemistry 54 (4), 1100–1110. doi:10.1021/bi5010359

Date, Y., Nakazato, M., Hashiguchi, S., Dezaki, K., Mondal, M. S., Hosoda, H., Kojima, M., Kangawa, K., Arima, T., Matsuo, H., Yada, T., and Matsukura, S. (2002). Ghrelin is present in pancreatic alpha-cells of humans and rats and stimulates insulin secretion. Diabetes, 51(1), 124–129. https://doi.org/10.2337/diabetes.51.1.124

De Meyer S ,Schaeverbeke JM , Verberk IMW , et al. Comparison of ELISA- and SIMOA-based quantification of plasma Aβ ratios for early detection of cerebral amyloidosis. Alzheimers Res Ther 2020;12:162. doi:10.1186/s13195-020-00728-w pmid:http://www.ncbi.nlm.nih.gov/pubmed/33278904

De Strooper, B., & Karran, E. (2016). The cellular phase of Alzheimer's disease. Cell, 164(4), 603-615.

Diano, S., Farr, S. A., Benoit, S. C., McNay, E. C., da Silva, I., Horvath, B., Gaskin, F. S., Nonaka, N., Jaeger, L. B., Banks, W. A., Morley, J. E., Pinto, S., Sherwin, R. S., Xu, L., Yamada, K. A., Sleeman, M. W., Tschöp, M. H., and Horvath, T. L. (2006). Ghrelin controls hippocampal spine synapse density and memory performance. Nature neuroscience, 9(3), 381–388. https://doi.org/10.1038/nn1656

Disanto, G., Barro, C., Benkert, P., Naegelin, Y., Schädelin, S., Giardiello, A., Zecca, C., Blennow, K., Zetterberg, H., Leppert, D., Kappos, L., Gobbi, C., Kuhle, J., & Swiss Multiple Sclerosis Cohort Study Group (2017). Serum Neurofilament light: A biomarker of neuronal damage in multiple sclerosis. Annals of neurology, 81(6), 857–870. https://doi.org/10.1002/ana.24954

Dixit, V. D., Yang, H., Sun, Y., Weeraratna, A. T., Youm, Y. H., Smith, R. G., and Taub, D. D. (2007). Ghrelin promotes thymopoiesis during aging. The Journal of clinical investigation, 117(10), 2778–2790. https://doi.org/10.1172/JCI30248

Dole, M., Hines, R. L., Mack, L. L., Mobley, R. C., Ferguson, L. D., and Alice, M. B. (1968). Gas phase macroions. Macromolecules, 1(1), 96–97. https://doi.org/10.1021/ma60001a017

Domon, B., & Aebersold, R. (2006). Mass spectrometry and protein analysis. Science, 312(5771), 212-217.

Duncan, M. W., Roder, H., and Hunsucker, S. W. (2008). Quantitative matrix-assisted laser desorption/ionization mass spectrometry. Briefings in functional genomics and proteomics, 7(5), 355–370. https://doi.org/10.1093/bfgp/eln041

Elbehiry A, Aldubaib M, Abalkhail A, Marzouk E, ALbeloushi A, Moussa I, Ibrahem M, Albazie H, Alqarni A, Anagreyyah S, Alghamdi S, Rawway M. How MALDI-TOF Mass Spectrometry Technology Contributes to Microbial Infection Control in Healthcare Settings. Vaccines (Basel). 2022 Nov 8;10(11):1881. doi: 10.3390/vaccines10111881. PMID: 36366389; PMCID: PMC9699604.

Ellington, A. A., Kullo, I. J., Bailey, K. R., & Klee, G. G. (2010). Antibody-based protein multiplex platforms: Technical and operational challenges. *Clinical Chemistry*, 56(2), 186–193. https://doi.org/10.1373/clinchem.2009.127217

Eslami, Z., Torabizadeh, M., Talebpour, Z., Talebpour, M., Ghassempour, A., and Aboul-Enein, H. Y. (2016). Simple and Sensitive Quantification of Ghrelin Hormone in Human Plasma Using SBSE-HPLC/DAD-MS. Journal of chromatographic science, 54(9), 1652–1660. https://doi.org/10.1093/chromsci/bmw125

Eslami, M., Yousefi, B., Kokhaei, P., Hemati, M., Nejad, Z. R., & Arabkari, V. (2017). Ghrelin as a regulator of neurodegeneration, neuroinflammation, and neurogenesis: Implications for Alzheimer's disease. *Reviews in the Neurosciences, 28*(8), 769–780. https://doi.org/10.1515/revneuro-2017-0005

Fairchild J.N., Horvath K., Guiochon G. Theoretical advantages and drawbacks of on-line, multidimensional liquid chromatography using multiple columns operated in parallel. J. Chromatogr. A. 2009;1216:6210–6217. doi: 10.1016/j.chroma.2009.06.085.

FDA-NIH Biomarker Working Group. (2016). BEST (Biomarkers, EndpointS, and other Tools) Resource. National Institutes of Health.

FDA. (2025). FDA grants marketing authorization for first blood test to aid in evaluation of Alzheimer's disease. U.S. Food and Drug Administration. https://www.fda.gov/news-events/press-announcements

Fenn, J. B. (2003). Electrospray Wings for Molecular Elephants (Nobel Lecture). Angewandte Chemie, 42(33), 3871–3894. https://doi.org/10.1002/anie.200300605

Fernandez G, Cabral A, Cornejo MP, De Francesco PN, Garcia-Romero G, Reynaldo M, Perello M. Des-Acyl Ghrelin Directly Targets the Arcuate Nucleus in a Ghrelin-Receptor Independent Manner and Impairs the Orexigenic Effect of Ghrelin. J Neuroendocrinol. 2016 Feb;28(2):12349. doi: 10.1111/jne.12349. PMID: 26661382.

Fernandez, G., et al. (2016). Unacylated ghrelin binds to a subset of arcuate nucleus cells independently of GHSR. *Endocrinology*, 157(2), 769–784.

Ferré, G., Louet, M., Saurel, O., Delort, B., Czaplicki, G., M'Kadmi, C., Damian, M., Renault, P., Cantel, S., Gavara, L., Demange, P., Marie, J., Fehrentz, J. A., Floquet, N., Milon, A., and Banères, J. L. (2019). Structure and dynamics of G protein-coupled receptor-bound ghrelin reveal the critical role of the octanoyl chain. Proceedings of the National Academy of Sciences of the United States of America, 116(35), 17525–17530. https://doi.org/10.1073/pnas.1905105116

Foster-Schubert, K. E., Overduin, J., Prudom, C. E., Liu, J., Callahan, H. S., Gaylinn, B. D., Thorner, M. O., & Cummings, D. E. (2010). Acyl and total ghrelin are suppressed strongly by ingested proteins, weakly by lipids, and biphasically by carbohydrates. *The Journal of Clinical Endocrinology & Metabolism,* *95*(2), 827–834. https://doi.org/10.1210/jc.2009-1328

Frank, R., & Hargreaves, R. (2003). Clinical biomarkers in drug discovery and development. Nature Reviews Drug Discovery, 2(7), 566-580.

Fukumoto, H., Tennis, M., Locascio, J. J., Hyman, B. T., Growdon, J. H., and Irizarry, M. C. (2003). Age but not diagnosis is the main predictor of plasma amyloid β-protein levels. Archives of Neurology, 60(7), 958–964. https://doi.org/10.1001/archneur.60.7.958

Fukushima, N., Hanada, R., Teranishi, H., Fukue, Y., Tachibana, T., Ishikawa, H., Takeda, S., Takeuchi, Y., Fukumoto, S., Kangawa, K., Nagata, K., and Kojima, M. (2005). Ghrelin directly regulates bone formation. Journal of bone and mineral

research : the official journal of the American Society for Bone and Mineral Research, 20(5), 790–798. https://doi.org/10.1359/JBMR.041237

Furness, J. B., Hunne, B., Matsuda, N., Yin, L., Russo, D., Kato, I., Fujimiya, M., Patterson, M., McLeod, J., Andrews, Z. B., and Bron, R. (2011). Investigation of the presence of ghrelin in the central nervous system of the rat and mouse. Neuroscience, 193, 1–9. https://doi.org/10.1016/j.neuroscience.2011.07.063

Gahete, M. D., Córdoba-Chacón, J., Salvatori, R., Castaño, J. P., Kineman, R. D., & Luque, R. M. (2010). Metabolic regulation of ghrelin O-acyltransferase (GOAT) expression in the mouse hypothalamus, pituitary, and stomach. Molecular and Cellular Endocrinology, 317(1–2), 154–1627

Gahete M. D., Córdoba-Chacón J., Hergueta-Redondo M., Martínez-Fuentes A. J., Kineman R. D., Moreno-Bueno G., et al. (2011). A Novel Human Ghrelin Variant (In1-Ghrelin) and Ghrelin-O-Acyltransferase Are Overexpressed in Breast Cancer: Potential Pathophysiological Relevance. PLoS ONE 6 (8), e23302. doi:10.1371/journal.pone.0023302

Gale, S. A., Acar, D., and Daffner, K. R. (2018). Dementia. The American journal of medicine, 131(10), 1161–1169. https://doi.org/10.1016/j.amjmed.2018.01.022

Gao S., Casals N., Keung W., Moran T. H., Lopaschuk G. D. (2013). Differential Effects of central Ghrelin on Fatty Acid Metabolism in Hypothalamic Ventral Medial and Arcuate Nuclei. Physiol. Behav. 118, 165–170. 10.1016/j.physbeh.2013.03.030

Gauna C, Meyler FM, Janssen JA, Delhanty PJ, Abribat T, van Koetsveld P, Hofland LJ, Broglio F, Ghigo E, van der Lely AJ. Administration of acylated ghrelin reduces insulin sensitivity, whereas the combination of acylated plus unacylated ghrelin strongly improves insulin sensitivity. J Clin Endocrinol Metab. 2004 Oct;89(10):5035-42. doi: 10.1210/jc.2004-0363. PMID: 15472202.

Gisslén M, Price RW, Andreasson U, Norgren N, Nilsson S, Hagberg L, Fuchs D, Spudich S, Blennow K, Zetterberg H. Plasma Concentration of the Neurofilament Light Protein (NFL) is a Biomarker of CNS Injury in HIV Infection: A Cross-Sectional Study. EBioMedicine. 2015 Nov 22;3:135-140. doi: 10.1016/j.ebiom.2015.11.036. Erratum in: EBioMedicine. 2016 May;7:287-288. PMID: 26870824; PMCID: PMC4739412.

Glish, G. L., and Vachet, R. W. (2003). The basics of mass spectrometry in the twenty-first century. Nature reviews. Drug discovery, 2(2), 140–150. https://doi.org/10.1038/nrd1011

Gomez-Pinilla, F. (2008). Brain foods: the effects of nutrients on brain function. *Nature Reviews Neuroscience, 9*(7), 568–578. https://doi.org/10.1038/nrn2421

Grönberg, M., Ahlin, C., Naeser, Y., Tiensuu Janson, E., Holmberg, L., & Fjällskog, M.-L. (2017). Ghrelin is a prognostic marker and a potential therapeutic target in breast cancer. PLoS ONE, 12(4), e0176059. https://doi.org/10.1371/journal.pone.0176059

Gross, J. H. (2017). Mass spectrometry. In Springer eBooks. https://doi.org/10.1007/978-3-319-54398-7

Gutierrez, J. A., Dorocke, J. A., Knierman, M. D., Gelfanova, V., Higgs, R. E., Koh, N. L., and Hale, J. E. (2005). Quantitative determination of peptides using matrix-assisted laser desorption/ionization time-of-flight mass spectrometry. BioTechniques, Suppl, 13–17. https://doi.org/10.2144/05386su02

Gutierrez J.A., Solenberg P.J., Perkins D.R., Willency J.A., Knierman M.D., Jin Z., Witcher D.R., Luo S., Onyia J.E., Hale J.E. Ghrelin octanoylation mediated by an orphan lipid transferase. Proc. Natl. Acad. Sci. Unit. States Am. 2008;105:6320–6325.

Gutierrez, J. A., Willency, J. A., Knierman, M. D., Coskun, T., Solenberg, P. J., Perkins, D. R., Higgs, R. E., and Hale, J. E. (2012). From ghrelin to ghrelin's O-acyl transferase. Methods in enzymology, 514, 129–146. https://doi.org/10.1016/B978-0-12-381272-8.00009-X

Haag, A. M. (2016). Mass analyzers and mass spectrometers. In Advances in Experimental Medicine and Biology (pp. 157–169). https://doi.org/10.1007/978-3-319-41448-5_7

Hampel, H., O'Bryant, S. E., Molinuevo, J. L., Zetterberg, H., Masters, C. L., Lista, S., … Blennow, K. (2018, November 1). Blood-based biomarkers for Alzheimer disease: mapping the road to the clinic. Nature Reviews Neurology, Vol. 14, pp. 639–652. https://doi.org/10.1038/s41582-018-0079-7

Hampel H, Hu Y, Cummings J, Mattke S, Iwatsubo T, Nakamura A, Vellas B, O'Bryant S, Shaw LM, Cho M, Batrla R, Vergallo A, Blennow K, Dage J, Schindler SE. Blood-based biomarkers for Alzheimer's disease: Current state and future use in a transformed global healthcare landscape. Neuron. 2023 Sep 20;111(18):2781-2799. doi: 10.1016/j.neuron.2023.05.017. Epub 2023 Jun 8. PMID: 37295421; PMCID: PMC10720399.

Hamza, Ghaith M., Vladislav B. Bergo, Sergey Mamaev, Don M. Wojchowski, Paul Toran, Camilla R. Worsfold, M. Paola Castaldi, and Jeffrey C. Silva. 2020. "Affinity-Bead Assisted Mass Spectrometry (Affi-BAMS): A Multiplexed Microarray Platform for Targeted Proteomics" International Journal of Molecular Sciences 21, no. 6: 2016. https://doi.org/10.3390/ijms21062016

Han, X., Aslanian, A., and Yates, J. R., 3rd (2008). Mass spectrometry for proteomics. Current opinion in chemical biology, 12(5), 483–490. https://doi.org/10.1016/j.cbpa.2008.07.024

Hankin, J. A., Barkley, R. M., and Murphy, R. C. (2007). Sublimation as a method of matrix application for mass spectrometric imaging. Journal of the American Society for Mass Spectrometry, 18(9), 1646-1652.

Heneka, M. T., Golenbock, D. T., & Latz, E. (2015). Innate immunity in Alzheimer’s disease. *Nature Immunology, 16*(3), 229–236. https://doi.org/10.1038/ni.3102

Henriksen, K., O’Bryant, S. E., Hampel, H., Trojanowski, J. Q., Montine, T. J., Jeromin, A., … Weiner, M. W. (2014, January). The future of blood-based biomarkers for Alzheimer’s disease. Alzheimer’s and Dementia, Vol. 10, pp. 115–131. https://doi.org/10.1016/j.jalz.2013.01.013

Herskovits, A. Z., Locascio, J. J., Peskind, E. R., Li, G., and Hyman, B. T. (2013). A Luminex prawf detects amyloid β oligomers in Alzheimer's disease cerebrospinal fluid. PloS one, 8(7), e67898. https://doi.org/10.1371/journal.pone.0067898

Herr P., Basler K. (2012). Porcupine-Mediated Lipidation Is Required for Wnt Recognition by Wls. Developmental Biol. 361 (2), 392–402. doi:10.1016/j.ydbio.2011.11.003

Hirtz, C., Busto, G. U., Bennys, K., Kindermans, J., Navucet, S., Tiers, L., Lista, S., Vialaret, J., Gutierrez, A., Dauvilliers, Y., Berr, C., Lehmann, S., & Gabelle, A. (2023). Comparison of ultrasensitive and mass spectrometry quantification of blood-based amyloid biomarkers for Alzheimer's disease diagnosis in a memory clinic cohort. Alzheimer's Research & Therapy, 15. https://doi.org/10.1186/s13195-023-01188-8

Ho, C. S., Lam, C. W., Chan, M. H., Cheung, R. C., Law, L. K., Lit, L. C., Ng, K. F., Suen, M. W., and Tai, H. L. (2003). Electrospray ionisation mass spectrometry: principles and clinical applications. The Clinical biochemist. Reviews, 24(1), 3–12.

Hörber, S., Achenbach, P., Schleicher, E., & Peter, A. (2020). Harmonization of immunoprawfs for biomarkers in diabetes mellitus. Biotechnology advances, 39, 107359. https://doi.org/10.1016/j.biotechadv.2019.02.015

Hofmann K. A superfamily of membrane-bound O-acyltransferases with implications for wnt signaling. Trends Biochem Sci. 2000 Mar;25(3):111-2. doi: 10.1016/s0968-0004(99)01539-x. PMID: 10694878.

Hornsby A. K. E., Redhead Y. T., Rees D. J., Ratcliff M. S. G., Reichenbach A., Wells T., et al. (2016). Short-Term Calorie Restriction Enhances Adult Hippocampal Neurogenesis and Remote Fear Memory in a Ghsr-Dependent Manner. Psychoneuroendocrinology 63, 198–207. doi:10.1016/j.psyneuen.2015.09.023

Hornsby A. K. E., Buntwal L., Carisi M. C., Santos V. V., Johnston F., Roberts L. D., et al. (2020). UnacylatedUnacylatedatedated-Ghrelin Impairs Hippocampal Neurogenesis and Memory in Mice and Is Altered in Parkinson's Dementia in Humans. Cell Rep. Med. 1 (7), 100120. doi:10.1016/j.xcrm.2020.100120

Hornsby, W. E., et al. (2022). Mass spectrometry for ghrelin isoform quantification. Analytical Chemistry, 94(2), 897–905.

Hosoda, H., M, Kojima., H. Matsuo, and K. Kangawa. 2000. Ghrelin and des-acyl ghrelin: two major forms of rat ghrelin peptide in gastrointestinal tissue. Biochem. Biophys. Res. Comm. 279:909–913.

Hosoda, H., Kojima, M., Mizushima, T., Shimizu, S., and Kangawa, K. (2003). Structural divergence of human ghrelin. Identification of multiple ghrelin-derived

molecules produced by post-translational processing. The Journal of biological chemistry, 278(1), 64–70. https://doi.org/10.1074/jbc.M205366200

Hosoda, H., Kangawa, K. (2004). Ghrelin Measurement: Present and Perspectives. In: Ghigo, E., Benso, A., Broglio, F. (eds) Ghrelin. Endocrine Updates, vol 23. Springer, Boston, MA. https://doi.org/10.1007/1-4020-7971-0_15

Hossain, M. The Mass Spectrometer and Its Components. in Selected Reaction Monitoring Mass Spectrometry (SRM-MS) in Proteomics 17–52 (Springer International Publishing, 2020). doi:10.1007/978-3-030-53433-2_2.

Hou, J., Charron, C. L., Fowkes, M. M., and Luyt, L. G. (2016). Bridging computational modeling with amino acid replacements to investigate GHS-R1a-peptidomimetic recognition. European journal of medicinal chemistry, 123, 822–833. https://doi.org/10.1016/j.ejmech.2016.07.078

Hu Q, Noll RJ, Li H, Makarov A, Hardman M, Cooks RG. The Orbitrap: A new mass spectrometer. Journal of Mass Spectrometry. 2005;40:430–443

Hu Y, Kirmess KM, Meyer MR, Rabinovici GD, Gatsonis C, Siegel BA, Whitmer RA, Apgar C, Hanna L, Kanekiyo M, Kaplow J, Koyama A, Verbel D, Holubasch MS, Knapik SS, Connor J, Contois JH, Jackson EN, Harpstrite SE, Bateman RJ, Holtzman DM, Verghese PB, Fogelman I, Braunstein JB, Yarasheski KE, West T (2022) Assessment of a plasma amyloid probability score to estimate amyloid positron emission tomography findings among adults with cognitive impairment. JAMA Netw Open 5, e228392.

Inhoff T, Mönnikes H, Noetzel S, Stengel A, Goebel M, Dinh QT, Riedl A, Bannert N, Wisser AS, Wiedenmann B, Klapp BF, Taché Y, Kobelt P. Desacyl ghrelin inhibits the orexigenic effect of peripherally injected ghrelin in rats. Peptides. 2008 Dec;29(12):2159-68. doi: 10.1016/j.peptides.2008.09.014. Epub 2008 Sep 30. PMID: 18938204; PMCID: PMC2586396.

Inoue, M., Suzuki, H., Meno, K., Liu, S., Korenaga, T., & Uchida, K. (2023). Identification of Plasma Proteins as Biomarkers for Mild Cognitive Impairment and Alzheimer's Disease Using Liquid Chromatography–Tandem Mass Spectrometry. International Journal of Molecular Sciences, 24(17), 13064. https://doi.org/10.3390/ijms241713064

Jack, C. R., Bennett, D. A., Blennow, K., Carrillo, M. C., Dunn, B., Haeberlein, S. B., … Silverberg, N. (2018, April 1). NIA-AA Research Framework: Toward a biological definition of Alzheimer's disease. Alzheimer's and Dementia, Vol. 14, pp. 535–562. https://doi.org/10.1016/j.jalz.2018.02.018

Janda C. Y., Waghray D., Levin A. M., Thomas C., Garcia K. C. (2012). Structural Basis of Wnt Recognition by Frizzled. Science 337 (6090), 59–64. doi:10.1126/SCIENCE.1222879

Janelidze, S., Stomrud, E., Palmqvist, S., Zetterberg, H., Van Westen, D., Jeromin, A., … Hansson, O. (2016). Plasma β-amyloid in Alzheimer's disease and vascular disease. Scientific Reports, 6. https://doi.org/10.1038/srep26801

Janelidze, S., Mattsson, N., Palmqvist, S., Smith, R., Beach, T. G., Serrano, G. E., Chai, X., Proctor, N. K., Eichenlaub, U., Zetterberg, H., Blennow, K., Reiman, E. M., Stomrud, E., Dage, J. L., & Hansson, O. (2020). Plasma P-tau181 in Alzheimer's disease: relationship to other biomarkers, differential diagnosis, neuropathology and longitudinal progression to Alzheimer's dementia. Nature medicine, 26(3), 379–386. https://doi.org/10.1038/s41591-020-0755-1

Janelidze S, Teunissen CE, Zetterberg H, Allué JA, Sarasa L, Eichenlaub U, Bittner T, Ovod V, Verberk IMW, Toba K, Nakamura A, Bateman RJ, Blennow K, Hansson O (2021) Head-to-head comparison of 8plasma amyloid-β 42/40 prawfs in Alzheimer disease. JAMA Neurol 78, 1375–1382.

Janelidze, S. et al. Head-to-head comparison of 10 plasma phospho-tau prawfs in prodromal Alzheimer's disease. Brain https://doi.org/10.1093/brain/awac333 (2022).

Janelidze, S., Mattsson-Carlgren, N., Palmqvist, S., Cullen, N. C., Hansson, O. (2022). Performance of plasma p-tau217 in the prediction of Alzheimer's disease pathology. Nature Medicine, 28(6), 1057–1063. https://doi.org/10.1038/s41591-022-01702-5

Jennings KR, Dolnikowski GG (1990) Mass analyzers. Method Enzymol 193:37–61

Julien, M., Kay, R. G., Delhanty, P. J., Allas, S., Granata, R., Barton, C., Constable, S., Ghigo, E., van der Lely, A. J., and Abribat, T. (2012). In vitro and in vivo stability and pharmacokinetic profile of unacylatedunacylatedatedated ghrelin (UAG)

analogues. European journal of pharmaceutical sciences : official journal of the European Federation for Pharmaceutical Sciences, 47(4), 625–635. https://doi.org/10.1016/j.ejps.2012.07.014

Kaiya H., Kojima M., Hosoda H., Koda A., Yamamoto K., Kitajima Y., et al. (2001). Bullfrog Ghrelin Is Modified by N-Octanoic Acid at its Third Threonine Residue. J. Biol. Chem. 276 (44), 40441–40448. doi:10.1074/jbc.M105212200

Kaneko, N., Yamamoto, R., Sato, T. A., & Tanaka, K. (2014). Identification and quantification of amyloid beta-related peptides in human plasma using matrix-assisted laser desorption/ionization time-of-flight mass spectrometry. Proceedings of the Japan Academy. Series B, Physical and biological sciences, 90(3), 104–117. https://doi.org/10.2183/pjab.90.104

Karas, M., and Hillenkamp, F. (1988). Laser desorption ionization of proteins with molecular masses exceeding 10,000 daltons. Analytical chemistry, 60(20), 2299–2301. https://doi.org/10.1021/ac00171a028

Karikari, T. K., Pascoal, T. A., Ashton, N. J., Janelidze, S., Benedet, A. L., Rodriguez, J. L., … Blennow, K. (2020). Blood phosphorylated tau 181 as a biomarker for Alzheimer's disease: a diagnostic performance and prediction modelling study using data from four prospective cohorts. The Lancet Neurology, 19(5), 422–433. https://doi.org/10.1016/S1474-4422(20)30071-5

Kebarle, P., and Verkerk, U. H. (2009). Electrospray: from ions in solution to ions in the gas phase, what we know now. Mass spectrometry reviews, 28(6), 898–917. https://doi.org/10.1002/mas.20247

Keller, B. O., Sui, J., Young, A. B., and Whittal, R. M. (2008). Interferences and contaminants encountered in modern mass spectrometry. Analytica chimica acta, 627(1), 71–81. https://doi.org/10.1016/j.aca.2008.04.043

Kennaway D. J. (2020). Measuring melatonin by immunoprawf. Journal of pineal research, 69(1), e12657. https://doi.org/10.1111/jpi.12657

Kent B. A., Beynon A. L., Hornsby A. K. E., Bekinschtein P., Bussey T. J., Davies J. S., et al. (2015). The Orexigenic Hormone Acyl-Ghrelin Increases Adult Hippocampal

Neurogenesis and Enhances Pattern Separation. Psychoneuroendocrinology 51, 431–439. doi:10.1016/j.psyneuen.2014.10.015

Kern, A., Grande, M. T., & Smith, R. G. (2014). Apo-ghrelin receptor (apo-GHS-R1a) regulates dopamine signaling in the brain. Frontiers in Neuroscience, 8, 157. https://doi.org/10.3389/fnins.2014.00157

Kern, A., Apikian, C., & Smith, R. G. (2015). Hippocampal dopamine/DRD1 signaling is dependent on the ghrelin receptor. Cell, 163(6), 1512–1528. https://doi.org/10.1016/j.cell.2015.11.015

Keshavan, A., Pannee, J., Karikari, T. K., Rodriguez, J. L., Ashton, N. J., Nicholas, J. M., Cash, D. M., Coath, W., Lane, C. A., Parker, T. D., Lu, K., Buchanan, S. M., Keuss, S. E., James, S. N., Murray-Smith, H., Wong, A., Barnes, A., Dickson, J. C., Heslegrave, A., Portelius, E., … Schott, J. M. (2021). Population-based blood screening for preclinical Alzheimer's disease in a British birth cohort at age 70. Brain : a journal of neurology, 144(2), 434–449. https://doi.org/10.1093/brain/awaa403

Klingelhoefer, L., & Reichmann, H. (2017). Pathogenesis of Parkinson disease—the gut–brain axis and environmental factors. *Nature Reviews Neurology*, 13(11), 653–668.

Khatib, N. (2014). Ghrelin: Ghrelin as a regulatory peptide in growth hormone secretion. Journal of Clinical and Diagnostic Research, 8(8), MC13–MC17.

Kojima, M., Hosoda, H., Date, Y., Nakazato, M., Matsuo, H., Kangawa, K.; Ghrelin is a growth-hormone-releasing acylated peptide from stomach; Nature, (1999); 402(6762): 656–660

Kojima, M., Hosoda, H., Matsuo, H., Kangawa, K.; Ghrelin: discovery of the natural endogenous ligand for the growth hormone secretagogue receptor; Trends in Endocrinology and Metabolism, (2001); 12(3): 118–122.

Kojima M., Kangawa K. (2005). Ghrelin: Structure and Function. Physiol. Rev. 85, 495–522. doi:10.1152/physrev.00012.2004

Kovalchuk, S. I., Anikanov, N. A., Ivanova, O. M., Ziganshin, R. H., and Govorun, V. M. (2015). Bovine serum albumin as a universal suppressor of non-specific peptide

binding in vials prior to nano-chromatography coupled mass-spectrometry analysis. Analytica chimica acta, 893, 57–64. https://doi.org/10.1016/j.aca.2015.08.027

Knochenmuss, R., and Zhigilei, L. V. (2010). Molecular dynamics simulations of MALDI: laser fluence and pulse width dependence of plume characteristics and consequences for matrix and analyte ionization. Journal of Mass Spectrometry, n/a. https://doi.org/10.1002/jms.1732

Kuhle J, Barro C, Andreasson U, Derfuss T, Lindberg R, Sandelius AA, Liman V, Norgren N, Blennow K, Zetterberg H (2016) Comparison of three analytical platforms for quantification of the neurofilament light chain in blood samples: ELISA, electrochemiluminescence immunoprawf and Simoa. Clin Chem Lab Med 54, 1655–1661.

Kwon, H. S., Lee, H., Kim, Y. S., Choi, H., Lee, K. Y., Lee, Y. J., Lee, E. H., Hwang, M., Park, H., & Koh, S. H. (2023). Comparing Neurofilament Light Chain Levels in Serum and Plasma. Dementia and neurocognitive disorders, 22(3), 109–111. https://doi.org/10.12779/dnd.2023.22.3.109

Lanckmans, K., Sarre, S., Smolders, I., and Michotte, Y. (2007). Use of a structural analogue versus a stable isotope labeled internal standard for the quantification of angiotensin IV in rat brain dialysates using nano-liquid chromatography/tandem mass spectrometry. Rapid communications in mass spectrometry : RCM, 21(7), 1187–1195. https://doi.org/10.1002/rcm.2950

Landau, S. M., Lu, M., Joshi, A. D., Pontecorvo, M., Mintun, M. A., Trojanowski, J. Q., … Jagust, W. J. (2013). Comparing positron emission tomography imaging and cerebrospinal fluid measurements of β-amyloid. Annals of Neurology, 74(6), 826–836. https://doi.org/10.1002/ana.23908

Lau, K., Kotzur, R., & Richter, F. (2024). Blood–brain barrier alterations and their impact on Parkinson's disease pathogenesis and therapy. Translational Neurodegeneration, 13(1), 37. https://doi.org/10.1186/s40035-024-00430-z

Lewczuk, P., Kornhuber, J., Vanmechelen, E., Peters, O., Heuser, I., Maier, W., … Wiltfang, J. (2010). Amyloid β peptides in plasma in early diagnosis of Alzheimer's disease: A multicenter study with multiplexing. Experimental Neurology, 223(2), 366–370. https://doi.org/10.1016/j.expneurol.2009.07.024

Lewczuk, P., Esselmann, H., Otto, M., Maler, J. M., Henkel, A. W., Henkel, M. K., ... & Kornhuber, J. (2010). Neurochemical diagnosis of Alzheimer's dementia by CSF Aβ42, Aβ42/Aβ40 ratio and total tau. Neurobiology of Aging, 31(5), 778–788. https://doi.org/10.1016/j.neurobiolaging.2008.06.013

Li E., Kim Y., Kim S., Park S. Ghrelin-induced hippocampal neurogenesis and enhancement of cognitive function are mediated independently of GH/IGF-1 axis: lessons from the spontaneous dwarf rats. Endocr. J. 2013;60:1065–1075.

Li, E., Chung, H., Kim, Y., Kim, D. H., Ryu, J. H., Sato, T., Kojima, M., and Park, S. (2013). Ghrelin directly stimulates adult hippocampal neurogenesis: implications for learning and memory. Endocrine journal, 60(6), 781–789. https://doi.org/10.1507/endocrj.ej13-0008

Lista, S., Faltraco, F., Prvulovic, D., and Hampel, H. (2013, February). Blood and plasma-based proteomic biomarker research in Alzheimer's disease. Progress in Neurobiology, Vol. 101–102, pp. 1–17. https://doi.org/10.1016/j.pneurobio.2012.06.007

Lippi, G., Salvagno, G. L., Montagnana, M., & Guidi, G. C. (2006). Stability of blood samples drawn in K3EDTA tubes for routine hematologic testing. LaboratoriumsMedizin, 30(1), 33–38.

Lifke, V., Kollmorgen, G., Manuilova, E., Oelschlaegel, T., Hillringhaus, L., Widmann, M., von Arnim, C. A. F., Otto, M., Christenson, R. H., Powers, J. L., Shaw, L. M., Hansson, O., Doecke, J. D., Li, Q. X., Teunissen, C., Tumani, H., and Blennow, K. (2019). Elecsys® Total-Tau and Phospho-Tau (181P) CSF prawfs: Analytical performance of the novel, fully automated immunoprawfs for quantification of tau proteins in human cerebrospinal fluid. Clinical biochemistry, 72, 30–38. https://doi.org/10.1016/j.clinbiochem.2019.05.005

Lim M. D. (2018). Dried Blood Spots for Global Health Diagnostics and Surveillance: Opportunities and Challenges. The American journal of tropical medicine and hygiene, 99(2), 256–265. https://doi.org/10.4269/ajtmh.17-0889

Liu B., Garcia E. A., Korbonits M. (2011). Genetic Studies on the Ghrelin, Growth Hormone Secretagogue Receptor (GHSR) and Ghrelin O-Acyl Transferase (GOAT) Genes. Peptides 32 (11), 2191–2207. doi:10.1016/j.peptides.2011.09.006

Loo, R. R., Dales, N., and Andrews, P. C. (1994). Surfactant effects on protein structure examined by electrospray ionization mass spectrometry. Protein science : a publication of the Protein Society, 3(11), 1975–1983. https://doi.org/10.1002/pro.5560031109

Lupo, S., and Kahler, T. (2020). New Advice on an Old Topic: Buffers in Reversed-Phase HPLC. Chromatography Online. https://www.chromatographyonline.com/view/new-advice-old-topic-buffers-reversed-phase-hplc

Leeuwendaal, N. K., Cryan, J. F., and Schellekens, H. (2021). Gut peptides and the microbiome: focus on ghrelin. Current opinion in endocrinology, diabetes, and obesity, 28(2), 243–252. https://doi.org/10.1097/MED.0000000000000616

Lingervelder, D., van Rijn, M., Ruijter, W., & Moons, K. G. (2021). Cost-effectiveness of point-of-care testing: A systematic review. *BMJ Open, 11*(2), e040725. https://doi.org/10.1136/bmjopen-2020-040725

Lutter, M., Sakata, I., Osborne-Lawrence, S., Rovinsky, S. A., Anderson, J. G., Jung, S., Birnbaum, S., Yanagisawa, M., Elmquist, J. K., Nestler, E. J., and Zigman, J. M. (2008). The orexigenic hormone ghrelin defends against depressive symptoms of chronic stress. Nature neuroscience, 11(7), 752–753. https://doi.org/10.1038/nn.2139

Makarov A. Electrostatic axially harmonic orbital trapping: A high-performance technique of mass analysis. Analytical Chemistry. 2000;72:1156–1162.

Mann, M., & Jensen, O. N. (2003). Proteomic analysis of post-translational modifications. Nature Biotechnology, 21(3), 255-261.

Mani BK, Zigman JM. Ghrelin as a Survival Hormone. Trends Endocrinol Metab. 2017 Dec;28(12):843-854. doi: 10.1016/j.tem.2017.10.001. Epub 2017 Oct 30. PMID: 29097101; PMCID: PMC5777178.

Matsumoto, M., Kitajima, Y., Iwanami, T., Hayashi, Y., Tanaka, S., Minamitake, Y., Hosoda, H., Kojima, M., Matsuo, H., and Kangawa, K. (2001). Structural similarity of

ghrelin derivatives to peptidyl growth hormone secretagogues. Biochemical and biophysical research communications, 284(3), 655–659. https://doi.org/10.1006/bbrc.2001.5014

Mattsson N, Andreasson U, Zetterberg H, Blennow K; Alzheimer's Disease Neuroimaging Initiative. Association of Plasma Neurofilament Light With Neurodegeneration in Patients With Alzheimer Disease. JAMA Neurol. 2017 May 1;74(5):557-566. doi: 10.1001/jamaneurol.2016.6117. PMID: 28346578; PMCID: PMC5822204.

Mattson, M. P., & Arumugam, T. V. (2018). Hallmarks of brain ageing: Adaptive and pathological modification by metabolic states. *Cell Metabolism, 27*(6), 1176–1199. https://doi.org/10.1016/j.cmet.2018.05.011

Mattsson-Carlgren, N., Collij, L. E., Stomrud, E., Pichet Binette, A., Ossenkoppele, R., Smith, R., Karlsson, L., Lantero-Rodriguez, J., Snellman, A., Strandberg, O., Palmqvist, S., Ashton, N. J., Blennow, K., Janelidze, S., & Hansson, O. (2024). Plasma Biomarker Strategy for Selecting Patients With Alzheimer Disease for Antiamyloid Immunotherapies. JAMA neurology, 81(1), 69–78. https://doi.org/10.1001/jamaneurol.2023.4596

Masumoto N., Lanyon-Hogg T., Rodgers U. R., Konitsiotis A. D., Magee A. I., Tate E. W. (2015). Membrane Bound O-Acyltransferases and Their Inhibitors. Biochem. Soc. Trans. 43, 246–252. 10.1042/BST2015001

Mayeux, R. (2004). Biomarkers: potential uses and limitations. NeuroRx, 1(2), 182-188.

Mendel, C. M., and Mendel, D. B. (1985). ynon-specific' binding. The problem, and a solution. The Biochemical journal, 228(1), 269–272. https://doi.org/10.1042/bj2280269

McGovern-Gooch, K. R., Rodrigues, T., Darling, J. E., Sieburg, M. A., Abizaid, A., and Hougland, J. L. (2016). Ghrelin Octanoylation Is Completely Stabilized in Biological Samples by Alkyl Fluorophosphonates. Endocrinology, 157(11), 4330–4338. https://doi.org/10.1210/en.2016-1657

Melby, J. A.; De Lange, W. J.; Zhang, J.; Roberts, D. S.; Mitchell, S. D.; Tucholski, T.; Kim, G.; Kyrvasilis, A.; McIlwain, S. J.; Kamp, T. J.; Ralphe, J. C.; Ge, Y. Functionally Integrated Top-Down Proteomics for Standardized Assessment of Human Induced Pluripotent Stem Cell-Derived Engineered Cardiac Tissues. J. Proteome Res. 2021, 20, 1424– 1433, DOI: 10.1021/acs.jproteome.0c00830

Menzies M., Seim I., Josh P., Nagaraj S. H., Lees M., Walpole C., et al. (2014). Cloning and Tissue Distribution of Novel Splice Variants of the Ovine Ghrelin Gene. BMC Veterinary Research 10 (1). doi:10.1186/s12917-014-0211-x

Meyer J. G., Komives E. A. (2012) Charge state coalescence during electrospray ionization improves peptide identification by tandem mass spectrometry. J. Am. Soc. Mass Spectrom. 23, 1390–1399

Mielke, M. M., Frank, R. D., Dage, J. L., Jeromin, A., Ashton, N. J., Blennow, K., Karikari, T. K., Vanmechelen, E., Zetterberg, H., Algeciras-Schimnich, A., Knopman, D. S., Lowe, V., Bu, G., Vemuri, P., Graff-Radford, J., Jack, C. R., Jr, & Petersen, R. C. (2021). Comparison of Plasma Phosphorylated Tau Species With Amyloid and Tau Positron Emission Tomography, Neurodegeneration, Vascular Pathology, and Cognitive Outcomes. JAMA neurology, 78(9), 1108–1117. https://doi.org/10.1001/jamaneurol.2021.2293

Molina, R. D., Conzatti, L. P., da Silva, A. P. B., Goi, L. D. S., da Costa, B. K., Machado, D. C., & Sato, D. K. (2020). Detection of autoantibodies in central nervous system inflammatory disorders: Clinical application of cell-based prawfs. Multiple sclerosis and related disorders, 38, 101858. https://doi.org/10.1016/j.msard.2019.101858

Molinuevo, J. L., Ayton, S., Batrla, R., Bednar, M. M., Bittner, T., Cummings, J., … Blennow, K. (2018). Current state of Alzheimer's fluid biomarkers. Acta Neuropathologica, 136(6). https://doi.org/10.1007/s00401-018-1932-x

Moon, M., Kim, H. G., Hwang, L., Seo, J.-H., Kim, S., Hwang, S., Kim, K.-T., Lee, K.-T., Chung, H., Oh, M.-S., & Lee, K.-W. (2009). Neuroprotective effect of ghrelin in the 1-methyl-4-phenyl-1,2,3,6-tetrahydropyridine mouse model of Parkinson's disease by blocking microglial activation. Neurotoxicology Research, 15(4), 332–347. https://doi.org/10.1007/s12640-009-9037-x

Moon M., Cha M.-Y., Mook-Jung I. (2014). Impaired Hippocampal Neurogenesis and its Enhancement with Ghrelin in 5XFAD Mice. Jad 41 (1), 233–241. doi:10.3233/JAD-132417

Montagne, A., Barnes, S. R., Sweeney, M. D., Halliday, M. R., Sagare, A. P., Zhao, Z., … Zlokovic, B. V. (2015). Blood-Brain barrier breakdown in the aging human hippocampus. Neuron, 85(2), 296–302. https://doi.org/10.1016/j.neuron.2014.12.032

Montoliu-Gaya, L., Barthelemy, N. R., Long, K. R., et al. (2023). Quantification of multiple tau isoforms by targeted immunoprecipitation mass spectrometry in plasma. *Alzheimer's & Dementia, 19*(12), 444–452. https://doi.org/10.1002/alz.13025

Muñoz-Prieto, A., Martínez-Subiela, S., Cerón, J. J., & Tvarijonaviciute, A. (2019). A new highly sensitive immunoprawf for the detection of adiponectin in serum and saliva of dogs and its application in obesity and canine leishmaniosis. Research in veterinary science, 125, 374–381. https://doi.org/10.1016/j.rvsc.2019.07.019

Murtuza, M. I., and Isokawa, M. (2018). Endogenous ghrelin-O-acyltransferase (GOAT) acylates local ghrelin in the hippocampus. Journal of neurochemistry, 144(1), 58–67. https://doi.org/10.1111/jnc.14244

Nagaya, N., Uematsu, M., Kojima, M., Ikeda, Y., Yoshihara, F., Shimizu, W., Hosoda, H., Hirota, Y., Ishida, H., Mori, H., and Kangawa, K. (2001). Chronic administration of ghrelin improves left ventricular dysfunction and attenuates development of cardiac cachexia in rats with heart failure. Circulation, 104(12), 1430–1435. https://doi.org/10.1161/hc3601.095575

Nakamura, A., Kaneko, N., Villemagne, V. L., Kato, T., Doecke, J., Doré, V., … Yanagisawa, K. (2018). High performance plasma amyloid-β biomarkers for Alzheimer's disease. Nature, 554(7691), 249–254. https://doi.org/10.1038/nature25456

Nakazato M., Murakami N., Date Y., Kojima M., Matsuo H., Kangawa K., et al. (2001). A Role for Ghrelin in the Central Regulation of Feeding. Nature 409 (6817), 194–198. 10.1038/35051587

Navarro, G., Rea, W., Quiroz, C., Moreno, E., Gomez, D., Wenthur, C. J., Casadó, V., Leggio, L., Hearing, M. C., & Ferré, S. (2022). Complexes of ghrelin GHS-R1a, GHS-R1b, and dopamine D1 receptors localized in the ventral tegmental area as main

mediators of the dopaminergic effects of ghrelin. Journal of Neuroscience, 42(6), 940–956. https://doi.org/10.1523/JNEUROSCI.1151-21.2021

Neagu, A. N., Jayathirtha, M., Baxter, E., Donnelly, M., Petre, B. A., and Darie, C. C. (2022). Applications of Tandem Mass Spectrometry (MS/MS) in Protein Analysis for Biomedical Research. Molecules (Basel, Switzerland), 27(8), 2411. https://doi.org/10.3390/molecules27082411

NHS England. (2021). *Point of care testing (POCT): Guidance for NHS Trusts and clinical teams*. https://www.england.nhs.uk/publication/point-of-care-testing-guidance

Niemeyer, C. M., Adler, M., and Wacker, R. (2005, April). Immuno-PCR: High sensitivity detection of proteins by nucleic acid amplification. Trends in Biotechnology, Vol. 23, pp. 208–216. https://doi.org/10.1016/j.tibtech.2005.02.006

Nile A. H., Hannoush R. N. (2016). Fatty Acylation of Wnt Proteins. Nat. Chem. Biol. 12 (2), 60–69. doi:10.1038/nchembio.2005

Nishi, Y., Hiejima, H., Hosoda, H., Kaiya, H., Mori, K., Fukue, Y., Yanase, T., Nawata, H., Kangawa, K., and Kojima, M. (2005). Ingested medium-chain fatty acids are directly utilized for the acyl modification of ghrelin. Endocrinology, 146(5), 2255–2264. https://doi.org/10.1210/en.2004-0695

Nishi, Y., Yoh, J., Hattori, Y., & Sugimoto, H. (2011). Ghrelin acylation and its biological significance. Endocrine Journal, 58(6), 403–410.

Ntai, I.; Fornelli, L.; DeHart, C. J.; Hutton, J. E.; Doubleday, P. F.; LeDuc, R. D.; van Nispen, A. J.; Fellers, R. T.; Whiteley, G.; Boja, E. S.; Rodriguez, H.; Kelleher, N. L. Precise Characterization of KRAS4b Proteoforms in Human Colorectal Cells and Tumors Reveals Mutation/Modification Cross-Talk. Proc. Natl. Acad. Sci. U. S. A. 2018, 115 (16), 4140– 4145,

O'Bryant, S. E., Edwards, M., Johnson, L., Hall, J., Villarreal, A. E., Britton, G. B., … Graff-Radford, N. R. (2016). A blood screening test for Alzheimer's disease. Alzheimer's and Dementia: Diagnosis, Assessment and Disease Monitoring, 3, 83–90. https://doi.org/10.1016/j.dadm.2016.06.004

O'Bryant, S. E., Mielke, M. M., Rissman, R. A., Lista, S., Vanderstichele, H., Zetterberg, H., … Hampel, H. (2017, January 1). Blood-based biomarkers in Alzheimer disease: Current state of the science and a novel collaborative paradigm for advancing from discovery to clinic. Alzheimer's and Dementia, Vol. 13, pp. 45–58. https://doi.org/10.1016/j.jalz.2016.09.014

Ossenkoppele, R., Jansen, W. J., Rabinovici, G. D., Knol, D. L., van der Flier, W. M., van Berckel, B. N., Scheltens, P., Visser, P. J., Amyloid PET Study Group, Verfaillie, S. C., Zwan, M. D., Adriaanse, S. M., Lammertsma, A. A., Barkhof, F., Jagust, W. J., Miller, B. L., Rosen, H. J., Landau, S. M., Villemagne, V. L., Rowe, C. C., … Brooks, D. J. (2015). Prevalence of amyloid PET positivity in dementia syndromes: a meta-analysis. JAMA, 313(19), 1939–1949. https://doi.org/10.1001/jama.2015.4669

Outeiro, T.F., Koss, D.J., Erskine, D. et al. Dementia with Lewy bodies: an update and outlook. Mol Neurodegeneration 14, 5 (2019). https://doi.org/10.1186/s13024-019-0306-8

Ovod, V., Ramsey, K. N., Mawuenyega, K. G., Bollinger, J. G., Hicks, T., Schneider, T., … Bateman, R. J. (2017). Amyloid β concentrations and stable isotope labeling kinetics of human plasma specific to central nervous system amyloidosis. Alzheimer's and Dementia, 13(8), 841–849. https://doi.org/10.1016/j.jalz.2017.06.2266

Oxford Health NHS Foundation Trust. (2025, January). *Trial for blood tests to diagnose dementia accepts first participants at Warneford Hospital* [News release]. Retrieved from https://www.oxfordhealth.nhs.uk/news/trial-for-blood-tests-to-diagnose-dementia-accepts-first-participants-at-warneford-hospital/

Pais MV, Forlenza OV, Diniz BS. Plasma Biomarkers of Alzheimer's Disease: A Review of Available Assays, Recent Developments, and Implications for Clinical Practice. Journal of Alzheimer's Disease Reports. 2023;7(1):355-380. doi:10.3233/ADR-230029

Palmqvist, S., Zetterberg, H., Mattsson, N., Johansson, P., Minthon, L., Blennow, K., … Hansson, O. (2015). Detailed comparison of amyloid PET and CSF biomarkers for identifying early Alzheimer disease. Neurology, 85(14), 1240–1249. https://doi.org/10.1212/WNL.0000000000001991

Palmqvist, S., Janelidze, S., Stomrud, E., Zetterberg, H., Karl, J., Zink, K., ... & Hansson, O. (2020). Performance of fully automated plasma assays as screening tests for Alzheimer disease–related β-amyloid status. JAMA Neurology, 77(9), 1060–1069. https://doi.org/10.1001/jamaneurol.2020.1123

Pan, W., Tu, H., and Kastin, A. J. (2006). Differential BBB interactions of three ingestive peptides: obestatin, ghrelin, and adiponectin. Peptides, 27(4), 911–916. https://doi.org/10.1016/j.peptides.2005.12.014

Pannee, J., Törnqvist, U., Westerlund, A., Ingelsson, M., Lannfelt, L., Brinkmalm, G., … Portelius, E. (2014). The amyloid-β degradation pattern in plasma-A possible tool for clinical trials in Alzheimer's disease. Neuroscience Letters, 573, 7–12. https://doi.org/10.1016/j.neulet.2014.04.041

Pannee, J., Portelius, E., Minthon, L., Wallin, A., Blennow, K., & Zetterberg, H. (2014). Reference measurement procedures for Alzheimer's disease cerebrospinal fluid biomarkers: Progress and challenges. Frontiers in Neurology, 5, 182. https://doi.org/10.3389/fneur.2014.00182

Pasch, H., and Schrepp, W. (2003). MALDI-TOF Mass spectrometry of synthetic polymers. In Springer eBooks. https://doi.org/10.1007/978-3-662-05046-0

Pemberton, J., & Richards, P. (2008). Isoforms of circulating ghrelin: biological relevance and measurement. Endocrine Reviews, 29(4), 443–462.

Peng, J., Liang, D., & Zhang, Z. (2024). Palmitoylation of synaptic proteins: roles in functional regulation and pathogenesis of neurodegenerative diseases. *Cellular & Molecular Biology Letters, 29*(1), 108. https://doi.org/10.1186/s11658-024-00625-2

Pepe, M. S., et al. (2001). Phases of biomarker development for early detection of cancer. Journal of the National Cancer Institute, 93(14), 1054–1061.

Preische O, Schultz SA, Apel A, Kuhle J, Kaeser SA, Barro C, Gräber S, Kuder-Buletta E, LaFougere C, Laske C, Vöglein J, Levin J, Masters CL, Martins R, Schofield PR, Rossor MN, Graff-Radford NR, Salloway S, Ghetti B, Ringman JM, Noble JM, Chhatwal J, Goate AM, Benzinger TLS, Morris JC, Bateman RJ, Wang G, Fagan AM, McDade EM, Gordon BA, Jucker M; Dominantly Inherited Alzheimer Network. Serum neurofilament dynamics predicts neurodegeneration and clinical progression in

presymptomatic Alzheimer's disease. Nat Med. 2019 Feb;25(2):277-283. doi: 10.1038/s41591-018-0304-3. Epub 2019 Jan 21. PMID: 30664784; PMCID: PMC6367005.

Piórkowska, E., Musijowski, J., Buś-Kwaśnik, K., and Rudzki, P. J. (2017). Is a deuterated internal standard appropriate for the reliable determination of olmesartan in human plasma?. Journal of chromatography. B, Analytical technologies in the biomedical and life sciences, 1040, 53–59. https://doi.org/10.1016/j.jchromb.2016.11.021

Quanterix. (2025). Quanterix receives FDA clearance for first blood-based Alzheimer's test. Quanterix Corporation. https://www.quanterix.com/newsroom

Quest Diagnostics. [online] Available at: https://testdirectory.questdiagnostics.com/test/test-guides/TS_AD_Detect_BetaRatioPlasma/quest-ad-detect-beta-amyloid-4240-ratio-plasma?p=td.

Rabinovici, G. D., Gatsonis, C., Apgar, C., Chaudhary, K., Gareen, I., Hanna, L., … Carrillo, M. C. (2019). Association of Amyloid Positron Emission Tomography with Subsequent Change in Clinical Management among Medicare Beneficiaries with Mild Cognitive Impairment or Dementia. JAMA - Journal of the American Medical Association, 321(13), 1286–1294. https://doi.org/10.1001/jama.2019.2000

Radha, R., Shahzadi, S. K., & Al-Sayah, M. H. (2021). Fluorescent Immunoprawfs for Detection and Quantification of Cardiac Troponin I: A Short Review. Molecules (Basel, Switzerland), 26(16), 4812. https://doi.org/10.3390/molecules26164812

Ranjit R, Van Remmen H, Ahn B. Acylated Ghrelin Receptor Agonist HM01 Decreases Lean Body and Muscle Mass, but Unacylated Ghrelin Protects against Redox-Dependent Sarcopenia. Antioxidants (Basel). 2022 Nov 28;11(12):2358. doi: 10.3390/antiox11122358. PMID: 36552566; PMCID: PMC9774605.

Rauh, M., Gröschl, M., and Rascher, W. (2007). Simultaneous quantification of ghrelin and desacyl-ghrelin by liquid chromatography-tandem mass spectrometry in plasma,

serum, and cell supernatants. Clinical chemistry, 53(5), 902–910. https://doi.org/10.1373/clinchem.2006.078956

Rhea, E. M., Salameh, T. S., Gray, S., Niu, J., Banks, W. A., & Tong, J. (2018). Ghrelin transport across the blood–brain barrier can occur independently of the growth hormone secretagogue receptor. Molecular Metabolism, 18, 88–96.

Rigamonti, A. E., Pincelli, A. I., Corrà, B., Viarengo, R., Bonomo, S. M., Galimberti, D., Scacchi, M., Scarpini, E., Cavagnini, F., and Müller, E. E. (2002). Plasma ghrelin concentrations in elderly subjects: comparison with anorexic and obese patients. The Journal of endocrinology, 175(1), R1–R5. https://doi.org/10.1677/joe.0.175r001

Rissin, D. M., Kan, C. W., Campbell, T. G., Howes, S. C., Fournier, D. R., Song, L., … Walt, D. R. (2010). Single-molecule enzyme-linked immunosorbent assay detects serum proteins at subfemtomolar concentrations. Nature Biotechnology, 28(6), 595–599. https://doi.org/10.1038/nbt.1641

Rissman, R. A. et al. Plasma Aβ42/Aβ40 and phospho-tau217 concentration ratios increase the accuracy of amyloid PET classification in preclinical Alzheimer's disease. Alzheimers Dement. https://doi.org/10.1002/alz.13542 (2023).

Roeben, B., Maetzler, W., Vanmechelen, E., Schulte, C., Heinzel, S., Stellos, K., … Berg, D. (2016). Association of Plasma Aβ40 Peptides, but Not Aβ42, with Coronary Artery Disease and Diabetes Mellitus. Journal of Alzheimer's Disease, 52(1), 161–169. https://doi.org/10.3233/JAD-150575

Roeben, B., Schliebs, R., Hartig, W., Schramm, M., & Bigl, V. (2016). Amyloid-β(1–42) plasma levels correlate with peripheral cholesterol metabolism in elderly non-demented individuals. Journal of Alzheimer's Disease, 54(2), 627–637. https://doi.org/10.3233/JAD-160314

Rieder, R., Wisniewski, P. J., & Alderman, B. L. (2017). The gut–brain axis: An emerging role for the gut microbiome in psychiatric and neurodegenerative disorders. *Neuroscience & Biobehavioral Reviews*, 83, 793–803.

Rogers, J. C., and Bomgarden, R. D. (2016). Sample Preparation for Mass Spectrometry-Based Proteomics; from Proteomes to Peptides. Advances in experimental medicine and biology, 919, 43–62. https://doi.org/10.1007/978-3-319-41448-5_3

Rutledge, J., Lehallier, B., Zarifkar, P., Losada, P. M., Shahid-Besanti, M., Western, D., Gorijala, P., Ryman, S., Yutsis, M., Deutsch, G. K., Mormino, E., Trelle, A., Wagner, A. D., Kerchner, G. A., Tian, L., Cruchaga, C., Henderson, V. W., Montine, T. J., Borghammer, P., Wyss-Coray, T., … Poston, K. L. (2024). Comprehensive proteomics of CSF, plasma, and urine identify DDC and other biomarkers of early Parkinson's disease. Acta neuropathologica, 147(1), 52. https://doi.org/10.1007/s00401-024-02706-0

Sakata, I., Nakano, Y., Osborne-Lawrence, S., Rovinsky, S. A., Lee, C. E., Perello, M., Anderson, J. G., Coppari, R., Xiao, G., Lowell, B. B., Elmquist, J. K., and Zigman, J. M. (2009). Characterization of a novel ghrelin cell reporter mouse. Regulatory peptides, 155(1-3), 91–98. https://doi.org/10.1016/j.regpep.2009.04.001

Sakata, I., Takemi, S., Kaminoda, A., Aizawa, S., Ojima, S., Gong, Z., ... & Sakata, T. (2018). β-Oxidation in ghrelin-producing cells is important for ghrelin acyl-modification. Scientific Reports, 8, 9176.

Sampson, T. R., & Mazmanian, S. K. (2016). Control of brain development, function, and behavior by the microbiome. *Cell Host & Microbe*, 17(5), 565–576.

Sanchez, E., Wilkinson, T., Coughlan, G., Mirza, S., Baril, A. A., Ramirez, J., Binns, M. A., Black, S. E., Borrie, M., Dilliott, A. A., Dixon, R. A., Dowlatshahi, D., Farhan, S., Finger, E., Fischer, C. E., Frank, A., Freedman, M., Goncalves, R. A., Grimes, D. A., Hassan, A., … Masellis, M. (2024). Association of plasma biomarkers with cognition, cognitive decline, and daily function across and within neurodegenerative diseases: Results from the Ontario Neurodegenerative Disease Research Initiative. Alzheimer's & dementia : the journal of the Alzheimer's Association, 20(3), 1753–1770. https://doi.org/10.1002/alz.13560

Sassi, M., Morgan, A. H., & Davies, J. S. (2022). Ghrelin acylation: A post-translational tuning mechanism regulating adult hippocampal neurogenesis. Cells, 11(5), 765. https://doi.org/10.3390/cells11050765

Satou M, Sugimoto H. The study of ghrelin deacylation enzymes. Methods Enzymol. 2012;514:165-79. doi: 10.1016/B978-0-12-381272-8.00011-8. PMID: 22975053.

Satou, M., Nishi, Y., Yoh, J., Hattori, Y., & Sugimoto, H. (2010). Identification and characterization of acyl-protein thioesterase 1/lysophospholipase I as a ghrelin

deacylation/lysophospholipid hydrolyzing enzyme in fetal bovine serum and conditioned medium. Endocrinology, 151(10), 4765–4775.

Schopfer LM, Lockridge O, Brimijoin S. Pure human butyrylcholinesterase hydrolyzes octanoyl ghrelin to desacyl ghrelin. Gen Comp Endocrinol. 2015 doi:10.1016/j.ygcen.2015.05.017.

Schultz H. S., Østergaard S., Sidney J., Lamberth K., Sette A. (2018). The Effect of Acylation with Fatty Acids and Other Modifications on HLA Class II:peptide Binding and T Cell Stimulation for Three Model Peptides. PLOS ONE 13 (5), e0197407. doi:10.1371/JOURNAL.PONE.0197407

Seemüller, E., Lupas, A., Stock, D., Lowe, J., Huber, R., and Baumeister, W. (1995) Science 268, 579–582

Shaw, L. M., Hansson, O., Manuilova, E., Masters, C. L., Doecke, J. D., Li, Q. X., Rutz, S., Widmann, M., Leinenbach, A., and Blennow, K. (2019). Method comparison study of the Elecsys® β-Amyloid (1-42) CSF prawf versus comparator prawfs and LC-MS/MS. Clinical biochemistry, 72, 7–14. https://doi.org/10.1016/j.clinbiochem.2019.05.006

Shiimura, Y., Horita, S., Hamamoto, A., Asada, H., Hirata, K., Tanaka, M., Mori, K., Uemura, T., Kobayashi, T., Iwata, S., and Kojima, M. (2020). Structure of an antagonist-bound ghrelin receptor reveals possible ghrelin recognition mode. Nature communications, 11(1), 4160. https://doi.org/10.1038/s41467-020-17554-1

Shiiya, T., Nakazato, M., Mizuta, M., Date, Y., Mondal, M. S., Tanaka, M., Nozoe, S., Hosoda, H., Kangawa, K., and Matsukura, S. (2002). Plasma ghrelin levels in lean and obese humans and the effect of glucose on ghrelin secretion. The Journal of clinical endocrinology and metabolism, 87(1), 240–244. https://doi.org/10.1210/jcem.87.1.8129

Sidibé, J., Varesio, E., and Hopfgartner, G. (2014). Quantification of ghrelin and des-acyl ghrelin in human plasma by using cubic-selected reaction-monitoring LCMS. Bioanalysis, 6(10), 1373–1383. https://doi.org/10.4155/bio.14.108

Sinha, A., and Mann, M. (2020). A beginner's guide to mass spectrometry–based proteomics. The Biochemist, 42(5), 64–69. https://doi.org/10.1042/bio20200057

Smith, R. M. (2004). Understanding Mass Spectra: A Basic Approach. In John Wiley and Sons, Inc. eBooks. https://doi.org/10.1002/0471479357

Snyder, H. M., Carrillo, M. C., Grodstein, F., Henriksen, K., Jeromin, A., Lovestone, S., … Fillit, H. M. (2014). Developing novel blood-based biomarkers for Alzheimer's disease. Alzheimer's and Dementia, 10(1), 109–114. https://doi.org/10.1016/j.jalz.2013.10.007

Song F, Poljak A, Valenzuela M, Mayeux R, Smythe GA, Sachdev PS (2011) Meta-analysis of plasma amyloid-β levels in Alzheimer's disease. J Alzheimers Dis 26, 365–375.

Song, N., Wang, W., Jia, F., Du, X., Xie, A., He, Q., Shen, X., Xie, J., & Jiang, H. (2017). Assessments of plasma ghrelin levels in the early stages of Parkinson's disease. Movement Disorders, 32(10), 1487–1491. https://doi.org/10.1002/mds.27095

St-Onge M.-P., Wolfe S., Sy M., Shechter A., Hirsch J. (2014). Sleep Restriction Increases the Neuronal Response to Unhealthy Food in Normal-Weight Individuals. Int. J. Obes. 38 (3), 411–416. 10.1038/ijo.2013.114

Staes, E., Rozet, E., Ucakar, B., Hubert, P., and Préat, V. (2010). Validation of a method for the quantitation of ghrelin and unacylated ghrelin by HPLC. Journal of pharmaceutical and biomedical analysis, 51(3), 633–639. https://doi.org/10.1016/j.jpba.2009.09.040

Stokvis, E., Nan-Offeringa, L. G., Ouwehand, M., Tibben, M. M., Rosing, H., Schnaars, Y., Grigat, M., Romeis, P., Schellens, J. H., and Beijnen, J. H. (2004). Quantitative analysis of D-24851, a novel anticancer agent, in human plasma and urine by liquid chromatography coupled with tandem mass spectrometry. Rapid communications in mass spectrometry : RCM, 18(13), 1465–1471. https://doi.org/10.1002/rcm.1493

Stokvis, E., Rosing, H. and Beijnen, J.H. (2005), Stable isotopically labeled internal standards in quantitative bioanalysis using liquid chromatography/mass spectrometry: necessity or not?. Rapid Commun. Mass Spectrom., 19: 401-407. https://doi.org/10.1002/rcm.1790

Strimbu, K., & Tavel, J. A. (2010). What are biomarkers? Current Opinion in HIV and AIDS, 5(6), 463-466.

Suda, Y., Kuzumaki, N., Sone, T., Narita, M., Takei, N., et al. (2018). Down-regulation of ghrelin receptors on dopaminergic neurons in the substantia nigra contributes to Parkinson's disease–like motor dysfunction. Molecular Brain, 11(1), 5. https://doi.org/10.1186/s13041-018-0349-8

Sun R., Wang H., Shi Y., Gao D., Sun Z., Chen Z., et al. (2019). A pilot study of urinary exosomes in Alzheimer's disease. Neurodegener. Dis. 19 184–191. 10.1159/000505851

Szentirmai, E., Kapás, L., Sun, Y., Smith, R. G., and Krueger, J. M. (2007). Spontaneous sleep and homeostatic sleep regulation in ghrelin knockout mice. American journal of physiology. Regulatory, integrative and comparative physiology, 293(1), R510–R517. https://doi.org/10.1152/ajpregu.00155.2007

Takada R., Satomi Y., Kurata T., Ueno N., Norioka S., Kondoh H., et al. (2006). Monounsaturated Fatty Acid Modification of Wnt Protein: Its Role in Wnt Secretion. Developmental Cell 11 (6), 791–801. doi:10.1016/j.devcel.2006.10.003

Taylor M. S., Ruch T. R., Hsiao P.-Y., Hwang Y., Zhang P., Dai L., et al. (2013). Architectural Organization of the Metabolic Regulatory Enzyme Ghrelin O-Acyltransferase. J. Biol. Chem. 288 (45), 32211–32228. 10.1074/jbc.M113.510313

Tian, D. Y., Cheng, Y., Zhuang, Z. Q., He, C. Y., Pan, Q. G., Tang, M. Z., Hu, X. L., Shen, Y. Y., Wang, Y. R., Chen, S. H., Sun, H. L., Sun, P. Y., Yu, Z. Y., Fan, D. Y., Bu, X. L., Tan, C. R., Zeng, G. H., Wang, J., Zhao, H. W., & Wang, Y. J. (2021). Physiological clearance of amyloid-beta by the kidney and its therapeutic potential for Alzheimer's disease. Molecular psychiatry, 26(10), 6074–6082. https://doi.org/10.1038/s41380-021-01073-6

Ten Have, S., Boulon, S., Ahmad, Y., and Lamond, A. I. (2011). Mass spectrometry-based immuno-precipitation proteomics - the user's guide. Proteomics, 11(6), 1153–1159. https://doi.org/10.1002/pmic.201000548

Teunissen, C. E., Chiu, M. J., Yang, C. C., Yang, S. Y., Scheltens, P., Zetterberg, H., & Blennow, K. (2018). Plasma Amyloid-β (Aβ42) Correlates with Cerebrospinal Fluid

Aβ42 in Alzheimer's Disease. Journal of Alzheimer's disease : JAD, 62(4), 1857–1863. https://doi.org/10.3233/JAD-170784

Tezenas du Montcel, C., Duriez, P., Lebrun, N., Grouselle, D., de Grimaudet, B., Dardennes, R., Epelbaum, J., Cuenca, M., Viltart, O., Gorwood, P., and Tolle, V. (2022). Methodological considerations for ghrelin isoforms prawf in clinical evaluation in anorexia nervosa. Comprehensive psychoneuroendocrinology, 11, 100140. https://doi.org/10.1016/j.cpnec.2022.100140

Therriault, J., Woo, M.S., Salvadó, G. et al. Comparison of immunoprawf- with mass spectrometry-derived p-tau quantification for the detection of Alzheimer's disease pathology. Mol Neurodegeneration 19, 2 (2024). https://doi.org/10.1186/s13024-023-00689-2 Thomas A, Krombholz S, Wolf C, Thevis M. Determination of ghrelin and desacyl ghrelin in human plasma and urine by means of LC-MS/MS for doping controls. Drug Test Anal. 2021 Nov;13(11-12):1862-1870. doi: 10.1002/dta.3176. Epub 2021 Oct 26. PMID: 34633773.

Thijssen, E. H., La Joie, R., Wolf, A., Strom, A., Wang, P., Iaccarino, L., Bourakova, V., Cobigo, Y., Heuer, H., Spina, S., VandeVrede, L., Chai, X., Proctor, N. K., Airey, D. C., Shcherbinin, S., Duggan Evans, C., Sims, J. R., Zetterberg, H., Blennow, K., Karydas, A. M., … Advancing Research and Treatment for Frontotemporal Lobar Degeneration (ARTFL) investigators (2020). Diagnostic value of plasma phosphorylated tau181 in Alzheimer's disease and frontotemporal lobar degeneration. Nature medicine, 26(3), 387–397. https://doi.org/10.1038/s41591-020-0762-2

Thomas, A. S., Sassi, M., Angelini, R., Morgan, A. H., and Davies, J. S. (2022). Acylation, a Conductor of Ghrelin Function in Brain Health and Disease. Frontiers in physiology, 13, 831641. https://doi.org/10.3389/fphys.2022.831641

Thomson, B. A., and Iribarne, J. V. (1979). Field induced ion evaporation from liquid surfaces at atmospheric pressure. Journal of Chemical Physics, 71(11), 4451–4463. https://doi.org/10.1063/1.438198

Tsai FJ, Chen SY, Liu YC, Liao HY, Chen CJ. The comparison of CHCA solvent compositions for improving LC-MALDI performance and its application to study the impact of aflatoxin B1 on the liver proteome of diabetes mellitus type 1 mice. PLoS

One. 2017 Jul 24;12(7):e0181423. doi: 10.1371/journal.pone.0181423. PMID: 28738076; PMCID: PMC5524319.

Tschöp, M., Smiley, D. L., and Heiman, M. L. (2000). Ghrelin induces adiposity in rodents. Nature, 407(6806), 908–913. https://doi.org/10.1038/35038090

Tucholski, T.; Cai, W.; Gregorich, Z. R.; Bayne, E. F.; Mitchell, S. D.; McIlwain, S. J.; de Lange, W. J.; Wrobbel, M.; Karp, H.; Hite, Z.; Vikhorev, P. G.; Marston, S. B.; Lal, S.; Li, A.; Dos Remedios, C.; Kohmoto, T.; Hermsen, J.; Ralphe, J. C.; Kamp, T. J.; Moss, R. L.; Ge, Y. Distinct Hypertrophic Cardiomyopathy Genotypes Result in Convergent Sarcomeric Proteoform Profiles Revealed by Top-down Proteomics. Proc. Natl. Acad. Sci. U. S. A. 2020, 117 (40), 24691– 24700,

Unger, M. M., Möller, J. C., Mankel, K., Eggert, K. M., Bohne, K., Bodden, M., Stiasny-Kolster, K., Kann, P. H., Mayer, G., Tebbe, J. J., & Oertel, W. H. (2011). Postprandial ghrelin response is reduced in patients with Parkinson's disease and idiopathic REM sleep behaviour disorder: A peripheral biomarker for early Parkinson's disease? Journal of Neurology, 258(6), 982–990. https://doi.org/10.1007/s00415-010-5864-1

Uriarte M., De Francesco P. N., Fernandez G., Cabral A., Castrogiovanni D., Lalonde T., et al. (2019). Evidence Supporting a Role for the Blood-Cerebrospinal Fluid Barrier Transporting Circulating Ghrelin into the Brain. Mol. Neurobiol. 56 (6), 4120–4134. doi:10.1007/s12035-018-1362-8

Van Berkel, G. J., and Kertesz, V. (2007). Using the electrochemistry of the electrospray ion source. Analytical chemistry, 79(15), 5510–5520. https://doi.org/10.1021/ac071944a

Verberk, I. M. W., Thijssen, E., Koelewijn, J., Mauroo, K., Vanbrabant, J., de Wilde, A., Zwan, M. D., Verfaillie, S. C. J., Ossenkoppele, R., Barkhof, F., van Berckel, B. N. M., Scheltens, P., van der Flier, W. M., Stoops, E., Vanderstichele, H. M., & Teunissen, C. E. (2020). Combination of plasma amyloid beta(1-42/1-40) and glial fibrillary acidic protein strongly associates with cerebral amyloid pathology. Alzheimer's research & therapy, 12(1), 118. https://doi.org/10.1186/s13195-020-00682-7

Villarreal, D., Pradhan, G., Zhou, Y., Xue, B., & Sun, Y. (2022). Diverse and complementary effects of ghrelin and obestatin. Biomolecules, 12(4), 517.

Vogelgsang, J., Shahpasand-Kroner, H., Vogelgsang, R., Streit, F., Vukovich, R., & Wiltfang, J. (2018). Multiplex immunoprawf measurement of amyloid-β42 to amyloid-β40 ratio in plasma discriminates between dementia due to Alzheimer's disease and dementia not due to Alzheimer's disease. Experimental brain research, 236(5), 1241–1250. https://doi.org/10.1007/s00221-018-5210-x

Vorm, O., Roepstorff, P., and Mann, M. (1994). Improved resolution and very high sensitivity in MALDI TOF of matrix surfaces made by fast evaporation. Analytical Chemistry, 66(19), 3281–3287. https://doi.org/10.1021/ac00091a044

Vortmeier, G., DeLuca, S. H., Els-Heindl, S., Chollet, C., Scheidt, H. A., Beck-Sickinger, A. G., Meiler, J., and Huster, D. (2015). Integrating solid-state NMR and computational modeling to investigate the structure and dynamics of membrane-associated ghrelin. PloS one, 10(3), e0122444. https://doi.org/10.1371/journal.pone.0122444

Vuckovic D., Dagley L.F., Purcell A.W., Emili A. Membrane proteomics by high performance liquid chromatography–tandem mass spectrometry: Analytical approaches and challenges. Proteomics. 2013;13:404–423. doi: 10.1002/pmic.201200340.

Walker A. K., Rivera P. D., Wang Q., Chuang J.-C., Tran S., Osborne-Lawrence S., et al. (2015). The P7C3 Class of Neuroprotective Compounds Exerts Antidepressant Efficacy in Mice by Increasing Hippocampal Neurogenesis. Mol. Psychiatry 20 (4), 500–508. doi:10.1038/mp.2014.34

Walsh, C. T., Garneau-Tsodikova, S., & Gatto Jr, G. J. (2005). Protein posttranslational modifications: the chemistry of proteome diversifications. Angewandte Chemie International Edition, 44(45), 7342-7372.

Wan, W. Y., and Milner-White, E. J. (1999). A recurring two-hydrogen-bond motif incorporating a serine or threonine residue is found both at alpha-helical N termini and in other situations. Journal of molecular biology, 286(5), 1651–1662. https://doi.org/10.1006/jmbi.1999.2551

Wang, H., Dou, S., Zhu, J., Shao, Z., Wang, C., & Cheng, B. (2020). Ghrelin protects dopaminergic neurons against MPTP neurotoxicity through promoting autophagy and

inhibiting endoplasmic reticulum stress–mediated apoptosis. Brain Research, 1746, 147023. https://doi.org/10.1016/j.brainres.2020.147023

Wang, Y., Guo, S., Zhuang, Y. et al. Molecular recognition of an acyl-peptide hormone and activation of ghrelin receptor. Nat Commun 12, 5064 (2021). https://doi.org/10.1038/s41467-021-25364-2

Wei, J., Wong, L. C., & Boland, S. (2024). Lipids as emerging biomarkers in neurodegenerative diseases. *International Journal of Molecular Sciences, 25*(1), 131. https://doi.org/10.3390/ijms25010131

Wiley, W. C., and McLaren, I. H. (1955). Time-of-Flight Mass Spectrometer with Improved Resolution. Review of Scientific Instruments, 26(12), 1150–1157. https://doi.org/10.1063/1.1715212

Wilson DH, Rissin DM, Kan CW, Fournier DR, Piech T, Campbell TG, Meyer RE, Fishburn MW, Cabrera C, Patel PP, Frew E, Chen Y, Chang L, Ferrell EP, von Einem V, McGuigan W, Reinhardt M, Sayer H, Vielsack C, Duffy DC (2016) The Simoa HD-1 Analyzer: A novel fully automated digital immunoprawf analyzer with single-molecule sensitivity and multiplexing. J Lab Autom 21, 533–547.

Willert K., Brown J. D., Danenberg E., Duncan A. W., Weissman I. L., Reya T., et al. (2003). Wnt Proteins Are Lipid-Modified and Can Act as Stem Cell Growth Factors. Nature 423 (6938), 448–452. doi:10.1038/nature01611

Winston Timp and Gregory Timp Beyond mass spectrometry, the next step in proteomics.Sci. Adv.6,eaax8978(2020).DOI:10.1126/sciadv.aax8978

World Health Organization. (2021). *Dementia*. Retrieved from https://www.who.int/news-room/fact-sheets/detail/dementia

Yang, J., Brown, M. S., Liang, G., Grishin, N. V., & Goldstein, J. L. (2008a). Identification of the acyltransferase that octanoylates ghrelin, an appetite-stimulating peptide hormone. *Cell, 132*(3), 387–396. https://doi.org/10.1016/j.cell.2008.01.017

Yang J., Zhao T.-J., Goldstein J. L., Brown M. S. (2008b). Inhibition of Ghrelin O-acyltransferase (GOAT) by Octanoylated Pentapeptides. Proc. Natl. Acad. Sci. U.S.A. 105 (31), 10750–10755. doi:10.1073/pnas.0805353105

Yang, S., Mu, L., Feng, R., and Kong, X. (2019). Selection of Internal Standards for Quantitative Matrix-Assisted Laser Desorption/Ionization Mass Spectrometric Analysis Based on Correlation Coefficients. ACS omega, 4(5), 8249–8254. https://doi.org/10.1021/acsomega.9b00566

Yang, J., and Sumbria, R. K. (2021). The concentration of brain homogenates with the Amicon Ultra Centrifugal filters. MethodsX, 8, 101584. https://doi.org/10.1016/j.mex.2021.101584

Young, E. R., & Jialal, I. (2023). Biochemistry, ghrelin. In *StatPearls* [Internet]. Treasure Island (FL): StatPearls Publishing. Retrieved from https://www.ncbi.nlm.nih.gov/books/NBK547692/

Yurtsever, D., & Lorent, J. H. (2020). Structural modifications controlling membrane raft partitioning and curvature in human and viral proteins. *The Journal of Physical Chemistry B, 124*(35), 7574–7585. https://doi.org/10.1021/acs.jpcb.0c03435

Xiao, X., Tang, T., Bi, M., Liu, M., Liu, J., Jiao, Q., Chen, X., Yan, C., Du, X., & Jiang, H. (2024). GHSR deficiency exacerbates Parkinson's disease pathology by impairing autophagy. Redox Biology, 76, 103322. https://doi.org/10.1016/j.redox.2024.103322

Zarkali, A., McColgan, P., Ryten, M., Reynolds, R. H., Leyland, L. A., Lees, A. J., Rees, G., and Weil, R. S. (2020). Dementia risk in Parkinson's disease is associated with interhemispheric connectivity loss and determined by regional gene expression. NeuroImage. Clinical, 28, 102470. https://doi.org/10.1016/j.nicl.2020.102470

Zeidman R., Jackson C. S., Magee A. I. (2009). Protein Acyl Thioesterases (Review). Mol. Membr. Biol. 26 (1–2), 32–41. doi:10.1080/09687680802629329

Zemenova, J., Sykora, D., Adamkova, H., Maletinska, L., Elbert, T., Marek, A., and Blechova, M. (2017). Novel approach to determine ghrelin analogs by liquid chromatography with mass spectrometry using a monolithic column. Journal of separation science, 40(5), 1032–1039. https://doi.org/10.1002/jssc.201601141

Zetterberg, H., and Burnham, S. C. (2019, March 28). Blood-based molecular biomarkers for Alzheimer's disease. Molecular Brain, Vol. 12, p. 26. https://doi.org/10.1186/s13041-019-0448-1

Zhou Q., Yang D., Wu M., Guo Y., Guo W., Zhong L., et al. (2019). Common Activation Mechanism of Class a GPCRs. ELife 8, e50279. doi:10.7554/ELIFE.50279

Zhu X., Cao Y., Voodg K., Steiner D. F. (2006). On the Processing of Proghrelin to Ghrelin. J. Biol. Chem. 281 (50), 38867–38870. doi:10.1074/jbc.M607955200

Zhu, N., Santos-Santos, M., Illán-Gala, I., Montal, V., Estellés, T., Barroeta, I., Altuna, M., Arranz, J., Muñoz, L., Belbin, O., Sala, I., Sánchez-Saudinós, M. B., Subirana, A., Videla, L., Pegueroles, J., Blesa, R., Clarimón, J., Carmona-Iragui, M., Fortea, J., Lleó, A., … Alcolea, D. (2021). Plasma glial fibrillary acidic protein and neurofilament light chain for the diagnostic and prognostic evaluation of frontotemporal dementia. Translational neurodegeneration, 10(1), 50. https://doi.org/10.1186/s40035-021-00275-w

Zipser, B. D., Johanson, C. E., Gonzalez, L., Berzin, T. M., Tavares, R., Hulette, C. M., … Stopa, E. G. (2007). Microvascular injury and blood-brain barrier leakage in Alzheimer's disease. Neurobiology of Aging, 28(7), 977–986. https://doi.org/10.1016/j.neurobiolaging.2006.05.016